Fall 12-20-2019

The Role of Reactive Oxygen Species in Regulating Macrophage and Fibroblast Activation Within the Breast Cancer Tumor Microenvironment

Brandon J. Griess
University of Nebraska Medical Center

THE ROLE OF REACTIVE OXYGEN SPECIES IN REGULATING MACROPHAGE AND FIBROBLAST ACTIVATION WITHIN THE BREAST CANCER TUMOR MICROENVIRONMENT

By

Brandon Joseph Griess

A DISSERTATION

Presented to the Faculty of

The University of Nebraska Graduate College

In Partial Fulfillment of the Requirements

For the Degree of Doctor of Philosophy

Department of Biochemistry and Molecular Biology

Under the Supervision of Professor Melissa Teoh-Fitzgerald

University of Nebraska Medical Center

Omaha, Nebraska

December, 2019

Supervisory Committee:

Hamid Band, M.D., Ph.D.

Kaustubh Datta, Ph.D.

Ming-Fong Lin, Ph.D.

ACKNOWLEDGMENTS

First and foremost, I would like to thank my mentor, Dr. Melissa Teoh-Fitzgerald. You were able to take a lump of clay and mold it into a scientist. I have learned a lot under your tutelage ranging from how to answer questions scientifically, how to analyze data, how to write grants and papers, and how to train summer students. You provide the direction when I needed it most, while also providing me the freedom to stand on my own and develop as a well-rounded scientist. Thank you for all your help.

Next, I would like to acknowledge the other members of the Teoh-Fitzgerald lab. Dr. Briana Ormsbee Golden played a vital and pivotal role during my early days at UNMC. I shudder to think of where I would be without the guidance and patience you displayed while teaching and training me to become a scientist. I want to thank Dr. Shakeel Mir for expanding my horizons both scientifically and culturally. Additionally, I would like to thank Michelle Desler and Drs. Eric Tom and Raghupathy Vengoji for all of their help and support throughout their limited time in our lab. Also, I would like to thank all the other co-authors on my papers. Without your help, I never would have been able to take those projects across the goal line and get them published. I would also like to thank the following labs for their help throughout, the Hyde, Oberley-Deegan, Datta, Lin, and Mott lab. Your collaborative help has greatly improved my ability to finish this work in a timely manner. I would especially like to thank, Dr. Elizabeth Kosmacek. You have always provided excellent advice and support whenever I needed it.

I would also like to acknowledge the role my supervisory committee has played in helping me focus and shape this project. Without the help of Drs. Band, Datta, and Lin, this project would not have gone as smoothly as it did. Thank you for providing the guidance needed for me to see this challenging project to its conclusion.

Next, I would like to acknowledge all of the friends that I have made throughout my time here at UNMC. The stress of a doctoral degree by its nature forces one to commiserate with fellow graduate students. I have been fortunate to find many friends at UNMC in large part through various intramural sports, such as volleyball, softball, and curling. These stolen amounts away from lab were beneficial to both my mind and body. I would like to especially thank, Bailee, Brittany, and Lisa, who took the brunt of my misplaced anxiety after a failed experiment. I will not soon forgot the fun of movie and game nights, especially due to my new found addition to board games. I thank you for all the good times and look forward to see what you accomplish in the next phase of your careers.

Finally, I would like to thank my family. Mom and Dad, you have been a constant inspiration throughout my entire life. Without your help and encouragement, I would not be half the man that I am today. You have instilled a sense of curiosity that has aided me throughout my life and, especially, while earning my graduate degree. I will always be grateful for the limited time that I was lucky enough to have with you, Mom. To my brothers and sisters, thank you for keeping me grounded and providing a consistent outlet to unplug from the treadmill that is scientific research. Thank you Jill for providing a near unending supply of motherly support. Your impact on our family cannot be understated. I would also like to thank my extended family. I apologize for the extended long-winded responses to the simple question, “What are you up to?”. To my long-term friends, thank you for never letting me get a big head and bringing me back to earth.

THE ROLE OF REACTIVE OXYGEN SPECIES IN REGULATING MACROPHAGE AND FIBROBLAST ACTIVATION WITHIN THE BREAST CANCER TUMOR MICROENVIRONMENT

Brandon Joseph Griess, Ph.D.

University of Nebraska, 2019

Supervisor: Melissa Teoh-Fitzgerald, Ph.D.

The tumor microenvironment (TME) is a key determining factor in breast cancer, especially the more aggressive subtype triple negative breast cancer (TNBC). The activated fibroblasts and macrophages within the TME have many tumor promoting functions. Therefore, targeting their activation presents a novel therapeutic approach in TNBC. My work studied the role of reactive oxygen species (ROS) during fibroblast and macrophage activation in breast cancer.

My studies showed that expression of the secreted antioxidant enzyme, EcSOD, is silenced in breast cancer samples, in part, via increased promoter methylation. The re-expression of EcSOD inhibited c-Met activation in the TNBC cell line, MDA-MB231. HGF, the ligand for c-Met, is secreted by surrounding fibroblasts in breast cancer. Due to its extracellular localization, EcSOD significantly inhibited the paracrine HGF/c-Met signaling during co-culture of MDA-MB231 with HGF overexpressing mammary fibroblast, RMF-HGF. EcSOD and a SOD mimetic, MnTE-2-PyP, inhibited the HGF-mediated 3D growth and invasion of MDA-MB231 in co-culture with RMF-HGF. EcSOD also inhibited RMF-HGF-stimulated orthotopic tumor growth of MDA-MB231. Interestingly, long-term co-culture showed that EcSOD expression in MDA-MB231 inhibited the aggressive phenotype in RMF-HGF. Additionally, upregulation of the ROS

generating enzyme, Nox4, increased the aggressiveness of RMF-HGF over control RMF cells.

Tumor associated macrophages (TAM), which resemble the M2 type, enhance the aggressiveness of breast cancer. M2 polarization was selectively inhibited by MnTE-2-PyP. MnTE-2-PyP reduced M2 markers and inhibited the macrophage-mediated cancer cell growth. Additionally, MnTE-2-PyP inhibited M2-mediated T cell suppression, in part, via decreased PD-L2 levels. This study also determined that M2 macrophages have lower levels of reactive oxygen species (ROS) and lower production of extracellular hydrogen peroxide compared to the anti-tumor M1 macrophages, due to reduced levels of pro-oxidants enzymes and higher levels of antioxidant enzymes. Despite lower ROS levels, M2 macrophages require ROS for proper polarization as MnTE-2-PyP reduced ROS levels. Additionally, inhibition of Nox-derived ROS with DPI inhibited M2 markers, while adding hydrogen peroxide increased M2 markers. Mechanistically, MnTE-2-PyP and DPI inhibited M2 polarization via decreased Stat3 activation.

Overall, my work shows ROS promotes an aggressive phenotype in macrophages and fibroblasts, which can be significantly inhibited using the redox active drug MnTE-2-PyP.

TABLE OF CONTENTS

LIST OF FIGURES

LIST OF TABLES

LIST OF ABBREVIATIONS

3D	Three Dimensional
5-aza-dC	5-Aza-2'-Deoxycytidine
5-mC	5-Methylcytosine
AhR-XRE	Aryl Hydrocarbon Receptor-Xenobiotic Response Element
ARE	Antioxidant Response Element
BCCR	Breast Cancer Collaborative Registry
BHA	Butylated Hydroxyanisole
BMI	Body Mass Index
CAF	Cancer-Associated Fibroblast
CC	Co-Culture
CCL2	MCP-1
CEP	2-(ω-carboxyethyl)pyrrole
CFSE	Carboxyfluorescein Succinimidyl Ester
CM	Conditioned Media
CMH	1-Hydroxy-3-Methoxycarbonyl-2,2,5,5-Tetramethylpyrrolidine
CNV	Copy Number Variation
COPD	Chronic Obstructive Pulmonary Disease
CPP	Cell Penetrating Peptides
Cu/ZnSOD	Copper Zinc Superoxide Dismutase, SOD1
CYBA	p22phox
DCFH	2',7'-Dichlorodihydrofluorescein Diacetate

DETC	Diethyldithiocarbamic Acid Sodium Salt
DF	Deferoxamine
DHE	Dihydroethidium
DPI	Diphenyleneiodonium
Ec.20	EcSOD Overexpressing MDA-MB231 Cell Line
ECM	Extracellular Matrix
EcSOD	Extracellular Superoxide Dismutase
EGFR	Epidermal Growth Factor Receptor
EMSA	Electrophoretic Mobility Shift Assay
EPR	Electron Paramagnetic Resonance
ER	Oestrogen Receptor
FAK	Focal Adhesion Kinase
FAP	Fibroblast Activating Protein
FSP	Fibroblast Stimulating Protein
GCPII	Glutamate Carboxypeptidase II
Gpx	Glutathione Peroxidase
GSH	Glutathione
GSSG	Oxidized glutathione
GST	Glutathione-S-Transferase
GWAS	Genome-Wide Association Study
HAT	Histone Acetyltransferase
HBD	Heparin Binding Domain

HBSS	Hank's Buffered Salt Solution
HDAC	Histone Deacetylase
Her2	Human Epidermal Growth Factor Receptor 2
HGF	Hepatocyte Growth Factor
HMEC	Human Mammary Epithelial Cell
HR	Hazard Ratio
IHC	Immunohistochemistry
LOH	Loss of Heterozygosity
LRP	Lipoprotein Receptor-Related Protein
MAPK	Mitogen-Activated Kinases
MHC	Major Histocompatibility Complex
MMP	Matrix Metallopeptidase
MMTV	Mouse Mammary Tumor Virus
MnP	Manganese Poryphrin
MnSOD	SOD2
MnTE	MnTE-2-PyP^{5+},
	Manganese (III) Meso-Tetrakis-(N-Methylpyridinium-2-yl) Porphyrin
MOI	Multiplicity of Infection
MSC	Mesenchymal Stem Cell
NAC	N-Acetyl Cysteine
NAF	Nipple Aspiration Fluid
NGPPBCP	Northern Great Plains Personalized Breast Cancer Program

NIH	National Institute of Health
NL20	Non-transformed Immortalized Human Bronchial Epithelial Cells
NOS	Nitric Oxide Synthase
Nox4	NADPH Oxidase 4
oxTME	Oxidized Tumor Microenvironment
PBL	Peripheral Blood Leukocytes
PBS	Phosphate-Buffered Saline
PCDCD4	Programmed Cell Death Protein 4
PDGRFα/β	Platelet-derived Growth Factor Receptors Alpha and Beta
PD-L1	Programmed Death-Ligand 1
pkb	Protein Kinase b/akt
pkd	Protein Kinase d
PP	Protein Phosphatases
PR	Progesterone Receptor
Prx	Peroxiredoxin
PTP	Protein Tyrosine Phosphatase
PyMT	Polyoma Virus Middle T Antigen
qRT-PCR	Quantitative Real-Time Polymerase Chain Reaction
RECK	Reversion-inducing Cysteine-rich Protein
RFS	Relapse Free Survival
rHGF	Recombinant Human HGF
RMF	Reduction Mammary Fibroblast

RMF-HGF	HGF-overexpressing Mammary Fibroblasts
ROS	Reactive Oxygen Species
RTK	Receptor Tyrosine Kinase
SDF-1	Stroma Derived Factor 1
SEER	Surveillance, Epidermiology, and End Results
SELECT	Selenium and Vitamin E Cancer Prevention Trial
shRNA	Short Hairpin RNA
SMA	Alpha Smooth Muscle Actin
SNO	S-Nitrosothiol
SNP	Single Nucleotide Polymorphism
SOD	Superoxide Dismutase
TAM	Tumor Associated Macrophages
TAT	HIV Transactivtor Protein
TCGA	The Cancer Genome Atlas
TCR	T Cell Receptor
Tet	Ten-eleven Translocation
TGF-β	Transforming Growth Factor beta
TME	Tumor Microenvironment
TNBC	Triple Negative Breast Cancer
TPA	12-O-tetradecanoylphorbol-13-acetate
TPM-1	Tropomyosin 1
TRX	Thioredoxin

TSP	thrombospondin
V.1	Vector Control MDA-MB231 Cell Line for Ec.20

CHAPTER 1:

Introduction

1. Introduction

1.1 Breast Cancer

Breast cancer is the most common type of cancer diagnosed in United States women. It is the second leading cause of cancer-related deaths in women surpassed only by lung cancer. This year alone, there are an estimated 268,600 newly diagnosed cases of invasive breast cancer and 41,760 deaths [1]. The lifetime risk for women to develop invasive breast cancer is 1 in 8 or 13%. There are several known risk factors for breast cancer development; body mass index (BMI), age at menarche, age at first live birth, number of births, hormone usage, alcohol usage, and smoking [2, 3]. The incidence rate within the US has varied depending on those factors. For example, the large drop in incidence rate between 1999 and 2004 was due in large part to a reduction in hormone therapy [4]. Since 2004, the breast cancer incidence rate has remained steady with a slight increase of about 0.3% [1]. The reduction in births are estimated to be the major factor accounting for the current changes in incidence rate [2]. Despite the increase in incidence, the mortality rate has dropped by 40% from 1975 to 2017 due to increases in early detection and improvements in treatment [1, 5]. This has resulted in a 5-year survival rate of ~90%. However, these improvements have not benefitted all breast cancer patient, as survival rates and treatment options are varied amongst the different subtypes.

Breast cancer, like all cancers, is not one type of cancer. Initial research indicated that breast cancer can be fractionated into 4 major subtypes based on the presence or absence of certain markers. These markers are the oestrogen receptor (ER), progesterone receptor (PR), and the human epidermal growth factor receptor 2

(Her2). There is the Luminal A subtype that is ER/PR positive, Her2 negative, most common and least aggressive. The luminal B subtype is similar with ER/PR expression, Her2 expression, and a faster proliferation rate. The Her2 subtype is ER/PR negative and Her2 positive. The triple negative breast cancer (TNBC) subtype is negative for all three markers. These markers help stratify breast cancer patients to help determine severity of the disease and treatment options. The following data is taken directly from the Surveillance, Epidemiology, and End Results (SEER) program from patients between 2012 and 2016. Luminal A and luminal B made up 67% and 10% of patients with a 5-year survival rate of 94% and 90% respectively. Her2 only made up 4% of patients diagnosed with a survival rate of 83%. TNBC was more common making up 10% of patients with an even further reduced survival rate of 77%. The remaining 8% of patients had an unknown status and resulting 77% survival rate.

Treatment for all localized breast cancer subtypes is surgical resection with addition of either radiation or chemotherapy [6]. There are targeted systemic therapies for BC presenting with ER/PR or Her2 expression. ER/PR positive cancers receive endocrine therapy, typically tamoxifen, which is a selective estrogen receptor inhibitor. While, Her2 positive cancers typically receive chemotherapy in combination with trastuzumab, a monoclonal antibody targeting Her2. Inclusion of trastuzumab has significantly increased survival in Her2 positive patients compared to chemotherapy alone [7]. TNBC to date lacks any targeted therapy. Therefore, the treatment regimen for TNBC is chemotherapy. However, newer clinical trials are being performed combining chemotherapy with immunotherapies, such as atezolizumab that target programmed death-ligand 1 (PD-L1). However, these combinatorial treatments are only currently in metastatic TNBC [8].

Due to the advances in DNA/RNA sequencing, there has been a further classification of subtypes amongst breast cancer to help determine driving factors that could be targeted. The immunohistochemistry (IHC) analysis of ER/PR/Her2, while hugely beneficial, has not been able to accurately account for the complexity found using gene signatures. The unbiased analysis of gene signature revealed 5 main clusters. It caused a split in the TNBC subtype into two different subtypes, the basal-like breast cancer and the normal-like breast cancer [9]. The basal-like tumors expression keratins 5/6 and 17 indicative of basal breast cells. The normal-like tumors are similarly express high basal-like and low luminal gene expression in combination with higher adipose cell and non-epithelial gene expression [10]. Other studies have developed different methods of stratification to help determine potential drivers and targets using a larger size of TNBC samples [11]. Interestingly, two of three large scale studies found distinct subtypes of TNBC are dependent on the immune response to the tumor [12, 13]. The study done by Jézéquel et al. is particularly interesting in the context of this dissertation. They showed a subset of TNBC samples that have a low immune response and a high M2-like macrophage signature had a higher grade and lower survival than other TNBC clusters [12]. Additionally, this cluster was the purest basal-like cluster. The importance of these findings will become more clear when the role of the tumor microenvironment on breast cancer outcome is discussed later in this dissertation.

Interestingly, the risk factors associated with breast cancer incidence do not affect all subtypes equally. The known risk factors stated earlier are largely indicative of incidence in the luminal A subtype with breastfeeding, a higher premenopausal BMI, a higher number of births, and use of oral contraceptives having a negative association and alcohol use, younger age at menarche, older age at first birth, and older age at menopause having a positive association [14]. Most of the risk factors had unknown

effect on luminal B and Her2 subtypes [14]. While, TNBC was affected by the known risk factors in a similar manner as luminal A [14]. The disparate risk factors between luminal A and TNBC were an increased risk in TNBC with a higher number of births, a higher premenopausal BMI, and a weak increase risk with the use of oral contraceptives [14]. This study serves to further highlight the distinct differences found throughout breast cancer and how those differences affect both outcome and incidence rates.

1.2 Reactive Oxygen Species & Reactive Nitrogen Species

Reactive oxygen species, or ROS, and the closely related reactive nitrogen species, or RNS, are aptly named chemicals that contain either oxygen or nitrogen respectively and readily and easily react with surrounding chemicals and molecules. While there are many different species included under the ROS/RNS banner, the main species studied are superoxide, hydrogen peroxide, the hydroxyl radical, nitric oxide and peroxynitrite, as they are the most common species produced by mammalian cells. These species are also involved in a complex web of reactions that ultimately dictates their effect within the cell. They affect mechanisms throughout the cell via their ability to oxidize surrounding molecules, such as proteins, lipids, RNA, and DNA. This oxidation can result in cellular damage, such as mutations of DNA, increased membrane permeability, and modification of protein activity. However, ROS and RNS are integrally engrained into signal propagation within eukaryotic physiology and have essential roles in metabolism, innate immunity, differentiation and cell survival. As such, ROS signaling has been linked to aging, cardiovascular pathologies, inflammation, neurodegeneration and cancer [15-19]. Due to this dual-sided nature of ROS as an effector of cell signaling and a damage inducing molecule, it has results in the idea of a Goldilocks zone of ROS

within cells. Very low levels of ROS lead to cytostatic effects on cells, while high levels can lead to tumorigenesis or cytotoxic ROS-mediated cell death as seen in figure 1.1. Therefore, insights into ROS produced by regulated processes and the defenses evolved to protect against these disruptions of homeostatic redox states have fueled intense interest in the search for drug targets and clinical antioxidants. Additionally, ROS is implicated as an important secondary messenger in most of the hallmarks of cancer [20]. Thus, ROS remains an attractive target when developing cancer therapies.

1.2.1 Superoxide

In order to understand the complexities of ROS and its effect within the cell, the web of reactions between ROS and RNS must be further explained. Within the cell, ROS is commonly generated first as superoxide. Superoxide is a formed when molecular oxygen gains an additional electron. This often occurs when electrons from the electron transport chain leak out of the inner mitochondrial membrane on to oxygen creating superoxide. However, superoxide is also produced by cellular enzymes, called NAPDH oxidases, further indicating that ROS is required for normal cellular function [21]. However, it is difficult to directly measure due to a short half-life and is quickly converted to other ROS, which makes studying the direct effects of superoxide difficult. However, its unique position as the progenitor for most cellular ROS, as indicated in figure 1.2, making it vitally important for cells to control its levels to regulate ROS levels as a whole. Once generated, superoxide can head in three main directions. The first direction is to either spontaneously or enzymatically dismutate as indicated in figure 1.2 [22]. This requires two superoxide molecules to form water and hydrogen peroxide. This hydrogen peroxide is another of the main ROS species, which will be discussed shortly. This reaction can occur spontaneously. However, the enzyme family superoxide dismutases,

Figure 1.1. The effect of cellular ROS levels on cell proliferation

The diagram indicates potential intracellular ROS levels in the red wedge and its effect on cell proliferation. Proteins known to modify cellular ROS are listed below the ROS wedge.

Figure from:

Schieber M. and Chandel N.S. ROS Function in Redox Signaling and Oxidative Stress. Current Biology. 2014; 24 (10): R453-R462.

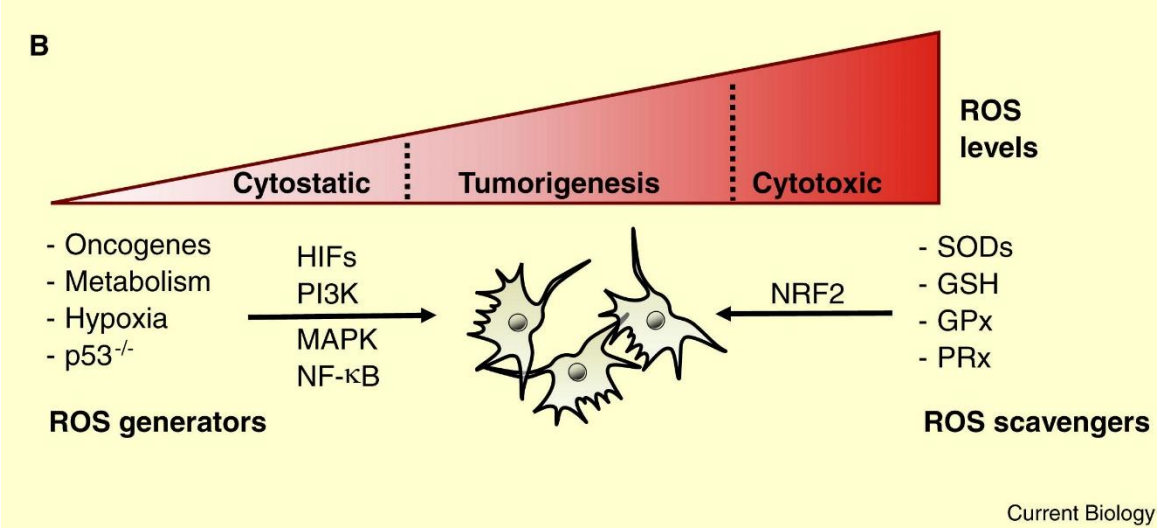
B
ROS levels
Cytostatic
Tumorigenesis
Cytotoxic
- Oncogenes
- Metabolism
- Hypoxia
- p53-/-
HIFs
PI3K
MAPK
NF-κB
NRF2
- SODs
- GSH
- GPx
- PRx
ROS generators
ROS scavengers
Current Biology

Figure 1.2. Interconnections between ROS and RNS

The diagram represents the interconnected nature of ROS and RNS with a main focus on superoxide (shown in red). It also highlights the main molecules shown to affect cellular signaling.

Figure from:

Wang Y., Branicky R., Noë A., Hekimi S. Superoxide dismutases: Dual roles in controlling ROS damage and regulating ROS signaling. Journal of Cell Biology. 2018; 217 (6): 1915-1928.

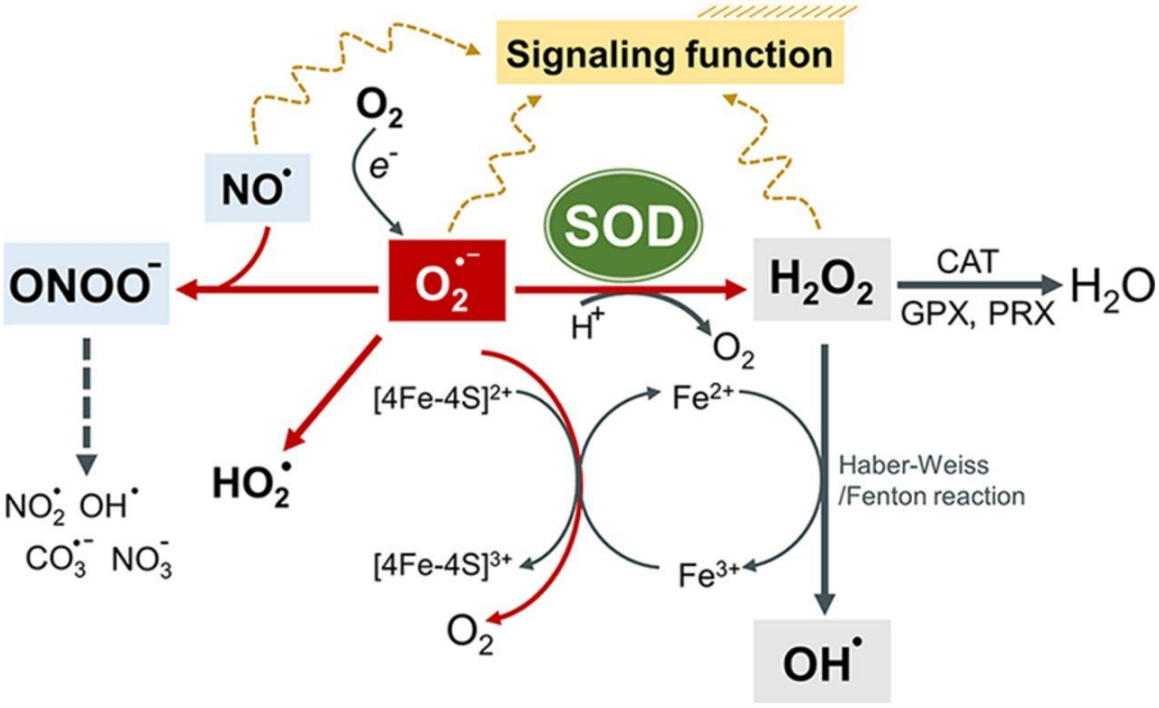
Signaling function
O_2
e^-
NO•
SOD
$ONOO^-$
$O_2^{\bullet -}$
H_2O_2
CAT
GPX, PRX
H_2O
H^+
O_2
$[4Fe\text{-}4S]^{2+}$
Fe^{2+}
$HO_2^•$
Haber-Weiss
/Fenton reaction
$NO_2^•$ $OH^•$
$CO_3^{•-}$ NO_3^-
$[4Fe\text{-}4S]^{3+}$
Fe^{3+}
O_2
OH•

or SODs, speed up this reaction to 2 x 10^9 $M^{-1}s^{-1}$, which is a diffusion-limited reaction that is ~10^4 faster than spontaneous dismutation [22]. This family of enzymes is vital to my research and will be discussed in more detail later in this dissertation. The second direction for superoxide is the forming the hydroxyl radical, one of the most reactive ROS, via the Haber-Weiss reaction (Figure 1.2). This reaction requires free transition metal ions, such as iron or copper, to act as a catalyst. This reaction rate is very slow (3 $M^{-1}s^{-1}$) making it unlikely to occur in biological systems [23]. The third direction for superoxide is to interact with nitric oxide to form peroxynitrite, which is a strong oxidant that can modify proteins via nitration of specific amino, like tyrosine, tryptophan, methionine, and cysteine [24]. This direction for superoxide is where the webs of ROS and RNS meet and add complexity to the situation, since nitric oxide and peroxynitrite are RNS. This reaction is also diffusion-limited with speeds at 6.7 x 10^9 $M^{-1}s^{-1}$ (Figure 1.2) [25]. The effect of these different directions for superoxide will become clear as each species of ROS and RNS have different effects and different targets, which unsurprisingly result in varying effects on cellular function.

Due to its negative charge, superoxide does not easily cross cellular membranes. This combined with the short half-life has led to idea that superoxide acts where it is produced. Thus, it is important to know any additional biological targets of superoxide. First, it can promote iron release from Fe-S cluster enzymes via oxidation or from the iron storing protein, ferritin, via reduction. This reaction occurs at a range of rates from 10^6 to 10^7 $M^{-1}s^{-1}$, depending on the exact Fe-S cluster enzyme [26]. The release of iron from these enzymes can further contribute to oxidative stress induced by superoxide as it is a required catalyst for the Haber-Weiss and Fenton reactions. Thus, unregulated levels of superoxide can lead to a cascade of even more reactive species, such as the hydroxyl radical. Secondly, superoxide can also directly oxidize thiols. However, the

exact rate of this reaction is disputed. The rate has been measured as high as > 10^5 $M^{-1}s^{-1}$ and as low as 15 $M^{-1}s^{-1}$ [27]. PTP1B, a common cellular protein tyrosine phosphatase, is oxidized by superoxide at a rate of 334 $M^{-1}s^{-1}$ for example [28]. However, this reaction speed is orders of magnitude slower that its reaction with nitric oxide, SOD enzymes, or Fe-S clusters. Thus, thiols are unlikely to outcompete these other superoxide sinks making thiol oxidation an unlikely reaction to occur inside cells. Additionally, the steady state levels of superoxide are in the range of 10^{-11} – 10^{-12} mol l^{-1} [29]. Therefore, it is hypothesized that while vitally important to control the levels of superoxide to regulate ROS levels, a different species may be the main culprit acting as a secondary messenger during cell signaling.

1.2.2 Hydrogen Peroxide

The most oft cited species responsible for acting as that secondary messenger is hydrogen peroxide. Hydrogen peroxide is one of the major products downstream of superoxide production. Also, like superoxide, there are enzymes (26 of them) that produce hydrogen peroxide [30]. However, hydrogen peroxide is usually produced as a by-product of these reactions not the main product like is seen with superoxide. Hydrogen peroxide is also 3 orders of magnitude more abundant than superoxide, as levels are estimated to be 10^{-9} – 10^{-7} M [29]. Hydrogen peroxide is also uncharged and can easily to diffuse across cellular membranes, especially through aquaporin channels [31]. Additionally, the cytosolic lifespan of H_2O_2 has been determined to be one millisecond, enabling diffusion from endogenous sources approximately 1 μm from its origin [32, 33]. In addition to its greater ability to diffuse across membranes, there is also a hydrogen peroxide gradient across the cell membrane as extracellular levels within the blood are ~ 1 – 5 μM [34]. Various studies have attempted to determine how step the

gradient is actually. The studies range from 7 to 5000 times as much extracellular hydrogen peroxide as intracellular [34]. Thus, removal of hydrogen peroxide from within the cell is likely a greater determent of cellular hydrogen peroxide levels than intracellular production. To further support this claim, cells *in vitro* treated with either a bolus or steady dose of exogenous hydrogen peroxide returned to steady state levels within 90 minutes of either treatment [35].

Within the cell, there are three main directions for hydrogen peroxide to go once produced. The first direction is to react with iron and superoxide in the Haber-Weiss reaction as mentioned above (Figure 1.2). The next direction is elimination of ROS by the cellular antioxidant network. These include scavenging through three different types of enzymes; glutathione peroxidases (Gpx), peroxiredoxin (Prx), and catalase (Figure 1.2). These reactions are quite quick with reaction rates ranging from 3×10^5 up to 6×10^7 $M^{-1}s^{-1}$ [36]. These enzymes will be examined more closely later in this dissertation. The other direction is reacting with low pKa thiols, typically found on reactive site cysteines within certain proteins. This occurs most commonly on protein tyrosine phosphatases, such as PTP1B and PTEN, which require an active site cysteine with a low pKa for their activity [37-40]. However, much like superoxide, the oxidation rate of PTPs ($10^1 – 10^3$ M^{-1} s^{-1}) is orders of magnitude slower than scavenging by enzymes [39, 40]. Therefore, PTPs are unlikely to outcompete hydrogen peroxide scavengers. Thus, it is currently unclear the exact mechanism that superoxide or hydrogen peroxide oxidize proteins within the cell. The effect of both hydrogen peroxide and superoxide on cellular signaling will be explained in section 1.2.4.

1.2.3 Reactive Nitrogen Species

Nitric oxide, $NO^{\bullet}$, generated by nitric oxide synthases (NOSs) plays an important role as neurotransmitter, in regulating vessel relaxation in endothelial cells, and in mediating neutrophil and macrophage functions. Since superoxide reacts at a diffusion-limit rate with $NO^{\bullet}$, oxidation of this $NO^{\bullet}$ into $ONOO^{-}$ can result in alterations of cellular function as well [41]. The actions of $NO^{\bullet}$ are mainly mediated through increasing cGMP-mediated signaling. The non-cGMP-dependent actions of $NO^{\bullet}$ are carried out mainly in three ways: (i) interaction with proteins containing transition metal, (ii) interaction with proteins, and (iii) modulation of cell signaling by forming S-nitrosothiol- (SNO) modification on proteins. $NO^{\bullet}$ has been shown to either facilitate cancer-promoting effects or act as an anti-cancer agent. Pro-tumor effects of $NO^{\bullet}$ were linked to the expression of $NO^{\bullet}$-producing enzymes in tumor progression [42]. While, anti-tumor effects were mediated by utilizing the immune defense mechanisms in animal models of various human cancers [43]. Recent evidence indicates that most of the cytotoxicity attributed to $NO^{\bullet}$ is rather due to $ONOO^{-}$, produced from the diffusion-controlled reaction between $NO^{\bullet}$ and superoxide anion. Peroxynitrite interacts with lipids, DNA, and proteins. These reactions result in cellular responses that vary from modulations of cell signaling to nitrosylative stress that triggers necrotic or apoptotic cell death [24]. In vivo, $ONOO^{-}$ generation has been implicated in many conditions such as stroke, chronic heart failure, diabetes, chronic inflammatory diseases, cancer, and neurodegenerative disorders [24]. Hence, novel pharmacological strategies aimed at removing $ONOO^{-}$ might represent powerful therapeutic tools in the future. EcSOD, in preserving bioavailability of $NO^{\bullet}$, is expected to have an indirect consequential effect in cancer through alterations of these $NO^{\bullet}/ONOO^{-}$ signaling. The seemingly paradoxical role of

$NO^{\bullet}$ in cancer has been quite extensively covered in other reviews [44] and is not discussed in detail here.

1.2.4 Role of Superoxide versus H_2O_2 Signaling in Oncogenesis

Deregulation of redox homeostasis has long been implicated in a variety of diseases and the role of ROS in oncogenesis remains an area of major interest. Nevertheless, ROS should not be considered as one single biochemical entity that has a single global effect in cancer. Rather, ROS function as cellular secondary messengers, with each reactive species orchestrating unique signaling events, in a temporal and spatial manner. Although H_2O_2 has been the main focus as the ROS-mediated signaling molecule, partly due to the conception that it is more stable and longer lived than superoxide, the insight starts to emerge that $O_2^{\bullet-}$ may also be an important mediator of cellular effects. This is further supported by the fact that most cells possess enzymatic systems that are capable of producing $O_2^{\bullet-}$, whereas to date no cellular system is known that exclusively generates H_2O_2 and not as a by-product of other reactions mentioned earlier [45].

Superoxide is believed to function as a signaling molecule in a distinct manner from those mediated by H_2O_2, $^{\bullet}OH$, and $ONOO^-$, although the mechanism is not fully understood. The name, superoxide is misleading in a sense that it is not a super-oxidant but a relatively moderate reductant. However, superoxide, being both a radical and an anion, can react with organic molecules by nucleophilic mechanism. Owing to this nucleophilic property, superoxide is able to rapidly deprotonize alcohols, phenols, and thiols, and hydrolyze esters as proposed [46]. By deprotonation of protein serine or threonine residues, superoxide is able to mediate phosphorylation of numerous proteins by protein kinases, thereby accelerating the rates of nucleophilic reaction between

kinases and phosphorylating proteins. For examples, superoxide has been shown to mediate the activation of many protein kinases including PKC, PKD (protein kinase D), PKB (Akt) (protein kinase B), and mitogen-activated (MAPK) kinases, p42/44, p38, and ERK [47-50]. Another important stimulus of enzymatic phosphorylation by superoxide signaling is via phosphatidylinositol 3-kinase activation, which subsequently activates PKB and MAPK [48, 51].

Furthermore, $O_2^{\bullet-}$ can promote protein phosphorylation by inhibiting dephosphorylation catalyzed by protein phosphatases. Superoxide affects both serine/threonine protein phosphatases (PPs) and protein tyrosine phosphatases (PTPs), by oxidizing the metal ion center of the former class of phosphatases and via nucleophilic attack of the cysteine residue in the later class [52, 53]. While H_2O_2 has also been demonstrated to inactivate PTPs, the rate of superoxide signaling is about 10-100 times higher than that of hydrogen peroxide signaling [54, 55]. In addition to being kinetically more efficient, $O_2^{\bullet-}$ is chemically more specific than H_2O_2 in this process as the catalytic site of PTP-1B is surrounded by positively charged residues [28]. Moreover, $O_2^{\bullet-}$-inactivated PTP-1B is more reversible than that of H_2O_2 since significantly more methionine residues are oxidized by H_2O_2. This provides an efficient fine-tuning ability of $O_2^{\bullet-}$ in regulating PTP-1B in signal transduction. This emphasizes an importance of $O_2^{\bullet-}$ signaling in many oncogenic signaling processes and the potential application of the specific superoxide inhibitors for their regulation.

It has long been recognized that low levels of $O_2^{\bullet-}$ and H_2O_2 are involved in proliferative signaling, partly via alterations in the activities of protein kinases and oxidative inactivation of phosphatases, as discussed earlier. Although these two major ROS are considered oncogenic ROS, there is strong evidence to support that these two ROS diverge in their roles in cellular survival/death pathways. Indeed, it is the ratio of

intracellular superoxide to H_2O_2 that could dictate the fate of cells as discussed in detail by Pervaiz and Clement [56]. A prominent increase in superoxide in the absence of cytotoxic levels of H_2O_2 supports cell survival and promotes oncogenesis by inhibiting activation of the pro-apoptotic pathway [57, 58]. In contrast, a rise in H_2O_2 levels with an accompanying decrease in superoxide facilitates apoptotic execution by activating caspase proteases [59, 60]. Superoxide, due to its specific anti-apoptotic effect in creating an environment conducive for cellular survival and proliferation in favor of oncogenesis, has been termed “Onco-ROS” [56]. However, competition between superoxide and hydrogen peroxide in cells might be more complicated.

1.3 Extracellular Superoxide Dismutase

1.3.1 Distribution and Function of the Three Sods in Mammalian Cells

One of the essential enzymatic components of the antioxidant defense system are the metal ion-dependent superoxide dismutases (SODs). There are three members of the SOD family present in mammalian physiology, with tightly regulated localization patterns. Of these, there are two copper/zinc containing members, CuZnSOD (SOD1) within the cytosol, mitochondrial inter membrane space, and nucleus, and EcSOD (*SOD3*) is the predominant antioxidant enzyme secreted into the extracellular space [61, 62]. The manganese-containing MnSOD (SOD2), localizes to the mitochondrial matrix, is the most divergent and displays minimal similarity to the other SODs, which share 60% homology around the catalytic and metal-binding domains [63]. All SOD family members require metal cofactors for catalyzing one-electron oxidation followed by one-electron reduction of two $O_2^{\bullet-}$ anions to affect disproportionation. Due to their distinct localizations,

and membrane impermeability of $O_2^{\bullet-}$, each member of the SOD family is expected to have specific compartmentalized roles, such as regulation of redox sensitive transcription factors [64], mitochondrial oxygen level sensing [65], or protection of surrounding tissue from oxidative inflammation during infection [66]. This implies SOD functions are non-redundant, despite having similar rate constants. Tumor suppressive effects of Cu/ZnSOD and MnSOD have been well described [67-69]. In this review, we will focus on EcSOD, its features and potential role in oncogenesis.

1.3.2 EcSOD Tissue-Specific Expression and Localization

While the other SODs are ubiquitously expressed, EcSOD is more restricted in a cell type and tissue dependent manner. EcSOD demonstrates high levels of protein expression within the cardiovascular endothelium, lungs, and placenta, displays moderately within kidney, pancreas and uterus, cartilage, skeletal muscle, adipose tissue, brain, and eye [62]. Abundantly secreted into the extracellular compartment, presence of EcSOD is detectable in milk, plasma, synovium, and lymph [61, 70]. Once secreted, EcSOD is bound to cell surface proteoglycans through its positively charged heparin-binding domain (HBD). A portion of secreted EcSOD is subjected to intracellular proteolytic cleavage removing the HBD, which precludes tethering to the cell surface, and facilitates distribution in the extracellular milieu and circulation [71, 72]. The secreted full length enzyme has been observed to be taken up by cells via endocytosis, facilitated by surface binding to proteoglycans and internalized through clathrin-coated pits [73]. In addition, EcSOD has been detected in nuclei associated with chromatin [74, 75], and trafficking through the endo-lysosome system has been suggested [73-75]. Thus, although EcSOD, as the name implies, mainly resides in the extracellular space this enzyme has other intracellular localizations.

1.3.3 Molecular Characteristics: EcSOD

The monomeric subunit of human EcSOD is synthesized as a 32 kDa monomeric protein that exhibits higher order dimers, tetramers and octamers cross-linked through disulfide bridges between cysteine residues in the C-terminal region [76-79]. A 240 amino acid propeptide contains a signal peptide on the N-terminal required for secretion and is cleaved to generate a 222 amino acid protein making up the mature form [80] (Figure 1.3). Mature EcSOD can be separated into 3 regions, the amino-terminal features an asparagine at position 89 revealed by mass spectrometry to be a singular glycosylated residue greatly enhancing protein solubility and has been demonstrated as required for secretion but not activity [81-83]. The second domain bears 60% homology to CuZnSOD and contains the conserved active site and ion binding folds for the singular copper and zinc ions required for catalysis [84, 85]. EcSOD is remarkably stable and resistant to extreme temperature, pH, urea and guanidinium chloride concentrations [84].

1.3.3.1 Heparin Binding Domain

The third domain is unique to EcSOD and tethers it to the surface glycocalyx with high affinity, via a cleavable C-terminal heparin-binding domain (HBD). The HBD comprises a cluster of positively-charged arginine and lysine residues (SERKKRRR) which associates electrostatically with proteoglycans, notably heparin but also collagen type I and fibulin-5, on endothelial surfaces and tissue matrix, where it protects against oxidative fragmentation [80, 86-88]. Intracellular proteolytic cleavage by a furin-like protease followed by carboxypeptidase activity within the HBD is expected to account for

Figure 1.3. Schematic illustration of human EcSOD protein structure

The 240 amino acid pro-peptide features an N-terminal signal peptide (green) cleaved to generate the 222 amino acid matured protein. Asparagine 89 is depicted as the singular glycosylated residue. The C-terminal heparin binding domain is depicted (blue).

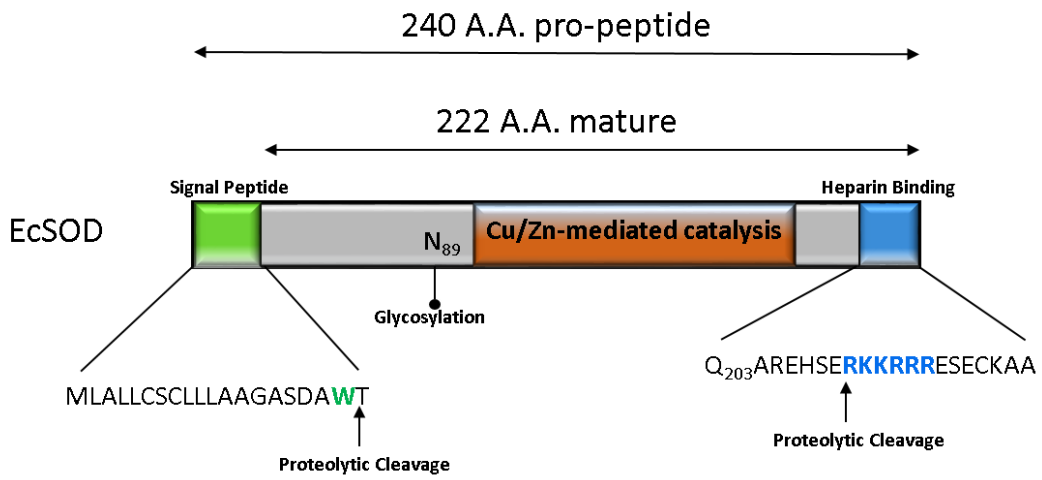
240 A.A. pro-peptide
222 A.A. mature
Signal Peptide
Heparin Binding
EcSOD
N89
Cu/Zn-mediated catalysis
Glycosylation
MLALLCSCLLLAAGASDAWT
Proteolytic Cleavage
Q203AREHSERKKRRRESECKAA
Proteolytic Cleavage

release of EcSOD into plasma and fluids [71, 89, 90]. Secreted distribution of hetero-oligomers possess a range of binding affinities and enzymatic activity. Tetramers separate into three fractions entirely with or without the HBD, or as a mixture of intact and truncated monomers [71, 72, 82, 91]. Secretion of both full length and truncated forms of EcSOD with varying degrees of heparin affinity allows for differential tissue distribution in regulating specific protection from ROS [91]. Endothelial cells prominently feature EcSOD bound to the surface, do not synthesize the protein on their own, and acquire secreted EcSOD from vascular smooth muscle cells [92]. The positively charged HBD resembles a nuclear localization signal. Heparin binding not only enables $O_2^{\bullet -}$ scavenging on cell surfaces and where EcSOD is tethered, but also mediates endocytosis [75]. Internalized EcSOD has been observed to be associated with lysosomes, suggesting a possible degradation pathway. This HBD-mediated endocytosis has also been linked to localization of EcSOD to the nucleus [74, 75]. The EcSOD crystal structure has been solved at a resolution of 1.7 angstroms. The overall tetramer is held together by disulfide bonds positioned towards the N-terminal, and uniquely features two grooves (‘major’ and ‘minor’) at polar ends, a result of dimeric organization [93]. Molecular modeling indicates the major groove accommodates binding of the heparin molecule some distance from the active site, consistent with previous reports that enzymatic activity is not inhibited while retained at the cell surface [86]. While missing from the overall structure, the C-terminal HBD is expected to be located along the top of this major groove to facilitate heparin binding, a conformational change ‘locking’ heparin into place protects EcSOD from proteolysis [94]. The minor groove on the reverse face is proposed to interact with collagen and involves electrostatic interaction with the C-terminus.

A naturally occurring polymorphism at arginine 213 (R213G) located in the HBD impairs heparin binding, increasing the concentration of EcSOD released into plasma. This results in no overt clinical phenotype, and does not appear to affect its intracellular distribution [95, 96]. Interestingly, this renders EcSOD resistant to trypsin-like proteases [97]. The R213G polymorphism also confers resistance to furin protease activity, promoting secretion of an active, full-length molecule unable to bind heparin [90]. Full length EcSOD has a significantly longer tissue half-life than the truncated and released form (85 versus 7 hours respectively), while the HBD-null form shows less clearance by the liver due to its reduced ability to be endocytosed [98].

In diabetic patients, elevated blood glucose promotes non-enzymatic glycation products of EcSOD disrupting heparin binding but not catalytic activity [99, 100]. While the R213G polymorphism has not been directly linked to diabetic susceptibility, diabetic patients on hemodialysis exhibit increased risk of ischemic complications of the cardiovascular system due to diminished EcSOD protection when absent from the surface endothelium [101, 102]. Presence of R213G correlates with decline in lung function and susceptibility to chronic obstructive pulmonary disease [103]. Controversially, other studies have suggested a protective role, the polymorphism being more common among smokers resistant to COPD development [104].

Development of therapeutic intervention strategies for ameliorating the negative effects of oxidative stress have produced both pharmacological and gene therapy based approaches for preventing tissue injury in disease models [105, 106]. SODs have shown promise as treatment in the laboratory, yet clinical efforts are stymied by source purification, clearance rate, and distribution [107-109]. To circumvent these challenges, a chimeric fusion of MnSOD with the EcSOD HBD, designed to promote its cellular internalization, successfully prevented vascular edema in two models of inflammation

[109]. The highly basic residues of the HBD domain of EcSOD that form a predominantly helical structure is similar to the features described for cell penetrating peptides (CPPs), such as the HIV transactivator protein (TAT) and other experimental CPPs [110, 111]. This unique domain of EcSOD has been demonstrated to possess efficacy as a CPP, where synthetic peptide corresponding to this region translocates into the cytoplasm and nucleus when added exogenously [111]. When this peptide is linked with apoptin (chicken anemia virus-derived protein), the recombinant apoptin-HBD fusion protein exhibited a significant and specific anti-tumor effect versus the apoptin protein alone, in the Lewis Lung carcinoma model in mice [111]. Although the uptake mechanism and intracellular fate of this highly basic EcSOD HBD peptide is not clear at this point, EcSOD HBD exhibits potential clinical application as a delivery tool to translocate cargo molecules into cells.

1.3.3.2 Catalytic Domain and Reaction Mechanism

EcSOD scavenges $O_2^{\bullet-}$ through the catalyzed dismutation of two molecules of $O_2^{\bullet-}$ to bimolecular oxygen and H_2O_2, which is subsequently reduced to water by catalase, peroxiredoxins and other enzymes [112]. EcSOD requires a redox-active $Cu^{1+/2+}$ ion at its active site. Three histidine residues anchor the catalytic copper in place. One of these, the “bridging histidine”, also ligates the zinc ion, which itself requires an aspartic acid and additional electrostatic contributions from three separate histidines. The zinc ion is not required for catalytic activity, but facilitates protonation between the bridging histidine and confers thermal stability [113]. Electrostatic guidance of $O_2^{\bullet-}$ into the positively-charged catalytic active site requires Lys134 and Glu131 for approach from longer-range, and Arg141 for a more local orienting effect [114].

Superoxide disproportionation occurs by a ping-pong mechanism which proceeds in two steps. Step one begins as the $O_2^{\bullet-}$ substrate binds to copper^{2+}. Superoxide anion donates an electron to become molecular oxygen, in the process reducing copper^{2+} to copper^{1+}. The bond between copper and its anchoring histidine is broken, and histidine becomes protonated. In step two, this proton is donated along with the electron from copper^{1+} to a second $O_2^{\bullet-}$ anion, forming H_2O_2, and copper^{2+} reforms its histidine bond [115]. A transfer of one electron from $O_2^{\bullet-}$ to copper reduces the oxidized copper ion. The reduced copper is oxidized, donating an electron to a second $O_2^{\bullet-}$ anion at rates close to diffusion limits [116]. The overall stoichiometry results in formation of molecular oxygen and H_2O_2 from two $O_2^{\bullet-}$ molecules. The remarkable structure of SODs have pioneered mechanistic studies of 'electrostatic guidance', described in intricate detail within an excellent review [117].

1. $Cu^{2+}ZnSOD + O_2^{\bullet-} \rightarrow Cu^{+}ZnSOD + O_2$
2. $Cu^{+}ZnSOD + O_2^{\bullet-} + 2H^{+} \rightarrow Cu^{2+}ZnSOD + H_2O_2$

Despite abundant documentation on SODs as anti-oxidants, a theme suggesting a pro-oxidant role is also coming into focus, with generation of H_2O_2 suggested to account for deleterious effects seen in some SOD overexpression systems [118]. In consideration, dismutation, spontaneous or catalyzed, yields identical amounts of H_2O_2, though with significantly different kinetics. In single-celled *E.coli*, endogenous SOD expression levels conferred 95% protection from $O_2^{\bullet-}$ induced damage to sensitive targets, this suggests the effects of SOD overexpression on H_2O_2 production should be negligible as $O_2^{\bullet-}$ concentrations would already be limited [118, 119]. This however does not account for the rapidity of H_2O_2 formation or subcellularly localized bursts of increased H_2O_2 concentration. Such phenomena arguably would result from the

presence of NADPH oxidase (NOX) enzymes not found in prokaryotic organisms, having made their first appearance later in evolution and function as compartmentalized producers of $O_2^{\bullet-}$ [120]. Whether SODs have pro-oxidant effects is likely to remain a conflicting issue. It is critical to know the answer to this antioxidant conundrum as there is accumulating evidence to support divergent effects on cell proliferation and death signaling for the two major intracellular ROS, $O_2^{\bullet-}$ and H_2O_2, as discussed in a later section. In addition to scavenging $O_2^{\bullet-}$, SODs exhibit less efficient, non-specific peroxidase activity [121-124]. Here, the Cu/Zn-containing enzymes require CO_2, ultimately generating a diffusible carbonate radical. This in turn disables the enzyme and thus the peroxidase action of both CuZnSOD and EcSOD functions as a 'suicide reaction' [121-124]. Determination of the precise mechanism has been notably contentious, and it remains to be seen whether SOD peroxidase activity is significant within living organisms, or can occur at physiological concentrations of H_2O_2 [118, 125].

1.3.4 EcSOD as a Primary Defense Against Other ROS and RNS

The primary function of EcSOD is a superoxide scavenger, as the name implies. However, its redox modulation effect is not limited to controlling the levels of this radical. Superoxide is a precursor of many ROS and RNS as described [126]. By suppressing the accumulation of superoxide, EcSOD also prevents spontaneous dismutation of superoxide into H_2O_2. Generation of $^{\bullet}OH$ via Fenton reaction and Harber Weiss reaction, can also be inhibited by EcSOD. Furthermore, by preventing the superoxide-mediated oxidation of $NO^{\bullet}$, EcSOD also controls the formation of $ONOO^-$, which as discussed earlier plays a significant role in the pathogenesis of diseases, such as stroke, myocardial infarction, chronic heart failure, diabetes, circulatory shock, chronic inflammatory diseases, cancer, and neurodegenerative disorders.

1.3.5 Gene Regulation and Transcription

Human *SOD3* is located on chromosome 4p with approximately 5.9 kilobase pairs, and contains two exons and one intron [127]. The entirety of the 722 bp coding region is within exon 2. The promoter contains two CAAT-box elements but is without a TATA promoter sequence [127]. Features in common with the other two SOD family members include antioxidant response elements (ARE), AP-1 and AP-2 binding sites, and NF-κB motifs. A more recent study of EcSOD transcriptional regulation that looked at tissue-specific expression in the mouse revealed a repressor role for myeloid zinc finger 1 and Krüppel-like transcription factors, whereas Ets family members, Elf-1 and GA-binding protein α and β, were transcriptional activators [128]. The farnesoid x receptor was found to bind an inverted repeat, IR-1 element promoting transcription [129].

Various growth factors, cytokines and ions likely play a role in transcriptional control of EcSOD mRNA expression. EcSOD was reportedly induced in response to interferon-γ and IL-4, but downregulated by TNF-α [130]. Rat brain astrocytes were protected from H_2O_2 by purinergic receptor agonists, which increased expression of both MnSOD and EcSOD, an effect likely dependent on intracellular calcium ion, cyclic AMP and PKA activity [131]. Leukemia inhibitor factor increases EcSOD expression and activity in brain tissue, protecting neurons from ischemic damage [132]. Exendin-4, a glucagon-like peptide-1 receptor agonist, induced the expression of EcSOD through epigenetic regulation at its proximal promoter by influencing the acetylation of histone H3 [133]. Lastly, the presence of metal ions bear influence on modulating EcSOD expression. Dietary copper/zinc levels [134, 135] influence EcSOD levels, and the intrinsic transcriptional activity of copper chaperone Atox1, can be stimulated to

translocate to the nucleus and bind a response element in the EcSOD promoter [136]. Unexpectedly, the application of various oxidizing conditions reduced EcSOD expression levels, although these results may be confounded by general toxicity [137].

1.3.6 *SOD3* KO Models

Whole body EcSOD null mice are born at Mendelian ratios, are fertile, appear to develop normally, and adult mice are healthy to 14 months of age [138]. Other antioxidant genes (catalase, glutathione peroxidase, glutathione reductase, glucose-6-phosphate dehydrogenase), were also reported as unchanged. Common hematological markers reported as normal. Significantly, *SOD3*$^{-/-}$ mice were more susceptible to oxidative stress resulting from hyperoxic exposure, with considerably diminished survival rates to wild type counterparts. When exposed to hyperoxic conditions whole body KO mice developed severe and sudden, inflammatory pulmonary edema, with enhanced neutrophil recruitment, signs of intra-alveolar hemorrhage, vascular congestion and thickening of alveolar septa. The expression levels of the other two SOD family members were examined, but no compensatory changes were observed. Moreover, a double knockout model for both *SOD1* and *SOD3* reported mild phenotypes, suggesting limited or no functional redundancy exists between these two family members [139].

Whole body KO mice do not have increased tumor incidence. Possibly, these conditions are not ideal to study the role of EcSOD in tumorigenesis. In dramatic contrast to the whole body knockout, an inducible deletion of EcSOD in adult mice exhibited an 85% mortality rate in ambient air conditions, 3-7 days after tamoxifen injection, and demonstrated severe respiratory distress, highlighting the critical role of EcSOD at the oxygen interface in the lungs [140]. This suggests that animals with an embryonic deletion of EcSOD have compensated/adapted, and will not demonstrate

accurate phenotypic identities as reflected upon deletion in adult mice. While the whole body KO model suggests loss of EcSOD expression alone is not an initiating factor in inducing tumorigenesis, reduced function of this antioxidant will likely contribute to oncogenesis as demonstrated by numerous studies further discussed in the following.

1.3.7 Expression Levels and Effects of EcSOD in Cancers

Oncomine analysis of neoplastic versus normal tissues showed that EcSOD (or *SOD3*) expression levels were significantly down-regulated across a majority of cancers including breast cancer, head and neck cancer, lung cancer, and sarcoma (Figure 1.4), suggesting that loss of EcSOD could contributes to oncogenesis. Amongst the Oncomine datasets, the breast cancer category shows the highest number of analyses that met the threshold, where 18 out of 53 analyses in 5 out of 14 breast cancer datasets met the thresholds for *P*-value < 0.01 and changes in EcSOD expression is scored in the top 10% of gene rank for most significantly under-expressed genes. Specific studies examining the expression level and function of EcSOD in various cancers are further discussed in the following.

1.3.7.1 Breast Cancer

In breast cancer cells, overexpression of EcSOD inhibited *in vitro* proliferation, clonogenic survival, and invasion of a triple negative breast cancer cell line partly via suppressing heparanase-mediated fragmentation of cell surface proteoglycans and by reducing VEGF bioavailability [141]. Overexpression of EcSOD also significantly inhibited tumor metastasis in both an experimental lung and a spontaneous metastasis mouse model [142], further suggesting a role for this extracellular enzyme as in

Figure 1.4. Oncomine gene analysis of SOD1-3 in solid cancers versus normal counterparts.

Oncomine gene summary view comparing the number of datasets that had significant changes in mRNA expression for EcSOD (*SOD3*), CuZnSOD (SOD2), and MnSOD (SOD2) in cancer versus normal tissues. Thresholds were set for P<0.01 and top 10% score in gene rank for most significantly changed genes. Blue boxes indicate downregulation and red represents upregulation. Number in each box shows the number of analyses that met the thresholds.

Analysis Type by Cancer	Cancer vs. Normal SOD3		Cancer vs. Normal SOD1		Cancer vs. Normal SOD2	
Bladder Cancer		5				2
Brain and CNS Cancer		3	2	8	9	2
Breast Cancer		18	7	1	2	9
Cervical Cancer		4			5	1
Colorectal Cancer	2	4		2	12	
Esophageal Cancer	1	1			1	1
Gastric Cancer		5		5	6	
Head and Neck Cancer		13	3		13	1
Kidney Cancer		6	1	4	10	1
Leukemia	1	1	4	2	2	10
Liver Cancer	2			2	1	3
Lung Cancer		12				3
Lymphoma	7		10		14	
Melanoma	1	2	1		1	1
Myeloma			5			1
Other Cancer		14	2	1	5	1
Ovarian Cancer	1	2		3	3	
Pancreatic Cancer		2	3	1	1	2
Prostate Cancer		5	1	1	1	4
Sarcoma	1	6		1	2	1
Significant Unique Analyses	16	102	39	31	86	43
Total Unique Analyses	436		455		455	

suppressing tumor progression. Concurrently, in a normal mammary epithelial cell line, siRNA-mediated knockdown of EcSOD promoted clonogenic capacity, tumorsphere formation, and wound healing in MCF10A cells [143]. In addition to the Oncomine analysis showing a prominent down-regulation of EcSOD expression in breast carcinomas, an inverse correlation between the mRNA expression levels of EcSOD and breast cancer stage has been reported [142, 144]. Immunohistochemistry data also show a significant decrease in EcSOD protein expression in both ductal carcinoma in situ and invasive breast carcinoma compared to normal tissue [142], further suggesting that loss of EcSOD provides a selective advantage in cancer cells. In contrast to the tumor suppressive role, EcSOD may be an important mediator in VEGF-C-promoted oncogenesis. Expression levels of EcSOD were found to be down-regulated when VEGF-C is knocked down in claudin-low breast cancers, and EcSOD was partly required for VEGF-C-mediated cell survival in response to oxidative stress and for VEGF-C-mediated metastasis [145]. This apparent discrepancy in the role of EcSOD in breast cancer hints at the complexity of redox-mediated cellular processes. It should be emphasized that these experiments were performed in a single murine mammary carcinoma cell line that constitutively expressed EcSOD. Since EcSOD expression is downregulated or absent in the majority of human breast cancer cases, the relevance of these studies with respect to the role of EcSOD in human breast cancer progression remain unclear.

Interesting, long-term estradiol stimulation resulted in significantly downregulated EcSOD in normal mammary epithelial cells, and in tumors derived from the ACI rat model of breast cancer [143, 146, 147]. The exact mechanism involved in the estrogen-mediated loss of EcSOD is not clear. The induction of neoplastic transformation by estrogen can be mediated through non-receptor alpha regulated mechanisms, via a

direct genotoxic effect. Russo *et al* [148] found that loss of chromosome 4 is associated with a tumorigenic phenotype by using an *in vitro* transformation model of normal mammary epithelial cells treated with 17-beta estradiol to elucidate a sequence of chromosomal changes correlating with specific stages of neoplastic progression. The authors implicated *Slit2* as a candidate tumor suppressor located at 4p15.2 that was silenced in the estrogen-induced tumors. However, considering the fact that the EcSOD gene or *SOD3* is also located in the chromosome 4p15.2 region, it is tempting to speculate that re-expression of EcSOD in their C5 cells (tumorigenic cell line derived from estrogen treated MCF10A cells) would inhibit tumorigenicity. Chromosome 4p15.1-15.3 is one of the most commonly deleted region (57%) reported in breast cancer [149], which would deplete expression of EcSOD in these cancers.

Loss of EcSOD expression, in addition to having a tumor promoting effect, also contributes to tumor recurrence and poor patient outcome. Local relapse remains a significant issue for breast cancer patients who have undergone breast conserving surgery [150]. In a murine 4T1 cytoreductive surgery model study aimed at identifying mechanisms driving local recurrence, EcSOD was found to be one of the top 40 genes underexpressed in the recurrent tumors versus primary tumors (fold change = 4.8) [151]. The recurrent tumors grew at a significantly accelerated rate compared to controls, suggesting that down-regulation of EcSOD is one of the contributing factors leading to tumor aggressiveness. More significantly, low expression levels of EcSOD are associated with reduced relapse-free survival in multiple subtypes of breast cancer. An integrative microarray data analysis using the Kaplan Meier Plotter [152] shows that low EcSOD expression is associated with significantly reduced relapse free survival in all breast cancers, as well as in Luminal A (ER+ and/or PR+, Her2−), Luminal B (ER+ and/or PR+, Her2+), Her2+, or basal-like (ER−, PR−, Her2−, CK 5/6+, and/or EGFR+)

breast cancers (Figure 1.5). More profound changes in the hazard ratio (HR) for the association are seen when restriction was set to exclude untreated patients (systemic therapies) in the analysis (right panel). Taken together, all of the evidence discussed here underscores the importance of *EcSOD* as a potential tumor suppressor gene, inhibiting the progression of malignant phenotype in human breast cancer.

1.3.7.2 Lung Cancer

Despite the protective role of EcSOD in normal lung function, relatively little information describes its role in lung cancer. EcSOD expression is significantly down-regulated in primary human lung cancer compared to normal lung tissue, with further reduction occurring between stages I and IV [153-155]. Overexpression of this extracellular enzyme in lung cancer cells reduced clonogenic survival and invasion via inhibition of NF-κB activation [153, 156], suggesting a tumor suppressive role of EcSOD in lung cancer. EcSOD may also play a role in gemcitabine resistance, as it is was identified amongst the gene set that was found to be upregulated in resistant non-small cell lung cancer cell lines [157]. However, it is not known if EcSOD directly confers resistance of cells against gemcitabine or upregulation of this gene is merely an indirect response to the cytotoxic effects of gemcitabine. In summation, EcSOD likely functions as a tumor suppressor and further investigation of its direct involvement in mediating sensitivity to gemcitabine would help to shed light on its role in drug resistance in lung cancer.

1.3.7.3 Prostate Cancer

Confirming Oncomine analysis, IHC studies of prostate tissue revealed a significant reduction of EcSOD expression in cancer tissue compared to the normal

Figure 1.5. Analysis of breast cancer data by Kaplan-Meier Plotter stratifying patient outcomes based on EcSOD expression in breast cancer subtypes

Kaplan-Meier plots (http://kmplot.com) show that low EcSOD expression is significantly associated with poor outcome (relapse free survival, RFS) in all types of breast cancer examined. Left panel shows analyses performed on all patients regardless of treatments while systemically untreated patients were excluded in analyses shown on the right. In red, patients with expression above the median and in black, patients with expressions below the median. The numbers of samples in each group are indicated in parentheses, and the hazard ratios (HR) and log rank p values are shown. Gene expression data and survival information are downloaded from GEO (Affymetrix HGU133A and HGU133+2 microarrays), EGA and TCGA.

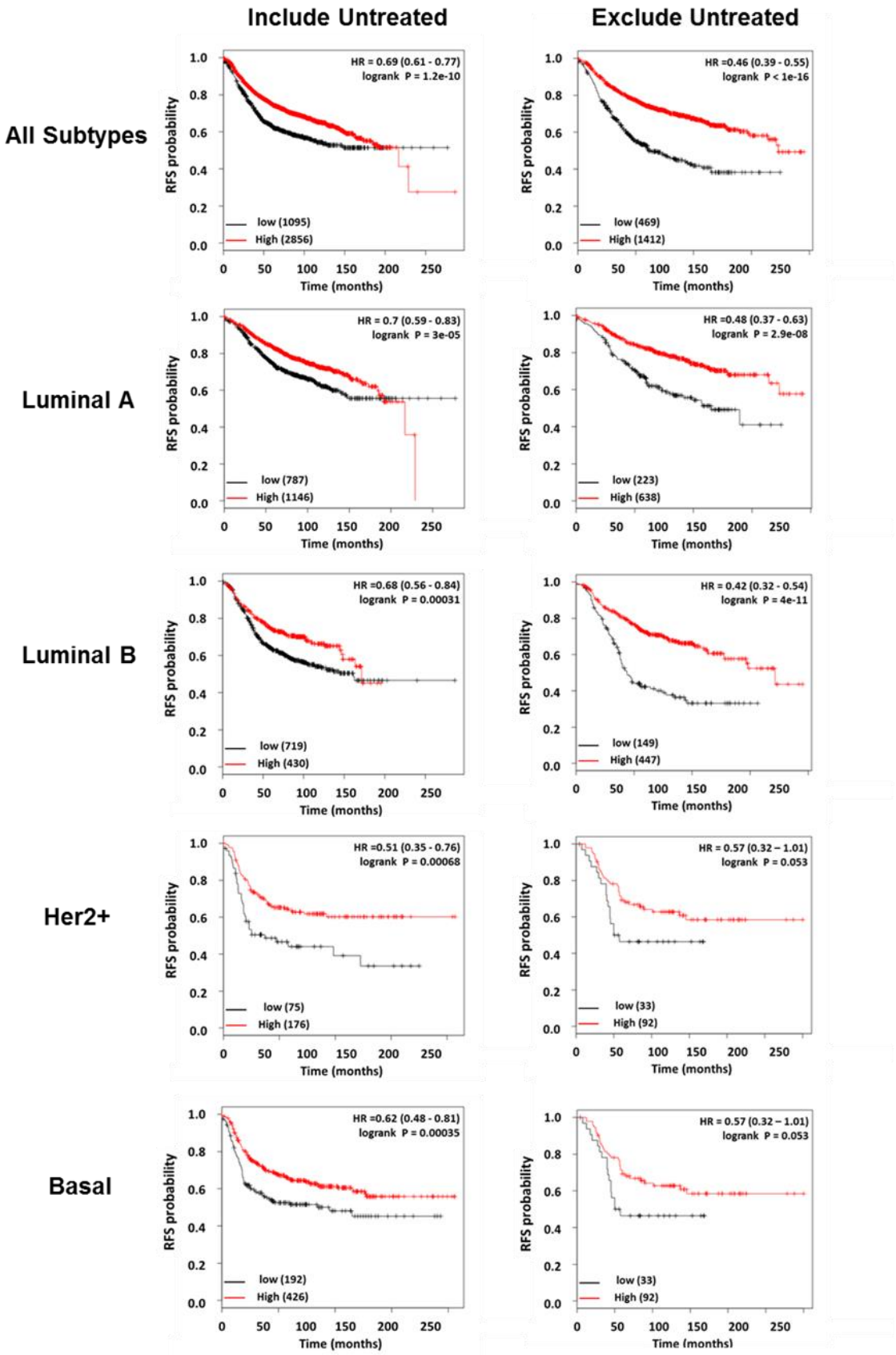
Include Untreated
Exclude Untreated
All Subtypes
HR = 0.69 (0.61 - 0.77)
logrank P = 1.2e-10
low (1095)
High (2856)
HR =0.46 (0.39 - 0.55)
logrank P < 1e-16
low (469)
High (1412)
Luminal A
HR = 0.7 (0.59 - 0.83)
logrank P = 3e-05
low (787)
High (1146)
HR =0.48 (0.37 - 0.63)
logrank P = 2.9e-08
low (223)
High (638)
Luminal B
HR =0.68 (0.56 - 0.84)
logrank P = 0.00031
low (719)
High (430)
HR = 0.42 (0.32 - 0.54)
logrank P = 4e-11
low (149)
High (447)
Her2+
HR =0.51 (0.35 - 0.76)
logrank P = 0.00068
low (75)
High (176)
HR = 0.57 (0.32 – 1.01)
logrank P = 0.053
low (33)
High (92)
Basal
HR =0.62 (0.48 - 0.81)
logrank P = 0.00035
low (192)
High (426)
HR = 0.57 (0.32 – 1.01)
logrank P = 0.053
low (33)
High (92)
RFS probability
Time (months)

counterparts [158]. Additionally, EcSOD levels and activity significantly decreased between high and intermediate grade prostate carcinomas, as well as in prostate cancer cell lines compared to normal prostate epithelial cells [159]. Migration and cell growth was also inhibited in a dose-dependent manner by overexpression of EcSOD or addition of recombinant human EcSOD [158]. The authors further showed that the inhibitory effects of EcSOD are due to reduced MMP2/MMP9 expression and activity, as well as increased H_2O_2 production. Other groups have since further correlated EcSOD expression with reduction of MMP2 activity and invasion in prostate cancer [159, 160]. These studies highlight the role of this secreted antioxidant in regulating key extracellular enzymatic activities that promote invasion and metastasis.

1.3.7.4 Pancreatic Cancer

EcSOD mRNA expression and IHC analysis reveal significantly decreased levels of EcSOD in tumor tissue compared to normal pancreatic ductal epithelium in paired and unpaired samples [161]. EcSOD loss is associated with a reduction in mean survival from 11.0 to 6.5 months in patients with pancreatic adenocarcinoma [161]. EcSOD over-expression inhibits *in vitro* cell proliferation, invasion, and clonogenic capacity of pancreatic cancer cells in a dose-dependent manner [161-163]. Furthermore, both transient and stable over-expression of EcSOD inhibited primary tumor growth and increased survival in tumor xenograft models [161-163]. EcSOD was also found to decrease levels of VEGF and HIF-1α protein levels in pancreatic cancer cell lines [162, 163]. Since HIF-1α and VEGF promote angiogenesis, EcSOD is likely inhibitory, restricting blood flow to the tumor. However, EcSOD may also promote survival of quiescent pancreatic cancer cells as revealed by Deng *et al* [164] where they showed that Mirk/Dyrk1B kinase maintains the viability of quiescent pancreatic cancer cells by

upregulation of both CuZnSOD and EcSOD thereby lowering ROS levels in quiescent SU86.86 and Panc1 cells.

1.3.7.5 Thyroid Cancer

Expression levels of EcSOD have been shown to be slightly increased in a benign thyroid tumor goiter model but gradually downregulated in cell lines that model advanced papillary and anaplastic thyroid cancers correlating with the level of Ras oncogene activation [165, 166]. Although growth promoting effects of EcSOD at lower levels have been shown in a thyroid cancer cell line, PCCL3 [167, 168], inhibitory effects of this antioxidant in cells harboring p53 mutations resulted in reductions in cell growth, invasion, and soft agar colony formation [169, 170]. Thus, EcSOD may have biphasic effects on tumor progression switching from a tumor promoter during tumorigenesis to a tumor suppresser shortly after transformation. The authors further implied that disparate effects seen with EcSOD overexpression are due to the dose-dependent responses. Interestingly, high levels of EcSOD, although inhibited cellular proliferation were found to promote phosphorylation of various receptor tyrosine and non-receptor tyrosine kinases such as EGFR, ERBB2, and FLT-3 [166, 169]. Propagation of cellular signaling was halted due to inhibition of small GTPases, (Ras, Rac, Rho, and CDC42), thereby decreasing activation of downstream effectors MEK and Erk [166, 169]. Thus, EcSOD overexpression can promote cell cycle arrest and apoptosis via activation of p53 and reduce cell growth via promoting inactivation of GTPases. Intriguingly, secretion of EcSOD in the tumor stroma by mesenchymal stem cells (MSCs) increased the growth of thyroid cancer cells in co-culture models despite having an inhibitory effect on their migration (106). Further studies are needed to assess the extent and role of stromal-derived EcSOD versus cancer cell-expressed EcSOD in thyroid cancer.

1.3.7.6 Melanoma

Overexpression of EcSOD showed a prominent inhibitory effect in melanomas. Inhibition of cell proliferation by IFNγ was mediated through increased expression of EcSOD [171]. Moreover, muscle cell-mediated EcSOD secretion inhibited the growth of B16 melanoma in mice via a decrease in VEGF expression [172]. Similarly, EcSOD overexpressing transgenic mice demonstrated reduced growth of metastatic cancer cells despite no effect on infiltration to the lungs after tail vein injection [171]. In a DMPA/TPA-induced skin carcinogenic model, skin-specific EcSOD transgenic mice showed half the number of tumors compared with the nontransgenic mice by reducing DNA damage associated with the carcinogens [173]. A metabolomics and transcriptomics analysis however, revealed EcSOD as one of the upregulated genes in tumors recovering from chemotherapy treatment [174]. This is likely due to the severe oxidative stress in both localized chemotherapy-treated and bystander tumors as suggested by the authors. Overall, EcSOD has a clear anti-proliferative and anti-tumor role in melanoma.

1.3.7.7 Additional Cancers

In addition to the cancer models described above, EcSOD expression is also decreased in colorectal cancer compared to paired normal controls [175]. In a liver cancer study, expression of EcSOD was increased by Farnesoid X receptor activity, which by inhibiting JNK activation, inhibited liver carcinogenesis, providing indirect evidence of the tumor suppressive role of EcSOD [129]. In renal cell carcinoma tissues, higher EcSOD expression correlated significantly with higher levels of apoptosis, as indicated by TUNEL staining [176]. Although down-regulation of EcSOD is reported in a

majority of cancers, serum levels of EcSOD were observed to be increased in patients with gastric adenocarcinoma and prolactinoma, a benign pituitary gland tumor, compared to healthy controls [177, 178]. However, the cause or role of increased serum EcSOD in either case remains unclear.

Other studies further indicate a potential role of EcSOD in therapy response and tumorigenesis. EcSOD expression can promote inhibition of radiation induced lung damage, such as myofibroblast expansion, oxidative stress, and fibrosis, via injection of mesenchymal stromal cells [179]. Additionally, EcSOD may play a role in obesity induced tumorigenesis, as EcSOD gene transfer in mice inhibited high fat diet-induced obesity and fatty liver [180]. It also reduced pro-inflammatory crowns, which are formed by the recruitment of macrophages to hypertrophic and necrotic adipose cells [180]. Both obesity and crown-like structures are associated with increased risk of breast cancer [181, 182]. These studies highlight the potential role of EcSOD in protecting healthy tissue from chronic inflammation and reducing the risk of cancer.

1.3.8 Plasma EcSOD in Cancer

Since EcSOD is a secreted protein, whether there is any correlations between the plasma levels of this antioxidant with cancer progression are of a high interest. Numerous studies have assessed the activity of serum/plasma SOD in cancer patients versus the normal patients but the results are controversial and largely inconclusive. For example, in breast cancer studies, plasma SOD activity has been found to be lower in patients with malignancy in comparison with the control group [183-185], while a reverse observation was reported showing higher SOD activities in patients with breast cancer versus the control patients [186-188]. Similar opposing results were also reported for prostate cancer [189, 190]. Importantly, these studies relied on commercially available

SOD activity kit assays which do not discern the 3 distinct forms of SODs. Specific activity of EcSOD can be further differentiated from the total SOD activities by including a Concanavalin A–based purification step. However, since Concanavalin A only binds to the full length ECSOD, this will exclude the detection of the truncated form of EcSOD, and therefore may not be a reliable method to account for the total EcSOD activity levels. Nevertheless, since circulating levels of EcSOD could be contributed by other tissues and organs, assessing plasma levels of this antioxidant is likely not an accurate measurement of the specific expression levels of EcSOD in localized tumor tissues. Furthermore, EcSOD exists in both tissue-bound and freely circulating form due to its unique HBD. A significant portion of the full length EcSOD, despite having a strong affinity for negatively charged ECM molecules, is also released into the circulation. Various factors such as heparin, a commonly used blood-thinning agent, also influence this dynamic redistribution of EcSOD. Therefore, a snap-shot measurement of this extracellular antioxidant in the blood is likely not a true reflection of the total levels of EcSOD secreted by cancer cells. Perhaps determining the released form of EcSOD locally i.e. in nipple aspiration fluid (NAF) may provide a better assessment in the breast cancer model. The levels of SOD1 protein expression in NAF has been reported to be similar between normal patients and breast cancer patients [191]. Although one would speculate an alteration in the extracellular levels of EcSOD due to its secretory nature, levels of EcSOD in NAF of breast cancer patients remain to be evaluated.

1.3.9 Deregulation of EcSOD in Cancers

The degree of difference in EcSOD expression in cancer versus normal cells/tissues is more pronounced and prevalent than for other SODs as shown in Oncomine analysis (Figure 1.5). Down-regulation of EcSOD expression in cancer has

been associated with epigenetic silencing, upregulation of oncomir microRNA-21, Ras oncogene-mediated gene silencing, chronic estrogen-induced gene suppression, single nucleotide polymorphisms, DNA copy number variation, and loss of heterozygosity. All of these observations imply that deregulation of EcSOD expression, distribution, or function has a clinical significance. In view of predominantly down-regulated EcSOD expression in a majority of cancers and a tumor suppressive role as supported by a large number of *in vitro* and *in vivo* models, understanding the mechanisms involved in deregulation of its expression could provide a tool towards therapeutic interventions. The mechanisms known to regulate EcSOD expression in cancers is discussed in the following sections.

1.3.9.1 Epigenetic

One of the most well studied mechanisms regulating EcSOD silencing is DNA methylation. EcSOD lacks a standard CpG island but contains a cluster of 18 CpG sites surrounding the transcriptional start site (-550 bp upstream to 100 bp downstream) with known transcription factor binding sites, such as Sp1/Sp3. *SOD3* CpG sites have been reported to be hypermethylated in tumor tissue from gallbladder, liver, prostate, lung, and breast cancer samples [142, 153, 192-194]. Furthermore, *SOD3* promoter hypermethylation correlated with decreased mRNA expression indicating epigenetic silencing via promoter DNA methylation [192]. *SOD3* is also hypermethylated and downregulated in other diseases, such as coronary artery disease [195]. Highlighting the functional role of epigenetic silencing of EcSOD, treatment with 5-aza-2'-deoxycytidine (5-aza-dC), an inhibitor of DNA methylation increased EcSOD expression in both normal and cancer cells [142, 153, 159, 196-198]. This methyltransferase inhibitor increased DNA accessibility via nucleosome remodeling thereby increasing RNA polymerase II and Sp3 binding to the *SOD3* promoter [198]. In Ras-driven thyroid

cancers, loss of EcSOD expression has also been shown to be affected with 5-aza-dC treatment, where mutant H-RasV12-mediated suppression of EcSOD was reverted [166].

Interestingly, methylation status of the EcSOD promoter can be influenced by the presence of extracellular matrix (ECM) or Matrigel in culture. While significant expression of EcSOD is detected in mammary epithelial cells in normal tissues, once the human mammary epithelial cells (HMECs) were isolated and plated as monolayer cells, there was a progressive loss of EcSOD mRNA expression as the cells were passaged without the ECM stimuli [142]. This was due to hypermethylated promoter of EcSOD when cells lose their polarity and acinari architecture. On the other hand, restoring the three dimensional (3D) acinar morphogenesis by culturing the HMEC cells in Matrigel induces re-expression of EcSOD and its promoter region became largely unmethylated [142]. Similarly, the expression pattern of another mammary-tissue specific gene, milk casein has also been shown to be regulated in this manner, where cell culture content and context can dictate gene expression via epigenetic mechanisms [199, 200]. Interestingly, the change to 3D culture did not restore EcSOD expression in the breast cancer cells, presumably due to inability to form normal acini but instead displayed an disorganized stellate growth in 3D culture [142]. These studies reveal a novel process by which ECM integrates structure and function in mammary epithelial cells through alterations of chromatin structure and epigenetic codes.

Additionally, *SOD3* methylation patterns may be impaired via a reduced ability to remove DNA methylation. DNA methylation removal is initiated by the ten-eleven translocation (Tet) family members, which are dioxygenases of 5-methylcytosine (5-mC). EcSOD expression is positively correlated with Tet1 expression in several tumor cell types, where Tet1 expression increases EcSOD expression via de-methylation of its

CpG sites [201]. Interestingly, Tet1 is often downregulated in several types of solid cancer, such as breast, lung, colorectal, and gastric cancer [202], suggesting a potential mechanism of EcSOD silencing in cancer via downregulation of Tet1 [201].

Alterations to the glutamate carboxypeptidase II (GCPII) also modify methylation patterns resulting in changes in EcSOD expression. GCPII promotes folate uptake, which promotes DNA methylation by regenerating the methyl donor S-adenosyl methionine. In prostate cancer, EcSOD expression correlates with mutations in GCPII [193]. The GCPII D191V mutation promotes *SOD3* hypermethylation and is associated with an increased risk of breast cancer [193, 203]. Additionally, the GCPII H475Y variant is associated with decreased *SOD3* methylation and decreased risk of breast and prostate cancer [193, 204]. These studies imply an interplay between EcSOD and GCPII variants associated with cancer risk via changes in the folate cycle and DNA methylation status of EcSOD.

Histone modifications and histone variants can also play a pivotal role in epigenetic regulation. Histone acetylation typically promotes gene expression by relaxing the condensed nucleosome complex allowing for easier access to genes. Inhibitors against histone acetyltransferases (HATs), such as GCN5, p300, and PCAF, prevented EcSOD increases in a stimulated monocytic leukemia cell line, THP-1 [196]. Additionally, several studies have demonstrated increased EcSOD expression with histone deacetylase (HDAC) inhibitors [142, 196, 197, 205, 206]. Specifically, inhibition or knockdown of HDAC3 led to increased EcSOD expression in pulmonary artery smooth muscle cells [205]. HDAC3 is upregulated in many solid cancers, such as lung, breast, pancreatic, liver, and colon, indicating another potential mechanism of EcSOD silencing in cancer [207-211]. Although, HDAC inhibition may also indirectly increase EcSOD expression via loss of thyroid stimulating hormone autocrine signaling [166, 168], these

studies indicate that decreased histone acetylation can contribute to silencing of EcSOD in cancer.

Not only are histone modifications able to modify EcSOD expression, but changes in histone variants have recently been shown to play a role in expression of this antioxidant. Histone variants mediate a variety of functions, such as modifying expression, controlling chromatin condensation, sensing DNA damage, and controlling the cellular response toward DNA damage repair or apoptosis [212]. MacroH2A isoforms are unique H2A histone variants due to the presence of a 30-kDa non-histone domain (macro domain) at their C-termini. MacroH2A variants are generally considered transcriptionally repressive in nature due to their association with forms of condensed chromatin such as the inactive X chromosome (Xi) and inactive genes [213, 214]. MacroH2A1, a variant in the H2A family, has dramatic effects on cancer progression dependent on its splice variant expression. The splice variant, macroH2A1.1, inhibits proliferation, invasion, migration, and is associated with better prognosis, while macroH2A1.2 is associated with cancer progression [212]. Interestingly, altered RNA splicing via increases in RNA helicase, Ddx5 and Ddx17 promoted macroH2A1.2 which resulted in suppression of EcSOD expression in a mouse mammary tumor cell line, 4T1 [215]. These macroH2A1 splice variants had opposing effects on *SOD3* expression. MacroH2A1.1 increased *SOD3* expression in 4T1 cells, while macroH2A1.2 decreased its expression [215]. Ddx5 and/or Ddx17 is overexpressed in a variety of solid cancers, such as breast, colon, prostate, non-small cell lung, head and neck, glioma, and leukemia [216-222]. Therefore, increases in Ddx5 and Ddx17 leading to higher macroH2A1.2 levels are an additional mechanism of EcSOD down-regulation in cancer.

1.3.9.2 Single Nucleotide Polymorphisms

Alterations of EcSOD expression, tissue distribution, and/or function can also occur via single nucleotide polymorphisms (SNPs). Here, we will highlight the research into EcSOD SNPs and their effect on cancer risk and progression. These SNPs include rs1799895, rs2536512, rs2284659, and rs699473 as shown in Table 1.1.

The most extensively studied SNP is rs1799895, which occurs in the protein coding region and results in an arginine to glycine mutation at position 213 (R213G). This missense mutation occurs within the heparin binding domain of EcSOD drastically reducing the binding of EcSOD to heparin, as a result increasing circulating EcSOD [95]. The R213G mutation also inhibits the ability of EcSOD to bind lipoprotein receptor-related protein (LRP), which promotes its uptake by LRP-mediated endocytosis and eventual clearance by the liver [98]. As a result, patients with R213G have a ~10-fold increase in plasma EcSOD activity levels [95]. It is also associated with decreased development of chronic obstructive pulmonary disease (COPD) in smokers [223]. Meta-analysis of many studies indicate smokers with COPD are associated with an increased risk of lung cancer [224]. These studies indicate it may provide protection to smokers from lung cancer development. Indeed, the R213G SNP in lung cancer is associated with a protective phenotype as it was enriched in healthy control smokers compared to lung cancer patients [225]. It is also associated with the number of lesions in metastatic gastric cancer [226]. Although, in a large study assessing the role of R213G SNP within the Danish population, the mutation was found to have no effect on the overall risk of cancer [227]. Despite the dramatic change in localization of *SOD3* caused by the R213G mutation, these studies suggest that it likely has no effect on cancer risk, except for a potential protective role in lung cancer.

Table 1.1. Summary of EcSOD SNPs with associated cancer risk.

SNP	Location	Mutation	Effect on Cancer
rs1799895 (Ex3-631C>G)	Coding region	C→G; R213G	Decreased risk of lung cancer [224] Increased number of lesions in metastatic gastric cancer [226]
rs2536512	Coding region	A→G; A58T	Increased risk of hepatocellular carcinoma [228] Increased risk of glioma [229] Associated with estrogen/progesterone receptor expression in breast cancer [144]
rs2284659	Promoter	G→T	In a 4 SNP set that results in increased risk of breast cancer [230]
rs699473 (IVS1+186C>T)	Promoter; AhR-XRE binding site, CpG Island	C→T	Enriched in high-grade prostate cancer [231] Decreased progression free survival in breast cancer [144]

The SNP, rs2536512, similarly occurs within the coding region of *SOD3* and results in a missense mutation of alanine to threonine at residue 58 (A58T). This mutation occurs within the oligomerization domain of EcSOD and is hypothesized to play a role in protein tetramerization. There are conflicting results about its effect on plasma EcSOD activity [232, 233]. However, to date there is little known about the effect of the A58T mutation on EcSOD activity, localization, or oligomerization. In cancer, it is associated with increased risk of hepatocellular carcinoma and glioma [228, 229]. Similarly, it is correlated with estrogen and progesterone receptor expression in breast cancer patients [144]. The A58T mutation also increases risk of other diseases, such a cerebral infarction in women, type 2 diabetes mellitus, and diminished lung function in children [234-236]. The functional effect of this mutation remains unclear and requires further study to fully understand its role in cancer.

The SNP rs2284659 occurs within the *SOD3* promoter. Due to its location in the promoter, it may modify expression of EcSOD. However, the effect of this SNP on EcSOD expression is unclear as it does not occur within any known transcription factor binding domains. In cancer, the SNP rs2284659 is associated with an increase in breast cancer incidence [230]. It is also associated with higher plasma levels of EcSOD in diabetic patients [237]. However, the mechanism behind the increase in patients with the SNP rs2284659 remains unclear.

Another EcSOD SNP shown to affect cancer risk is rs699473. This SNP occurs within the aryl hydrocarbon receptor-xenobiotic response element (AhR-XRE) binding motif of the EcSOD promoter. The mutation causes reduced binding capacity of nuclear proteins and alteration of a CpG site potentially perturbing DNA methylation at this location [153, 234]. The resulting effect on EcSOD expression remains unclear. In cancer, the SNP rs699473 is associated with increased risk of high-grade prostate

cancer [231]. Interestingly, this SNP was also found to protect patients from increased risk of high grade prostate cancer after selenium supplementation in the Selenium and Vitamin E Cancer Prevention Trial (SELECT) [238]. In breast cancer, SNP rs699473 is associated with a significant reduction in the progression-free survival in breast cancer compared to patients with wild type EcSOD [144]. This SNP has also been linked to an increased risk of adult brain cancer, specifically meningioma and possibly glioma [239].

1.3.9.3 Loss of Heterozygosity

SNPs are not the only genetic abnormality regulating EcSOD in cancer. Loss of heterozygosity (LOH), also known as allelic deletion, is the process by which a cell deletes one of the two copies of a gene. Allelic deletion in cancer cells results in hemizygotes containing only one parental copy of that gene. As EcSOD has several SNPs, it is likely that parentally inherited SNPs of EcSOD exist in a heterozygous state. Therefore, LOH may help expose functional roles of SNPs in EcSOD previously masked by the deleted allele. In addition to unmasking SNP phenotypes, allelic deletion often results in reduced gene expression. Several reports indicate the *SOD3* gene, located on chromosome 4p15.3-4p15.1, is a hotspot for LOH in cancer. The deletion of chromosome 4p15.1-15.3 has been observed in many types of solid cancers, such as cervical, breast, head and neck, liver, colorectal, lung, and bladder [149, 153, 240-248]. These loses range from 30% in bladder cancer up to 60% in lung cancer [245, 248]. LOH of this region increases dramatically between cervical intraepithelial neoplasia and grade I cervical cancer suggesting that allelic deletion occurs early in tumorigenesis [240]. LOH plays a role in EcSOD suppression in the lung cancer cell line, A549 indicating both LOH and DNA methylation mediate EcSOD silencing in these cells [153]. Moreover, 17β-estradiol induced transformation of the normal breast epithelial cell line,

MCF10F, resulted in loss of chromosome 4p [249]. Thus, indicating a potential role of estrogen in EcSOD deletion in breast cancer.

1.3.9.4 MicroRNA

Expression of EcSOD can also be regulated by microRNA, which are a class of small (~22 nucleotides) non-coding RNAs that negatively regulate gene expression post-transcriptionally [250]. Currently, miR-21 is the only known microRNA to directly target EcSOD, as it binds a 3' UTR site in EcSOD mRNA [251]. MiR-21 is considered an oncomir and is upregulated in both leukemias and solid cancers of the lung, breast, prostate, pancreas, stomach, colon, ovaries, cervix, and thyroid [252-256]. MiR-21 has diagnostic and prognostic value, as its expression typically increases with tumor grade [256]. Other targets of miR-21 are tropomyosin 1 (TPM-1), programmed cell death protein 4 (PCDCD4), reversion-inducing cysteine-rich protein with kazal (RECK), maspin, NFIB, Sporouty2, and PTEN [256]. Overexpression of miR-21 in non-transformed immortalized human bronchial epithelial cells (NL20) reduced EcSOD levels and increased transformation as shown via colony formation in soft agar [251]. Transformation was blunted by re-expression of EcSOD, supporting a tumor suppressive role for EcSOD [251]. Additionally, miR-21 levels were significantly increased after >10 fold increases in Ras activity via expression of mutant H-RasV12 leading to decreased EcSOD expression [166]. Therefore, cancer cells can also silence EcSOD expression via upregulation of the oncomir miR-21.

1.4 Redox-Active Drugs in Breast Cancer Treatment

As highlighted above, ROS is implicated in every hallmark of cancer. Therefore, researchers have set out to find a way to target ROS effectively in the context of cancer prevention and treatment. The first and most obvious choices for treatment were the dietary antioxidants, beta-carotene, vitamin A, C, and E, to reduce cancer risk. There have been many studies done to assess if low consumption of these antioxidants would increase the risk of cancer. A meta-analysis of 11 different studies indicated that dietary intake of β carotene, vitamin A, C, or E had no effect on breast cancer risk [257]. While further analysis of serum levels of these same antioxidants also showed an inconsistently mild effect or no effect at all on breast cancer risk [257]. Furthermore, there have been several high-profile randomized clinical trials set up to test the idea of antioxidant and/or multivitamin supplementation to reduce cancer risk. These trials include the SELECT, SU.VI.MAX, CARET, and ATBC trials. These trials found no evidence of reduction in cancer risk in women [258]. However, when using a multivitamin, men had a slight reduction in cancer incidence in the SU.VI.MAX and Physicians' Health Study II trials [259, 260]. Therefore, while ROS may play a role during tumor initiation, the use of dietary antioxidants is ultimately ineffective at preventing cancer formation.

Despite the contention over the role ROS plays during cancer formation, it plays an undeniable role during cancer treatment. Due to the inherent high levels of ROS in cancer cells, there are two options for modifying ROS levels in cancer; increase ROS levels to promote cell death or decrease ROS levels to inhibit cancer cell growth as indicated in figure 1.1. This concept is oft referred to as the "double-edged" sword of ROS in cancer treatment. The most common examples of ROS inducing cancer

therapies are radiation and chemotherapy, which both rely on ROS to induce apoptosis. Ionizing radiation generates ROS/RNS directly as it is absorbed by water or organic molecules, which leads to toxic levels of ROS in cancer cells [261]. Chemotherapies are a broad category of drugs that target cell growth. These chemotherapy drugs can result in both a direct and an indirect increase of ROS levels ultimately leading to cytotoxic effects [262]. This phenomenon is evident by analysis of chemoresistant breast cells. These resistant cells have significantly increased genes required to produce glutathione [263]. Furthermore, addition of antioxidants decreases cell death induced by doxorubicin [264]. However, these therapies also have off-target effects due to damage induced to normal cells. Due to the severity of these negative effects, the idea of combining chemotherapy/radiation with antioxidants to reduce off-target effects has been tested. The use of dietary antioxidants has been found to slightly reduce the severity of off-target effects with little to no effect on tumor response [265].

Furthermore, the current therapeutic approach in cancer treatment is combination of multiple drugs to enhance efficacy. In the context of redox-active drugs, there are several drugs in clinical trials built on the idea of modifying ROS levels; increasing ROS to enhance efficacy and reducing ROS to decrease off-target toxicity. Targeting the antioxidant thioredoxin (TRX) system has been a promising approach. The TRX system is upregulated in many cancers and is associated with higher proliferation, metastasis, and chemoresistance, as well as decreased apoptosis [266, 267]. Thus, TRX inhibitors, aurofin and arsenic trioxide, are both currently in multiple phase I/II clinical trials for solo and combination therapy as cancer treatment [268]. Additionally, sulindac, a non-steroidal anti-inflammatory drug, inhibited mammary carcinogenesis and cancer cell growth, as well as induced apoptosis in breast cancer cell lines [269]. Later studies determined that sulindac-derived ROS induced apoptosis via activation of p38

mitogen-activated protein kinase and p53 [270]. A phase II clinical trial was launched to determine if combination of docetaxel and sulindac would improve efficacy in advanced breast cancer patients (NCT00039520).

Despite their lack of efficacy in cancer prevention, dietary antioxidants are currently being tested for their efficacy as a treatment in cancer. Fenretinide is a synthetic retinoid that induces apoptosis in a ROS-dependent mechanism [271]. A phase III clinical trial in breast cancer patients showed that it decreased breast cancer recurrence, especially in younger pre-menopausal patients [272]. Additionally, it is currently being tested in a clinical trial in recurrent ovarian cancer patients (NCT01535157). Vitamin C has also made a reappearance in cancer treatment. It was found that high-dose vitamin C, which requires intravenous injection, generates ROS in cancer cells. Due to the uniquely high intracellular free iron found in cancer cells, vitamin C redox cycles with iron to generate H_2O_2, which ultimately creates toxic levels of ROS, resulting in cancer cell death [273, 274]. The high-dose vitamin C, or pharmacological ascorbate, therapy is currently in many phase II clinical trials for lymphoma (NCT03418038), acute myeloid leukemia (NCT03397173), hepatocellular carcinoma (NCT04033107), gastric cancer (NCT04033107), glioblastoma (NCT02344355), colon cancer (NCT04035096, NCT03146962, NCT04033107), lung cancer (NCT02905591, NCT02420314, NCT03146962) and pancreatic cancer (NCT03410030, NCT03146962, NCT04033107, NCT02905578), as well as a phase III trial in gastric cancer (NCT03015675). These trials highlight the optimism around this therapy, as well as demonstrate the potential duplicity of redox-active drugs.

Current use of drugs to lower ROS levels are largely focused on reducing off-target cytotoxic effects. Vitamin E has been used to reduce oral mucositis, an off-target effect of radiation in head and neck cancers [275]. Additionally, N-acetyl cysteine

(NAC), a well-known antioxidant and GSH precursor, is also being tested in a phase II clinical trial to reduce oral mucositis in head and neck cancer patients undergoing radiation therapy (NCT02123511). NAC was also used a phase IV clinical trial to reduce cisplatin-induced toxicities in head and neck cancer patients (NCT02241876). Furthermore, SOD mimetics are also being used to reduce the negative effects of high ROS levels induced by chemotherapy and radiation. GC4419, a SOD mimetic, completed a phase IIb clinical trial and has started a phase III trial to reduce severe oral mucositis in head and neck patients that receive radiotherapy and cisplatin treatment [276]. The rationale for this study was piloted by the work done with a different class of SOD mimetics, the manganese porphyrin drugs. Due to the heavy use of the manganese porphyrin in my work, the following is a more in-depth overview on this class of redox-active drugs.

1.4.1 Manganese Porphyrin

Manganese (III) porphyrin (MnPs) are a family of redox-active drugs. They were initially designed as a SOD mimetic. The manganese core of MnPs can accept and donate electrons, which is a required a characteristic of SOD enzymes as mentioned above. The structure of the porphyrin ring pulls electrons away from the Mn core preventing stabilization of Mn(III) and allowing it to accept electrons from $O_2^{\bullet-}$ and other ROS species. Thus, MnPs undergo a redox couple with Mn^{III}/Mn^{II}, whereby MnPs react two $O_2^{\bullet-}$ molecules to create O_2 and H_2O_2 and regenerate Mn(III)P [277]. Several analogs have been made over the years based off the initial MnTR-2-PyP^{5+} design, where R indicates different substitutions. The main analog used in these studies is MnTE-2-PyP^{5+} (MnTE) shown in figure 1.6. MnTE is well tolerated in pre-clinical trials and is currently in clinical trials for acne vulgaris (NCT03752242), rosacea

Figure 1.6. MnTE-2-PyP^{5+} chemical structure

The diagram represents the chemical structure of MnTE-2-PyP^{5+}.

Figure from:

Tovmasyan A.G., Rajic Z., Spasojevic I., Reboucas J.S., Chen X., Salvemini D., Sheng H., Warner D.S., Benov L., Batinic-Haberle I. Methoxy-derivation of alkyl chains increases the in vivo efficacy of cationic Mn porphyrins. Synthesis, characterization, SOD-like activity, and SOD-deficient E. coli study of meta Mn(III) N – methoxyalkylpyridylporphyrins. Dalton Transactions. 2011; 40 (16): 4111-4121.

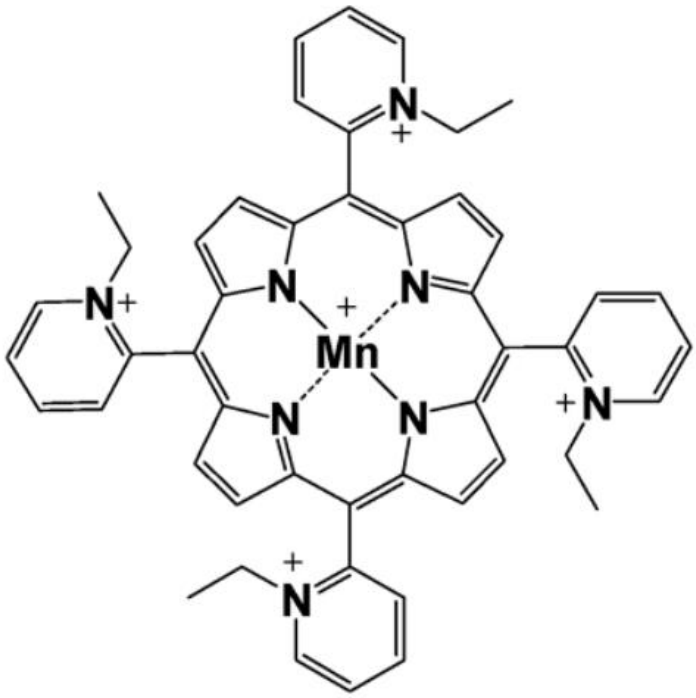

MnTE-2-PyP^{5+}

(NCT03756389), atopic dermatitis and plaque psoriasis (NCT03381625) [278]. Another analog of MnPs, MnTnBuOE-2-PyP^{5+}, is also in clinical trials for anal cancer (NCT03386500), glioma (NCT02655601), head and neck cancer (NCT02990468), and patients with multiple brain metastases (NCT03608020) as a radioprotectant.

Interestingly, over the years, researchers have discovered that MnPs have much a wider range of potential reactions than just mimicking SOD activity. The SOD enzymes have the bulky tertiary protein structure that provides selectivity toward $O_2^{\bullet-}$. However, the MnPs lack this bulkiness allowing for a wider range of reactions to occur. MnPs have been shown to react with $ONOO^-$, H_2O_2, GSH, and ascorbate to name a few [279, 280]. Similarly, MnPs can act as both an oxidizing and reducing agent resulting in the production of hydrogen peroxide [277]. These effects usually occur with combination of MnPs and ascorbate and/or radiation [279, 281, 282]. MnPs may also redox couple via Mn^{IV}/Mn^{III} adding further complexity to range of MnP activity [277]. Due to the large complex array of MnP reactions, the overall function of MnPs within the cell is highly dependent on ROS levels, MnP concentration, and the associated rate constants of the reaction. Thus, one can no longer generalize MnPs as a SOD mimetic requiring more intense research on the exact effect of MnPs in each cellular context.

Studies have also found that MnPs affect not only ROS levels but also modify signaling pathways and transcription factors. NF-κB, Nrf2, and Hif-1α are the transcription factors that have their activity modified by MnPs. NF-κB is inactivated by MnPs through glutathionylation of p65 [283]. Additionally, MnPs can increase protein glutathionylation of mitochondrial proteins, Complex I and Complex III, inhibiting their activity [284]. AP-1 activity, as assessed via an electrophoretic mobility shift assay (EMSA), was inhibited via MnPs in the skin carcinogenesis mouse model induced via 12-O-tetradecanoylphorbol-13-acetate (TPA) treatment [285]. While the mechanism for

this inhibition was never assessed, it is believed the mechanism is through MnP-mediated ROS reduction, since ROS is a known activator of AP-1. Hif-1α protein levels are decreased by MnPs during hypoxia in breast cancer cell line, MCF-7 [286]. MnPs also decrease Hif-1α activity via disruption of the DNA binding of the CREB/HIF-1α complex as seen in prostate cancer cell line, PC3 [281]. MnPs inhibited ROS-dependent 6-hydroxydopamine activation of ERK in neuronal B65 cells [287]. Additionally, epigenetics is also regulated via MnPs. The histone acetyltransferase, p300, is inhibited by MnPs in prostate cancer cells reducing HIF-1a [281]. Interestingly, MnPs can regulate histone deacetylases as well. Recent studies have shown MnPs can modify the activity of sirtuins via changes in the levels of their essential co-factor, NAD^+, within the cell. The NAD^+ levels were increased via Nrf2-upregulation of Nqo1, a NAD(P)H dehydrogenase that reduces quinones using NADPH or NADH in the process [288].

The effect of the MnPs on immune cells within the tumor is of particular interest to my studies. In alveolar macrophages, MnPs reduces TGF-β and VEGF production [289]. Also, macrophage infiltration in the 4T1 mouse model of stage IV breast cancer was reduced by MnPs, along with reduced levels of angiogenesis and metastasis, which are both induced by macrophages [290]. In other tumor mouse models, MnTnBuOE-2-PyP^{5+} reduced monocyte infiltration and macrophage polarization [291]. Furthermore, other immune cells, such as T cells, are affected by MnP treatment. $CD4^+$ T cells polarization is affected by MnP treatment with a skew toward T_H1 [292-294]. Furthermore, splenic levels of T cells, B cells, and NK cells are increased after MnP treatment [294].

1.5 Breast Cancer Microenvironment

No man is an island. This is a common sayings used throughout academia to highlight the collaborative work required to generate data while the spotlight is one individual. These same sayings apply to cancer. Tumors are more than just the cancer cells themselves. For many years, analyzing cancer cells growing in two dimensions on plastic in hyperoxic conditions was the norm. Little energy was put into understanding the three-dimensional nature of tumors could affect cancer cell aggressiveness. Additionally, little research was done to understand the effect stromal cells within the tumor on patient outcomes. However, in the last decade there has been an influx of research into how the three-dimensional structure and the non-transformed surrounding cells contribute to disease outcomes. These traits are all loosely grouped under the umbrella term, the tumor microenvironment. The tumor microenvironment is an acidic, oxidized, and hypoxic region made up of cancer cells, fibroblasts, endothelial cells, lymphocytes, and myeloid cells held together by aberrant extracellular matrices. Furthermore, a larger tumor stroma is a strong prognostic factor indicative poor survival independent of breast cancer subtype [295, 296]. Many studies were launched to determine if any of these characteristics within the tumor microenvironment play a role in cancer growth, metastasis, recurrence, and patient survival to find new therapeutic targets. I will focus on the role of fibroblasts and macrophages within the tumor microenvironment, as well as the role of the oxidized nature of tumor, in this dissertation.

1.5.1 Cancer Associated Fibroblasts

Cancer associated fibroblasts, or CAFs, are one of the most abundant cells in the breast TME. These cells are commonly believed to originate from tissue resident fibroblast. There are additional theories which suggest transdifferentiation of cancer cells and other cell types, such as mesenchymal stem cells or pericytes, as an additional source of CAFs [297]. Normal fibroblast activation into CAFs follows similar pathways as myofibroblast activation. This activation is largely driven by transforming growth factor beta (TGF-β) [298]. However, recent studies have determined that cancer cells secrete a variety of additional factors that promote CAF activation, such as Wnt7a, osteopontin, and breast cancer cell-derived exosomes [299-302]. Additionally, CAFs release TGF-β and SDF-1 inducing signaling pathways in surrounding normal fibroblasts promoting their activation [303]. These activated CAFs have higher levels of α-smooth muscle actin (SMA), fibroblast activating protein (FAP), fibroblast stimulating protein (FSP), and platelet-derived growth factor receptors alpha and beta (PDGFRα/β) [297]. CAFs are also characterized by increased secretion of many cytokines, such as HGF, SDF-1, IL-6, IL-10, and VEGF, and chemokines, such as CCL2, CCL5, and CCL20, which act to directly promote tumor aggressiveness, metastasis, angiogenesis, and suppression of the immune system [297, 304-306].

Additionally, CAFs cause dramatic changes to the extracellular matrix (ECM). Interestingly, in breast cancer, there are specific ECM signatures that correlates with breast cancer subtype and outcome [307]. The ECM components correlated with poor survival in breast cancer are fibronectin, collagen, and tenascin-C, while laminins, hyaluronic acid, and heparins are associated with a better outcome [308]. CAFs in breast cancer produce high levels of fibronectin, collagen, and tenascin-C compared to normal mammary fibroblasts, which promotes cancer cell migration [309-311]. CAFs

also participate heavily in degrading the surrounding normal ECM with matrix metallopetidases, MMPs. MMP-1, MMP-7, MMP-9, MMP-11, MMP-12, and MMP-14 are all associated with a poor prognosis in breast cancer [297, 312]. Many of these MMPs are upregulated during CAF activation [313, 314]. The combination of increased ECM degradation with MMPs and increased ECM deposition results in a dramatic remodeling of the ECM. This ECM remodeling promotes invasion of surrounding tissue by orienting collagen perpendicular to the tumor boundary to allow for easier cancer cell migration along these collagen highways [315]. Furthermore, increase ECM secretion enhances the stiffness of the tumor and increases metastasis and tumor progression, as well as promotes fibroblast growth and migration [316-319].

A newer study has also examined the stroma of breast cancer tumors to determine what TME is indicative of a more aggressive disease. They found that stroma with high levels of collagen or fibroblasts were indicative of a poor prognosis [320]. Additionally, many studies have begun using known CAF markers, α-SMA, FSP1, and tenascin C, to determine if the number of activated fibroblasts within the tumor resulted in a poorer prognosis [321-323]. These studies have repeatedly found that high level of activated fibroblasts, or CAFs, are indicative of faster tumor growth, more metastasis, and reduced survival independent of breast cancer subtype. Therefore, CAFs have a vital role in determining the aggressiveness, especially in the most aggressive forms of breast cancer, TNBC.

Interestingly, many studies are also beginning to highlight the heterogeneity that exists within CAFs. Not only are there differences between normal fibroblasts and CAFs as noted above, there are differences based on cancer cell that stimulates the transition from normal fibroblast to CAF. The molecular subtype of breast cancer can result in CAFs that have distinct gene and protein expression compared to the other subtypes

[324, 325]. The data suggests that CAFs from Her2+ breast cancer were more divergent than CAFs from either TNBC or ER+ breast cancer. These CAFs also had different levels of aggressiveness as CAFs from TNBC and Her2+ breast cancer promoted migration of breast cancer cells more than normal fibroblasts or CAFs from ER+ breast cancer.

Newer studies have begun to use of single cell RNA-seq highlighting that there is even CAF heterogeneity within tumors. Two new studies used this single cell sequencing data to reveal that there are distinct populations of CAFs present within the tumor. Busch et al. suggests that the distinct populations occur due to fibroblast differentiation [326]. This model suggests stem-like fibroblasts progress through the differentiation to activated CAFs that are predominantly either ECM-regulating myofibrolasts or secretory myofibroblasts. However, Bartoschek et al. performing a similar experiment on CAFs in the MMTV-PyMT mouse model found the cell of origin to be the distinguishing factor between the different CAF populations. They found three distinct CAFs populations originated from either resident fibroblasts, the perivascular niche (potentially pericytes), or from malignant cells that had undergone epithelial-mesenchymal transition [327]. The gene signature of the different CAF populations were correlated with different levels of metastatic risk in patients from the TCGA database indicative of different functions within the tumor.

In addition to the high-powered RNA-seq studies, loss of Cav1 has begun to be recognized as a marker of a lethal TME in breast cancer, as it is linked to drug resistance, metastasis, recurrence, and reduced survival [328, 329]. For example, low stromal Cav1 TNBC had a ≤ 5 year survival rate, while high stromal Cav1 TNBC had a 12 year survival rate [330]. Unsurprisingly, Cav1 knockout fibroblasts have higher myofibroblasts markers and collagen expression. However, these fibroblasts also have

increased glycolytic markers, such as PKM2 and LDHA, suggesting these Cav1 loss promotes increased glycolysis. Further research confirmed that Cav1 loss increased aerobic glycolysis and lactate secretion through HIF-1α dependent mechanism [331]. Interestingly, the lactate was secreted by CAFs via increased levels of MCT4, a lactate exporter, and taken up by nearby breast cancer cells expressing the lactate importer, MCT1, suggesting CAFs may also modify the metabolism of the cancer cells within the tumor [332]. Of particular interest to my research is the role ROS plays during activation. Addition of hydrogen peroxide alone increased CAF markers and reduced Cav-1 levels suggesting ROS plays a role during fibroblast activation toward CAFs [333].

1.5.2 Tumor Associated Macrophages

Macrophages are a key immune cell within the innate immune system. These white blood cells are the first line of defense against most threats, including cancer. These cells eat and degrade bacteria or defective/dying human cells via a process called phagocytosis [334]. They also eat lipid particles and other non-cell particles. Thus, during a typical wound response, macrophages play a key role during both the initial pro-inflammatory disinfect phase and the secondary wound closure phase. To provide both functions' macrophages undergo a process called polarization. Broadly, macrophages can polarize toward two main extremes. This includes the pro-inflammatory M1 state and immunosuppressive M2 state [335]. Macrophages polarize toward either of these states depending on the external stimuli given to each individual cell. In practice, macrophage polarization is much more complicated than either M1 or M2 states. Previously, IL-4, IL-10, and conditioned media from cancer cells were thought to all produce M2 macrophages. However, recent studies using expression profiling and novel function assays have determined these macrophages behave quite differently. Thus, some

researchers have begun to subclassify M2 macrophages into M2a, M2b, and M2c class depending on the stimulating agent [336]. Furthermore, recent studies have found novel polarization states in macrophages, such as Mox and M4 in in atherosclerosis [337, 338]. While these systems provide a more nuanced view of macrophage polarization and function, the initial M1/M2 model is still widely used and useful shorthand during surface level discussions of macrophages in disease states.

To further stratify macrophage classifications, macrophages that invade into the tumor stroma are called tumor associated macrophages (TAMs). TAMs are one of the most abundant immune cells within breast cancer. TAMs typically have a M2-like phenotype [339]. Functionally, TAMs play a key role in promoting an aggressive phenotype in breast cancer via stimulating angiogenesis, metastasis, tumor growth, and suppression of the immune system [340]. Co-culture experiments with macrophages and a variety of breast cancer cell lines determined that TNBC cell lines polarized macrophages more dramatically than other subtypes of breast cancer [341-343]. Analysis of cytokines secreted by these different cancer cell lines generated several potential candidates responsible for polarizing macrophages, such as M-CSF, and GM-CSF [342, 343]. Due to the high plasticity and ease at which macrophages adapt to their surroundings, it is likely that it is a combination of signals that result in TAM formation.

Furthermore, cancer cells may not be the only cells within the tumor that affect macrophage polarization. Recent evidence correlates macrophage infiltration and fibroblast activation. M2 macrophages were positively correlated with CAF levels in TNBC tumors before therapy as analyzed by IHC of CD163 as an M2 marker and α-SMA and FAP as a CAF marker [344]. This correlation was suggested after analysis of CAF secretome revealed secretion of cytokines and chemokines, such as IL-6, MCP-1, and SDF-1, which are known to recruit the macrophage precursor, monocytes [304].

Mechanistic studies using neutralizing antibodies revealed that CAFs secrete large amounts of SDF-1 and MCP-1, which promoted monocyte recruitment [305, 345]. This study also indicated that monocyte recruitment was similar in both CAFs and cancer cells. Thus, CAFs, as well as cancer cells, play a key role in the enhanced macrophage infiltration of breast tumors. Furthermore, CAFs also play a role in stimulating macrophage polarization. Conditioned media from CAFs increased levels of M2 surface markers, CD163 and CD206, as well as enhanced macrophage-mediated immunosuppression compared to conditioned media from normal fibroblasts [305, 346]. Conditioned media from these CAF-conditioned macrophages also stimulated cancer cell invasion further suggesting these macrophages are behaving as TAM. Interestingly, conditioned media from M2 macrophages increased the CAF marker, SMA, in normal fibroblasts suggesting a reciprocal interaction between CAFs and TAM [346]. These data provide evidence that TAM recruitment and polarization is not a phenomenon solely instituted by cancer cells but by multiple cells within the tumor.

Regardless of polarization state, the data is clear that macrophages overall promote an aggressive phenotype in breast cancer. Several studies correlate increased macrophage infiltration with increased metastasis and tumor size, as well as decreased disease-free survival. More recent studies have begun testing if M2 markers provide a better correlation than generic macrophage markers. These show similar trends from generic macrophage markers, CD68, and M2 specific markers, CD163 [347-351]. Thus, both macrophages generically and M2 specifically are associated with an aggressive cancer. To test if there is a casual relationship, cancer mouse models were treated with clodronate liposomes to remove macrophages [352]. The macrophage deficient mice had decreased tumor growth and metastasis compared to control mice suggesting macrophages play a casual role in the aggressiveness of breast cancer. Additionally,

reprogramming of macrophages to M1 reduced 4T1 tumor growth [353]. These studies provided the initial rationale for targeting macrophages moving forward.

The field is currently developing therapies to target macrophages through three main methods: inhibiting macrophage recruitment, reprogramming TAM to the anti-tumor M1 type, and depleting TAM by promoting cell death. The most well studied pathway involved in macrophage recruitment in cancer is the CCL2/CCR2 pathways. CCL2 (MCP-1), a chemokine expressed by cancer cells and stromal cells, like adipocytes, fibroblasts, endothelial cells, and macrophages, increases macrophage infiltration [354-356]. Silencing of CCL2, reduced M2 macrophage recruitment and inhibited TNBC progression in a humanized mouse model [357]. Similar to CCL2 inhibition, inhibition of CSF1R reduces macrophage levels in tumors. However, CSF1R depletes macrophages through removal a major survival pathway in macrophages [358, 359]. This results in reduced metastasis in preclinical mouse models. Reprogramming of TAM is the most diverse of the macrophage targeting strategies. These strategies range from targeting histone deacetylases, CD47, MARCO, or PI3Kγ to activation of TLR7 or CD40 [360-366]. All of these techniques have showed promise in mouse models and many of them are currently in clinical trials highlighting the role of TAM during cancer progression.

Few studies have investigated the role of ROS in TAM polarization and function. Modifying glutathione levels can alter macrophage secretion of IL-10 and IL-12 suggesting the redox status of macrophages could affect polarization [367]. Furthermore, the ROS inhibitor butylated hydroxyanisole (BHA), which prevents fatty acid oxidation, inhibits M-CSF mediated M2 polarization [368]. However, BHA also has off-target effects, which could also disrupt macrophage polarization [369]. Additionally, loss of Nox-derived ROS inhibits M2 polarization in a mouse model for diabetes [370]. Whereas, increasing ROS induced M2 polarization in mouse macrophages [371].

Despite these recent advances, the effect of ROS on polarization and function of TAM and human macrophage polarization remains unclear.

1.5.3 Oxidized Tumor Microenvironment

It is well known that tumors have high levels of oxidation. Breast tumors have increased levels of ROS markers, such as oxidized lipids, protein carbonyls, protein nitrosylation, and others, compared to normal breast tissue [372-377]. Since breast cancer cells have higher levels of ROS than normal breast epithelial cells, these data were unsurprising [378]. Despite all the research done on how the increased intracellular ROS levels affect breast cancer cells, very little data has been collected addressing the role of extracellular ROS on tumor development and growth. However, there are some studies that examined the role of exogenous ROS on cellular functions. Addition of H_2O_2 to fibroblasts promotes loss of Cav1, which as stated above promotes an aggressive CAF phenotype in those fibroblasts [333]. The activated CAFs have increased hydrogen peroxide secretion compared to normal fibroblasts, which inhibits PTEN activity in normal epithelial cells ahead of the tumor, as well as promote tumor growth [379]. Furthermore, exogenous ROS can have immunosuppressive functions by promoting Treg formation and by inhibiting the binding of the major histocompatibility complexes (MHC) with the T cell receptor (TCR) in CD4 and CD8 T cells by nitrosylating the TCR [380, 381].

Additionally, stromal cells within the TME are not the only thing affected by increased ROS levels. The ECM is also modified by the oxTME. ECM proteins are readily oxidized *in vitro* after addition of exogenous ROS. This oxidation causes conformational changes that often result in fragmentation and degradation. ECM fragments are known to have chemotactic activity for neutrophils and monocytes [382].

They also induce pro-inflammatory gene expression and cytokine release in monocytes, macrophages, and neutrophils. However, not all ECM fragments are created equal. Different ECM fragments will have different effects on different target cells. Hyaluronan fragments stimulates receptor CD44 and activates NF-κB activation and chemokine expression in macrophages [383-385]. In breast cancer, hyaluronan fragments are associated with poor outcome, disease recurrence, metastasis, and promote breast cancer cell survival and migration [386, 387]. Heparan sulfate is also known to be oxidized and fragmented via ROS. Oxidized heparan sulfate fragments activate the TLR4 receptor and induce neutrophil chemotaxis [388]. Collagen, on the other hand, undergoes proline oxidation causing backbone fragmentation into 2 pyrrolidone [389]. Oxidized type I collagen decreased cell survival in primary rat hepatocytes compared to normal type I collagen. It also increased transcription factor activity in AP-1, Egr-1, CREB, and NF-κB in these cells [390]. However, this effect may be cell-type specific as oxidized collagen stimulated cell growth in vascular smooth muscle cells [391]. The oxidized collagen may also affect the strength of attachment by smooth muscle cells as they were detached via trypsin much easier than those grown on non-oxidized collagen. In skeletal muscle cells, oxidized fibronectin increases focal adhesion kinase (FAK) activation and promotes adhesion to the myotendinous junction [392]. Furthermore, current studies are beginning to find that oxidation of polyunsaturated fats leads to 2-(ω-carboxyethyl) pyrrole (CEP) adducts that can bind to ECM proteins, such as fibrinogen. These CEP-adducts are recognized by integrins $\alpha_M\beta_2$ and $\alpha_D\beta_2$ [393]. Macrophages that express these integrins bind the CEP-adducts and increases their migration and retention at the target site [394]. Interestingly, even amongst macrophages expression of integrins $\alpha_M\beta_2$ and $\alpha_D\beta_2$ is varied depending on the polarization state. M1 macrophages have higher levels of $\alpha_D\beta_2$ compared to M2, while both M1 and M2 macrophages have moderate levels of $\alpha_M\beta_2$ compared to resident macrophages [395]. However, integrin

expression has a biphasic effect on migration, where both high and low expression reduce migration. Therefore, CEP-adducts caused by the oxTME likely increase migration of M2 macrophages preferentially over M1 macrophages. Thus, the role of oxidized ECM is highly dependent on both the cell-type interacting with the ECM and on which member of the ECM is oxidized.

Due to its unique extracellular localization and ability to scavenge superoxide, EcSOD is a key regulator in the oxTME. Unsurprisingly, EcSOD is a key enzyme to prevent oxidative damage to ECM proteins. The first hints were found in the EcSOD knockout mouse model. After bleomycin-induced pulmonary damage, the knockout mice had enhanced 2-pyrrolidone levels, which is a marker of oxidized proline residues and indicates fragmentation of collagen [396]. Future studies confirmed that EcSOD expression reduced ROS-mediated fragmentation of type I collagen, hyaluronan, and heparan sulfate [87, 388, 397]. Therefore, it is unsurprising that overexpression of EcSOD reduced immune cell infiltration in mouse model of ischemia, inflammatory skin disease, and radiation-induced lung damage [398-401].

Furthermore, the oxidative tumor microenvironment can play a role in the tumor immune response, as EcSOD can regulate both innate and adaptive immune cell infiltration and function. Macrophage infiltration, which is correlated with poor prognosis in cancer [402], is reduced with EcSOD overexpression in acute inflammation mouse models [401]. In addition to its role in the innate immune system, EcSOD selectively inhibited Th2 and Th17 differentiation with no effect on Th1 [403], which are implicated in tumor progression [404]. Additionally, macrophage-derived superoxide induces Treg formation [381], indicating EcSOD may serve a potential inhibitory role for Tregs in cancer. Therefore, EcSOD likely plays a key role controlling the activation of stromal cells through its ability to regulate the oxTME.

1.6 Dissertation Hypothesis

It is becoming increasingly clear that the TME can act as an active participant during tumorigenesis rather than as a passive bystander. It can actively promote many negative aspects of cancers, such as enhanced tumor growth, chemoresistance, and metastasis. Therefore, therapeutic strategies targeting the TME and its interactions with cancer cells opens a novel avenue of intervention. However, the TME is an extremely complex network of many different cell types communicating back and forth with each other and cancer cells within a tumor that is highly oxidatively stressed. Despite the knowledge of the oxidative state within the tumor, it remains an understudied area of research with the TME field. Therefore, in the broadest terms possible, the main goal of this dissertation was to determine the role of ROS in promoting an aggressive phenotype in the breast cancer TME and to use this knowledge to discover novel therapeutic targets.

This work is predicated on previous findings of the loss of EcSOD in breast cancer, as well as many other solid cancers. Previously, our laboratory found that re-expression of EcSOD in TNBC cell lines reduces proliferation, clonogenic survival, and invasion. Low expression of EcSOD is also associated with a poorer relapse free survival in all subtype of BC. Taken together these data suggests EcSOD acts a tumor suppressor. However, it remained unclear exactly how EcSOD was having these effects. Therefore, we sought to elucidate potential mechanisms behind the tumor suppressive function of EcSOD, with a particular interest in TNBC. EcSOD is uniquely localized extracellularly and attached via its heparin binding domain on the cell surface. Therefore, we hypothesize that EcSOD plays a unique role in regulating signaling by controlling ROS levels, since ROS is a well-established secondary messenger. To test this

hypothesis, we re-expressed EcSOD in a TNBC cell line and analyzed activation of receptor tyrosine kinases, which are located on the cell surface and ROS-sensitive. The results of this screen returned c-Met, a receptor that is overexpressed in 20-30% of breast cancer patients and is a prognostic indicator of poor survival. Due to the relatively poor expression of the c-Met ligand, hepatocyte growth factor (HGF), in cancer cells, we hypothesized that CAFs secreted HGF to activate c-Met on cancer cells. Furthermore, we hypothesized that the oxTME created by loss of EcSOD promotes a HGF/c-Met paracrine signaling axis between cancer cells and CAFs. Due to the high level of oxidative stress within the TME, we hypothesized that ROS may play a role in activation of fibroblasts.

Additionally, due to the effect of EcSOD on paracrine signaling between CAFs and BC cells, we sought to expand the role of the oxTME plays on additional cell types within the TME. The next most common cell type found within breast tumors is macrophages. Previous studies into macrophages focused almost entirely on the classically activated anti-tumor M1 macrophages, which are known to produce high levels of ROS to kill microbes. However, there was very little information on the alternatively activated pro-tumor M2 macrophages and how ROS affects them. Additionally, previous studies found that modification of the reduced and oxidized levels of glutathione, a key cellular antioxidant. Therefore, we hypothesized that there are inherent differences in how M1 and M2 macrophages produce and control ROS, which thereby modify their sensitivities to ROS manipulation allowing for targeting of the pro-tumor M2 macrophages. Furthermore, much like ROS contributing to activation of CAFs, we hypothesized that increased exogenous ROS levels would result in increased polarization to the pro-tumor M2 macrophage. To test this hypothesis, we utilized polarized human macrophages derived from primary human monocytes of healthy

donors to analyze any inherent differences between M1 and M2 macrophages. Furthermore, we utilized MnTE-2-PyP^{5+}, a MnP class redox-active drug currently in clinical trials, to assess its ability to modify macrophage polarization based on the assumption that it would be equivalent to re-expression of EcSOD in breast cancer cells. This study was done to provide initial data to further examine the role of the oxTME, caused in part by reduction in EcSOD levels, in controlling signaling between cancer cells and the surrounding stromal cells.

Finally, we sought to determine potential mechanisms of EcSOD loss in breast cancer patients. Based on previous data collected in our laboratory, we knew EcSOD was regulated in part by DNA methylation of its promoter in cancer cell lines compared normal breast epithelial cell lines and in a limited number of patient samples. We sought to expand upon this work by analyzing DNA methylation patterns of the EcSOD promoter compared to mRNA expression levels in a larger cohort of breast cancer patients. Due to differences in genome stability and methylation rate of breast cancer subtypes, we hypothesized that different subtypes of BC, specifically luminal B, would have higher levels of DNA methylation mediated suppression of EcSOD expression. We also hypothesized that EcSOD genomic deletion would be highest in TNBC, the subtype with the highest genomic instability. To test this hypothesis, we used patient samples from the Northern Great Plains Personalized Breast Cancer Program, which were initially collected for whole exome sequencing to identify specific genetic driver mutations, to examine the methylation status of key CpG sites within the EcSOD promoter. Furthermore, we used microarray expression data to examine any correlation between expression levels and promoter methylation.

CHAPTER 2:

Materials and Methods

2.1 Cells Lines and Culture Conditions

2.1.1 Cell Lines

Breast cancer cell lines, MDA-MB231 and MDA-MB468, were purchased from the American Type Cell Culture Collection (Manassas, VA, USA). A firefly luciferase expressing stable cell line, MDA-MB231.luc, was previously generated as described [405]. Stable EcSOD overexpressing MDA-MB231 cell line, Ec.20 were generated as previously described [142]. Reduction mammoplasty fibroblasts expressing human HGF (RMF-HGF) and their parental normal fibroblasts (RMF) were generated by Dr. Charlotte Kuperwasser (Tufts University, Boston, MA, USA) [406]. Primary human monocytes and Peripheral blood leukocytes (PBLs) were purchased from the UNMC Elutriation core after isolation and separation from human donor whole blood. Cells were tested routinely for mycoplasma contamination using the MycoAlert Mycoplasma Detection Kit (LT07-118, Lonza). Diphenyleneiodonium chloride (DPI) (Sigma #D2926), recombinant human Hepatocyte Growth Factor (EMD Millipore #GF116), MnTE-2-PyP (a kind gift from Dr. James Crapo), and N-acetyl cysteine (NAC, MP Bio #02100098) were all added to cells as indicated in their respective figures.

2.1.2 2D Culture Conditions

Human monocytes, PBLs, and MDA-MB231 were maintained in RPMI1640 containing 10% FBS and 1X Pen/Strep. MDA-MB468, RMF, RMF-HGF, and MDA-MB231 during co-culture with fibroblasts were grown in DMEM + 10% fetal bovine serum media and 1X Pen/Strep. All cells are maintained at 37ºC, 5% O_2.

2.1.3 2D Co-culture

For prolonged 2D co-culture between fibroblasts and cancer cells, 6 well transwell plates (3450, Corning) were used to allow for easier separation of each cell type. Fibroblasts (1×10^5) were grown in the bottom of a 6-well plate and 1×10^5 MDA-MB231 cells were seeded on the 0.4 uM polyester membrane of a transwell insert to prevent invasion of cancer cells through the membrane. Cells were co-cultured in DMEM + 10% fetal bovine serum media and 1X Pen/Strep. After 48h of co-culture, these two cell types were trypsinized, counted and seeded in subsequent co-cultures for a total of 4 passages.

2.1.4 3D Monoculture

Mammary epithelial cell were propagated in 3D culture using the 'on-top assay' as described [407]. Briefly, 4-chamber slides were coated with 150 uL of Matrigel (BD Biosciences, San Jose, CA, USA). While the matrigel was solidifying in the incubator, cells were trypsinized and counted. Single cells were then overlaid on the Matrigel at 2×10^4 cells per chamber in 350 µL of 3D culture media. The 3D culture media is DMEM/F12 with the following additives: 250 ng/mL insulin (I-6634, Sigma), 10 µg/mL transferrin (T-2252, Sigma), 2.6 ng/mL sodium selenite (40201, Sigma), 10^{10} M estradiol (E-2758, Sigma), 1.4×10^{-6} M hydrocortisone (H-0888, Sigma), and 5 µg/mL prolactin (559006, BioLegend) [142]. Cells were allowed to attach to the matrigel for 30 minutes. After attachment, an additional 350 µL of 3D culture media with 4% matrigel was added to the top of the cells gently to provide coating "on-top" of the cells for a final 2% matrigel concentration. The media was replaced every 3 days with 3D media containing 2% matrigel. Any solution containing matrigel was kept on ice until added to the plate to ensure that it would not prematurely solidify.

This protocol was also adapted to the µ-Slide angiogenesis with ibiTreat (#81506, iBidi USA, Fitchburg, Wisconsin, USA) using 10uL of matrigel coating the well and 2.5 x 10^3 cells per well overlayed in 40 µL of 3D media. After attachment, 10 µL of 10% matrigel solution in the 3D media to provide the 2% matrigel coating.

Breast cancers were also grown in 3D conditions using conditioned media from fibroblasts. The following are the adjustments to the protocol to collect and use the conditioned media. To generate the conditioned media, 5 x 10^4 fibroblasts were plated per well on a 24 well plate in complete media. On the following day, the media was changed to 1 mL of DMEM/F12 in 1% fetal bovine serum. After 48 hours, the media was collected and filtered through a 0.22 µm filter. The 3D media was prepared at 10x solution and diluted to 1x with the collected conditioned media. The new solution is called the 3D conditioned media. Breast cancer cells were seeded and grown in the 3D conditioned media.

2.1.5 3D Co-culture

The 3D co-culture method follows the 3D monoculture method with the following exceptions. The bottom of the chamber was coated with 100 µL of matrigel to prevent direct interaction with plate. The matrigel was allowed to solidify in the incubator for 30 minutes, while the fibroblasts were trypsinized and counted. To embed the fibroblasts into the matrigel, 3 x 10^4 fibroblasts were resuspended slowly in 100 µL matrigel per chamber of the 4-chamber slide. The matrigel and cell mixture was allowed to solidify for another 30 minutes in the incubator. Once solidified, 2 x 10^4 breast cancer cells were seeded on top of the matrix in 350 µL 3D media. After the cells are allowed to attach for 30 minutes, 350 µL of 4% matrigel in 3D media was added to the plate. The media was replaced every 3 days with 3D media containing 2% matrigel.

2.1.6 Generation of Catalytically Inactive Mutant EcSOD MDA-MB231 Cell Line

First, the catalytically inactive mutant EcSOD (N180A, R186A) was generated using primers designed by Dr. Briana Ormsbee Golden to create the N180A and R186A mutations. The *SOD3* was amplified into separate DNA segments using these two sets of primers: the first set (forward primer 5'-TCTTATACTTGGATCCATGCTGGCGCTACTGTGTTCC-3' and reverse primer 5'-GCCCGGCCCGCGTTCCCGGCCTCCACGCTGGC-3') and the second set (forward primer 5'-GCCGGGAACGCGGGCCGGGCGCTGGCCTGC-3' and reverse primer 5'-GCCGGGGCGGCCGCTCAGGCGGCCTTGCACTCG-3'). The vector pLVX-TRE3G-IRES (Takara Bio USA) was digested in the multiple cloning site 1 using the restriction digest enzymes BamHI (FD0054, ThermoFisher) and NotI (FD0594, ThermoFisher). The cut vector and two *SOD3* gene segments were joined using InFusion cloning system (Takara Bio USA).

The doxycycline-inducible catalytically inactive mutant EcSOD expressing MDA-MB231 (iMutEcSOD) were generated using the Lenti-X Tet-On 3G Inducible Expression System (Takara Bio USA). Briefly, this is a two-vector system. One vector expresses a doxycycline-sensing transactivator protein, while the other vector expresses the gene-of-interest in a dox-inducible manner. Lentiviral particles were generated by transfection of the Lenti-X HTX packaging mix and either the transactivator vector (pLVX-EF1α-Tet3G, Takara Bio USA) or the generated mutant EcSOD vector into LentiX-293T (Takara Bio USA). The virus-containing media was collected after 72 hours and filtered through a 0.45 µm filter to avoid cellular debris. MDA-MB231 were seeded on a 6 well plate at 3 x 10^5 in complete media. The virus-containing media (150 µL for the Tet3G virus and 150 µL for the mutant*SOD3* virus) was diluted with 700 µL of complete media with the addition of 10 µg/mL polybrene. The media on the MDA-MB231 cells was replaced with

this new mixture. The cells were transduced for 24 hours before replacement with complete media with puromycin (0.6 µg/mL) and G418 (1.2 mg/mL). Selection was maintained for two weeks before reduction to half concentration for maintenance. A non-transduced control well of MDA-MB231 was also treated with puromycin and G418 to ensure cells without the required virus were selected against and died. Mutant EcSOD expression was confirmed by addition of doxycycline (100 ng/mL) for 3 days in complete media. The media was collected and the cells were lysed with non-reducing lysis buffer. An in-gel SOD activity was performed on the media and lysate to confirm that there was no EcSOD expression. A Western blot was performed to confirm that EcSOD expression was induced with addition of doxycycline.

2.1.7 Macrophage Differentiation and Polarization

Polarization of macrophages was induced as described [408] with the following modifications. Primary human monocytes were purchased from the University of Nebraska Medical Center Elutriation core facility. The monocytes were seeded on tissue culture treated plates/dishes at 1000 cells/mm^2 growth area in complete RPMI (RPMI 1640 +10% FBS +1x Pen/Strep). Monocytes were differentiated and polarized to M1 macrophages with GM-CSF (100ng/mL, BioLegend #572904) for seven days to promote monocyte differentiation and growth. The media was replaced one to two times during those seven days. Before the media was replaced, the plates were washed twice with phosphate buffer solution (PBS) to remove any undifferentiated monocytes or contaminating PBLs. Then, the GM-CSF stimulated macrophages were polarized to M1 by addition of IFN-γ (20ng/mL, BioLegend #570204) and LPS (20ng/mL, Sigma # L6529) for 24 hours. Monocytes were differentiated and polarized to M2 macrophages with M-CSF (100ng/mL, BioLegend #574806) for 7 days to promote monocyte differentiation

and growth. Like M1 macrophages, the media was replaced, and the cells were washed one to two times during differentiation. Then, the M-CSF stimulated macrophages were polarized to M2 by addition of IL-4 (20ng/mL, BioLegend #574002) for 24 hours. After 24 hours of polarization both M1 and M2 macrophages were ready for down-stream applications.

2.1.8 Macrophage Trypsinization

Macrophages were removed from the cell culture surface via Accutase (Corning #25-058-Cl). Macrophages were washed with cold PBS. Then, macrophages were incubated at room temperature with Accutase for 30 minutes. Macrophages were gentle pipetted up and down to help remove cell from the cell culture plate.

2.2 Genetic Manipulation

2.2.1 Adenovirus Transduction

Cells were transduced with adenovirus using the following protocol. Cells were seeded to be ~90% confluent 24 hours. For example, 2.5×10^5 MDA-MB231 cells were seeded into one well of a 6-well plate. To ensure an accurate multiplicity of infection (MOI), an extra well of cells was seeded to count just before addition of virus. After 24 hours of seeding, cells were washed with serum free media twice. The extra well of cells were counted. The appropriate amount of virus was added to 600 µL of serum free media. The multiplicity of infection (MOI) of 50 was used. Cells were transduced for 24 hours. After transduction, the media was replaced with complete media. The cells were harvested after an additional 24 hours for downstream applications. Overexpression of

EcSOD and Nox4 was achieved by this protocol. AdEcSOD, AdNox4, and Ad5CMVempty (AdEmpty) were purchased from University of Iowa Vector Core Facility.

2.2.2 Silencing RNA Transfection

Transfection with siRNA was performed using Lipofectamine RNAiMAX reagent (ThermoFisher Scientific #13778030) following the manufacturer's protocol. Cells were seeded to 75% confluency the night before transfection. For example, 2 x 10^5 RMF-HGF cells were seeded in a 6-well plate. In a microcentrifuge, 9 µL of the Lipofectamine RNAiMAX reagent was diluted into 150 µL of Opti-MEM medium (ThermoFisher Scientific #31985088) and mixed gently. In a separate microcentrifuge tube, 10 nM of siRNA was diluted into another 150 µL of Opti-MEM and mixed gently. The diluted siRNA was then added to the diluted Lipofectamine RNAiMAX reagent mixture. The combined solution was mixed gently and incubated at room temperature for 5-10 minutes. The media was changed on the RMF-HGF cells from DMEM to 700 µL Opti-MEM. The 300 µL combined solution was then added to the cells dropwise to bring the total volume up to 1 mL. Cell was transfected overnight before the media was changed to fresh DMEM. The siRNA used were siNC#1 (Thermo Fisher Scientific #4390843) and the siNox4 (Thermo Fisher Scientific #4392420; ID#s224159).

2.3 Cell Lysis

Protein lysate was isolated from cells using two different buffers, the denaturing RIPA buffer and the non-denaturing lysis buffer. Cells were lysed in either buffer depending on the downstream applications. In general, the RIPA buffer was used for

Western blotting, while the non-denaturing lysis buffer was used for either Western blotting or activity assays.

The RIPA buffer was made using the following recipe; 10 mM trisaminomethane chloride (pH 8.0), 1 mM ethylenediaminetetraacetic acid, 0.5 mM egtazic acid, 1% Triton X-100, 0.1% sodium deoxycholate, 0.1% sodium dodecyl sulfate, and 140 mM sodium chloride. Before use of the RIPA buffer, 1 mM phenylmethane sulfonyl fluoride and 1x Halt™ Protease and Phosphatase Inhibitor Cocktail (ThermoFisher Scientific #78440) was added before use to inhibit proteases and phosphatases. Before addition of the RIPA lysis buffer, cells were washed with cold PBS twice. RIPA buffer was then added (~100 µL per well for a 6-well plate). While keeping the plate on ice, cells were scrapped using a plastic cell scrapper to one edge of the well and collected in a clean microcentrifuge tube. The lysate was kept on ice for an additional 30 minutes with vortexing every 10 minutes. Cell debris was pelleted by centrifuge at max speed for 15 minutes at 4 °C. The supernant was transferred to a clean microcentrifuge and kept at -20 °C for later use.

The non-denaturing lysis buffer was purchased from Cell Signaling (Cell Signaling #9803S) and diluted from 10x to 1x. Like the RIPA buffer, PMSF and Halt™ was added before use. The protocol for this buffer was largely similar to the RIPA buffer protocol with the one exception. Instead of vortexing the samples, the samples were sonicated for 10 seconds with a 30 second incubation on ice three times to ensure throughout lysis of both the cell and nuclear membranes.

2.4 Electrophoresis and Western Blotting

2.4.1 Western Blotting

Protein lysates were diluted with water, 4x NuPAGE™ LDS Sample Buffer (ThermoFisher Scientific #NP0007), and 10x NuPAGE™ Sample Reducing Agent (ThermoFisher Scientific #NP0004). The samples were boiled at 80 °C for 10 minutes. Samples were cooled on ice and spun down to collect precipitated droplets. The wells of Novex™ 4-20% Tris-Glycine mini-gels (ThermoFisher #XP04200BOX) were washed. After washing, 10 µg of reduced protein lysate were run at 150V in tris-glycine buffer until the dye front has run out of the gel. The gel was removed from the plastic mold and rinsed in deionized water. Once rinsed, the proteins were transferred to a PVDF membrane using an iBlot Dry Blotting transfer system for 6 minutes and 30 seconds on program P3. Proteins were also transferred using wet transfer using the Mini Gel Tank and Blot Module (ThermoFisher Scientific #NW2000) for one hour at 23 V at room temperature. The transfer buffer was tris-glycine in 20% methanol. Membranes were blocked by rocking in 5% dry milk in TBST for one hour at room temperature. Membranes were then probed overnight in the primary antibody that was diluted in 3% BSA TBST solution. After probing with primary antibodies, membranes were washed with TBST four times for 10 minutes each. After washing, membranes were probed with secondary antibodies conjugated to HRP for 1-2 hours in 5% milk or 3% BSA at room temperature. The secondary antibody was washed off the membrane with TBST for 10 minutes for four times. Protein quantity was measured using Classic Autoradiography Film (MidSci #BX57) exposed to membranes incubated in either SuperSignal™ West Pico (ThermoFisher Scientific #34577) or West Femto (ThermoFisher Scientific #34094) depending on protein quantity. The intensity of the protein bands were quantified using

ImageJ software (NIH). The list of primary and secondary antibodies is included in Table 2.1.

2.4.2 Electrophoresis for In-Gel Activity Assays

In-gel activity assays were performed to determine SOD or GPX activity of specific members of each protein family. The GPX and SOD activity assays were performed as previously described [409, 410]. Briefly, both assays rely on native polyacrylamide gel electrophoresis with different staining protocols. The native gel protocol is as follows. Native polyacrylamide gels were poured with 10% acrylamide for SOD assays and 8% acrylamide for GPX assays. The electrophoresis buffer (50 mM Tris pH 8.3, 5 mM EDTA pH 8.0, 0.34 M glycine) was pre-chilled to 4 °C. Samples were loaded on the gel (~40 µg of lysate for SOD assays and 100 µg of lysate for GPX assays) with an empty lane between the samples and the reduced kaleidoscope prestained protein standards (BioRad #1610375). Cu/ZnSOD migrates near the green band. MnSOD migrates near the pink band. EcSOD runs above the pink band. None of the GPX family members have been matched up to this ladder. Therefore, running an extra gel alongside to transfer and probe with antibodies is advised. Additionally, 0.5 units of bovine Cu/ZnSOD or 0.5 µg of bovine GPX (Sigma #G-6137) can be used as positive controls. An empty lane between the positive controls and samples is also advised. Lysates were mixed with a 10x sample loading buffer (50 mM Tris pH 6.8, 5 mM EDTA, 9.5 mL 100% glycerol, and small amount of bromophenol blue) and added to the wells. Gels were run at 80 mA for 3-4 hours at 4 °C to prevent protein degradation due to heat.

TABLE 2.1. Antibody list

The table includes all antibodies used throughout the dissertation. The source, concentration, and vendor of each antibody are also included in the list

Antibody	Company	Part Number	Concentration	Source
β-Actin	Sigma	A2066	1:5,000	rabbit
p-c-Met [D26] (Tyr1234/Tyr1235)	Cell Signaling	3077	1:1,000	rabbit
c-Met	Cell Signaling	4560S	1:1,000	rabbit
p-Erk1/2 (Thr202/Tyr204)	Cell Signaling	9101	1:1,000	rabbit
Erk1/2	Cell Signaling	9102	1:1,000	rabbit
GAPDH [14C10]	Cell Signaling	2118	1:5,000	rabbit
Gpx1 [13B2AF]	ThermoFisher	LF-MA0206	1:1,000	mouse
Gpx4 [EPNCIR144]	Abcam	ab125066	1:10,000	rabbit
Nox2 [EPR6991]	Abcam	ab129068	1:5,000	rabbit
Nox4 [UOTR1B493]	Abcam	Ab133303	1:1,000	rabbit
p47phox	Cell Signaling	4312	1:1,000	rabbit
RhoGDI	Santa Cruz	sc-360	1:5,000	rabbit
SOD1	[411]		1:5,000	rabbit
SOD2	[411]		1:5,000	rabbit
SOD3	A kind gift from Dr.	National Jewish Medical and	1:5,000	rabbit
p-Stat3 (Tyr705)	Cell Signaling	9145	1:1,000	rabbit
Stat3 [79D7]	Cell Signaling	4904	1:2,000	rabbit
Anti-rabbit HRP	EMD Millipore	AP187P	1:20,000	goat
Anti-mouse HRP	Proteintech	SA00001-1	1:5,000	goat

SOD activity assays were incubated in solution A (2.5 mM nitro blue tetrazolium chloride) for 20 minutes rocking at room temperature in the dark. After incubation in solution A, the gel was incubated in solution B (28 mM TEMED, 28 µM riboflavin-5'-monophosphate diluted in a 36 mM phosphate buffer pH 7.8). The gels were incubated on a light box while shaking to avoid precipitate settling on the gel. After five minutes, gels were incubated for an additional five minutes in fresh solution B. Once the gel begins to turn purple and the clear SOD bands became clear, solution B was replaced with deionized water. Gels were left on the light box in deionized water to enhance the signal to noise ratio. All stains were done in a glass container not a plastic one to reduce background.

For GPX activity assays, the gel was incubated in 1 mM reduced glutathione (Sigma #G-4251) in deionized water for 10 minutes 3 times. The gel was rocked during incubation to ensure even distribution of GSH. The gel was incubated deionized water contained 0.008% cumene hydroperoxide (Sigma #247502) for 10 minutes. The gel was rinsed with deionized water twice. The gel was stained simultaneously with two separate solutions; 2% ferric chloride and 2% potassium ferricyanide. The gel was mixed with freshly mixed dyes for a few minutes until clear bands appeared and the gel was stained dark green. All stains were done in a glass container not a plastic one to reduce background.

2.4.3 Receptor Tyrosine Kinase Array

Cell lysates were quantified by Bradford assay (Protein Assay, Bio-Rad, USA) and incubated with the PathScan RTK signaling kit array chip (#7949, Cell Signaling Technology, USA) according to the protocol provided by the manufacturer. Briefly, after incubation of the samples, biotin-labeled anti-pan-phospho-tyrosine antibodies and

specific anti-phospho-residue antibodies were used to detect phosphorylated proteins captured on each spot on the nitrocellulose membrane. After incubation with DyLight 680-linked streptavidin, the chip was washed, fully dried and imaged using a Li-COR Odyssey imager. The pixel density of the background was subtracted from the pixel density of each spot, and the average of duplicate spots was determined. Next, Signal intensity was calculated by the normalization of mean pixel density in each spot against the pixel density of the positive control.

2.5 Flow Cytometry

2.5.1 ROS Measurements

ROS was measured using dihydroethidium (DHE) (ThermoFisher Scientific #D1168), 2',7'-dichlorodihydrofluorescein diacetate (DCFH) (ThermoFisher Scientific #C400), and CellRox Deep Red reagent (ThermoFisher Scientific #C10422). Cells in single cell suspension were incubated in the dark with either DHE (10 µM), DCFH (10 µM), or CellRox (3 µM) for 40 minutes at 37°C in Hank's Balanced Salt Solution (HBSS). Cells were then diluted and washed with HBSS and strained to ensure single cell suspension. Fluorescence was measured via flow cytometry on a BD LSRII. For DHE, superoxide-enriched fluorescence was measured using the 405nm laser, while fluorescence induced by superoxide and non-specific ROS was measured using the 488nm laser. For DCFH and CellROX, the excitation was the 405nm laser and 633nm laser, respectively.

2.5.2 Surface Marker Expression

Cells in single cell suspension were counted and primary fluorescently tagged antibodies were added at a concentration of 5 µL antibody per $1x10^6$ cells in FACS buffer (1% BSA in HBSS without Ca^{2+}/Mg^{2+}). Cells were incubated in antibody mix for 30 minutes at room temperature in the dark. After diluting and washing in FACS buffer, cells were strained to remove cell clumps. Stained cells were measured using a LSRII flow cytometer. The antibodies used were FITC-CD80 (BioLegend #305205), PE/Dazzle-CD86 (BioLegend #305433), AlexaFluor647-CD163 (BioLegend #333619), BrillantViolet421-CD206 (BioLegend #321125), and Pe/Cy7-CD273 (BioLegend #345511). When used in combination with additional antibodies, single stain controls were used to compensate for bleed over between the fluorophores.

2.5.3 CFSE Cell Growth Measurements

Single cells were labeled with 7.5 µM carboxyfluorescein succinimidyl ester (CFSE) (BD Biosciences #565082) for 15 minutes in a 37 °C water bath in the dark. Cells were vortexed immediately after addition of CFSE to prevent uneven staining. Cells were diluted and washed with PBS. Cells were stimulated and grown for multiple days. The cells were then collected, washed, strained, and resuspended in FACS buffer. CFSE was measured using a LSRII flow cytometer using a 488nm laser.

2.6 Reverse Transcriptase and Quantitative PCR

2.6.1 Reverse Transcriptase

Total RNA was isolated using Quick RNA Miniprep (Zymo Research #R1054). Cells in a 6-well plate were lysed using 300 µL of RNA lysis buffer included in the kit.

The lysate was scrapped using an RNase-free cell scrapper and collected in an RNase-free microcentrifuge tube. RNA lysate was either frozen at -80 °C for later RNA isolation or RNA was immediately isolated. The Zymo-Spin™ columns were used to isolate RNA from the cell debris. Genomic DNA was digested by DNase treatment and rinsed away. RNA was eluted off the columns using RNase-Free water. RNA concentration and purity were measured using 2 µL of RNA on a NanoQuant Plate™ in the Tecan Infinite M200 PRO plate reader. After quantification, RNA was converted to cDNA using a High-Capacity cDNA Reverse Transcription Kit (ThermoFisher Scientific #4368813). The RNA was added to master mix of random primers, dNTPs, reverse transcriptase enzyme, and buffer. The final concentration of RNA was made to be multiples of 20 ng/µL up to 80 ng/µL to make it easier for use in quantitative real-time PCR (qRT-PCR).

2.6.2 Real-Time Quantitative PCR

Quantitative real-time PCR (qRT-PCR) was performed using Maxima SYBR Green (Thermo Fisher Scientific #K0221). RNA (40 ng) and primer pairs (µM) were diluted with water and SYBR Green master mix. Each primer pair and RNA sample were done in triplicate. The qRT-PCR was done on an ABI 7000 Fast machine. The fold change was calculated using the 2^(-ddCt) method using 18S as the reference gene. The primer pair sequences are found in Table 2.2.

2.7 Plate Reader Assays

2.7.1 Amplex Red Assay

Extracellular H_2O_2 production was measured using the Amplex Red Hydrogen Peroxide Assay kit (ThermoFisher Scientific #A22188). RMF and RMF-HGF fibroblasts

TABLE 2.2. Primer list for qRT-PCR

The list is of the primer sequences used during qRT-PCR throughout the dissertation. Both the forward and reverse primers for each gene are included in the 5’ → 3’ orientation.

Gene	Forward Primer 5’ → 3’	Reverse Primer 5’ → 3’
18S	CCTTGGATGTGGTAGCCGTTT	AACTTTCGATGGTAGTCGCCG
Catalase	TCCACTGTTGCTGGAGAATC	CGAGATCCCAGTTACCATCTTC
CCL18	AGCCAGGTGTCATCCTAA	CAGCTTCAGGTCGCTGATGTA
CD163	AGCATGGAAGCGGTCTCTGTGATT	AGCTGACTCATTCCCACGACAAGA
Cu/ZnSOD	AGGATGAAGAGAGGCATGTTG	ATGGTCTCCTGAGAGTGAGAT
CYBA	CGTCCTGCATCTCCTGCT	GTAGATGCCGCTCGCAAT
DuoxA1	CACATTGACCACAGGACTGC	CCAGCATGGGGTCTTCATCC
Duox1	ATGCTGCGGGACCACAATAG	CACTCTGGGAGAGGGACAGAT
FAP	TGTTTCGGTCCTGTCTATATGTG	CCCATCCAGTTCTGCTTTCT
Fibronectin1	GCTCCTGCACATGCTTTGG	TCTCTGTCAGCCTGTACATC
Gpx1	GGGCAAGGTACTTATCGAG	CTCGTTCATCTGGGTGTAGTC
Gpx4	AGATCAAAGAGTTCGCCGC	CTTGATGGCATTTCCCAGGAT
HGF	ATGTCAGCGTTGGGATTCTC	TCGGATGTTTGGATCAGTGG
IL-10	AGGCTGAGGCTACGGCGCT	TAGATGCCTTTCTCTTGGAG
IL-12b	ATTGAGGTCATGGTGGATG	TGATGTCCCTGAAGAAGC
MnSOD	GGCCTACGTGAACAACCTGAA	CTGTAACATCTCCCTTGGCCA
Nox1	GTTATGCACCCATCCAAAG	CTGGAGCAGAGGTCAAAGTAAA
Nox2	GGCTTCCTCAGCTACAACATCT	GTGCACAGCAAAGTGATTGG
Nox4	AACACCTCTGCCTGTTCATC	GATACTCTGGCCCTTGGTTATAC
Nox5	CACCCCTTCACCATCAGCAGT	AGTATCTCAGAGCCCTTGGACG
PDGFRα	TGCCTGACATTGACCCTGT	CCGTCTCAATGGCACTCTCT
SDF-1	GACCCAACGTCAAGCATCTC	CGGGTCAATGCACACTTGTC
SMA	GCGTGGCTATTCCTTCGTTA	TCAGGCAACTCGTAACTCTTCTC
TNFa	AGCCCATGTAGCAAACC	TATCTCTCAGCTCCACGCCA

(1.8x10^5 cells) were plated in a 12 well format for 48 hours. After washing with PBS, cells were incubated in 1mL of the Amplex Red reaction mixture consisting of 50µM Amplex Red reagent and 0.1 U/mL HRP in HBSS +Ca^{2+}/Mg^{2+}. For every measurement, 300µL (3 x 100µL) of the reaction mixture was removed from each sample and put into a 96-well black plate. The fluorescence product indicative of the amount of H_2O_2 produced was measured using a Tecan Infinite M200 PRO plate reader at excitation of 560nm and emission of 590nm. This assay was also done for macrophages and modified to a 24 well plate format.

2.7.2 GSH/GSSG Assay

Total (GSH) and oxidized glutathione (GSSG) levels were measured using the GSH/GSSG-Glo kit (Promega #V6611) following the manufacturer's protocol. In brief, this assay produces luminescence by coupling glutathione S-transferase with luciferase to produce light in a GSH-dependent manner. Cells were plated and lysed in 96-well white plate to measure total GSH levels (10,000 cells/well) or oxidized glutathione (20,000 cells/well). The cells were lysed using either the total glutathione lysis reagent or the oxidized glutathione lysis reagent that contains N-ethylmaleimide to block the reduced GSH from measurement. The cells are incubated at room temperature while shaking. After five minutes, luciferin generation reagent was added. The plate was shaken briefly and incubated for 30 minutes. After incubation, the luciferin detection reagent was added. The plate was shaken and incubated for 15 additional minutes. Finally, luminescence was measured using the Tecan Infinite M200 PRO plate reader.

2.8 Electron Paramagnetic Resonance Spectroscopy (EPR)

Superoxide levels were measured using 1-hydroxy-3-methoxycarbonyl-2,2,5,5-tetramethylpyrrolidine (CMH). CMH (200μM) was prepared in Krebs-Hepes Buffer (KHB) with deferoxamine (DF) and diethyldithiocarbamic acid sodium salt (DETC). After washing with KHB +DF/DETC, cells were incubated in CMH for 30 minutes at 37°C. Cells were scraped and resuspended before measuring the EPR signal in 100 μL of cell mixture. The EPR signal was measured using a Bruker E-Scan Table Top EPR spectrometer. The live and total cells were counted in 10 μL of cells using a TC20 Automated Cell Counter. The EPR signal was adjusted to the amount of signal per cell.

2.9 Collagen Contraction Assay

Human mammary fibroblasts were suspended (500,000 cells/mL) in a rat tail collagen I solution (2.2 mg/mL; BD Biosciences, San Jose, CA, USA) as described [412]. MEM (Invitrogen, Carlsbad, CA, USA) supplemented with 1.8 mg/mL $NaHCO_3$ (Sigma-Aldrich, St. Louis, MO, USA) and 2.3 mg/mL L-glutamine (Invitrogen) was used as a diluent and pH was adjusted with 0.22 M NaOH. For each replicate, 500 μL cell-collagen mixture was dispensed into a single well of a 24-well plate and incubated at 37°C for 1 hour to facilitate collagen polymerization. Next, the collagen gels were detached from the well using a pipet tip. Culture media (500 μL) was then added and plates were incubated at 37°C in a humidified, 5% CO_2–containing atmosphere. Images of the collagen matrix were taken at the end of contraction time point, and surface area was measured with ImageJ software (NIH).

2.10 Invasion Assay

The in vitro invasive properties of the breast cancer cells were performed using the BD Bio-Coat Matrigel invasion assay system (BD Biosciences) as previously described [141]. Briefly, 2 X 10^5 cancer cells in serum free media were seeded into the Matrigel inserts consisting with 8-um filter pores. After 16 h of incubation, the upper surface of the transwell chambers was removed with a cotton swab and cells that have invaded through the Matrigel were lysed with the Luc-Screen Extended-Glow Luciferase Reporter Gene Assay System kit (Thermo Fisher Scientific, # T1033) and analyzed for luciferase activity using the Tecan Infinite M200 Pro plate reader. In some experiments, invaded cells were counted after being fixed and stained using a crystal violet solution (2% crystal violet, 50% methanol, 10% acetic acid).

2.11 T Cell Activation Assay

Autologous T cells were procured as PBLs from the UNMC Elutriation Core after isolation from monocytes. T cells were labeled with 7.5 µM CFSE (BD Biosciences #565082) for 15 minutes at 37˚C. After washing, T cells were plated in empty wells or on top of treated macrophages after washing off treatment. Activation of T cells was achieved with anti-CD3 co-stimulation (OKT3, Biolegend #317302) at 0.1 ug/mL in RPMI with 10% FBS and Pen/Strep. The non-adherent T cells were washed out of the well using DPBS and re-suspended in FACS buffer before measuring CFSE using a LSRII flow cytometer.

2.12 MDA-MB231 Growth Assay

Conditioned media from treated and untreated macrophages was collected, spun down, and filtered. This media was stored at -80˚C until use. MDA-MB231.luc (MDA-

MB231 cells stably expressing luciferase) were plated in complete RPMI media in a 96 well white walled plate at a concentration of 2,000 cells per well. Conditioned media was added to the wells to make it a final concentration of 50% conditioned media. Luciferase activity was measured on day 1, 3 and 4, to assess cell growth over time in the various conditions. Luc-Screen Extended-Glow Luciferase Reporter Gene Assay system (ThermoFisher #T1035) was used according to the manufacturer's guidelines. Buffer 1 (50 µL) and buffer 2 (50 µL) were added directly to cells in 100 µL of culture media. Cells were mixed briefly and incubated for 10 minutes before measuring luciferase on a TECAN Infinite M200 Pro plate reader.

2.13 *In Vivo* Tumor Study

Eight-week-old female athymic nude mice were obtained from Harlan Laboratories Inc. (Indianapolis, IN, USA). The nude mice protocol was reviewed and approved by the Animal Care and Use Committee of the University of Iowa. Breast cancer cells (MDA-MB231.luc or Ec.20 at 1 X 10^6) were injected alone or co-injected with 3 x 10^5 mammary fibroblasts (RMF or RMF-HGF) into both sides of the 4^{th} mammary fad pads, in the presence of 50% Matrigel. Tumor growth was monitored weekly by bioluminescence imaging as previously described [142].

2.14 Patient Sample Preparation

Excess DNA samples collected through the Breast Cancer Collaborative Registry (BCCR) (IRB# 253-13 EP, PI: Dr. Kenneth Cowan) were used for pyrosequencing analysis. BCCR is a web-based biomedical data and biospecimen repository developed by the Fred & Pamela Buffett Cancer Center. The BCCR provides a critical platform for

the Northern Great Plains Personalized Breast Cancer Program (NGPPBCP) funded by The Leona M. and Harry B. Helmsley Charitable Trust. Seventy one locations across the U.S. including seven cancer centers in the Northern Great Plains that are actively enrolling patients on the BCCR. Formalin fixed tissue blocks collected from the cancer centers were sent to the FPBCC for centralized review. Specimens that are deemed adequate for whole exome DNA sequence studies were then sent to the tissue facility at the FPBCC for sectioning. Trained tissue technologist then performed macro-dissection on each specimen to concentrate the number of tumor cells and reduce the contamination of adjacent normal breast tissue. DNA isolation from the FFPE tumor specimens was performed by the Fred & Pamela Buffett Cancer Centers's Molecular Biology/High-Throughput Screening facility. DNA was extracted and purified using QIAamp DNA FFPE Tissue (QIAGEN) kits, quantified by Nanodrop 2000, followed by double-stranded DNA assessment using Qubit (3.0) dsDNA HS Assay kit (Invitrogen). Following the extraction of DNA from each patient's breast cancer, the quality and quantity of DNA in each sample is determined. RNAs were extracted by using the QIAGEN RNeasy FFPE kit. The gene array expression profiling was performed by Agendia Inc. USA.

2.15 *SOD3* Pyrosequencing

Only the DNA samples with available gene expression profiling data were used for the correlation analysis between the expression levels of *SOD3* and its promoter methylation pattern (N = 75 tumor samples and 14 normal tissues). Approximately 500 ng of breast tumor genomic DNA were treated with sodium bisulfite using the EZ DNA Methylation-Direct kit (Zymo Research, Orange, CA). This process deaminates unmethylated cytosine residues to uracil leaving methylated cytosine residues

unchanged. A 323 base pair region of the *SOD3* promoter was captured from each sample using PCR and custom designed primers: sense strand 5'-TGTTGTGTGTTGAAGGTTATTGGTTATA-3', anti-sense strand 5'-CAACTCCTCCAAAAAAACTTTCTCTCCT-3', and pyrosequencing primer 5'-TGTTGAAGGTTATTGGTTATAA-3'. Methylation percentage of each CpG (-19 to -108 relative to transcription start site) was determined using the PCR product generated using Roche Diagnostic Corporation (Indianapolis, IN) High Fidelity FastStart Taq DNA Polymerase kit and a Qiagen (Valencia, CA) Pyromark Q96 pyrosequencer according to manufacturer's recommendations. Along with the samples a positive (high methylation level) control, Roche Diagnostic Corporation (Indianapolis, IN) human lymphocyte genomic DNA was methylated using M. SssI (CpG) methylase kit (New England Biolabs, Ipswich, MA) and untreated Roche human lymphocyte genomic DNA served as a negative (low methylation level) control were sequenced to access proper sequencing performance. The area of the *SOD3* promoter examined includes the Sp1/Sp3 transcription factor binding site as previously described [413].

2.16 TCGA Database Analysis

Copy number and expression of *SOD3* within the Cancer Genome Atlas (TCGA) breast carcinoma samples were queried using the cBioPortal for Cancer Genomics multidimensional cancer genomics data sets search engine (http://www.cbioportal.org/).

2.17 Copy Number Variation Analysis

Copy number and expression of *SOD3* within the Cancer Genome Atlas (TCGA) breast carcinoma samples were queried using the cBioPortal for Cancer Genomics multidimensional cancer genomics data sets search engine (http://www.cbioportal.org/).

2.18 Statistical Analysis

All statistical analyses were done using three or more biological replicates unless otherwise stated. Statistical analyses were performed using GraphPad Prism 5 software. For some experiments, a single-factor ANOVA followed by post-hoc Tukey test was used to determine statistical differences between means. Statistical analyses were assessed using a two-tailed Student's t test. Statistical significance was achieved when $P < 0.05$. Unpaired t test or Mann-Whitney test was applied when comparing two groups. When comparing three or more groups, one-way ANOVA and post-hoc test were used. Spearman test was used for correlation analyses.

CHAPTER 3:

Extracellular Superoxide Dismutase Inhibits Hepatocyte Growth Factor-mediated Breast Cancer-Fibroblast Interactions

Data in this chapter have been published in the following manuscript:

Golden B. Ormsbee*, Griess B.*, Mir S., Fitzgerald M., Kuperwasser C., Domann F., Teoh-Fitzgerald M. Extracellular superoxide dismutase inhibits hepatocyte growth factor-mediated breast cancer-fibroblast interactions. Oncotarget. 2017; 8: 107390-107408.

*Contributed equally

3.1 Introduction

We have previously shown that expression levels of the extracellular form of SOD, (EcSOD or *SOD3*) is significantly down-regulated in a majority of breast carcinomas and its expression levels inversely correlated with clinical stage [142]. Overexpression of this antioxidant in breast cancer cells inhibited *in vitro* proliferation, clonogenic survival, invasion, tumor growth and metastasis [141, 142]. EcSOD is the only extracellular enzyme that scavenges superoxide ($O_2^{\bullet-}$) which is the essential first step in eliminating the downstream production of more potent ROS (e.g. H_2O_2, $^{\bullet}OH$, and $ONOO^-$). Considering its unique cell-surface localization and the fact that the substrate for EcSOD, $O_2^{\bullet-}$, crosses membranes poorly, loss of EcSOD is anticipated to promote an oxidative extracellular environment that will likely alter autocrine and/or paracrine signal transductions initiated at cell surface receptors.

Receptor tyrosine kinases (RTKs) such as the epidermal growth factor receptor (EGFR) have been shown to be ROS-sensitive or utilize ROS-dependent mechanisms for activation [414]. ROS can activate signal transduction pathways by oxidizing and therefore inhibiting the cysteine regions of the active sites of protein tyrosine phosphatases (PTPs), which promotes activation of tyrosine kinases. Recently, oxidative stress has also been suggested to be involved in activating c-Met signaling [415]. Therefore, loss of EcSOD expression and the resulting increase in extracellular $O_2^{\bullet-}$ is expected to promote HGF/c-Met signaling. Upon activation, c-Met undergoes phosphorylation that evokes a variety of oncogenic responses leading to increased proliferation, scattering and motility, invasion, survival, angiogenesis, and metastasis [416]. In breast cancer, c-Met is overexpressed in 20-30% of cases, and is a strong, independent predictor of decreased survival [417]. Moreover, several types of signal cooperation and cross-talk between c-Met and EGFR pathways have been

demonstrated in recent years [418]. This has driven the development of inhibitors that target c-Met as an anti-cancer strategy [419].

In addition to overexpression, c-Met activation can be promoted through mutations, or autocrine signaling in malignant cells. Mutations in c-Met that confer its constitutive activation independent of its ligand (hepatocyte growth factor, HGF) has been observed and autocrine upregulation of HGF has been reported in lung cancer [420]. However, breast cancer cells rarely express the c-Met ligand, but often acquire HGF from stroma fibroblasts or the cancer-associated fibroblasts (CAFs) via a paracrine interaction [421]. CAFs are now recognized to be one of the key players in the tumor microenvironment that not only supports cancer cells but also interacts with the other stroma cells such as macrophages and endothelial cells, in a community fashion, to promote cancer cell proliferation, survival, malignant progression, angiogenesis, and metastasis [422]. These fibroblasts differ from the normal quiescent fibroblasts in their activated phenotypes and their pro-tumorigenic secretory profile. Pro-inflammatory [423] and pro-oxidative [424] phenotype have also recently been associated with CAFs. Understanding factors that contribute to the paracrine HGF/c-Met signaling during cancer-fibroblast interactions will therefore have a positive clinical impact for c-Met overexpressing cancers.

The objective of this study is to determine the effect of EcSOD and oxidative stress on HGF/c-Met-signaling in breast cancer. We found that overexpression of EcSOD inhibited HGF-mediated c-Met phosphorylation and resulted in an inhibition of three-dimensional (3D) Matrigel growth of MDA-MB231. This antioxidant enzyme also inhibited HGF-mediated cancer-fibroblast interactions in our co-culture model. In a prolonged co-culture study where breast cancer cells were seeded for multiple passages with mammary fibroblasts, followed by re-isolation of individual cell types,

overexpression of EcSOD significantly suppressed the invasiveness of breast cancer cells that were pre-exposed to HGF-secreting fibroblasts, when compared to the parental MDA-MB231 cells. Concurrently, the isolated HGF secreting fibroblasts, which were co-cultured with EcSOD–overexpressing MDA-MB231 cells showed attenuated phenotype in their ability to promote naïve breast cancer cell invasion.

Furthermore, we have shown that upregulation of NADPH oxidase 4 (Nox4) contributes to the activated phenotype of HGF expressing fibroblasts, via promoting oxidative stress. Scavenging ROS with an SOD mimetic, MnTE-2-PyP significantly suppressed the HGF-stimulated 3D growth and invasion of MDA-MB231 cells. In addition, targeting the ROS-generating Nox4 enzyme inhibited the ability of activated fibroblasts to contract collagen matrix. Our *in vivo* study further showed that scavenging ROS with EcSOD in MDA-MB231 significantly inhibited HGF-mediated tumor growth in mice. Overall, our study indicates a contributing role of an oxidative tumor microenvironment in promoting an activated-phenotype of fibroblasts in addition to supporting HGF/c-Met signaling during cancer-fibroblast interactions.

3.2 Results

3.2.1 EcSOD Inhibits c-Met Phosphorylation

To determine if scavenging cell surface-generated ROS with EcSOD will affect the phosphorylation status of RTKs, we utilized PathScan® RTK Signaling Antibody Array Kit (Cell Signaling). As shown in Figure 3.1A, amongst the 28 RTKs screened, the most significant change is observed for c-Met phosphorylation (Pan-Tyr), where overexpression of EcSOD (Ec.20 cell line) drastically inhibited activation of this RTK

relative to its vector control MDA-MB231 cell line. Quantification of the pixel intensities is shown on the right bar graph (A), revealing a more than 85% decrease in c-Met phosphorylation in Ec.20 cells versus MDA-MB231. The array shown in Figure 3.1A also shows a down-regulation of c-Abl phosphorylation (pan-Tyr), a non-receptor tyrosine kinase which has recently been shown to be activated downstream of c-Met [425-427]. To further confirm that overexpression of EcSOD affects c-Met activation in MDA-MB231, we performed western blot analysis. Figure 3.1B shows that when cells were stimulated with a recombinant human HGF (rHGF), c-Met phosphorylation (at Y1234/1235) was significantly suppressed in Ec.20 cell line when compared to that of MDA-MB231 cells. Moreover, transient overexpression of this extracellular antioxidant using an adenovirus vector (AdEcSOD) at M.O.I. of 50 also resulted in an inhibition of c-Met activation relative to the control vector (AdEmpty) infected sample. To determine whether the superoxide scavenging activity of EcSOD is required for this inhibition, we overexpressed an inactive form of EcSOD where two critical residues were mutated as previously described [428]. The inactive EcSOD expression was generated to be expressed only under doxycycline induction and the cell line was named iMutEcSOD. When MutEcSOD cells were treated with doxycycline, we observed no alterations in c-Met signaling as shown on the right panel in Figure 3.1B. These data suggest that HGF/c-Met signaling is sensitive to ROS modulation. To further show that the inhibitory effect of wild type EcSOD on c-Met is not limited to MDA-MB231 cell line, we repeated the assay with another basal like breast cancer cell line, MDA-MB468 and demonstrated similar down-regulation of this signaling pathway (Figure 3.1C).

FIGURE 3.1. Overexpression of EcSOD inhibited c-Met phosphorylation and HGF-stimulated Matrigel growth of MDA-MB231 cells

(**A**) Cell lysates of the parental MDA-MB231 or an EcSOD overexpressing stable cell line (Ec.20) were screened for activation of a panel of receptor tyrosine kinases using the PathScan® RTK Signaling Antibody Array. A fluorescence image of the array chip revealing phosphorylation of c-Met and c-Abl in MDA-MB231 cells vs. EcSOD-overexpressing Ec.20 cells. Pixel intensities of the array signal is shown on the bar graph. (**B**) Left–western blot analysis confirming that either transient overexpression of EcSOD using adenovirus vectors (AdEcSOD) or stable overexpression in Ec.20 clones showed significant decreases in c-Met activation (phosphorylation at Y1234/1235). Cells were serum starved overnight followed by rHGF stimulation (50 ng/mL) for 15 min prior to cell lysate preparation. Right–Overexpression of inactive mutant EcSOD (N180A, R186A) did not affect c-Met activation in MDA-MB231 cells. Doxycycline (100 ng/mL) was used to induce the expression of the mutant EcSOD in iMutEcSOD cells. Cells were serum starved overnight followed by HGF stimulation (50 ng/mL) for 15 and 60 min prior to cell lysate preparation. Signal intensity of phosphorylated c-Met over total c-Met was analyzed by densitometry as shown. (**C**) Phosphorylation of c-Met (Y1234/1235) was also inhibited by EcSOD in MDA-MB468 cells. Cells were infected with AdEcSOD or AdEmpty for 24 hours prior to stimulation with 50 ng/mL of rHGF. Cell lysate was then harvested for western blot analysis after 15 min of stimulation. Representative blots from 3 independent experiments are shown. Signal intensity of phosphorylated c-Met over total c-Met and phosphorylated p44/42 over total p44/42 was analyzed by densitometry as shown. (**D**) Extracellular protein array analysis comparing the secreted factors in Ec.20 cultured media to that of the vector control MDA-MB231 cells. (**E**) EcSOD inhibited HGF-stimulated invasive morphology and growth in 3D co-culture. Top–Mammary fibroblasts (RMF or RMF-HGF) were embedded in Matrigel and breast cancer cells (MDA-MB231 or Ec.20) were seeded on top of the matrix as illustrated in the top panel. Bright field images showing the 3D growth of MDA-MB231 or Ec.20 cells when co-cultured with RMF-HGF for 4 days. Representative images of *N* = 3 separate experiments. Bottom–Cellular growth of breast cancer cells was quantified after 4 days of co-culture with a luciferase activity assay. RLU = Relative Light Units. Representative data from *N* = 3 separate experiments. Error bars = SD of 6 separate samples. (**F**) Catalytically inactive EcSOD did not affect the 3D morphology and growth of iMutEcSOD cells. Top–3D growth of iMutEcSOD in co-culture with RMF or RMF-HGF. 100 ng/mL of dox was used to induce the mutant EcSOD expression. Bottom–After 5 days of culture, cells were isolated from the matrix and counted for growth analysis. Error bars = SD of 4 separate samples. (**G**) Wild-type EcSOD but not the inactive mutant (N180A, R186A) inhibited breast cancer cells invasion, under the stimulation of RMF-HGF. Top–Representative Matrigel invasion of MDA-MB468 cells when EcSOD was overexpressed with AdEcSOD versus AdEmpty. Conditioned media (CM) harvested from fibroblasts (RMF and RMF-HGF) were used as chemoattractant. Invaded cells were analyzed after 20 hours of seeding. Data are mean ± SD of 3 separate samples. Bottom–Representative invasion of iMutEcSOD when the expression of an inactive mutant EcSOD was induced with 100 ng/mL of dox, in the presence of CM harvested from RMF and RMF-HGF. Data are mean ± SD of 3 separate samples.

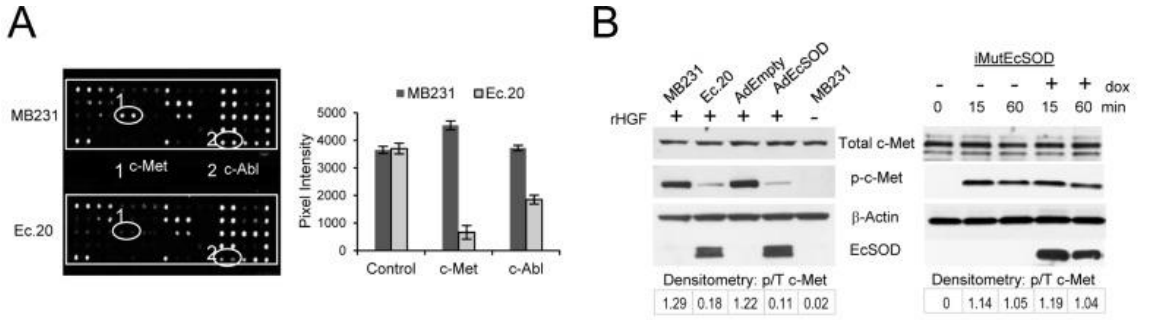
A
MB231
Ec.20
1 c-Met
2 c-Abl
MB231
Ec.20
Pixel Intensity
Control
c-Met
c-Abl
B
MB231
Ec.20
AdEmpty
AdEcSOD
MB231
rHGF
Total c-Met
p-c-Met
β-Actin
EcSOD
Densitometry: p/T c-Met
1.29 0.18 1.22 0.11 0.02
iMutEcSOD
dox
min
0 15 60 15 60
Densitometry: p/T c-Met
0 1.14 1.05 1.19 1.04

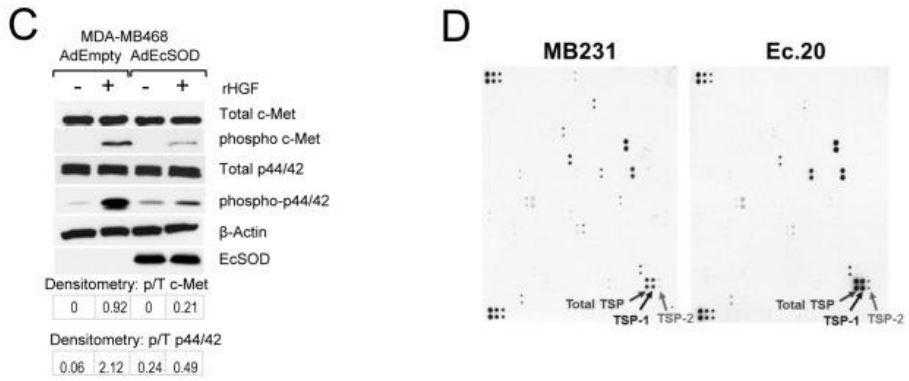
C
MDA-MB468
AdEmpty AdEcSOD
rHGF
Total c-Met
phospho c-Met
Total p44/42
phospho-p44/42
β-Actin
EcSOD
Densitometry: p/T c-Met
0 0.92 0 0.21
Densitometry: p/T p44/42
0.06 2.12 0.24 0.49
D
MB231
Ec.20
Total TSP
TSP-1
TSP-2

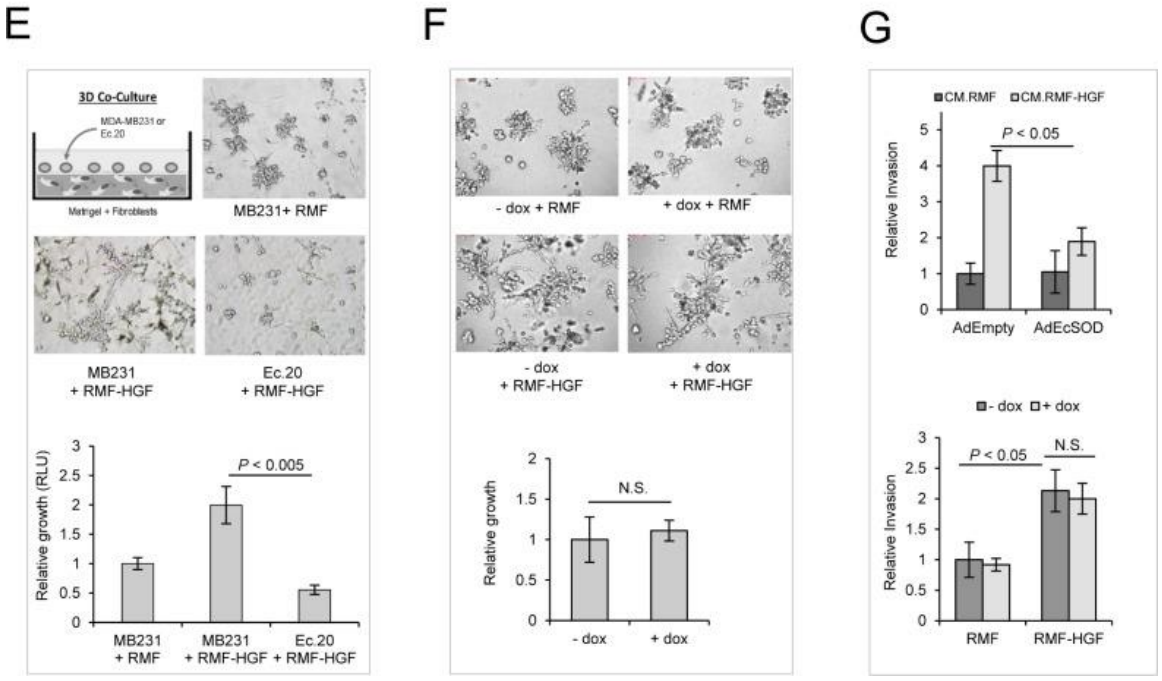
E
3D Co-Culture
MDA-MB231 or Ec.20
Matrigel + Fibroblasts
MB231+ RMF
MB231 + RMF-HGF
Ec.20 + RMF-HGF
Relative growth (RLU)
P < 0.005
MB231 + RMF
MB231 + RMF-HGF
Ec.20 + RMF-HGF
F
- dox + RMF
+ dox + RMF
- dox + RMF-HGF
+ dox + RMF-HGF
Relative growth
N.S.
- dox
+ dox
G
CM.RMF
CM.RMF-HGF
Relative Invasion
P < 0.05
AdEmpty
AdEcSOD
- dox
+ dox
P < 0.05
N.S.
Relative Invasion
RMF
RMF-HGF

3.2.2 EcSOD Upregulates Extracellular Thrombospondin Levels

To further determine whether EcSOD mediates suppression of c-Met signaling via an alteration of secreted factors, we performed an extracellular protein array analysis. As shown in Figure 3.1D, levels of thrombospondin-1 and 2 (TSP-1 and TSP-2) were significantly increased in conditioned media of Ec.20 compared to that of the vector control cells. Both TSP-1 and TSP-2 are anti-angiogenic and anti-metastatic factors that show inverse correlation with malignant progression in breast cancer [429, 430]. TSP-1 possesses a strong affinity for HGF [431] which mobilizes HGF away from the extracellular matrix and cell surface proteoglycans hence preventing its receptor binding [432]. Our results suggest that EcSOD inhibits c-Met activation partly through sequestering of its ligand via anti-angiogenic TSPs.

3.2.3 EcSOD Inhibits HGF-mediated Breast Cancer Invasive Morphology and Growth in 3D Culture

Since tumor stroma cells such as activated fibroblasts are the predominant source of HGF, we determined if EcSOD will affect the cancer cell-fibroblast interactions in the context of HGF stimulation. Here, we co-cultured MDA-MB231 cells with mammary fibroblasts that were generated to overexpress HGF (RMF-HGF) [406]. The parental fibroblasts, RMF are non-malignant fibroblasts isolated from reduction mammoplasty as described [406]. The 3D co-culture system (Figure 3.1E) shows that RMF-HGF greatly stimulated the growth and stellate formation of MDA-MB231 relative to the cells co-cultured with RMF. This stimulatory effect of RMF-HGF was inhibited in the presence of EcSOD, where Ec.20 cells showed stunted 3D growth with minimal stellate formation when co-cultured with RMF-HGF. Growth of MDA-MB231 and Ec.20 cells under the RMF-HGF stimulation was quantified using a luciferase activity assay and

presented on a bar graph in Figure 3.1E. The inactive mutant form of EcSOD on the other hand, did not affect the 3D stellate formation nor the growth of MDA-MB231, in the presence of HGF, as shown in Figure 3.1F. Moreover, overexpression of the wild type EcSOD with an adenovirus vector (AdEcSOD) suppressed the HGF-stimulated Matrigel invasion of MDA-MB468 cells (Figure 3.1 G-top panel), whereas the mutant EcSOD has no influence on the invasiveness of breast cancer cells, when conditioned media harvested from RMF-HGF fibroblasts were used as a chemoattractant (Figure 3.1G-bottom panel).

3.2.4 Prolonged Co-culture with EcSOD Overexpressing Breast Cancer Cells Attenuated Pro-invasive Phenotype of RMF-HGF

To determine the effects of scavenging extracellular ROS with EcSOD on the reciprocal interactions between cancer cells and activated fibroblasts, we performed serial passages of MDA-MB231 cells with mammary fibroblasts using a transwell co-culture chamber as illustrated in Figure 3.2A. After four passages, fibroblast-co-cultured MDA-MB231 and Ec.20 cells were isolated and tested for their invasiveness through Matrigel. Figure 3.2B shows that as expected, MDA-MB231 cells are more invasive after prolonged co-cultivation with RMF-HGF (CC.RMF-HGF) when compared to co-cultivation with RMF (CC.RMF). In contrast, invasiveness of Ec.20 cells was not affected by the pro-longed interactions with RMF-HGF (CC.RMF-HGF), suggesting that EcSOD inhibits HGF-mediated invasion of cancer cells.

In parallel, RMF and RMF-HGF were also isolated from the co-cultures and tested for their ability to promote breast cancer cell invasion. As shown in Figure 3.2A, fibroblasts were seeded into the bottom wells of invasion chambers where naïve MDA-MB231 cells were seeded on the Matrigel layer on the top inserts. The bar graph in

FIGURE 3.2. Prolonged co-culture with Ec.20 breast cancer cells inhibits pro-invasive phenotype of RMF-HGF

(**A**) Breast cancer cells were in-directly co-cultured with RMF or RMF-HGF for 4 passages using transwell chambers. Breast cancer cells were subsequently isolated and evaluated for their invasiveness through Matrigel as shown in (**B**). Fibroblasts were also isolated and examined for their ability to promote invasion of naïve MDA-MB231 cells (**C**). Error bars = SD of 3 separate samples, representative data from N = 3 separate experiments.

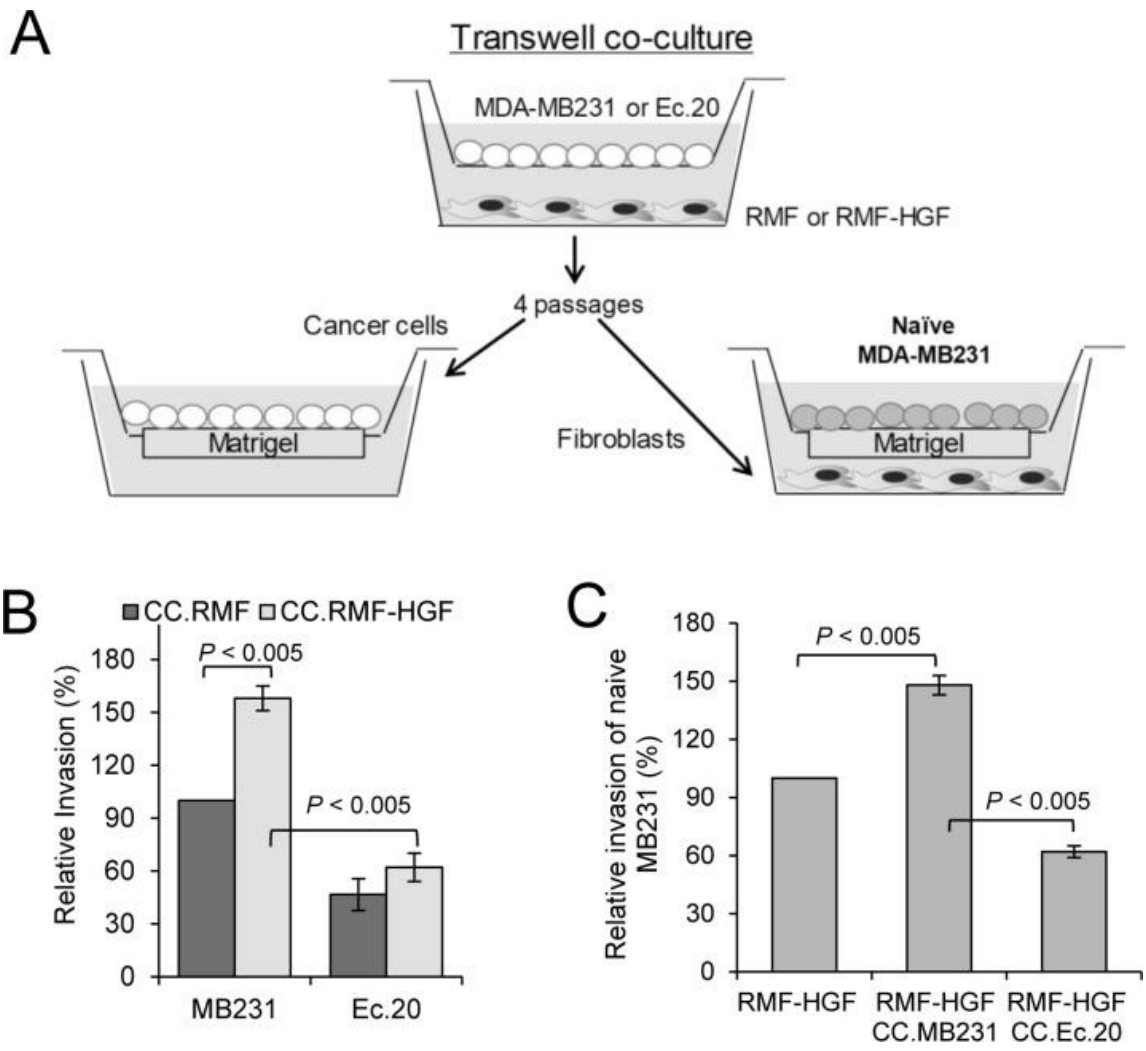
A
Transwell co-culture
MDA-MB231 or Ec.20
RMF or RMF-HGF
4 passages
Cancer cells
Naïve
MDA-MB231
Matrigel
Fibroblasts
Matrigel
B
CC.RMF
CC.RMF-HGF
Relative Invasion (%)
P < 0.005
P < 0.005
MB231
Ec.20
C
Relative invasion of naive MB231 (%)
P < 0.005
P < 0.005
RMF-HGF
RMF-HGF CC.MB231
RMF-HGF CC.Ec.20

Figure 3.2C shows that RMF-HGF that were pre-educated by MDA-MB231 in this co-culture system (CC.MDA-MB231) became more aggressive in their ability to promote breast cancer cell invasion when compared to the fibroblasts that have not been co-cultured with the cancer cells. This shows a reciprocal pro-oncogenic stimulation between the fibroblasts and the breast cancer cells. However, RMF-HGF that were co-cultured with Ec.20 cells (CC.Ec.20) exhibited suppressed ability of this process. These data imply that ROS are involved in regulating the reciprocal cancer cell-fibroblast interactions in the context of HGF/c-Met activation.

3.2.5 HGF Expressing Fibroblasts Exhibit Higher Levels of ROS and an Upregulation of NADPH Oxidase 4.

Since RMF-HGF shows an attenuated phenotype after the prolonged co-culture with Ec.20 cells (Figure 3.2C), we next determined if this oncogenic cytokine promotes oxidative stress in the activated fibroblasts. Figure 3.3A shows an increase in DHE oxidation in RMF-HGF when compared to RMF, indicating a higher level of $O_2^{\bullet-}$ generation in the HGF expressing fibroblasts. As expected, DHE oxidation decreased when RMF-HGF were treated with an SOD mimetic, MnTE. Despite performing the DHE oxidation assay using a more superoxide-specific setting at 405 nm excitation (instead of the non-specific 488 nm excitation) and 570 nm emission, as described [433], we have further determined the $O_2^{\bullet-}$ levels in the fibroblasts with electron paramagnetic resonance (EPR) spectroscopy. As shown Figure 3.3B, RMF-HGF indeed possess ~ 53% increase in superoxide-specific EPR amplitude per cell as compared to RMF. We also utilized another oxidative stress indicator, CellROX® reagent, which is sensitive to ROS modifications. An increase in CellROX oxidation further shows that HGF overexpression promoted generation of ROS in mammary fibroblasts and this increase in ROS was

FIGURE 3.3. RMF-HGF fibroblasts generate higher levels of ROS in comparison to RMF

(**A**) Intracellular $O_2^{\bullet-}$ level was quantified with DHE by FACS analysis in fibroblasts. Cells were treated with 15 uM of MnTE for 16 h prior to DHE labeling. Data are mean ± SD of 3 separate samples, representative data from *N* = 3 independent studies. (**B**) Representative electron paramagnetic resonance (EPR) spectroscopy analysis of $O_2^{\bullet-}$ using a superoxide-specific probe, 1-hydroxy-3-methoxycarbonyl-2,2,5,5-tetramethylpyrrolidine (CMH). Data are mean ± SD of 3 separate samples. (**C**) ROS level was determined using CellRox reagent. Fibroblasts were treated with NAC (5 mM) for 16 h prior to labeling cells with CellRox reagent. Representative data from *N* = 3 independent studies. Data are mean ± SD of 3 separate samples. (**D**–**F**) RMF-HGF show significantly increased levels of both the total GSH and the oxidized form, GSSG, when compared to RMF, resulting in a reduction in the GSH:GSSG ratio. Data are mean ± SD of 3 independent experiments. (**G**) Real time-PCR analysis shows an upregulation of Nox4 and CYBA in RMF-HGF vs. RMF fibroblasts. Data are mean ± SD of 3 independent experiments. (**H**) Representative superoxide-specific EPR analysis of RMF-HGF. Fibroblasts were exposed to CM harvested from Ec.20 versus vector control MDA-MB231 cells (V.1) for 48 hours. Data are mean ± SD of 4 separate samples. (**I**) Extracellular H_2O_2 levels as determined by Amplex Red assay. RMF and RMF-HGF were co-cultured (CC) with V.1 or Ec.20 cells for 48 prior. RMF-HGF were also treated with 10 μM of diphenyleneiodonium (DPI), a pan Nox and flavoprotein inhibitor, as a control. Data are mean ± SD of 3 separate samples.

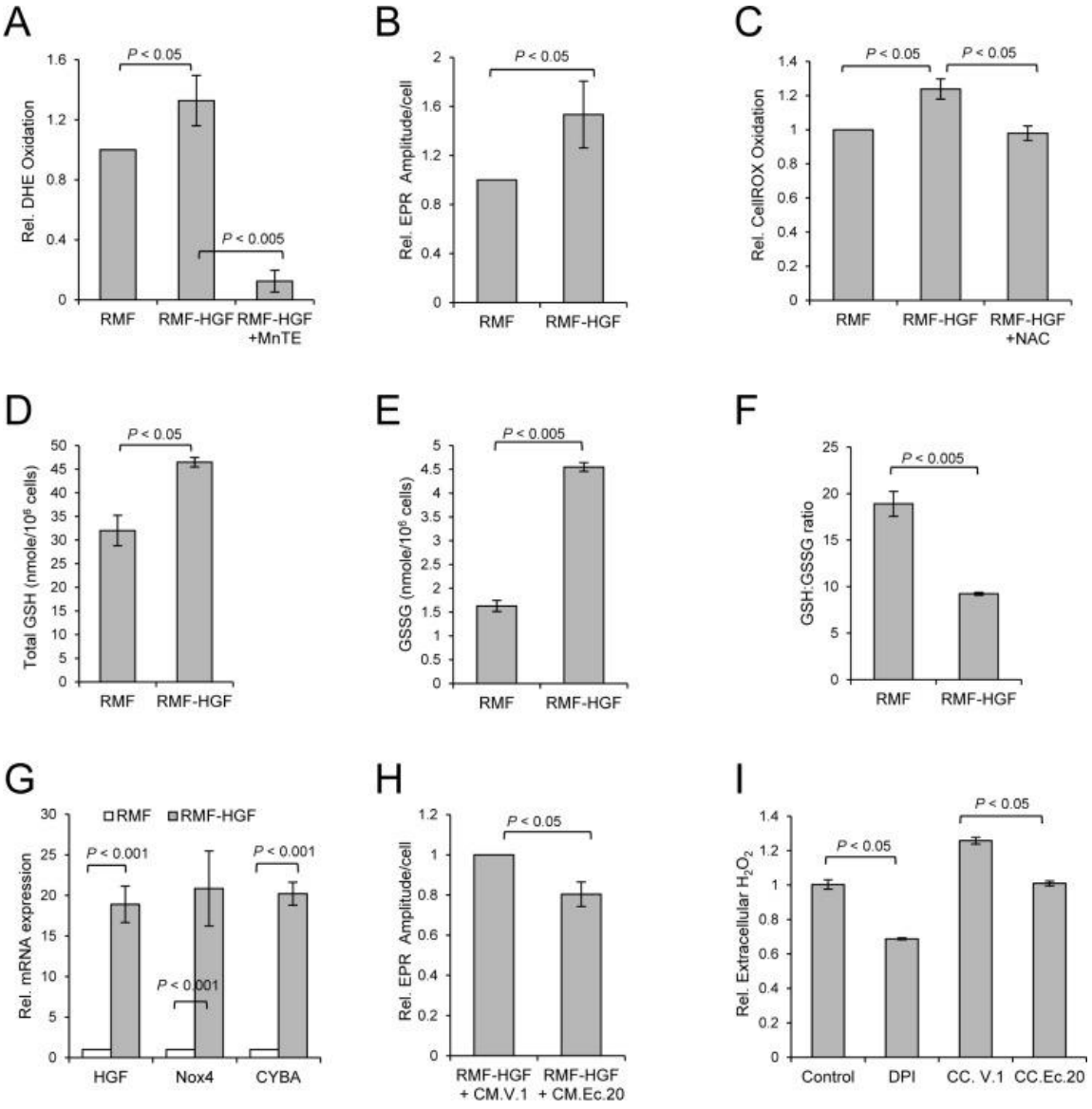
A
Rel. DHE Oxidation
P < 0.05
P < 0.005
RMF
RMF-HGF
RMF-HGF +MnTE
B
Rel. EPR Amplitude/cell
P < 0.05
RMF
RMF-HGF
C
Rel. CellROX Oxidation
P < 0.05
P < 0.05
RMF
RMF-HGF
RMF-HGF +NAC
D
Total GSH (nmole/10^6 cells)
P < 0.05
RMF
RMF-HGF
E
GSSG (nmole/10^6 cells)
P < 0.005
RMF
RMF-HGF
F
GSH:GSSG ratio
P < 0.005
RMF
RMF-HGF
G
RMF
RMF-HGF
Rel. mRNA expression
P < 0.001
P < 0.001
P < 0.001
HGF
Nox4
CYBA
H
Rel. EPR Amplitude/cell
P < 0.05
RMF-HGF + CM.V.1
RMF-HGF + CM.Ec.20
I
Rel. Extracellular H2O2
P < 0.05
P < 0.05
Control
DPI
CC. V.1
CC.Ec.20

reduced when cells were treated with an H_2O_2 scavenger, NAC (Figure 3.3C). In addition, cellular glutathione (GSH) levels were also analyzed as an overall indicator of cellular redox status. GSH is the most abundant antioxidant in aerobic cells and a decrease in the ratio of reduced to oxidized form (GSH:GSSG) indicates an increase in cellular oxidative stress, as often detected in cancer cells. We found that not only is GSH generation increased in RMF-HGF (Figure 3.3D), these fibroblasts also possess a close to 3-fold higher levels of oxidized GSSG (Figure 3.3E), resulting in a significantly reduced GSH:GSSG ratio (Figure 3.3F), when compared to that of RMF. Taken together, all of these indicate an increase oxidative stress in RMF-HGF versus RMF, due in parts to accumulation of $O_2^{\bullet-}$ and other ROS.

To gain insight into the mechanisms that promoted oxidative stress in RMF-HGF versus its parental fibroblast strain, RMF we profiled mRNA expression of a small panel of antioxidant related genes in these fibroblasts using TaqMan® Array Human Antioxidant Mechanisms kit. We found that CYBA (also known as p22phox) is highly upregulated in RMF-HGF when compared to the RMF. CYBA is an essential component of the membrane-associated enzyme NADPH-oxidases (Noxs), more specifically Nox1-4. An increase in expression of CYBA suggests that activation of Noxs is one of the contributing factors in promoting oxidative stress in RMF-HGF. We have indeed confirmed that there is a 20-fold increase in Nox4 mRNA expression in RMF-HGF versus RMF (Figure 3.3G), while no significant difference was observed in the mRNA expression levels of Nox1-3 (data not shown). This suggests that Nox4 is the predominant source of ROS in HGF-overexpressing fibroblasts.

To show the effect of cancer-fibroblast co-culture on cellular redox status of the fibroblasts, we determined the $O_2^{\bullet-}$ levels in RMF-HGF when cultured in the presence of conditioned media harvested from Ec.20 breast cancer cells. Figure 3.3H shows that

there was a significant reduction in superoxide-specific EPR amplitude in these fibroblasts in the presence of EcSOD-containing media. Since H_2O_2 can cross membrane, we also measured the extracellular levels of this peroxide as an indirect indicator of the cellular H_2O_2 levels. Figure 3.3I shows that the extracellular H_2O_2 levels of RMF-HGF were also significantly reduced, when co-cultured with Ec.20 breast cancer cells. These suggest that exogenous sources of EcSOD can regulate cellular redox status of RMF-HGF.

3.2.6 Nox4 Promotes Collagen Contraction Activity of Fibroblasts

To determine the effects of Nox4-generated ROS on the activity of fibroblasts, we performed collagen contraction assays where Nox4 was overexpressed in RMF using an adenovirus vector (AdNox4). This 3D collagen gel contraction is a standard assay utilized for functionally quantifying a contractile phenotype of activated fibroblasts. Figure 3.4A shows that the control adenovirus vector (AdEmpty) infected RMF showed similar contraction rate compared to the mock infected control sample. However, in the presence of Nox4, a reduction in the collagen disc area was observed, indicating an increase in collagen contraction activity of AdNox4 infected RMF. Figure 3.4B shows that when compared to RMF, HGF-overexpressing fibroblasts showed a significant increase in collagen contraction, indicating a more activated and aggressive phenotype of the RMF-HGF. In the presence of a Nox inhibitor DPI, RMF-HGF showed an attenuated ability to contract collagen. This suggests that ROS-generating Nox enzymes contribute to fibroblast activation. Since DPI targets the activity of all Noxs, we specifically inhibited Nox4 expression in RMF-HGF using a siRNA and observed that down-regulation of Nox4 also significantly impaired the ability of RMF-HGF to contract collagen (Figure 3.4C). Protein expression levels of Nox4 in these fibroblasts was

FIGURE 3.4. Nox4 promotes collagen gel contraction ability of fibroblasts

(**A**) RMF was induced to overexpress Nox4 with adenovirus vector (AdNox4 vs AdEmpty as a control). Collagen contraction activity of fibroblasts was then analyzed after 16 h of seeding the cells, where area of contracted collagen discs were quantified by Image J. The effect of Nox4 on contraction activity of RMF-HGF was determined by (**B**) inhibiting the ROS-generating activity of Nox4 with DPI and by (**C**) suppressing expression of Nox4 using a siRNA (siNox4 vs siNC#1 as a control). White bar marks 1cm in length. Representative images from *N* = 3 independent collagen contraction experiments. Error bar = SD of 3 separate samples. (**D**) Western blot analysis showing the expression levels of Nox4 in fibroblasts. Representative images from 3 independent experiments. (**E**) Nox4 knockdown in RMF-HGF down-regulates mRNA expression of myofibroblast markers. Real time PCR analysis of siRNA transfected RMF-HGF. Error bar = SD of 3 separate experiments.

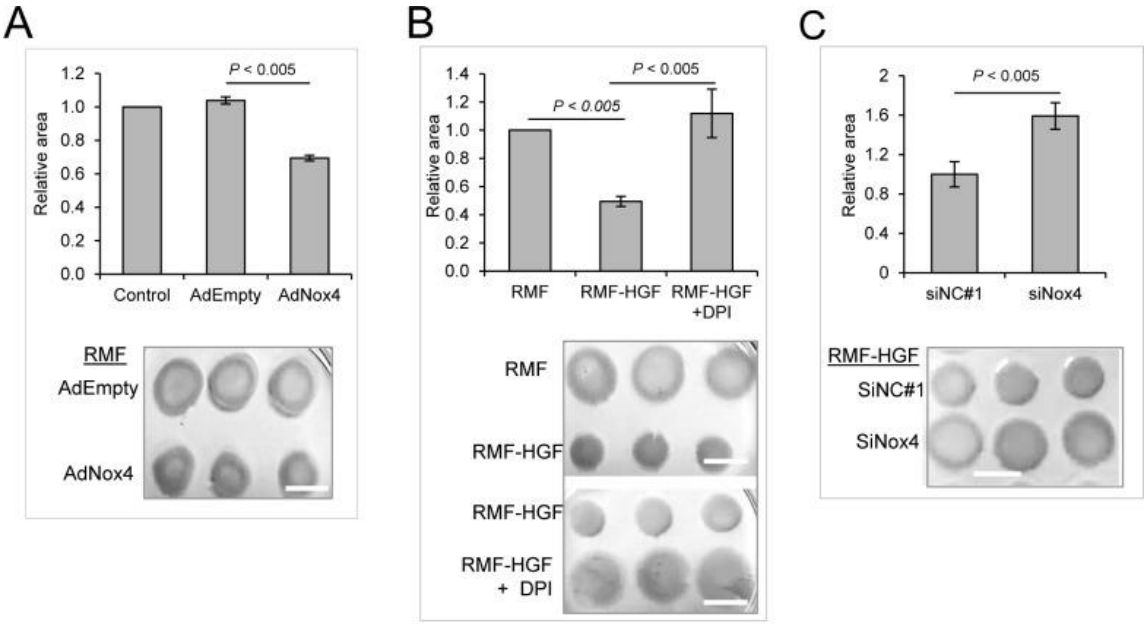
A
Relative area
P < 0.005
Control
AdEmpty
AdNox4
RMF
AdEmpty
AdNox4
B
Relative area
P < 0.005
P < 0.005
RMF
RMF-HGF
RMF-HGF +DPI
RMF
RMF-HGF
RMF-HGF
RMF-HGF + DPI
C
Relative area
P < 0.005
siNC#1
siNox4
RMF-HGF
SiNC#1
SiNox4

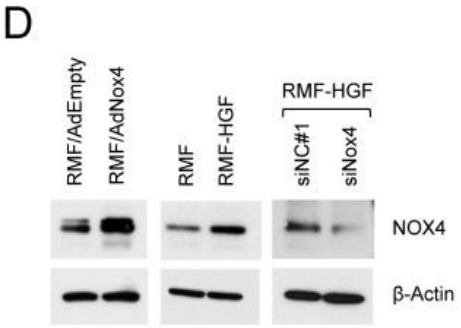
D
RMF/AdEmpty
RMF/AdNox4
RMF
RMF-HGF
RMF-HGF
siNC#1
siNox4
NOX4
β-Actin

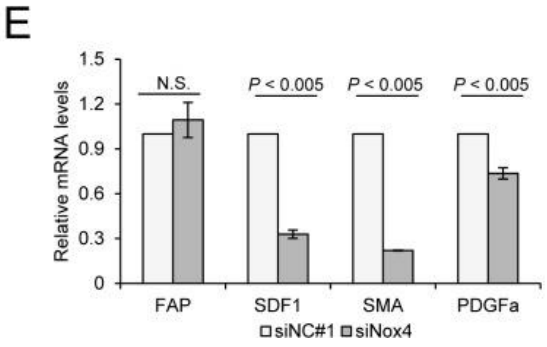
E
Relative mRNA levels
N.S.
P < 0.005
P < 0.005
P < 0.005
FAP
SDF1
SMA
PDGFa
siNC#1 siNox4

verified using western blot analysis as shown in Figure 3.4D. In addition to collagen gel contraction, we also evaluated the mRNA expression levels of some myofibroblast markers in Nox4-knocked down fibroblasts. Figure 3.4E shows that transfection with siNox4 down-regulated expression of stroma derived factor 1 (SDF1), smooth muscle actin (SMA), and platelet derived growth factor receptor alpha (PDGFRα) in RMF-HGF when compared to the control siNC#1 transfected cells. Together, this study indicates that Nox4 upregulation in RMF-HGF promotes an activated phenotype of the fibroblasts.

3.2.7 Scavenging ROS with an SOD Mimetic Inhibited HGF-mediated Growth and Invasion of Breast Cancer Cells

To further provide evidence that ROS contributes to HGF-mediated oncogenic stimulation, we treated breast cancer cells with an SOD mimetic, MnTE-2-PyP (MnTE). This compound has been demonstrated to effectively scavenge ROS [434]. We first stimulated 3D growth of MDA-MB231 with rHGF and observed that MnTE treatment inhibited the induction of breast cancer cell growth and stellate formation by HGF (Figure 3.5A). Next, we co-cultured breast cancer cells with RMF-HGF. In this co-culture, MnTE also greatly reduced the 3D colony sizes and invasive stellate formation of MDA-MB231 as seen in Figure 3.5B. Moreover, this inhibitory effect of MnTE is observed when cancer cells were stimulated with conditioned media harvested from RMF-HGF (Figure 3.5C). Cellular growth in conditioned media (shown in Figure 3.5C) was quantified using a luciferase activity assay and presented in Figure 3.5D. The antioxidant, MnTE inhibited HGF-mediated growth of breast cancer cells by 76% ($P = 0.017$). In addition to the 3D growth behavior, we also determined the effects of scavenging ROS with MnTE on HGF-mediated invasion of breast cancer cells. Figure 3.5E shows that while conditioned

FIGURE 3.5. Scavenging ROS with an SOD mimetic inhibited HGF-mediated 3D growth and Matrigel invasion of MDA-MB231

Growth of MDA-MB231 cells was stimulated with either rHGF (50 ng/mL, **A**) or in co-culture with RMF-HGF (**B**), or with conditioned media (CM) harvested from fibroblasts (C). Cells were treated with an ROS scavenger, MnTE-2-PyP (MnTE, 15 uM) for 4 days. Representative bright field images of *N* = 3. Quantitation of the proliferation of MDA-MB231 in (**C**) is shown in (**D**). After 4 days of culture with conditioned media from RMF or RMF-HGF, MDA-MB231 cells were lysed and luciferase activity was measured. (**E**) MDA-MB231 cells were seeded into Matrigel® invasion chamber and their ability to invade into conditioned media harvested from RMF or RMF-HGF in the present and absence of MnTE (15 uM) was analyzed. *N* = 3 independent studies. Data are mean ± SD of 3 separate samples. RLU = Relative light units.

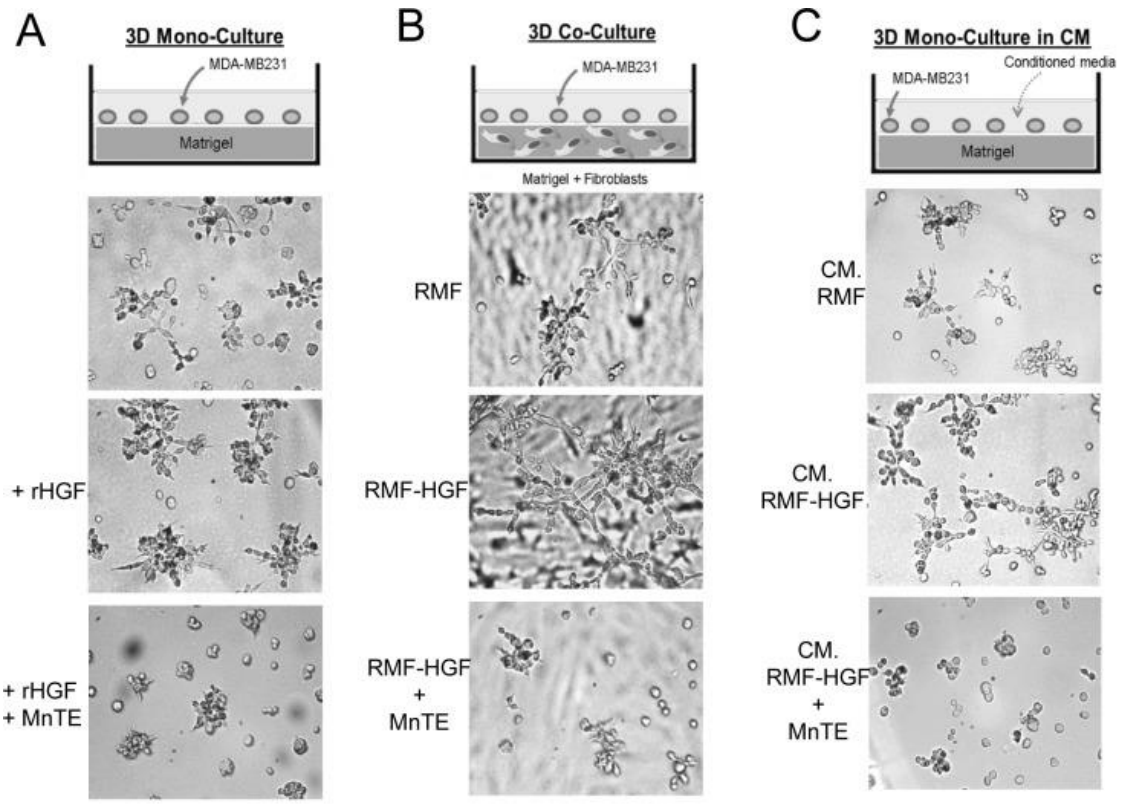
A
3D Mono-Culture
MDA-MB231
Matrigel
+ rHGF
+ rHGF
+ MnTE
B
3D Co-Culture
MDA-MB231
Matrigel + Fibroblasts
RMF
RMF-HGF
RMF-HGF
+
MnTE
C
3D Mono-Culture in CM
Conditioned media
MDA-MB231
Matrigel
CM.
RMF
CM.
RMF-HGF
CM.
RMF-HGF
+
MnTE

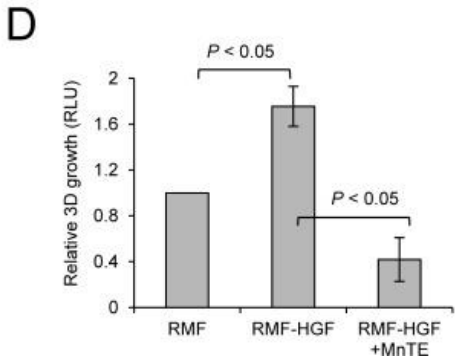
D
P < 0.05
P < 0.05
Relative 3D growth (RLU)
2
1.6
1.2
0.8
0.4
0
RMF
RMF-HGF
RMF-HGF
+MnTE

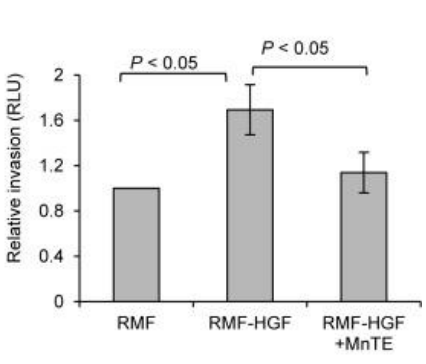
E
P < 0.05
P < 0.05
Relative invasion (RLU)
2
1.6
1.2
0.8
0.4
0
RMF
RMF-HGF
RMF-HGF
+MnTE

media from RMF-HGF promoted invasion of MDA-MB231, this stimulation was significantly reduced in the presence of MnTE. These studies reveal that HGF-mediated cancer cell-fibroblast interactions involve ROS and that administration of antioxidants can suppress the oncogenic HGF/c-Met signaling.

3.2.8 EcSOD Inhibited HGF-mediated Tumor Growth

To determine the regulation of HGF-stimulated tumorigenesis by ROS, we utilized an orthotopic mammary tumor model. RMF-HGF was co-injected with the cancer cells as the source of c-Met ligand as well as in providing a model for studying the tumor-fibroblast interactions. The top panel of Figure 3.6A shows the presence of the breast cancer cells following the mammary fat pad injection. After 6 weeks post injection, RMF-HGF greatly stimulated the primary tumor growth of MDA-MB231, as expected (bottom panel). In contrast, EcSOD overexpressing cells (Ec.20) were irresponsive to the growth stimulation by RMF-HGF. Quantitation of the primary tumor growth is presented in Figure 3.6B as determined by photon flux over time.

3.2.9 EcSOD is Significantly Under-expressed in Breast Carcinomas

To further evaluate the expression levels of EcSOD in breast carcinomas, we analyzed deposited Oncomine datasets. Differential expression analysis of breast carcinomas versus normal tissues showed that EcSOD (or *SOD3*) is significantly down-regulated in different types of breast carcinomas in two main datasets, TCGA and Curtis Breast (Figure 3.7A). Specifically, in invasive breast carcinomas, *SOD3* is ranked in the top 1% and 6% most significantly under-expressed genes as shown in the box plots in Figure 3.7B. The fold change of this gene is -5.475 in the TCGA and -2.654 in the Curtis

FIGURE 3.6. EcSOD suppresses HGF-stimulated tumor growth

(**A**) Bioluminescence imaging showing tumor growth of luciferase expressing breast cancer cell lines in athymic nude mice. At Day 0, 10^6 MDA-MB231 or Ec.20 cells were co-injected with 3×10^5 fibroblasts (RMF or RMF-HGF) into both sides of the 4^{th} mammary fad pads. Mice were imaged over time to monitor tumor growth as shown in representative images in (A) and the quantitation of the primary tumor growth is shown in (**B**). $N = 6$ per group. $^{*}P < 0.01$ Ec.20 + RMF-HGF vs. MB231 + RMF-HGF.

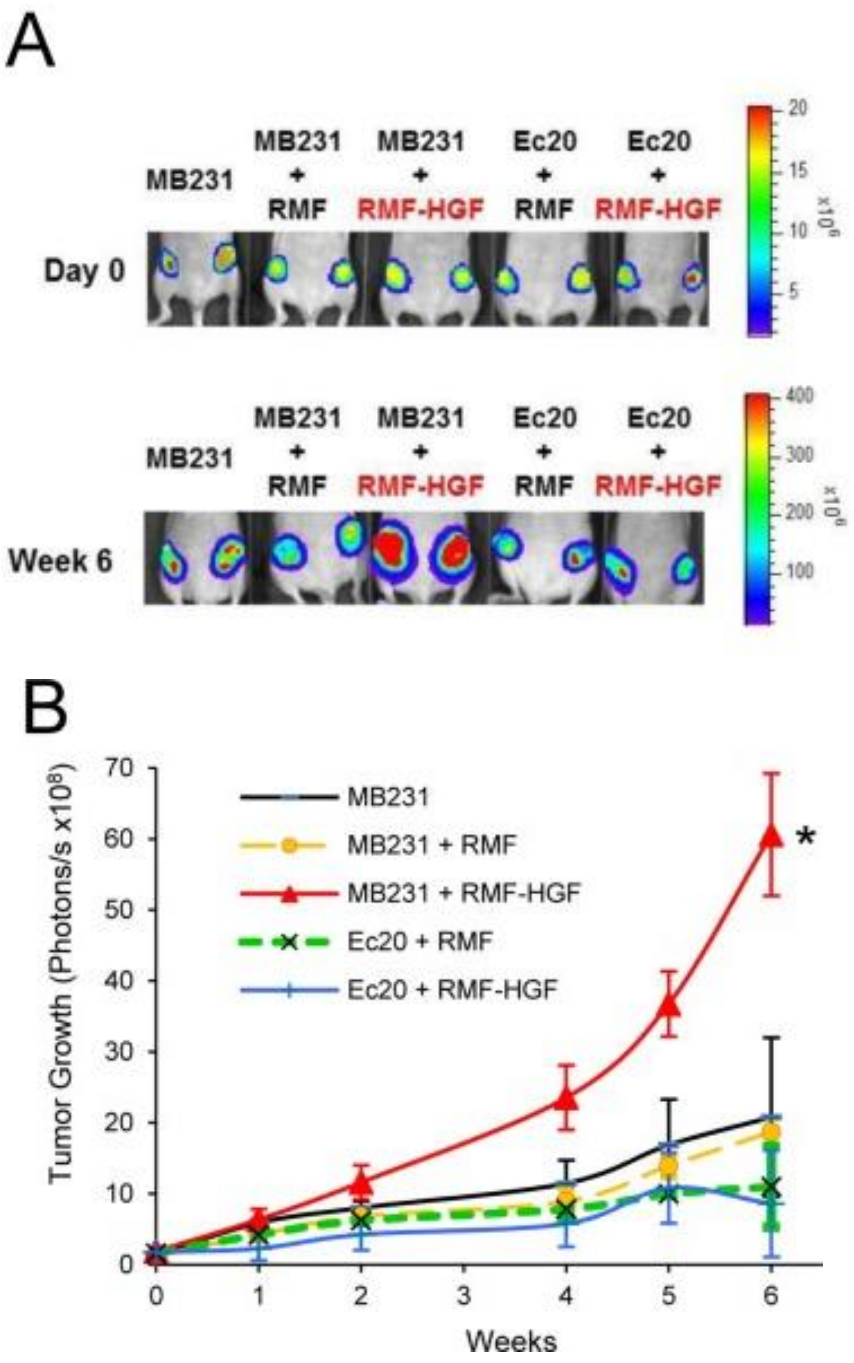
A
MB231
MB231 + RMF
MB231 + RMF-HGF
Ec20 + RMF
Ec20 + RMF-HGF
Day 0
Week 6
x10^6
B
Tumor Growth (Photons/s x10^8)
MB231
MB231 + RMF
MB231 + RMF-HGF
Ec20 + RMF
Ec20 + RMF-HGF
*
Weeks

FIGURE 3.7. Oncomine *SOD3* (EcSOD) gene analysis in breast cancer

(**A**) Comparison of *SOD3* expression across 14 breast cancer analyses. The heatmap represent the relative expression in patients with the indicated breast carcinomas compared with normal tissue. Blue indicates underexpression. The reported median rank and *P* value consider all indicated studies simultaneously. (**B**) Box plots derived from gene expression data comparing invasive ductal carcinomas to normal tissues from TCGA and Curtis studies. The number of samples in each group is indicated in brackets.

A

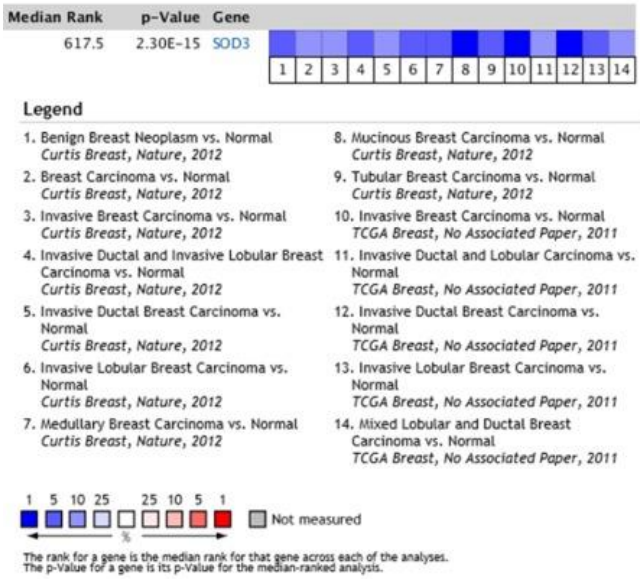
Median Rank
p-Value
Gene
617.5
2.30E-15
SOD3
1 2 3 4 5 6 7 8 9 10 11 12 13 14
Legend
1. Benign Breast Neoplasm vs. Normal
Curtis Breast, Nature, 2012
2. Breast Carcinoma vs. Normal
Curtis Breast, Nature, 2012
3. Invasive Breast Carcinoma vs. Normal
Curtis Breast, Nature, 2012
4. Invasive Ductal and Invasive Lobular Breast Carcinoma vs. Normal
Curtis Breast, Nature, 2012
5. Invasive Ductal Breast Carcinoma vs. Normal
Curtis Breast, Nature, 2012
6. Invasive Lobular Breast Carcinoma vs. Normal
Curtis Breast, Nature, 2012
7. Medullary Breast Carcinoma vs. Normal
Curtis Breast, Nature, 2012
8. Mucinous Breast Carcinoma vs. Normal
Curtis Breast, Nature, 2012
9. Tubular Breast Carcinoma vs. Normal
Curtis Breast, Nature, 2012
10. Invasive Breast Carcinoma vs. Normal
TCGA Breast, No Associated Paper, 2011
11. Invasive Ductal and Lobular Carcinoma vs. Normal
TCGA Breast, No Associated Paper, 2011
12. Invasive Ductal Breast Carcinoma vs. Normal
TCGA Breast, No Associated Paper, 2011
13. Invasive Lobular Breast Carcinoma vs. Normal
TCGA Breast, No Associated Paper, 2011
14. Mixed Lobular and Ductal Breast Carcinoma vs. Normal
TCGA Breast, No Associated Paper, 2011
1 5 10 25 25 10 5 1
%
Not measured
The rank for a gene is the median rank for that gene across each of the analyses.
The p-Value for a gene is its p-Value for the median-ranked analysis.

B

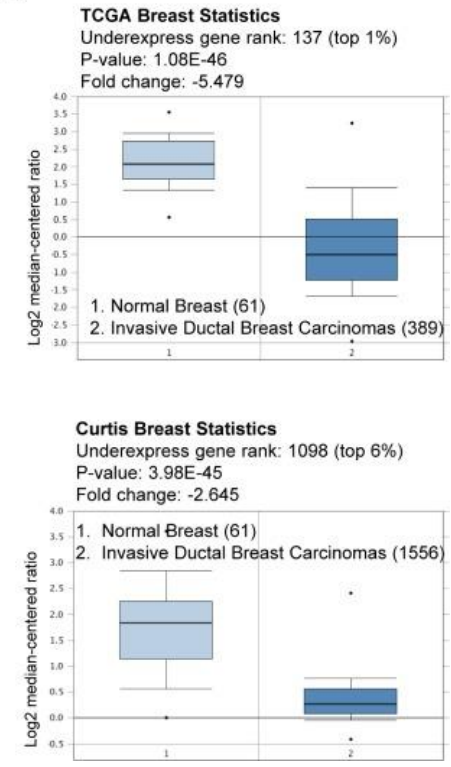
TCGA Breast Statistics
Underexpress gene rank: 137 (top 1%)
P-value: 1.08E-46
Fold change: -5.479
Log2 median-centered ratio
1. Normal Breast (61)
2. Invasive Ductal Breast Carcinomas (389)
Curtis Breast Statistics
Underexpress gene rank: 1098 (top 6%)
P-value: 3.98E-45
Fold change: -2.645
Log2 median-centered ratio
1. Normal Breast (61)
2. Invasive Ductal Breast Carcinomas (1556)

datasets.

3.2.10 Low EcSOD Expression Confers Poor Survival in Breast Cancer Patients

An integrative microarray data analysis using the Kaplan Meier Plotter [152] shows that low EcSOD expression is associated with significantly reduced relapse free survival in all breast cancer subtypes, including the basal-like (ER−, PR−, Her2−, CK 5/6+, and/or EGFR+) breast cancers (Table 3.1). Survival analysis was performed where restriction was set to exclude systemically untreated patients. The numbers of samples in each group are indicated in parentheses, and the hazard ratios (HR) and log rank p values are shown.

3.3 Discussion

A breast cancer genome-wide association study (GWAS) of the NCI Cancer Genetic Markers of Susceptibility project identified c-Met signaling as the second highest ranked pathway that may contribute to breast cancer susceptibility [435]. Since breast cancer cells primarily rely on their stroma fibroblasts for the c-Met ligand, understanding the contributing factors that fuel this reciprocal communication between cancer cells and their stroma partners will therefore, help in identifying novel targets for c-Met driven cancer. In this study, we identified c-Met as one of the RTKs regulated by an extracellular antioxidant enzyme, EcSOD in basal-like breast cancer cells via modulating the cellular redox status. Expression of this enzyme has been shown to be suppressed in a variety of cancers, including breast cancer [142, 165, 413]. Conversely, upregulation of EcSOD has been reported to inhibit both *in vitro* and *in vivo* growth as well as the oncogenic phenotype of breast cancer, prostate cancer, pancreas cancer, melanomas, and lung cancer [141, 158, 161, 162, 171, 172, 413], suggesting tumor

TABLE 3.1. Relapse free survival rate of breast cancer patients based on low versus high expression levels of EcSOD

Gene expression data and survival information are downloaded from GEO (Affymetrix HGU133A and HGU133+2 microarrays), EGA and TCGA (http://kmplot.com). Months shown are upper quartile RFS rate except for * which indicates median survival

	Low expression cohort (No. of patients)	High expression cohort (No. of patients)	Hazard Ratios (HR)	P values
All Subtypes	61* months (469)	173.2* months (1412)	0.46	1.00E-16
Luminal A	42 months (223)	97 months (638)	0.48	2.90E-08
Luminal B	43.9 months (149)	171.4 months (447)	0.42	4.00E-11
Her2+ve	16 months (33)	22.6 months (92)	0.57	5.30E-02
Basal-like	11.31 months (105)	30.42 months (194)	0.46	1.70E-05

suppressive effects of this antioxidant.

The oncogenic RTK, c-Met is one of the cell surface receptors known to be activated by ROS. Stimulation of lung cancer cells with exogenous ROS (i.e. H_2O_2) enhanced tyrosine phosphorylation of c-Met and activated its downstream signaling cascades in lung cancer cells [415]. In these same cells, an increase in ROS production was also observed when c-Met was activated by HGF treatment [415]. In addition, ROS-induced invasive activity of hepatoma cells has been demonstrated to be mediated through an autocrine/paracrine loop of HGF, where ROS directly augment mRNA expression of HGF [436]. Our study provides further evidence that a pro-oxidative environment is involved in activating and sustaining the oncogenic HGF/c-Met signaling and that re-expressing EcSOD in breast cancer cells inhibits HGF-stimulated oncogenesis. Further supporting an association of c-Met signaling with loss of EcSOD expression, a gene expression profiling study identified EcSOD as one of the genes that was down-regulated in both c-Met driven mouse liver tumors and human hepatocyte carcinomas, and that this change has a significant predictive power on overall and disease-free survival [437].

Although the second messenger role of ROS in cellular signaling is well recognized, it is not clear how EcSOD specifically regulates c-Met signaling amongst the other kinases screened in this study. Interestingly, phosphorylation of other RTKs such as EGFR, ERBB2, and FLT-3 have recently been shown to be promoted when EcSOD is overexpressed in thyroid cancer cells [169]. Despite increased phosphorylation of these RTKs, EcSOD overexpressing cells showed a reduced level of growth and migration signal transductions, through down-regulation of small GTPase regulatory genes [169]. The same study also showed a reduction of HGFR (or c-Met) phosphorylation in EcSOD enriched cells. The discrepancies between our RTK findings

with the exception of c-Met phosphorylation could be due to specificity issues related to the cell type examined and possibly also influenced by the dose-dependent effect of this ROS scavenger, as suggested by the authors.

In addition to c-Met, phosphorylation of c-Abl is also targeted by EcSOD in breast cancer cells (Figure 3.1A). This oncogene has been demonstrated to promote an aggressive phenotype of breast cancer cells [438]. Genetic and pharmacological knock-down of c-Abl impairs c-Met-triggered solid tumor formation *in vivo* and this kinase is required for c-Met-dependent cell scattering, tubulogenesis, migration, and invasion, through induction of Rho signaling [425]. In the same study, this kinase has also been demonstrated to promote the phosphorylation of c-Met at tyrosine residues required for engaging downstream signaling pathways, suggesting that down-regulation of c-Abl by EcSOD will block this feed-forward c-Abl→c-Met signaling and likely contribute to the overall suppression of c-Met signaling in breast cancer cells.

One mechanism by which EcSOD could inhibit c-Met signaling is by reducing bioavailability of its ligand HGF, via TSPs, as shown by our extracellular protein array analysis. Thrombospondin 1, TSP-1 is a well-known anti-angiogenic protein that elicits a variety of cellular processes, including a recently discovered role in maintaining dormancy of disseminated tumor cells [439]. The TSP-1 interactome is still not fully defined but HGF has been identified to be one of its ligands [440]. We have shown here for the first time that EcSOD expressing cells secrete higher levels of TSP-1 and TSP-2 (Figure 3.1 D). Not only is the function of HGF affected by TSP-1, the expression of this anti-angiogenic factor has also been shown to be down-regulated by HGF-c-Met interactions in breast cancer cells [441], indicating a negative regulatory circuit of TSP1 and HGF. Further supporting a regulatory effect of EcSOD on TSP-1, a microarray

expression analysis has identified TSP-1 as one of the growth suppressors upregulated by this antioxidant in thyroid cancer cells [169].

It is now well recognized that the progression from normal to benign, malignant, and metastatic, as well as therapeutic resistance is driven not just by what is happening inside the cancer cell but by reciprocal communication between the cancer cells and their stroma microenvironment. Our heterotypic co-culture studies indicate an ROS-mediated reciprocal interaction between cancer cells and fibroblasts (Figure 3.2). After a prolonged co-cultivation with CAF-like RMF-HGF, breast cancer cells showed a heightened aggressiveness in invasive properties and they also pre-educated RMF-HGF to increase their ability to promote breast cancer invasion. This symbiotic relationship is compromised when breast cancer cell overexpress EcSOD. The presence of EcSOD in breast cancer cells not only inhibited this RMF-HGF-stimulated invasion, but on top of that prevented the reprograming of RMF-HGF in their tumor-promoting phenotype. This suggests that an oxidative microenvironment is a contributing factor in regulating HGF-c-Met-mediated tumor stroma co-evolution. This is particularly important considering the fact that 86% of the aggressive basal-like tumors are positively correlated with the HGF signature [442]. Furthermore, among basal-like patients that are positive for the HGF signature, patients had worse overall survival [442]. These results emphasize the importance of HGF signaling in aggressive breast cancer, particularly the basal-like breast cancer. While some c-Met signaling can arise from an autocrine manner, the predominant activation mode of c-Met in breast cancer is through a paracrine tumor-stroma interactions. Immunohistochemitry analysis shows that the HGF/c-Met paracrine pattern is seen in 59.1% of tumors; and that this paracrine signaling is associated with a worse outcome when c-Met staining is more intense at the tumor front [443].

Cancer associated fibroblasts (CAFs) actively participate in the outcome of breast cancer by providing extracellular matrix components and secreting signaling factors that enhance cancer cell growth, survival, oncogenic progression, and metastasis. However, the intrinsic factor(s) contributing to the "activated" fibroblast phenotype of CAFs remains to be elucidated. A recent study showed that oxidative stress is necessary for triggering fibroblast activation in the pathological condition of fibrosis. NADPH oxidases (Noxs) are the predominant enzymes that produce $O_2^{\bullet -}$ on the plasma (and organelle) membrane and their activation has been linked to the etiology of cancer. Importantly, Nox4 is the only Nox that is expressed as an active enzyme. Thus, elevated Nox4 will lead to an increase in ROS generation. Nox4 has been suggested to play an important role in inducing fibroblast activation during fibrosis [444] in cardiac and pulmonary fibroblasts and in TGFβ-induced myofibroblast activation [445], but the role of Nox4 in CAFs is not known. Here we have shown that the HGF-induced activated phenotype of mammary fibroblasts involves Nox4-generated ROS (Figure 3.3 and 3.4). This explains the suppressive effects of EcSOD during co-cultivation of breast cancer cells with RMF-HGF as well as in our *in vivo* tumor model. Modulating the redox tumor microenvironment will therefore, not only inhibit the oncogenic c-Met pathway in cancer cells, but also target the activated phenotype of CAFs, thus suppressing their tumor-stroma interactions.

Despite the name implying that EcSOD is an extracellular antioxidant, the $O_2^{\bullet -}$ scavenging effect of this enzyme is not limited to cell surface and secreted compartment but more widely distributed to endocytic vehicles and nucleus. By harboring a heparin binding domain at its c-terminus, EcSOD interacts with cell surface heparin sulfate proteoglycan [446] once it is secreted. This interaction has been shown to be critical for the re-entry of this enzyme through a clathrine-mediated endocytosis [73] and its nuclear

tranlocation [75]. This feature renders EcSOD more readily available to cells or tissues that do not express this enzyme and internalization of exogenous EcSOD has been reported in mouse preadipocytes and endothelial cells [73, 447]. Here, the secreted EcSOD from Ec.20 cancer cells is also likely to be taken up by the co-cultured RMF-HGF, resulting in a decrease in $O_2^{\bullet-}$ levels of the fibroblasts (Figure 3.3H), thereby attenuating the tumor-promoting effects of RMF-HGF, as seen in Figure 3.2.

Although Nox4 has been historically considered as a superoxide generating enzyme, an increasing number of studies have reported that the major product of Nox4 is H_2O_2, although other studies have detected $O_2^{\bullet-}$ generation [120, 448-450]. It is plausible that some of the discrepancies may have resulted from non-specificity issues of the ROS detection reagents or that the $O_2^{\bullet-}$ produced (in membrane compartments) remains cryptic and inaccessible to assay reagents prior to its dismutation to form H_2O_2. Since the oxygen-reducing heme group at the catalytic site of Nox4 is an obligate one-electron donor, a direct formation of H_2O_2 without a $O_2^{\bullet-}$ intermediate is mechanistically implausible, implying that Nox4 is both a $O_2^{\bullet-}$ and H_2O_2 producers. This is supported by a recent study using cell-free isolated Nox4, where the authors found that approximately 80% of the product from the isolated Nox4 was detected as H_2O_2, while ~20% was detected as $O_2^{\bullet-}$ [448].

Since EcSOD catalyzes the dismutation of $O_2^{\bullet-}$ to H_2O_2, some may argue that EcSOD would exacerbate the H_2O_2 levels in Nox4-overexpressing RMF-HGF, and if so overexpression of EcSOD would not have inhibited but promoted c-Met signaling, which is known to be activated by H_2O_2 [415]. Whether overexpression of SOD can increase the production of H_2O_2 has been a hotly debated issue. Although some studies have attributed the consequences of SOD overexpression to this counter intuitive effect in increasing H_2O_2 levels, the views that SOD should elevate H_2O_2 formation merely

because it catalyzes an H_2O_2-producing reaction has been disputed. Liochev and Fridovich [451, 452] reasoned that an excess of SOD should decrease the steady-state levels of $O_2^{\bullet-}$ without increasing the endogenous formation of H_2O_2, at least *in vivo*. So it is doubtful that the inhibitory tumor-stroma effects seen with EcSOD overexpression in our current study, is due to an overproduction of H_2O_2. Moreover, the copper ion located in the catalytic domain of EcSOD are sensitive to H_2O_2 attack and by acting in a "suicidal mode", EcSOD can have peroxidase-like properties [121]. Our data showing a decrease in both cellular $O_2^{\bullet-}$ levels and the extracellular H_2O_2 levels in the co-cultures (Figure 3.3H and 3.3I) support the view that overexpression of this extracellular $O_2^{\bullet-}$ scavenger does not contribute to H_2O_2 accumulation.

Although H_2O_2 has long been the main focus as the ROS-mediated signaling molecule, partly due to it being a more stable and longer lived species than $O_2^{\bullet-}$, $O_2^{\bullet-}$ has recently been viewed as an important mediator of cellular effects. Superoxide affects both serine/threonine protein phosphatases (PPs) and protein tyrosine phosphatases (PTPs), by oxidizing the metal ion center of the former class of phosphatases and via nucleophilic attack of the cysteine residue in the later class [52, 53]. The rate of superoxide signaling has been estimated to be about 10-100 times higher than that of H_2O_2 signaling [54, 55]. In addition to being kinetically more efficient, $O_2^{\bullet-}$ is chemically more specific than H_2O_2 in this process as the catalytic site of PTP-1B is surrounded by positively charged residues [28]. This provides an efficient fine-tuning ability of $O_2^{\bullet-}$ in regulating signal transduction. Therefore, loss of EcSOD expression in cancer cells and the resulting increase of $O_2^{\bullet-}$ in the tumor will likely promote and sustain oncogenic signal transduction such as the c-Met pathway.

In comparison to the other two intracellular SODs, EcSOD is the new comer in terms of its tumor suppressive role in cancer and the mechanisms involved are less well

understood. The degree of differential expression of this antioxidant in cancer versus normal cells/tissues however, is more pronounced and prevalent than the other SODs in breast cancer. Oncomine gene expression signature analysis identifies EcSOD as one of the top 1% to 6% under-expressed genes in invasive ductal breast carcinomas versus normal tissues from both the TCGA and Curtis datasets (Figure 3.7). Down-regulation of EcSOD expression in cancer cells has been associated with epigenetic silencing, upregulation of oncomir microRNA-21, Ras oncogene-mediated gene silencing, chronic estrogen-induced gene suppression, single nucleotide polymorphisms, DNA copy number variation, and loss of heterozygosity as reviewed recently [453]. All of these observations imply that deregulation of EcSOD expression, distribution, or function provides a selective advantage in cancer cells. Furthermore, association of low EcSOD expression levels with poor relapse-free survival as shown in Table 3.1 underscores the importance of *EcSOD* as a potential tumor suppressor gene, inhibiting the progression of malignant phenotype in human breast cancer. However, the mechanisms of how EcSOD loss could promote oncogenesis is not fully understood.

Taken together, our study shows that ROS contributes to HGF-stimulated c-Met activation and that overexpressing the extracellular antioxidant enzyme, EcSOD suppresses this oncogenic cancer-fibroblast interaction. Modulating the redox tumor microenvironment not only inhibits the oncogenic c-Met pathway in cancer cells but also targets the redox-mediated activated phenotype of CAFs. ROS as merely a damaging bystander species that induce cytotoxic effects does not provide a complete picture of their biological effects. Rather, they should be considered as critical players in fine-tuning cellular signaling events in a temporal and purposeful manner in cancer. Future studies to unravel the specific modifications of signaling molecules/factors by $O_2^{\bullet -}$ and

H_2O_2 and how EcSOD regulates oncogenic signal transduction pathways will help to identify specific redox-mediators as potential cancer targets.

CHAPTER 4:

Scavenging Reactive Oxygen Species Selectively Inhibits M2 Macrophage Polarization and their Pro-tumorigenic Function in part via Stat3 Suppression

Data in this chapter have been published in the following manuscript:

Griess B., Mir S., Datta K., Teoh-Fitzgerald M. Scavenging reactive oxygen species selectively inhibits M2 macrophage polarization and their pro-tumorigenic function, in part via Stat3 suppression. Free Radical Biology & Medicine. 2019 (under revision)

4.1 Introduction

Macrophages are known to exhibit high plasticity which allows for dramatically different functions based on signals received from the microenvironment. In general, macrophages can polarize toward two extremes, the proinflammatory M1 and the immunosuppressive M2. The classically activated M1 macrophages are characterized by enhanced bacteria killing via an oxidative burst of reactive oxygen species (ROS), increased antigen presentation and phagocytosis, high IL-12 production, and promotion of a T_H1 response. Conversely, M2 macrophage are characterized by increased efferocytosis, high IL-10 secretion, high levels of scavenger receptors, such as CD163 and CD206, promotion of a T_H2 response, and immunosuppression. This is, however, an oversimplification of the complexity of macrophage polarization as recent studies indicate a much broader range of polarization states, such M2b, M2c, Mox, and M4, depending on the stimulating factor(s) within the milieu, as detailed in the these reviews [335, 336].

Macrophages are the most abundant immune cell in the tumor stroma and can account for up to 50% of tumor mass in breast cancer [454]. These tumor-associated macrophages (TAMs) are known to promote cancer cell growth, metastasis, and cancer cell evasion of the immune system [455]. Then unsurprisingly, TAMs are correlated with decreased survival in many types of solid cancers, such as breast, lung, and pancreatic, among others [348, 456-465]. While TAM are a heterogeneous population, they are mostly skewed toward a predominantly M2 phenotype [466]. The M2 surface marker, CD163, is correlated with poor patient survival, metastasis, and grade in breast cancer [349, 351, 467, 468]. Macrophage depletion in mouse models decreases tumor growth and metastasis [469-471]. Therefore, a further understanding of the M2 macrophages

polarization and function is required to develop therapies to target their detrimental effects seen in many different solid cancers.

During activation, M1 macrophages produce ROS via Nox2 to activate NF-κB, thereby stimulating phagocytosis and the inflammasome [472]. However, few studies have investigated the role of ROS in M2 polarization and function. Some studies suggest that M2 macrophages have key differences in ROS production and metabolism compared to M1 macrophages [472]. Promoting a pro-oxidative condition by lowering glutathione (GSH) levels has been shown to increase IL-10 and decreased IL-12 production in macrophages, indicative of a more M2 polarization state [367]. Conversely, increasing glutathione levels promoted M1 polarization as shown by an increase in IL-12 production and a decrease in IL-10 levels [367]. Therefore, the redox status of macrophages could be a contributing factor of macrophage polarization and function. Furthermore, butylated hydroxyanisole (BHA), a commonly used food preservative that prevents fatty acid oxidation, inhibits M-CSF mediated M2 polarization [368]. However, BHA also has off-target effects, such as disruption of the electron transport chain, which could also disrupt macrophage polarization [369]. Despite all the recent advancements in understanding macrophage biology, the direct role of ROS during TAM or M2 polarization and function remains unclear.

MnTE-2-PyP^{5+} (MnTE), also known as AEOL10113 and BMX-010, is a member of the manganese porphyrin (MnP) ring family of redox-active drugs. MnTE has been safely administered in preclinical models with very little negative side effects [278]. It is currently used in clinical trials for atopic dermatitis and plaque psoriasis. Additionally, an analog of MnTE, MnTnBuOE-2-PyP^{5+}, is also being tested as a radioprotectant in patients with multiple brain metastases, anal cancer, high grade glioma, and advanced head and neck cancer. MnPs were initially designed to mimic the activity of superoxide

dismutases (SODs). However, the small molecule MnPs lack the large protein bulk of SODs, which provide selectivity toward $O_2^{\bullet -}$ via steric hindrance. Thus, MnPs have a more promiscuous active site that can readily react with other reactive species, such as peroxynitrite and hydrogen peroxide [277]. Furthermore, recent evidence indicates that MnPs can act as a pro-oxidant in certain cancer cell lines and in tumor tissue. This effect is especially potent when MnPs are combined with high levels of intravenous ascorbate and/or radiation [279, 281, 282]. Interestingly, there is some circumstantial evidence that MnTE may affect macrophages in breast cancer. MnTE treatment in the 4T1 mouse model of stage IV breast cancer reduced macrophage infiltration, along with reduced levels of angiogenesis and metastasis, which are both processes induced by M2 macrophages [290]. This study provided rationale for determining the effect of MnTE on macrophage polarization and function directly.

Tumors are known to have a highly oxidative microenvironment compared to adjacent normal tissue, in part due to an increased ROS production from cancer cells [473]. The role of this highly oxidative tumor microenvironment on the interactions between cancer cells and the surrounding stromal cells is not clear. Particularly, the influence of this oxidative tumor microenvironment on TAM function is not known. Due to the high plasticity of macrophages and the key role they play in the immune response to cancer, we sought to determine the role of ROS on macrophage polarization and function. The objectives here were to characterize the redox profile in pro-tumorigenic M2 macrophages versus anti-tumorigenic M1 macrophages and to determine differences in their sensitivity to MnTE, with the goal of selectively targeting the M2 macrophages. We found that M2 macrophages showed an increase expression levels of some key antioxidant enzymes and lower levels of some pro-oxidants, when compared to the M1 macrophages, suggesting an increase ability to tolerate an oxidative

environment. Interestingly, despite the lower levels of ROS levels in M2 macrophages, these cells seem to require an optimum range of ROS to maintain their proper function and are more sensitive to ROS scavengers. Polarization of the M2 but not the M1 macrophages was attenuated by the redox-active drug, MnTE and the pan-Nox inhibitor, diphenyleneiodonium (DPI) [474]. These data suggest that the M1 macrophages can tolerate a wider range of ROS levels whereas the M2 macrophages are more vulnerable to alterations in cellular redox status. We have further shown that MnTE inhibited IL4-stimulated polarization of M2 macrophages by decreasing Stat3 activation. Consequently, MnTE treated macrophages showed reduced ability to promote breast cancer cell growth and T cell suppression. This study highlights a critical role of ROS in M2 macrophage function and implies that targeting the redox susceptibility of these macrophages could be a promising consideration for a more effective anti-cancer strategy.

4.2 Results

4.2.1 MnTE Reduces Expression Levels of M2 Markers

To determine the role of ROS during macrophage polarization, primary human macrophages were treated with MnTE during differentiation and polarization to M1 or M2. The changes to cellular morphology were the first indications this antioxidant affected macrophage polarization. When stimulated with M-CSF and IL-4, activated M2 macrophages showed an elongated morphology as demonstrated in Figure 4.1A, while M1 macrophages have a more rounded spherical cell shape. MnTE treatment inhibited

FIGURE 4.1. MnTE inhibits M2 polarization

Primary human macrophages were generated from isolated monocytes which were differentiated to macrophages and polarized to M1 or M2 types. The macrophages were analyzed 24 hours after polarization. (**A**) Representative phase contrast pictures of M1 and M2 macrophages treated with varying concentrations of MnTE. Expression of (**B**) M1 and (**C**) M2 mRNA markers in macrophages treated with or without 15 μM MnTE from 3 and 4 different donors, respectively. (**D**) A representative histogram of CD206 surface staining in M1 and M2 macrophages. (**E-F**) Box plots depicting flow cytometry analysis of M2 surface marker levels, (**E**) CD163 and (**F**) CD206, in M2 macrophages from 6 different donors treated with varying concentrations of MnTE. Relative values were calculated by comparing the change of MnTE treated samples to its untreated donor-specific control. Error bars are the standard deviation. Student t-test was used to calculate p-value with statistical significance being < 0.05. Symbols indicate significance between the treatment groups and M2 control (* < 0.05, $ < 0.005, # < 0.0005).

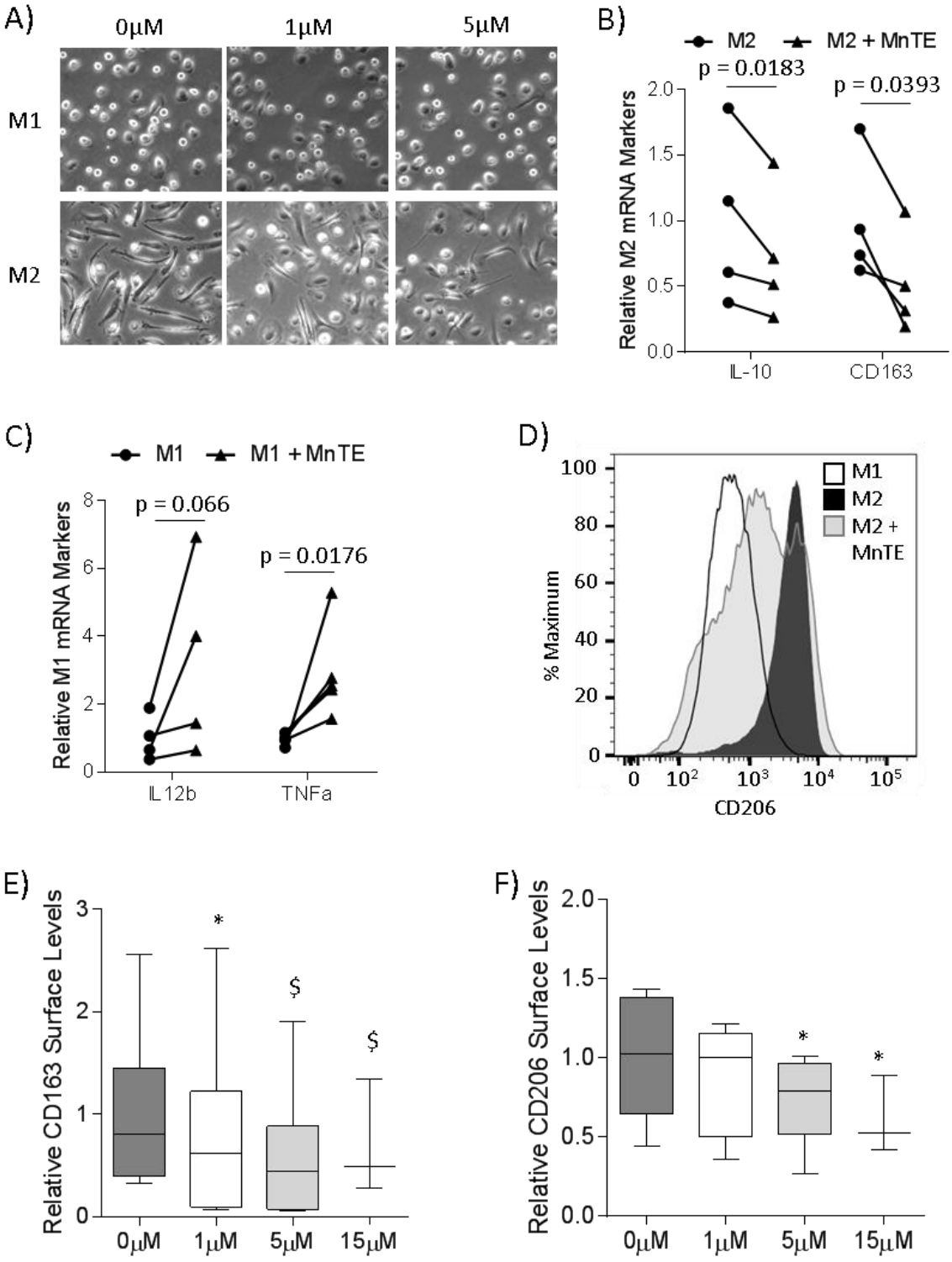
A)
0μM
1μM
5μM
M1
M2
B)
M2
M2 + MnTE
p = 0.0183
p = 0.0393
Relative M2 mRNA Markers
2.0
1.5
1.0
0.5
0.0
IL-10
CD163
C)
M1
M1 + MnTE
p = 0.066
p = 0.0176
Relative M1 mRNA Markers
8
6
4
2
0
IL12b
TNFa
D)
M1
M2
M2 + MnTE
% Maximum
100
80
60
40
20
0
0
10²
10³
10⁴
10⁵
CD206
E)
Relative CD163 Surface Levels
3
2
1
0
*
$
$
0μM
1μM
5μM
15μM
F)
Relative CD206 Surface Levels
2.0
1.5
1.0
0.5
0.0
*
*
0μM
1μM
5μM
15μM

the elongated phenotype of M2 macrophages in a dose-dependent manner (Figure 4.1A). The morphology of the MnTE treated M2 macrophages resembled that of the rounded phenotype in M1 macrophages. Contrary to the M2 macrophages, MnTE treatment did not affect the overall morphology of the M1 macrophages (Figure 4.1A). We then analyzed M1- vs. M2- specific marker expression in these macrophages and found that MnTE indeed decreased the mRNA expression of M2 markers, IL-10 and CD163 (Figure 4.1B). MnTE treated M1 macrophages had increased levels of the M1 marker, TNFα, as well as a trend toward an increase in IL12b, another M1 marker (Figure 4.1C). To further confirm the effect of MnTE on M2 polarization, we analyzed the surface levels of the M2 markers, CD163 and CD206. Flow cytometry analysis showed that both markers were significantly decreased in a dose-dependent manner with MnTE treatment (Figure 4.1D-F).

4.2.2 MnTE Inhibits M2 Macrophage Function *In Vitro*

We next determined the effect of MnTE on macrophage function. It is known that M1 macrophages inhibit the growth of cancer cells, while M2 macrophages promote cancer cell growth [475, 476]. Therefore, we isolated conditioned media (CM) from M1 and M2 macrophages with or without MnTE pre-treatment and examined its ability to affect cancer cell growth. As expected, MDA-MB231 breast cancer cells showed a decreased proliferation in the presence of CM isolated from the M1 macrophages, when compared to the CM from the M2 macrophages and unpolarized M0 macrophages (Figure 4.2A). While MnTE did not affect the ability of M1 macrophages to inhibit MDA-MB231 cancer cell growth, as shown in Figure 4.2B, CM from M2 macrophages pre-treated with MnTE significantly reduced cancer cell growth (Figure 4.2C). Since MnTE is still in the CM of treated macrophages, we assessed the effect of MnTE treatment alone

FIGURE 4.2. MnTE treatment inhibits M2-mediated cancer cell growth

MDA-MB231 breast cancer cells were grown in 50% conditioned media from M1 or M2 macrophages, with or without MnTE pre-treatment. (**A-C**) Line graphs depicting the relative growth of MDA-MB231 cancer cells in macrophage conditioned media from 4 different donors. (**A**) This line graph compares growth of MDA-MB231 in the control conditioned media (of unstimulated M0 macrophages) to M1 and M2 macrophages. (**B-C**). Line graphs depicting the effect of 5 μM MnTE pre-treatment on (**B**) M1 and (**C**) M2 macrophage conditioned media versus control conditioned media. (**D**) The relative cancer cell growth after 4 days in unconditioned media with the addition of varying MnTE doses. Error bars are the standard deviation. Student t-test was used to calculate p-value with statistical significance being < 0.05. P-values between MnTE pretreated conditioned media and their respective controls are indicated by lines between the different groups.

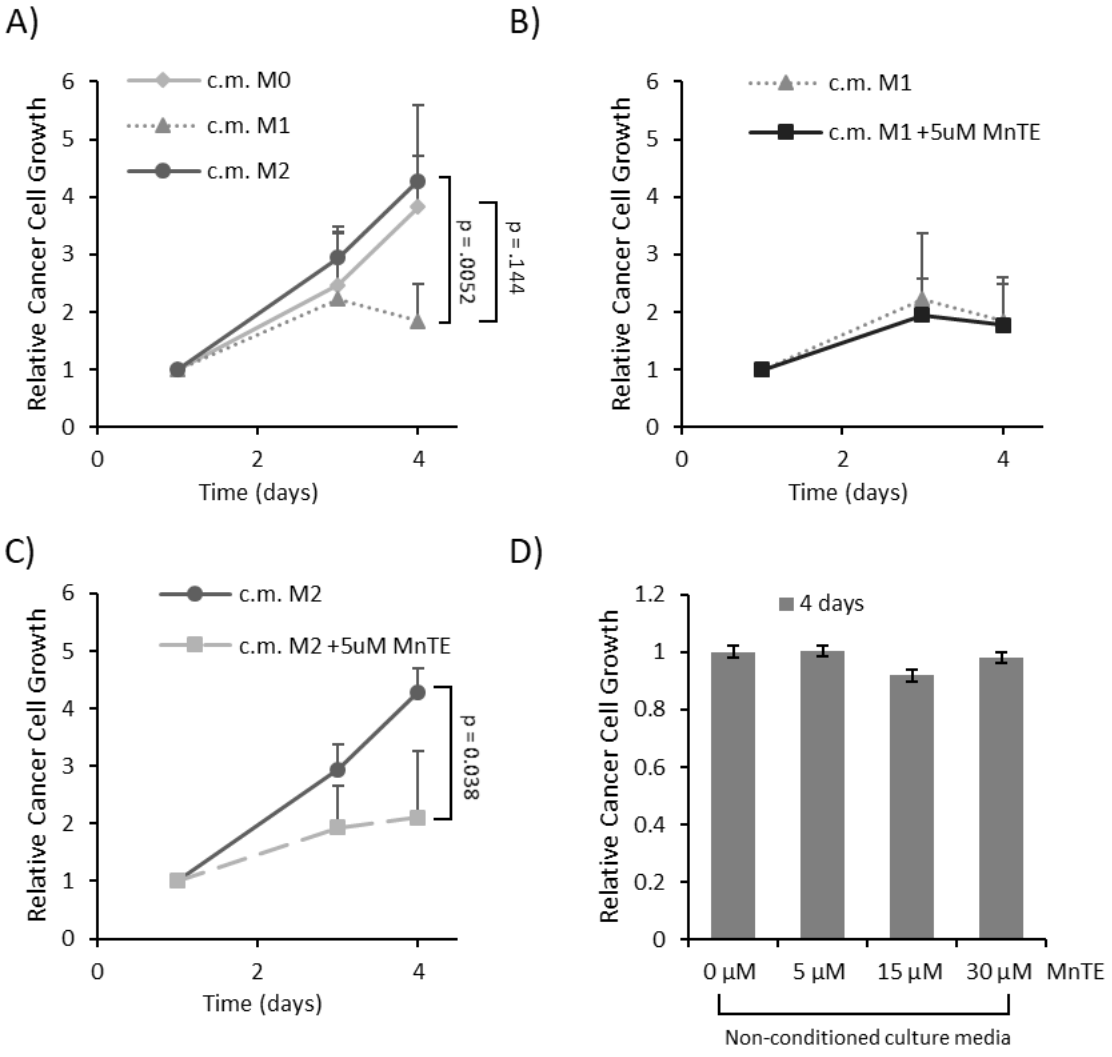
A)
B)
C)
D)
c.m. M0
c.m. M1
c.m. M2
c.m. M1 +5uM MnTE
c.m. M2 +5uM MnTE
4 days
Relative Cancer Cell Growth
Time (days)
p = .144
p = .0052
p = 0.038
0 µM
5 µM
15 µM
30 µM
MnTE
Non-conditioned culture media

on cancer cell growth over 4 days. Over this short time period, MnTE alone had no direct effect on the growth of breast cancer cells (Figure 4.2D). These data suggests that the growth inhibition of MnTE-treated M2 macrophages was due to changes to the macrophages not the effect of the drug alone. Thus, MnTE inhibits the M2 pro-tumor phenotype *in vitro*.

4.2.3 MnTE Inhibits M2-mediated T Cell Suppression

Next, we examined whether MnTE pre-treatment will affect the T cell suppressive function of the M2 macrophages. To do so, we utilized autologous T cells labeled with the fluorescent dye, CFSE, to track proliferation as a marker of T cell activation. The T cells were first stimulated with anti-CD3 to promote their activation. Then, macrophages were co-cultured with T cells where they provide the secondary signal that can promote or suppress T cell activation. M2 macrophages are known to suppress T cell activation in this method [477]. In figure 4.3A, a representative histogram indicates the activated T cell population as a leftward shift away from the unstimulated monocultured T cells. The histogram also shows that stimulated T cells co-cultured with M1 macrophages have more activated T cells than those co-cultured with M2 macrophages, as indicated by the higher peaks within the activated T cell bracket. The bar graph in figure 3B shows the results of four replicates from a representative donor. This experiment was repeated with similar results in two additional donors. As expected, anti-CD3 alone in the monoculture condition (mono) did not readily activate the T cells, while M1 macrophages activated T cells much better than their M2 counterparts. Furthermore, MnTE treatment, while having no effect on M1-stimulated T cell activation, dramatically reverted the T cell suppressive effect of the M2 macrophages (Figure 4.3B-C). MnTE pre-treated M2

FIGURE 4.3. MnTE inhibits M2-mediated T cell suppression

A T cell activation assay was performed to assess the ability of macrophages to modify T cell activation. Human peripheral blood lymphocytes (PBLs) were stained with CFSE to track their activation. PBLs were directly co-cultured with autologous control of pretreated macrophages and stimulated with anti-CD3. Flow cytometry was used to track the dilution of CFSE as a proxy for T cell activation. (**A**) A representative histogram of T cells comparing unstimulated mono-culture T cells with anti-CD3 stimulated T cells co-cultured with either M1 or M2 macrophages. The bracket delineates the activated T cells measured in the bar graph. (**B**) A bar graph depicting the average percent T cell activated after direct co-culture with the control or pre-treated M1 and M2 macrophages. Four technical replicates from a representative donor are shown here. Similar results were obtained in 3 different donors. (**C**) A representative histogram highlighting the ability of pre-treated M2 macrophages to promote T cell activation. (**D-F**) Flow cytometry analysis of surface markers known to affect T cell activation in treated M1 and M2 macrophages. The following co-activators of (**D**) CD80, (**E**) CD86 were analyzed. Relative expression levels of the coinhibitory molecule, PD-L2, in 2 different donors (**F**). Error bars are the standard deviation. Student t-test was used to calculate p-value with statistical significance being < 0.05. Symbols indicate significance between the groups indicated via the line (* < 0.05, $ < 0.005, # < 0.0005).

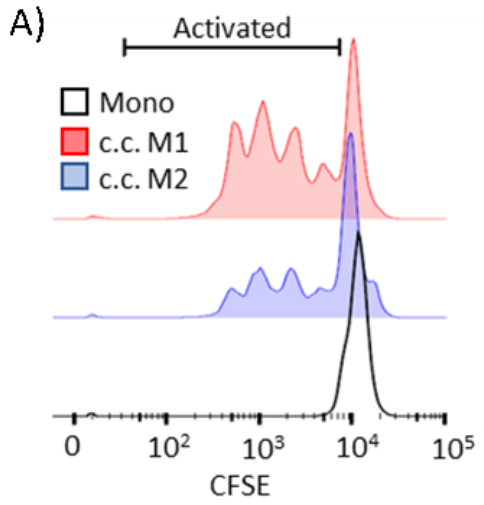
A)
Activated
Mono
c.c. M1
c.c. M2
0
10^2
10^3
10^4
10^5
CFSE

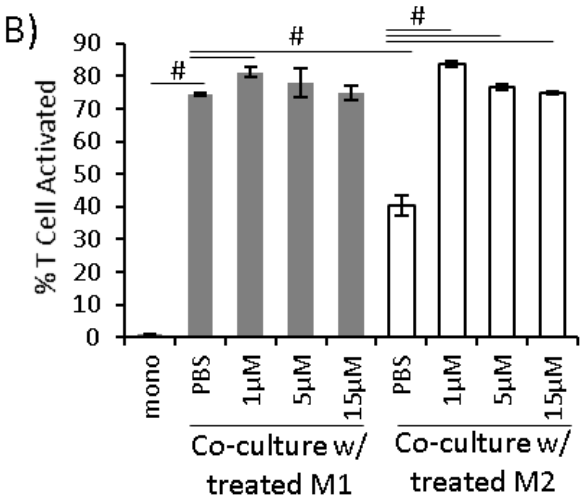
B)
% T Cell Activated
90
80
70
60
50
40
30
20
10
0
#
#
#
mono
PBS
1μM
5μM
15μM
PBS
1μM
5μM
15μM
Co-culture w/ treated M1
Co-culture w/ treated M2

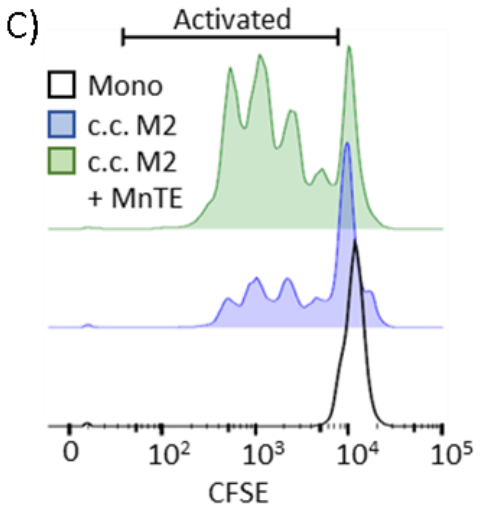
C)
Activated
Mono
c.c. M2
c.c. M2 + MnTE
0
10^2
10^3
10^4
10^5
CFSE

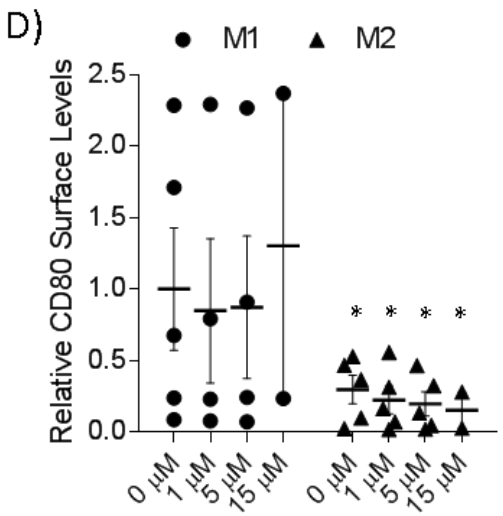
D)
M1
M2
Relative CD80 Surface Levels
2.5
2.0
1.5
1.0
0.5
0.0
* * * *
0 μM
1 μM
5 μM
15 μM
0 μM
1 μM
5 μM
15 μM

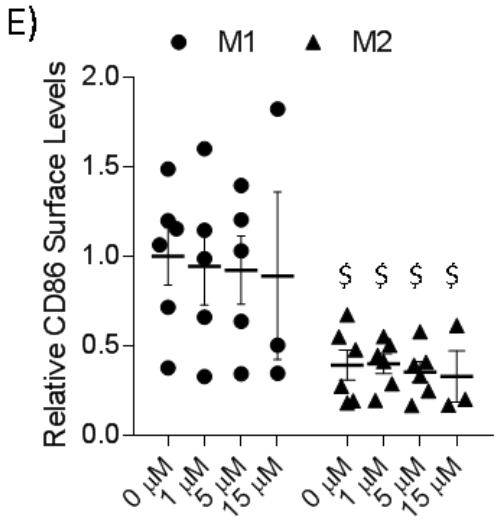
E)
M1
M2
Relative CD86 Surface Levels
2.0
1.5
1.0
0.5
0.0
$ $ $ $
0 μM
1 μM
5 μM
15 μM
0 μM
1 μM
5 μM
15 μM

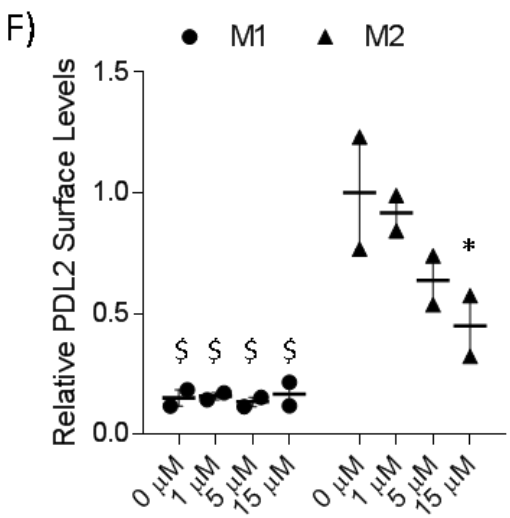
F)
M1
M2
Relative PDL2 Surface Levels
1.5
1.0
0.5
0.0
$ $ $ $
*
0 μM
1 μM
5 μM
15 μM
0 μM
1 μM
5 μM
15 μM

macrophages are now able to induce T cell proliferation to the same extent as the M1 macrophages.

To determine the mechanism behind this dramatic change, we analyzed some key co-activators and co-inhibitory molecules expressed by macrophages that are known to promote/inhibit T cell activation. Amongst these are the co-activators CD80 and CD86 [478], which we found to be significantly lower in M2 macrophages compared to M1 macrophages (Figure 4.3D-E). MnTE treatment had no effect on CD80 or CD86 levels in M1 or M2 macrophages suggesting neither CD80 nor CD86 plays a role in the dramatic change of treated M2 macrophages promoting T cell activation. We next evaluated PD-L2, a co-inhibitory molecule expressed on M2 macrophages that is known to play a key role in M2-mediated inhibition of T cell proliferation [479]. MnTE treatment significantly decreased surface levels of PD-L2 in a dose-dependent manner (Figure 4.3F). This suggests that MnTE treatment inhibits M2-mediated immunosuppression in part through reduction in PD-L2 surface levels.

4.2.4 M2 Macrophages Have Differential Redox Status Compared to M1 Macrophages

Our data suggests that M2 macrophages are more sensitive to ROS manipulation than M1. Therefore, we hypothesized that inherent differences in the redox status of M1 and M2 macrophages could explain the differential effect of ROS manipulation. To determine if there were any potential redox differences in these macrophages, we analyzed the ROS levels of fully polarized M1 and M2 macrophages. M2 macrophages showed significantly lower levels of ROS as assessed by DCFH staining (Figure 4.4A). Additionally, DHE labeling of the superoxide-enriched fluorescence (Ex. 405nm) and the non-specific ROS fluorescence (Ex. 488nm) were both trending lower in M2 macrophages compared to M1 (Figure 4.4B). To further

FIGURE 4.4. M2 macrophages have differential redox status compared to M1

Primary human macrophages were analyzed after 24 hours of polarization. The ROS levels of primary human macrophages from 7 different human donors were measured by (**A**) DCFH. (**B**) DHE measured ROS levels in primary human macrophages from 4 different donors. DHE excitation at 405nm and 488nm was used to measure superoxide-specific levels and general ROS levels respectively. (**C, D**) The levels of oxidized GSSG and total GSH were measured using GSH/GSSG-glo assay in 5 different donors. (**E**) The levels of extracellular H2O2 were measured using AmplexRed via plate reader from 4 different donors. (**F, G**) The levels of mitochondrial ROS production and mitochondrial number in macrophages from 4 different donors were assessed using MitoSox and MitoTrackerGreen respectively. Each line indicating changes between M1 and M2 for each specific donor. (**A, B, F, G**) Fluorescence was assessed using flow cytometry. Relative values were calculated by comparing the change of the M2 sample to its donor specific M1 sample making each change donor specific to account for the heterogeneity of different human donors. Error bars are the standard deviation between all donors M1 or M2 samples. Student t-test was used to calculate p-value with statistical significance being < 0.05.

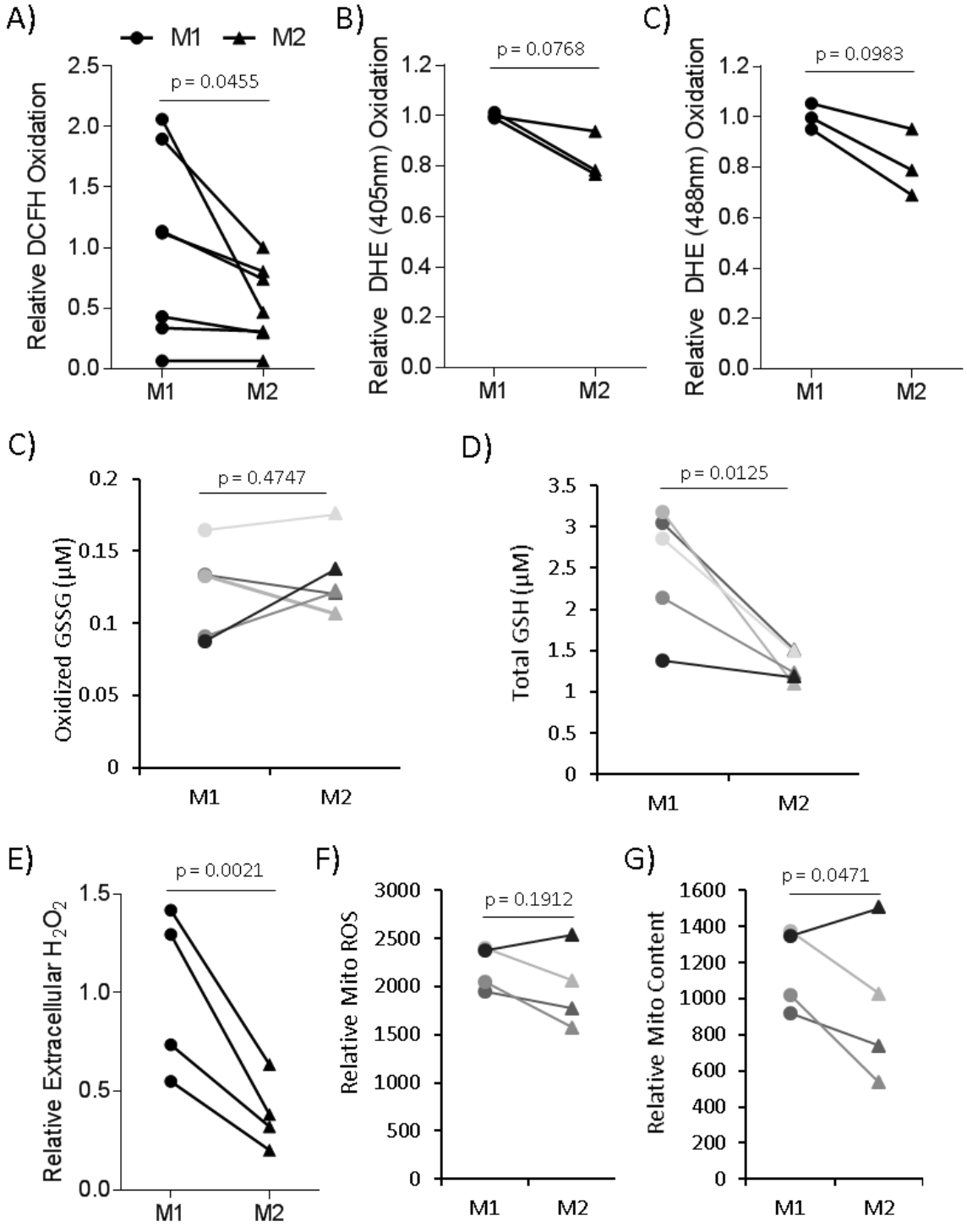
A)
M1
M2
Relative DCFH Oxidation
p = 0.0455
B)
Relative DHE (405nm) Oxidation
p = 0.0768
C)
Relative DHE (488nm) Oxidation
p = 0.0983
C)
Oxidized GSSG (µM)
p = 0.4747
D)
Total GSH (µM)
p = 0.0125
E)
Relative Extracellular H_2O_2
p = 0.0021
F)
Relative Mito ROS
p = 0.1912
G)
Relative Mito Content
p = 0.0471

assess the overall redox status of the cells, we analyzed the levels of cellular glutathione (GSH). In general, cells that exhibit a higher level of ROS will show a higher level of oxidized GSH (GSSG). However, Figure 4.4C shows no significant difference in GSSG levels between the M1 and M2 macrophages while the total levels of GSH are significantly increased in M1 versus M2 macrophages (Figure 4.4D). This suggests that M1 macrophages maintain a higher intracellular level of GSH to combat the increased ROS seen in these classically activated macrophages, whereas the M2 macrophages are less reliant on the GSH pathway. Next, we sought to determine if the cellular ROS differences were driven by certain cellular compartments, such as an extracellular oxidative burst or an internal spike in mitochondrial ROS production. Figure 4E shows that M2 macrophages had significantly reduced extracellular hydrogen peroxide production compared to M1 macrophages. While, mitochondrial ROS levels were unchanged between M1 and M2 macrophages (Figure 4.4F), despite a slight decrease in mitochondrial content in M2 macrophages (Figure 4.4E).

4.2.5 M2 Macrophages Have Reduced ROS Producing Enzymes

We next determined the sources of increased ROS levels in the M2 macrophages. Due to the large disparity in extracellular hydrogen peroxide levels, we analyzed the membrane bound ROS producing enzymes, NADPH oxidases (Nox). We found that mRNA expression of Nox2, Nox5, and CYBA (p22phox) was significantly lower in M2 macrophage compared to M1 (Figure 4.5A). Interestingly, Duox1 and its activator DuoxA1 both were dramatically increased in M2 whereas essentially no expression of these genes was detected in M1 macrophages (Figure 4.6A). Despite the dramatic increase in Duox1, Nox2 is still the most expressed Nox family member in both M1 and M2 macrophages (Ct values for real time-PCR analysis were 19 for Nox2 and 26

FIGURE 4.5. M2 macrophages have lower ROS producers than M1

(**A**) mRNA was isolated from M1 and M2 macrophages 24 hours after addition of polarizing cytokines. The mRNA expression of Nox family members and co-factors was measured using rt-qPCR. The differences between M1 and M2 were calculated using the ΔΔ Ct method with 18S as the loading control. Analysis of gene expression was performed using *N = 3-5* donors. (**B**) The protein expression of Nox2, p47phox, and β-actin in M1 and M2 macrophages was analyzed using Western blot analysis from 5 different donors. (**C**) Densitometry analysis of Nox2 and p47phox compared to the loading control, β-actin, is indicated in line graphs comparing the change of the change of M2 sample to its donor specific M1 sample to account for the heterogeneity of different human donors. The bar graphs indicate the average gene expression with error bars indicating the standard deviation. Student t-test was used to calculate p-value with statistical significance being < 0.05.

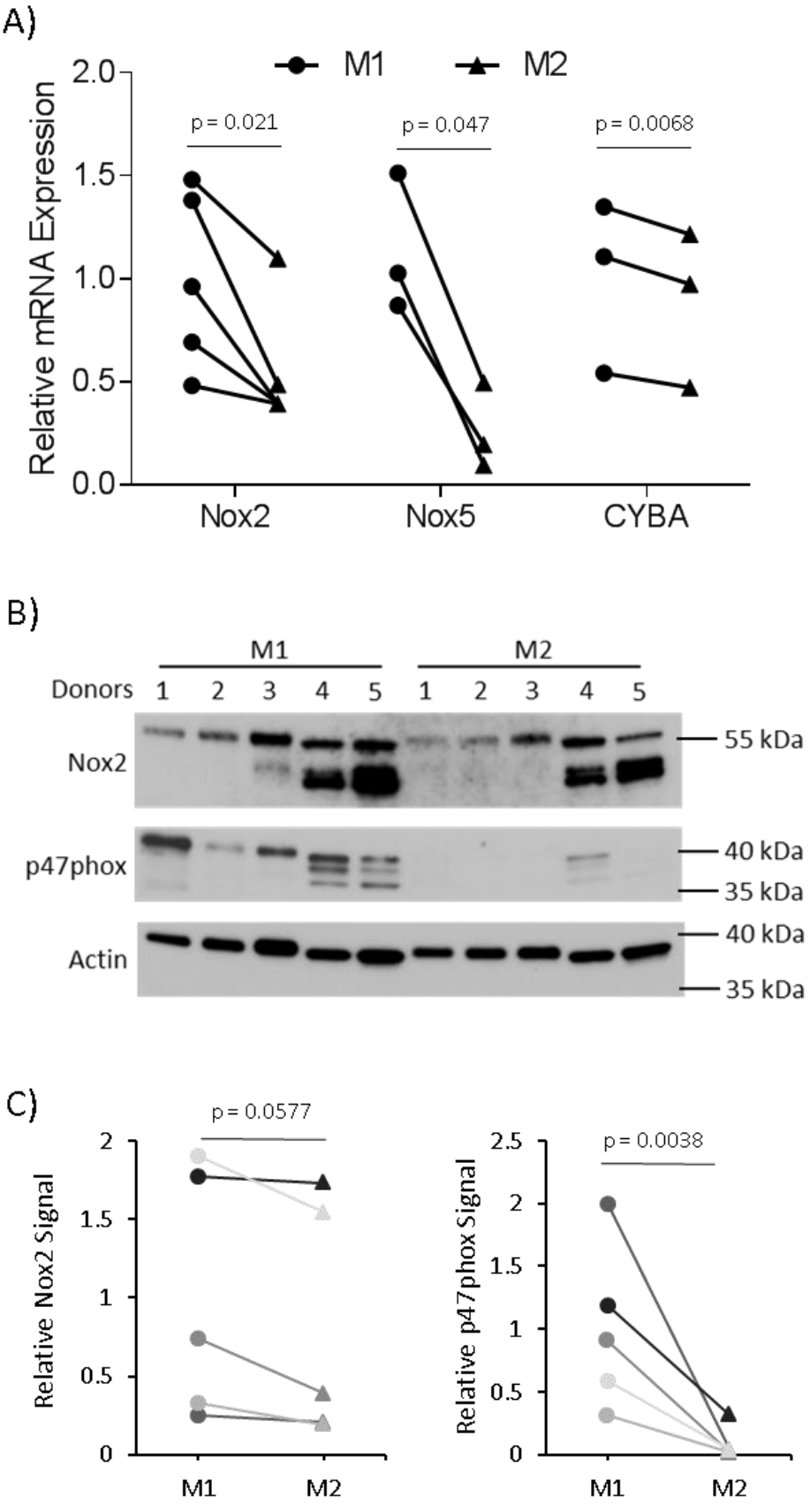
A)
M1
M2
Relative mRNA Expression
2.0
1.5
1.0
0.5
0.0
p = 0.021
p = 0.047
p = 0.0068
Nox2
Nox5
CYBA
B)
M1
M2
Donors 1 2 3 4 5 1 2 3 4 5
Nox2
55 kDa
p47phox
40 kDa
35 kDa
Actin
40 kDa
35 kDa
C)
p = 0.0577
Relative Nox2 Signal
2
1.5
1
0.5
0
M1
M2
p = 0.0038
Relative p47phox Signal
2.5
2
1.5
1
0.5
0
M1
M2

FIGURE 4.6. Nox family members are differentially expressed in M1 and M2 macrophages

(**A-B**) mRNA was isolated from M1 and M2 macrophages 24 hours after addition of polarizing cytokines. The mRNA expression of Nox family members was measured using rt-qPCR. (**A**) The differences between M1 and M2 were calculated using the ΔΔ Ct method with 18S as the loading control. Analysis of gene expression was performed using 4 different donors for DuoxA1 and 5 different donors Duox1. (**B**) Table indicates the raw Ct value for Nox family members in M1 and M2 macrophages averaged across different donors with the standard deviation included.

A)

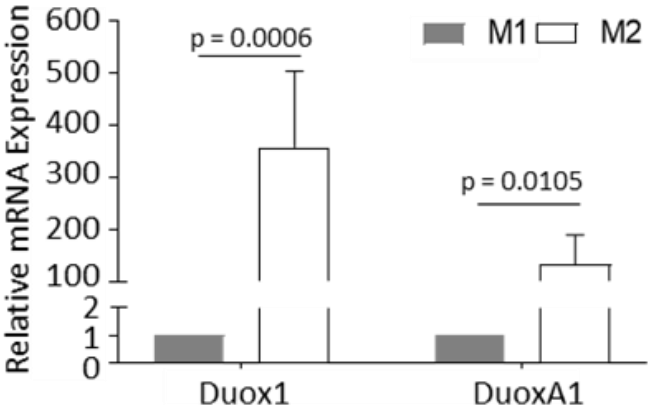

B)

Gene	C_t for M1 Macrophages	C_t for M2 Macrophages
Nox1	31.1 +/- 2.5	32.56 +/- 4.1
Nox2	17.9 +/- 0.8	19.3 +/- 0.8
Nox4	34.5 +/- 1.9	37.5 +/- 2.3
Nox5	30.7 +/- 0.6	32.9 +/- 1.2
Duox1	34.3 +/- 0.6	26.3 +/- 1.1
Duox2	33.72 +/- 0.8	33.1 +/- 0.1

for Duox1 in M2 macrophages). Additionally, both M1 and M2 macrophages expressed comparably low levels of Nox1 and Nox4 (Figure 4.6B). Western blot analysis showed a slight trend of Nox2 expression in M2 macrophages versus donor matched M1 macrophages (Figure 4.5C). The cytosolic subunit of Nox2 required for its activation and ROS production, p47phox, is also dramatically reduced in M2 macrophages (Figure 4.5C), suggesting that Nox2 activity is greatly reduced in these macrophages. These data may explain the dramatic differences in extracellular hydrogen peroxide production seen in figure 4E.

4.2.6 M2 Macrophages Have Differential Expression of ROS Scavenging Enzymes

In a further effort to determine the cause of the lower ROS levels in M2 macrophages, we examined several key antioxidant enzymes. Gene expression of both the superoxide scavenger, copper-zinc superoxide dismutase (Cu/ZnSOD), and hydrogen peroxide scavenging enzymes, glutathione peroxidase 1 (Gpx1), Gpx4, and catalase, was found to be increased in M2 macrophages (Figure 4.7A). The only antioxidant gene found to be increased in M1 macrophages was MnSOD (Figure 4.7A). However, contrary to the mRNA expression, there was no change in MnSOD protein levels and a slight increase in activity between M1 and M2 macrophages (Figure 4.7B-D). We found a trend toward increase in Cu/ZnSOD protein expression and activity in M2 macrophages. Additionally, M2 macrophages had higher levels of the hydrogen peroxide scavenging proteins, Gpx1 and GPX activity, with a trend toward increased Gpx4 protein levels (Figure 4.7B-D).

FIGURE 4.7. M2 macrophage have higher antioxidant enzyme expression and activity compared to M1

(**A**) Antioxidant gene expression was measured using rt-qPCR to determine differences between M1 and M2 macrophages. Analysis of gene expression was performed using *N = 3-4* donors. (**B**) Western blot analysis of antioxidant genes indicating the differential protein levels between M1 and M2 macrophages from 4 different donors. (**C**) Densitometry analysis of Gpx1, Gpx4, MnSOD, and Cu/ZnSOD compared to the loading control, RhoGDI. The line graphs indicate the relative difference between M1 and M2 samples of each individual donor. (**D**) In-gel activity assays for Gpx and SOD proteins using M1 and M2 whole cell lysate. (**E**) Line graph indicating relative difference between M1 and M2 for each specific donor. Relative values were calculated by comparing the change of the change of M2 sample to its donor specific M1 sample making each change donor specific to account for the heterogeneity of different human donors. Error bars are the standard deviation of the M2 samples relative to donor-specific M1 sample. Student t-test was used to calculate p-value with statistical significance being < 0.05.

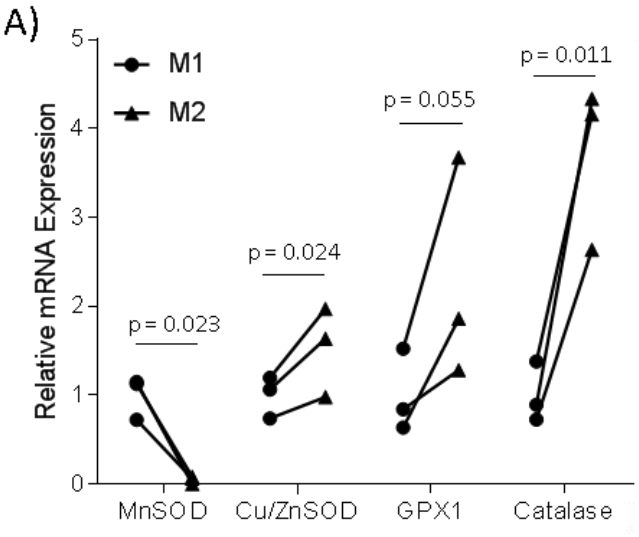
A)
M1
M2
Relative mRNA Expression
p = 0.023
p = 0.024
p = 0.055
p = 0.011
MnSOD
Cu/ZnSOD
GPX1
Catalase

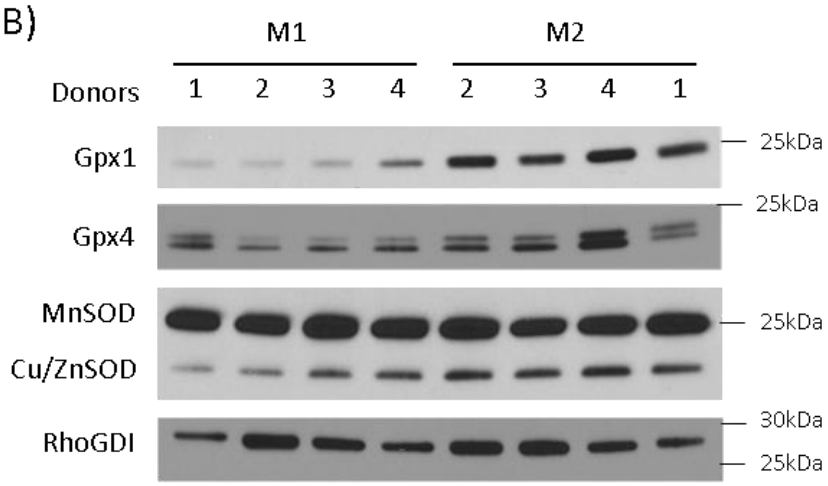
B)
M1
M2
Donors
1 2 3 4 2 3 4 1
Gpx1
Gpx4
MnSOD
Cu/ZnSOD
RhoGDI
25kDa
25kDa
25kDa
30kDa
25kDa

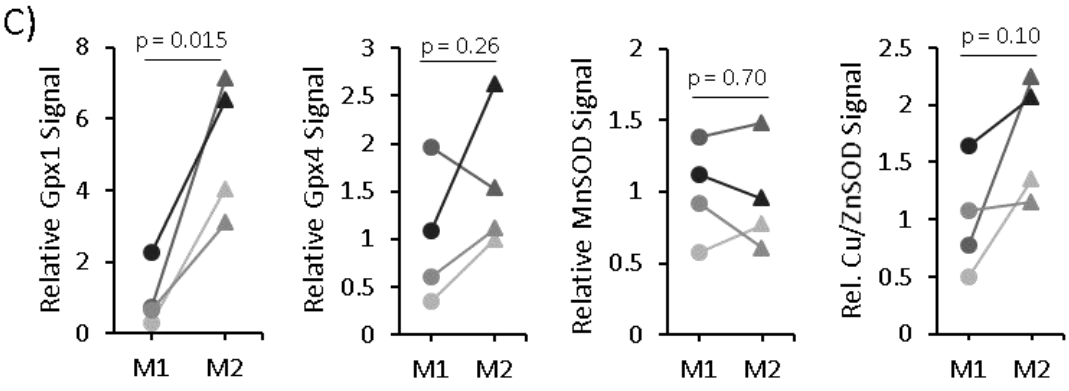
C)
Relative Gpx1 Signal
p = 0.015
Relative Gpx4 Signal
p = 0.26
Relative MnSOD Signal
p = 0.70
Rel. Cu/ZnSOD Signal
p = 0.10
M1 M2

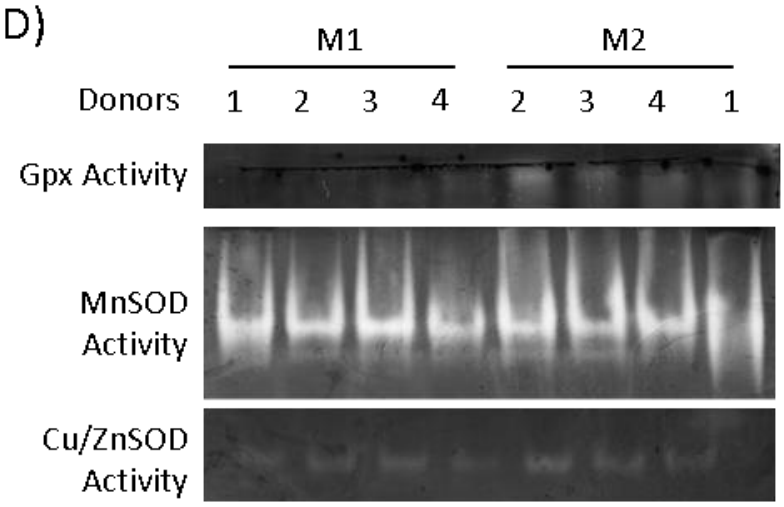
D)
M1
M2
Donors
1 2 3 4 2 3 4 1
Gpx Activity
MnSOD Activity
Cu/ZnSOD Activity

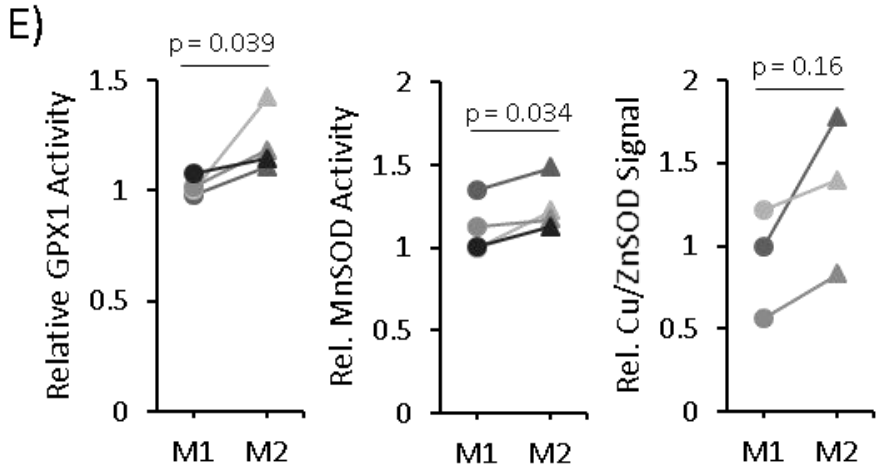
E)
p = 0.039
Relative GPX1 Activity
1.5
1
0.5
0
M1 M2
p = 0.034
Rel. MnSOD Activity
2
1.5
1
0.5
0
M1 M2
p = 0.16
Rel. Cu/ZnSOD Signal
2
1.5
1
0.5
0
M1 M2

4.2.7 ROS Promotes IL-4 Stimulated M2 Polarization

Next, we sought to determine the mechanism by which MnTE inhibits M2 polarization and function. Since MnTE is a redox-active drug, it can act as a pro-oxidant activating additional signaling pathways or an antioxidant reducing M2 signaling cascades. To determine how MnTE is acting in macrophages, both intracellular and extracellular ROS levels were measured in treated and control macrophages. Interestingly, intracellular ROS levels were unchanged in MnTE treated M1 macrophages compared to control (Figure 4.8A). However, MnTE significantly reduced ROS levels by almost 40% in M2 macrophages compared to control. Extracellular hydrogen peroxide levels were also reduced by 40% in MnTE-treated M2 macrophages compared to PBS control with no changes in M1 macrophages (Figure 4.8B). Thus, MnTE is functioning as an antioxidant during M2 polarization. To further test the role of ROS during M2 polarization, Nox-derived ROS production was inhibited using DPI. DPI reduced M2 markers similar to MnTE (Figure 4.8C). Additionally, directly adding exogenous hydrogen peroxide as a bolus injection during M2 polarization increased M2 markers (Figure 4.8D). However, the negative effects of high levels of hydrogen peroxide are seen as M2 markers begin to drop around 20 μM.

Additionally, EcSOD inhibited the ability of conditioned media from MDA-MB231 to increase M2 markers suggesting EcSOD inhibits M2 polarization (Figure 4.9A). Furthermore, TEMPO, another ROS scavenging drug, reduces M2 markers and increases M1 markers (Figure 4.9B-C). However, caution must be applied to not over interpret the data using conditioned media with EcSOD and TEMPO, as these data were only performed in one donor. Interestingly, addition of NAC, a commonly used antioxidant increased M2 polarization (Figure 4.9D). However, analysis of ROS levels indicated that NAC had no significant effect on ROS levels in either M1 or M2

FIGURE 4.8. ROS is a required secondary messenger during IL-4 stimulated M2 polarization
(**A**) Flow cytometry analysis of ROS levels using DCFH in M1 and M2 macrophages from 4 different donors treated with or without 15 μM MnTE. (**B**) Line graph depicting the relative change in extracellular H_2O_2 levels in control versus 15 μM MnTE treated M1 and M2 macrophages from 4 different donors. (**C, D**) Measurement of M2 mRNA markers 24 hours after addition of IL-4. Macrophages were treated with either (**C**) DMSO or 10 μM DPI for 1 hour before addition of IL-4 or (**D**) varying concentrations of exogenous H_2O_2 immediately after addition of IL-4. (**E, F**) Macrophages were treated with MnTE at different times throughout the differentiation and polarization protocol. (**E**) Diagram indicating the M2 polarization protocol with arrows indicating when MnTE was added in the different samples. (**F**) Relative M2 mRNA marker expression of macrophages compared to untreated control measured 48 hours after addition of IL-4. Error bars are the standard deviation. Student t-test was used to calculate p-value with statistical significance being < 0.05. Symbols indicate significance between the treatment groups and M2 control (* < 0.05, $ < 0.005, # < 0.0005).

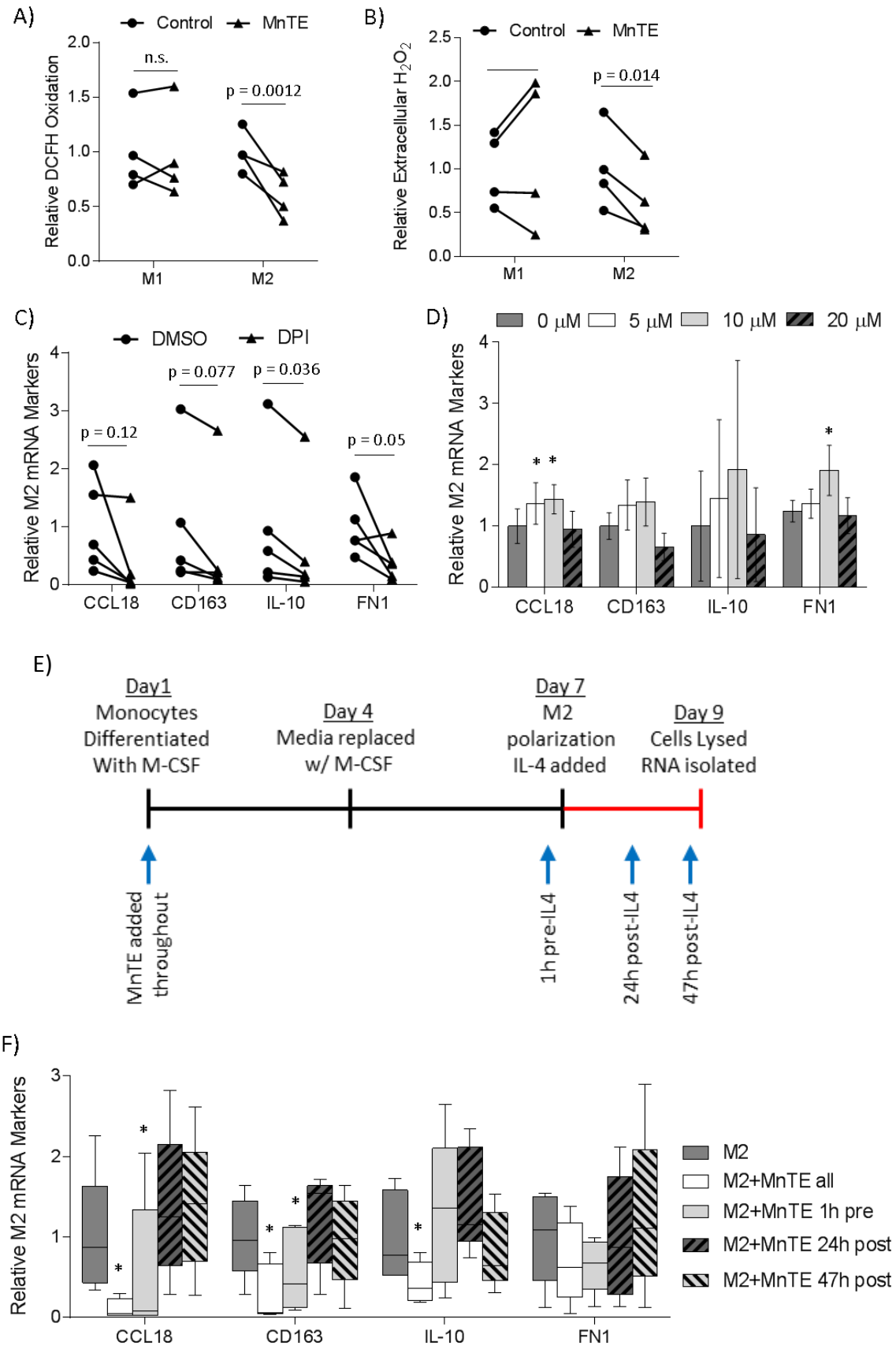
A)
Control
MnTE
Relative DCFH Oxidation
n.s.
p = 0.0012
M1
M2
B)
Control
MnTE
Relative Extracellular H_2O_2
p = 0.014
M1
M2
C)
DMSO
DPI
Relative M2 mRNA Markers
p = 0.12
p = 0.077
p = 0.036
p = 0.05
CCL18
CD163
IL-10
FN1
D)
0 μM
5 μM
10 μM
20 μM
Relative M2 mRNA Markers
CCL18
CD163
IL-10
FN1
E)
Day1
Monocytes
Differentiated
With M-CSF
Day 4
Media replaced
w/ M-CSF
Day 7
M2
polarization
IL-4 added
Day 9
Cells Lysed
RNA isolated
MnTE added throughout
1h pre-IL4
24h post-IL4
47h post-IL4
F)
Relative M2 mRNA Markers
CCL18
CD163
IL-10
FN1
M2
M2+MnTE all
M2+MnTE 1h pre
M2+MnTE 24h post
M2+MnTE 47h post

FIGURE 4.9. The effect of additional antioxidants on macrophage polarization

(**A**) Macrophages were polarized in 50% conditioned media from MDA-MB231 or EcSOD overexpressing cell line, Ec.20. M1 and M2 markers were analyzed after polarization. (**B-C**) Macrophages were treated with TEMPO throughout differentiation and polarization. M1 (**B**) and M2 (**C**) markers were analyzed after polarization. (**D**) Macrophages were treated with 5 mM NAC throughout differentiation and polarization. M2 markers were analyzed after polarization. (**E**) ROS levels were measured after polarization via DCFH. Macrophages were treated with NAC throughout differentiation and polarization.

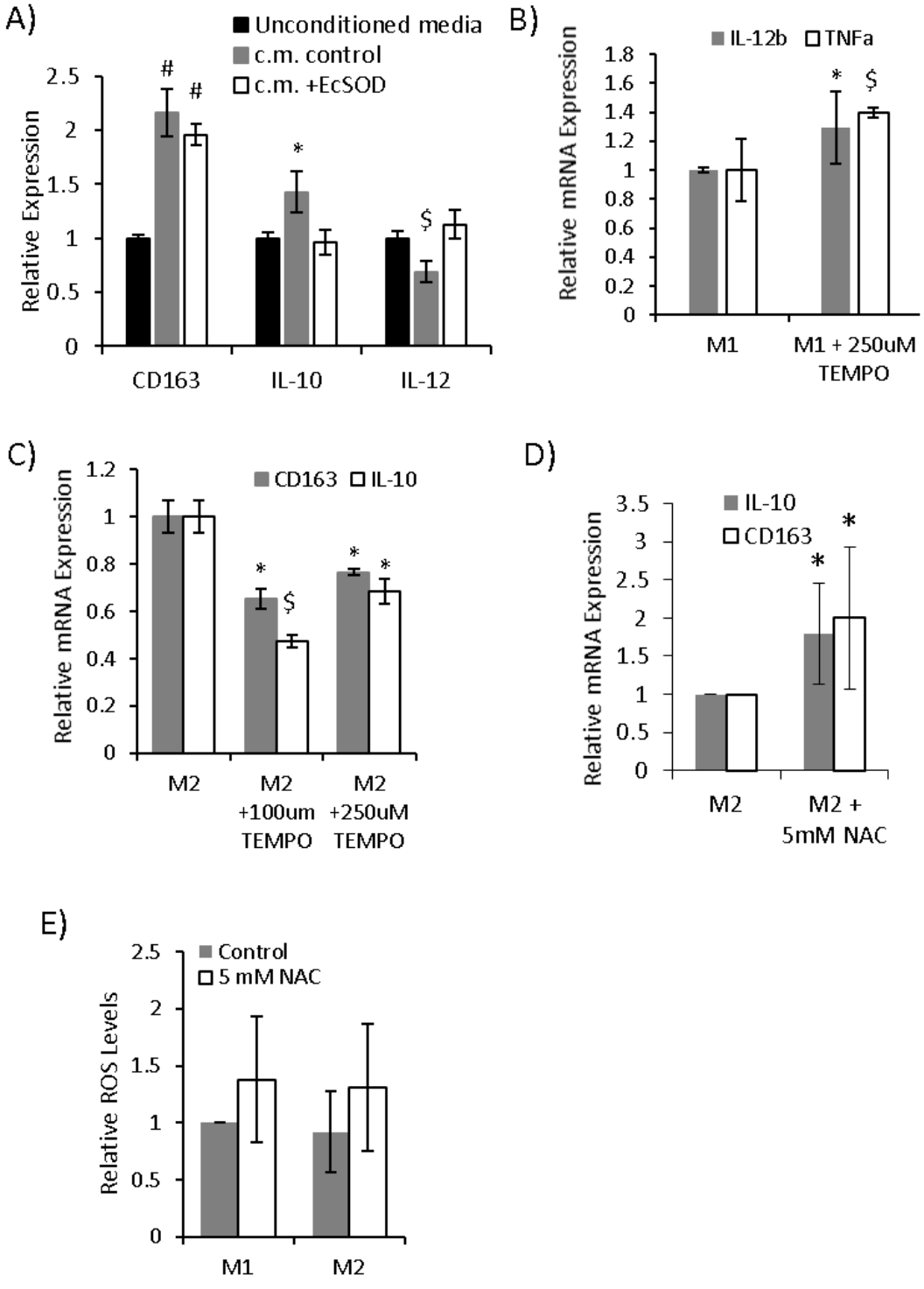
A)
Unconditioned media
c.m. control
c.m. +EcSOD
Relative Expression
2.5
2
1.5
1
0.5
0
#
#
*
$
CD163
IL-10
IL-12
B)
IL-12b
TNFa
Relative mRNA Expression
1.8
1.6
1.4
1.2
1
0.8
0.6
0.4
0.2
0
*
$
M1
M1 + 250uM TEMPO
C)
CD163
IL-10
Relative mRNA Expression
1.2
1
0.8
0.6
0.4
0.2
0
*
$
*
*
M2
M2 +100um TEMPO
M2 +250uM TEMPO
D)
IL-10
CD163
Relative mRNA Expression
3.5
3
2.5
2
1.5
1
0.5
0
*
*
M2
M2 + 5mM NAC
E)
Control
5 mM NAC
Relative ROS Levels
2.5
2
1.5
1
0.5
0
M1
M2

macrophages suggesting its effects are ROS-independent (Figure 4.9E). These data provide further evidence that reducing ROS levels inhibits M2 polarization.

Next, MnTE was added during different times throughout M2 polarization to test if MnTE was inhibiting IL-4 signaling during M2 polarization or activating other signaling pathways such as NF-κB and Nrf2 on its own that would shift macrophage polarization toward a more M1-like state. As indicated in Figure 4.8E, MnTE was added throughout differentiation and polarization, just prior to polarization, half-way through polarization, and just before RNA isolation. M2 mRNA markers were measured 48 hours after IL-4 addition. Figure 4.8F indicates pre-treatment is required for MnTE inhibition of M2 markers. Additionally, MnTE may affect M-CSF signaling since the effect of MnTE added just before polarization was not quite as strong as the effect of MnTE treatment throughout differentiation and polarization. However, MnTE treatment after IL-4 polarization had virtually no effect on M2 markers. Thus, MnTE modulates short-term IL-4 signaling. It is unlikely that MnTE is modifying macrophage polarization by activating other transcription factors via increased ROS production. These data indicate that ROS is required during M2 polarization, likely as a ROS burst during the initial signaling events, and that MnTE is inhibiting M2 polarization and acting as an antioxidant in this specific context.

4.2.8 ROS is Required for IL4-induced Stat3 Activation.

We next examined key signaling pathways during M2 polarization to determine the MnTE-mediated mechanism of inhibition. Stat6 is a major transcription factor during M2 polarization and is activated via canonical type I IL-4 signaling [480]. Additionally, Stat6 has been shown be regulated by H_2O_2 during IL-4 signaling [481-483]. Although

FIGURE 4.10. Stat6 activation is affected by MnTE in a small subset of donors

(**A-C**) Western blot analysis of p-Stat6, total Stat6, and loading control GAPDH in macrophages from three different donors treated with varying concentrations of MnTE.

A)

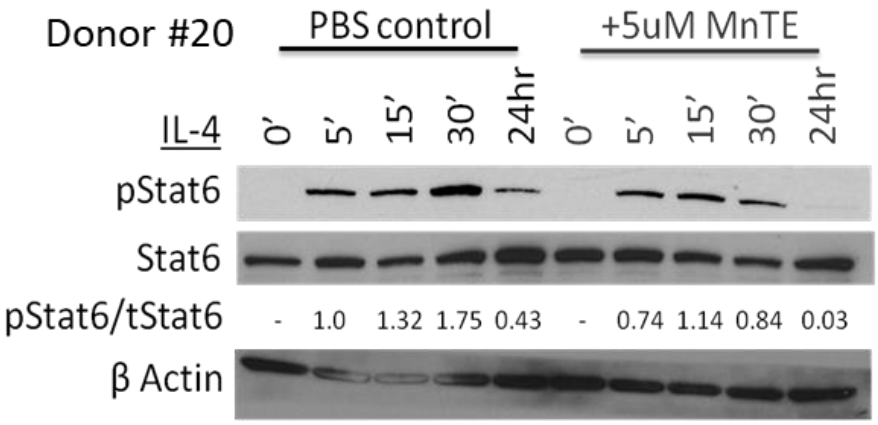
Donor #20
PBS control
+5uM MnTE
IL-4
0'
5'
15'
30'
24hr
0'
5'
15'
30'
24hr
pStat6
Stat6
pStat6/tStat6
- 1.0 1.32 1.75 0.43 - 0.74 1.14 0.84 0.03
β Actin

B)

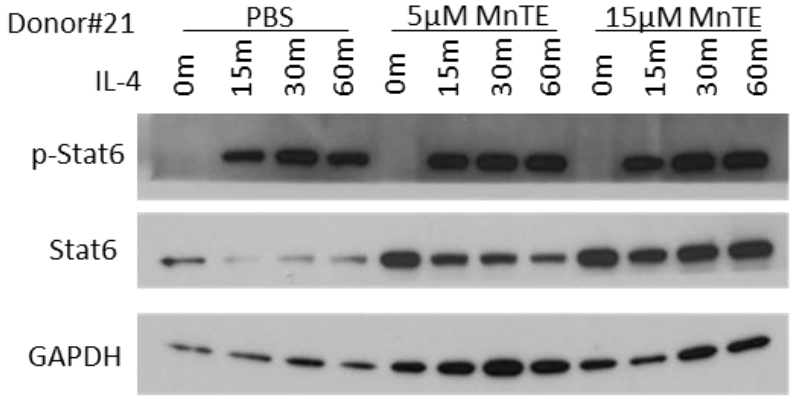
Donor#21
PBS
5µM MnTE
15µM MnTE
IL-4
0m
15m
30m
60m
0m
15m
30m
60m
0m
15m
30m
60m
p-Stat6
Stat6
GAPDH

C)

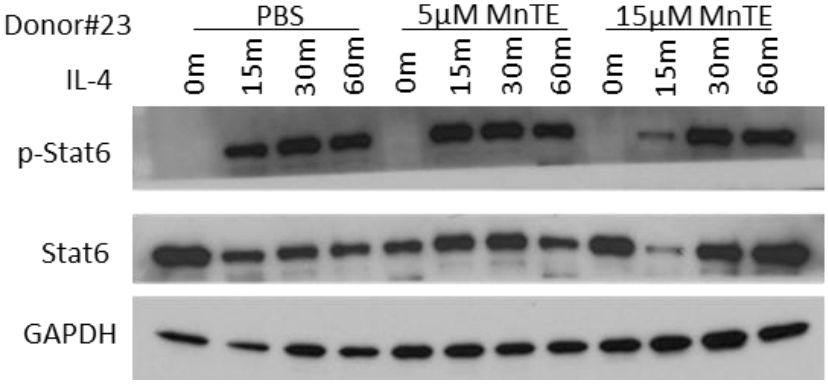
Donor#23
PBS
5µM MnTE
15µM MnTE
IL-4
0m
15m
30m
60m
0m
15m
30m
60m
0m
15m
30m
60m
p-Stat6
Stat6
GAPDH

FIGURE 4.11. MnTE inhibits Stat3 activation

(**A-C**) Western blot analysis of p-Stat3, total Stat3, and loading control GAPDH in macrophages from different donors treated with MnTE or DPI. Macrophages were serum starved overnight before IL-4 addition. Macrophages were stimulated with IL-4 for varying time points indicated above each lane. The densitometry indicating the relative p-Stat3/total Stat3 ratio is include below the total Stat3 blot. (**A**) Macrophages were treated with PBS or MnTE (5 μM or 15 μM) throughout differentiation and IL-4 stimulation. (**B**) Macrophages were treated with PBS or MnTE (15 μM) 1 hour before addition of IL-4. (**C**) Macrophages were treated with DMSO or DPI (10 μM) for 1 hour before stimulation with IL-4.

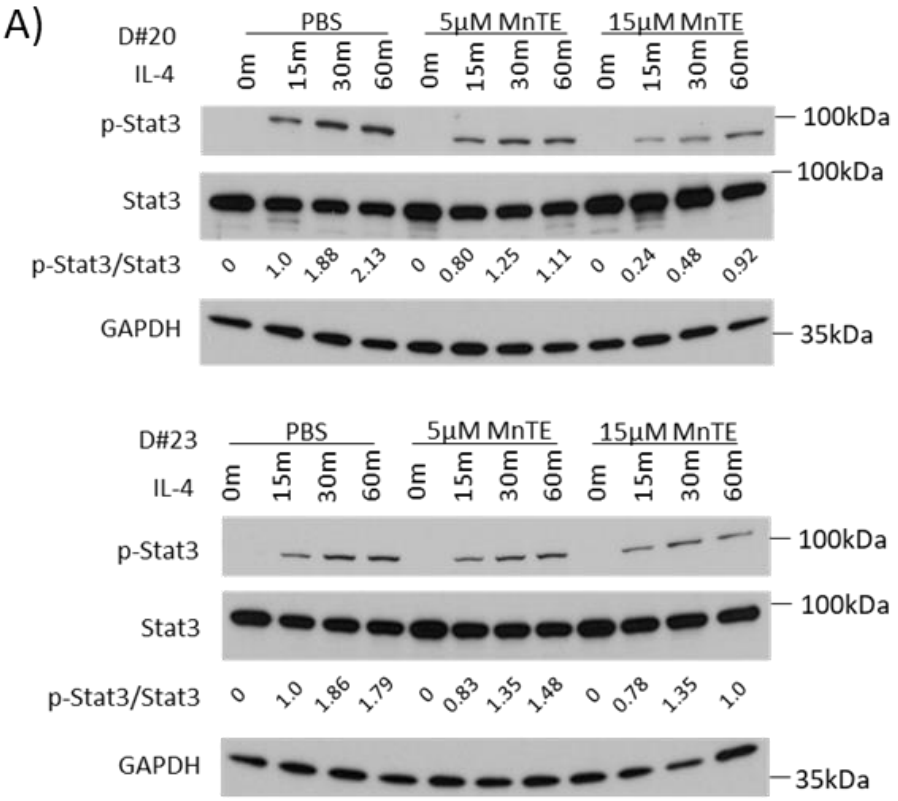
A)
D#20
PBS
5μM MnTE
15μM MnTE
IL-4
0m 15m 30m 60m 0m 15m 30m 60m 0m 15m 30m 60m
p-Stat3
100kDa
Stat3
100kDa
p-Stat3/Stat3
0 1.0 1.88 2.13 0 0.80 1.25 1.11 0 0.24 0.48 0.92
GAPDH
35kDa
D#23
PBS
5μM MnTE
15μM MnTE
IL-4
0m 15m 30m 60m 0m 15m 30m 60m 0m 15m 30m 60m
p-Stat3
100kDa
Stat3
100kDa
p-Stat3/Stat3
0 1.0 1.86 1.79 0 0.83 1.35 1.48 0 0.78 1.35 1.0
GAPDH
35kDa

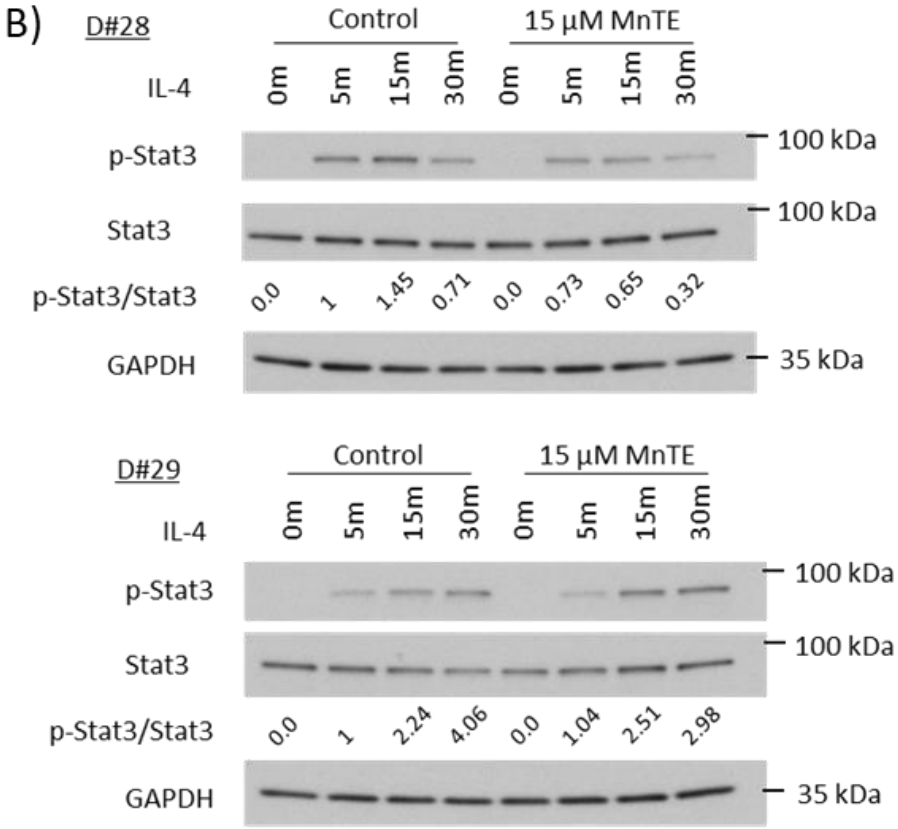
B)
D#28
Control
15 μM MnTE
IL-4
0m 5m 15m 30m 0m 5m 15m 30m
p-Stat3
100 kDa
Stat3
100 kDa
p-Stat3/Stat3
0.0 1 1.45 0.71 0.0 0.73 0.65 0.32
GAPDH
35 kDa
D#29
Control
15 μM MnTE
IL-4
0m 5m 15m 30m 0m 5m 15m 30m
p-Stat3
100 kDa
Stat3
100 kDa
p-Stat3/Stat3
0.0 1 2.24 4.06 0.0 1.04 2.51 2.98
GAPDH
35 kDa

C)

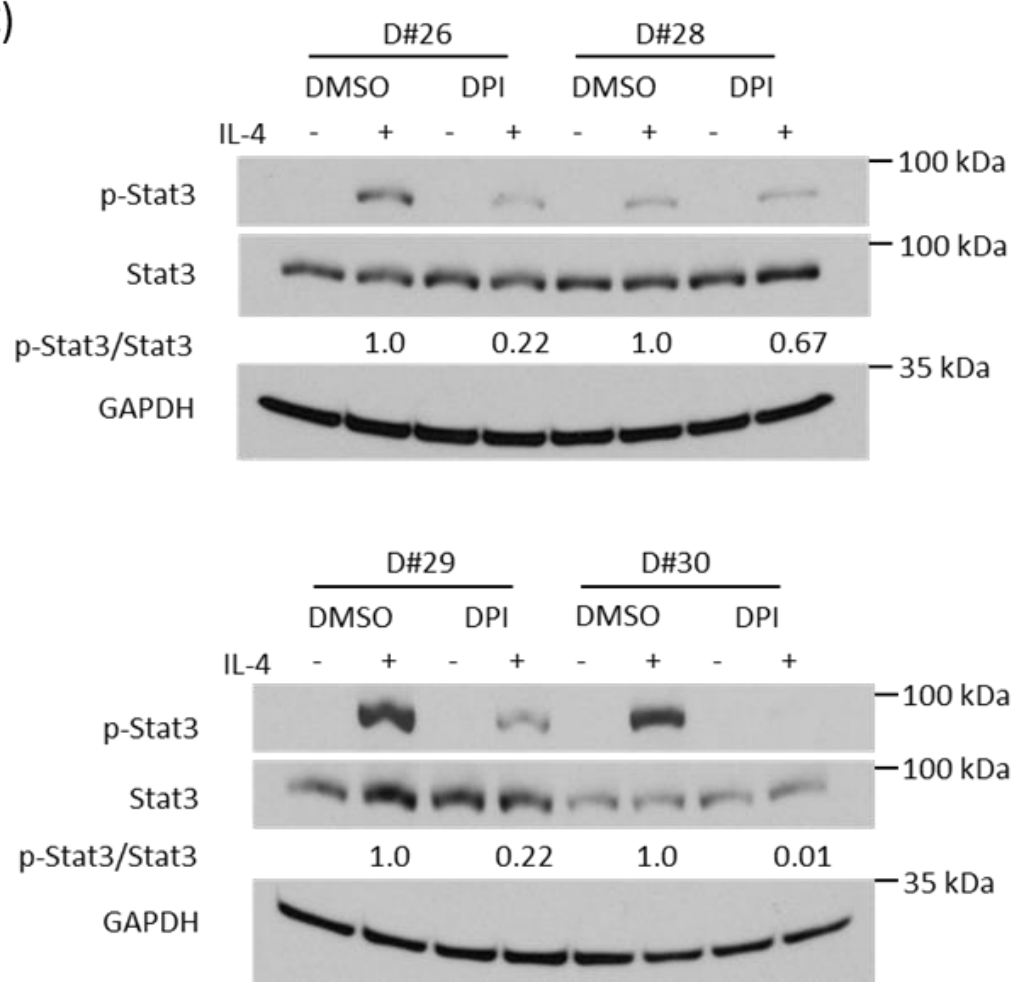
D#26
D#28
DMSO
DPI
DMSO
DPI
IL-4
- + - + - + - +
p-Stat3
100 kDa
Stat3
100 kDa
p-Stat3/Stat3
1.0 0.22 1.0 0.67
GAPDH
35 kDa
D#29
D#30
DMSO
DPI
DMSO
DPI
IL-4
- + - + - + - +
p-Stat3
100 kDa
Stat3
100 kDa
p-Stat3/Stat3
1.0 0.22 1.0 0.01
GAPDH
35 kDa

we found that MnTE inhibited IL4-mediated Stat6 activation in some cases, this effect is inconsistent amongst the various donor samples suggesting that another pathway was involved in this phenomena (Figure 4.10A-C). Therefore, we next turned our attention toward the less studied type II IL-4 signaling, which activates Stat3 via dimerization of the IL-4Rα with the IL-13Rα1 receptor [484, 485]. Additionally, ROS is known to activate Stat3 [486, 487]. Stimulation of macrophages with IL-4 clearly increased Stat3 phosphorylation at Y705, indicating activation (Figure 4.11A-B). MnTE treatment resulted in a reduction of phospho-Stat3 levels in four human donors and in a dose dependent manner compared to the PBS controls (Figure 4.11A-B). Furthermore, DPI was used to determine if inhibiting Nox-derived ROS would also inhibit Stat3 activation, as it reduced M2 markers. Similar to MnTE, DPI treatment reduced phospho-Stat3 levels compared to DMSO control (Figure 4.11C). Furthermore, the M2 markers genes, IL-10, CD163, and PD-L2, are known target genes of Stat3 [488-490]. These M2 markers are all suppressed by drug treatment as indicated earlier in this study. All these studies clearly showed that either scavenging ROS with MnTE or inhibiting Nox activities with DPI, reduce phospho-Stat3 levels and inhibit Stat3 activation.

4.3 Discussion

It is well known that cancer cells have higher intracellular ROS levels than their normal counterparts. It is also becoming clear that the tumor microenvironment (TME) is highly oxidized compared to their normal tissue counterparts. However, the role of the oxidative TME on cellular functions within the tumor remains relatively understudied. It has been shown that the oxidative TME contributes to immunosuppression in cancer, where increased extracellular ROS inhibited CD8+ T cell activation while inducing Treg activation [380, 381, 491-493]. Our data show that M2 or TAM-like macrophages have increased redox buffer, suggesting their high tolerance within the oxidative TME.

Additionally, this study indicates ROS is a necessary secondary messenger for proper M2 polarization and function. Furthermore, addition of exogenous hydrogen peroxide promotes M2 polarization. Thus, it is reasonable to speculate that the oxidative TME may actively promote an immunosuppressive environment via polarizing TAM to a M2-like phenotype, while also inhibiting T cell activation and increasing Tregs.

Due to the plasticity of macrophages, there are a plethora of studies examining the differences in M1 and M2 states via large scale transcriptomics. Some key differences in the expression levels of ROS producing and scavenging enzymes was identified by Beyer *et al* in M1 vs. M2 macrophages [494]. Their results show that M2 macrophages have increased expression of genes in the peroxiredoxin family, specifically PRDX1, PRDX3, and PRDX6, which may further contribute to the lower levels of ROS in M2 macrophages. Some of the largest changes in ROS-related genes were seen in the glutathione-S-transferase (GST) family, specifically lower GSTO1 and higher GSTP1, mGST2, and GSTT1, in M2 macrophages, which may lead to different glutathionylation patterns as a potential regulator of macrophage polarization and function. Our data agree with their RNA-seq data that Nox2 is the highest expressed Nox family member with the others being very lowly expressed or undetectable. Their observations also support our findings of differential expression of Nox2, Duox1, DuoxA1, MnSOD, catalase, Gpx1, and Cu/ZnSOD in M1 and M2 macrophages. Our study also takes these data a step further by analyzing the protein and activity levels of these genes, as well as analyze the effect of these changes on the redox status of M1 and M2 macrophages.

Our data implicate ROS as a required secondary messenger during IL-4 signaling for optimal Stat3 activation and M2 polarization. Futhermore, our data shows optimal M2 polarization, in part, requires Stat3 activation. The ability of ROS to promote

Stat3 activation by ROS has also been shown in other cell types [486, 495-499]. Additionally, hydrogen peroxide has been demonstrated to activate Jak2 and Tyk2, which are upstream activators of Stat3 [495, 499, 500]. Our studies imply that this ROS is likely generated from Nox2, as it is the most abundant ROS producing enzyme in these macrophages. Further supporting this, the pan-Nox inhibitor, DPI suppressed Stat3 activation and reduced M2 marker expression. However, DPI is a flavoprotein inhibitor that can inhibit enzymes other that Noxs, such as nitric oxide synthases, xanthine oxidases, and enzymes involved in the pentose phosphate pathway and TCA cycle [501]. Therefore, we cannot rule out the possibility that DPI may also inhibit M2 polarization through modulation of metabolic pathways [502]. Due to the use of primary human macrophages, the ability to genetic silence Nox members to test this hypothesis was limited. However, a study using mouse macrophages derived from the Nox1/2 double knockout mice noticed a similar M2 polarization deficiency [503]. Although, it was unclear whether this deficiency occurred during macrophage differentiation or during M2 polarization, this study supports our speculation that Nox-generated ROS contributes to M2 macrophage polarization and their pro-tumorigenic phenotype.

ROS typically act as a secondary messenger during signaling through reversible oxidation and inactivation of protein tyrosine phosphatases (PTPs), which are the off switches of many signaling pathways. Therefore, we hypothesize that Nox2-derived ROS oxidizes and inactivates PTPs that are negatively regulating the IL-4 signaling pathway. Among the long list of PTPs that have been shown to negatively regulate Stat3 are SHP-1, SHP-2, PTP1B, and TCPTP, all of which can be inhibited via ROS-mediated reversible oxidation [504-507]. Furthermore, this mechanism may also be applicable to additional pathways that activate Stat3. These include IL-6, IL-10, and IL-22, which polarize macrophages to similar states as the IL-4 stimulated M2 used in this study [508-

510]. Additionally, non-macrophage cells in the TME, such as myeloid-derived suppressor cells, are known to require Stat3 activation and ROS production for their immunosuppressive phenotype [380, 511]. Thus, MnTE may have a wider ability to inhibit Stat3-mediated immunosuppression in macrophages and MDSCs than what our study examined.

Additional research indicates that MnTE also acts on other immune cells besides macrophages. In $CD4^+$ T cells, it skews their polarization by promoting T_H1 response and inhibiting T_H2 *in vivo* [292, 293]. Interestingly, Stat3 is required for optimal T_H2 polarization and function [512]. Due to closely related process of macrophage and $CD4^+$ T cell polarization, we speculate that MnTE inhibits M2 polarization and T_H2 polarization via similar mechanisms [336]. Furthermore, MnTE increases both $CD4^+$ and $CD8^+$ T cells in the spleen, as well as B cells and NK cells, suggesting it is activating several different types of immune cells that may provide additional anti-tumor effects [294]. It also increased production of IL-2, an immunostimulatory cytokine released primarily via T_H1 $CD4^+$ T cells. Additionally, tumor mouse models treated with MnTE or its analog, MnTnBuOE-2-PyP^{5+} affect monocyte infiltration and have increased M1 macrophages [291]. Our study adds evidence that MnTE also stimulates the immune system through inhibiting M2 polarization.

Several strategies have been proposed to target TAM for antitumor therapy. These include blocking macrophage recruitment to the tumor, decreasing total macrophage number via targeting therapies, and reprogramming of TAMs from the pro-tumorigenic M2 to proinflammatory M1 macrophages [513]. Reprogramming TAM has shown efficacy as a single therapy in inhibiting tumor growth and metastasis, thereby promoting survival in mouse models [363, 514]. While MnTE does not entirely reverse the M2 markers, this study clearly shows that it inhibits some of the critical negative

effects of M2 macrophages. Additionally, the immunosuppressive function of TAM is a known mechanism of resistance to immune checkpoint blockade inhibitors [515]. Therefore, use of MnTE, to reprogram immunosuppressive TAM in combination with inhibitors for immune checkpoint blockade to stimulate T cell activation, presents a potentially promising and exciting combination approach to overcome this known resistance mechanism to immunotherapy.

In conclusion, this study further confirms key differences between M1 and M2 macrophages in their production and scavenging of superoxide and hydrogen peroxide hinted at in previous studies. Additionally, we show that clinically relevant redox-active drugs could be used as a promising approach to selectively target M2 macrophages to inhibit their pro-tumorigenic and immunosuppressive functions. This study also supports the concept of the oxidative TME in actively and purposefully promoting M2 polarization in TAM. Future studies are required to determine the direct role of the oxidative TME on cell-cell interactions within the tumor. Additionally, more studies are needed to determine the efficacy of MnTE to inhibit M2 polarization in tumor models *in vivo*, as well as in combination with T cell activating immunotherapy to synergistically reduce tumor growth.

CHAPTER 5:

Association of *SOD3* Promoter DNA with Its Expression Levels in Breast Carcinomas

Data in this chapter have been published in the following manuscript:

Griess B., Klinkebiel D., Kueh A., Desler M., Cowan K., Fitzgerald M., Teoh-Fitzgerald M. Association of SOD3 Promoter DNA methylation with its expression levels in Breast Carcinomas. Clinical Epigenetics. 2019 (submitted)

5.1 Introduction

Breast cancer is the most prevalent cancer in women and it is the second leading cause of cancer -related death. It is estimated that one out of eight women will be diagnosed with breast cancer throughout the lifetime. On the molecular level, breast cancer is a complex and heterogeneous disease. Therapeutic strategies are mainly guided by tumor burden and molecular subtypes. The four main breast cancer subtypes are categorized based on the presence of receptor(s), which include: Luminal A (estrogen receptor, ER+ and/or progesterone receptor, PR+, Her2-, and low ki67 index), Luminal B (ER/PR+, Her2+, and high ki67 index), Her2-enriched (ER/PR-, Her2+, and high ki67 index), and triple-negative (TNBC) (ER-, PR-, Her2-, and high ki67 index).The standard management of breast cancer is a multidisciplinary approach that involves local regional resection of tumor, systemic therapies (anti-hormonal, anti-Her2, or chemotherapies), and radiation therapies. Poly (ADP- ribose) polymerase, PARP inhibitors are also used for *BRCA* mutation carriers.

Our previous study indicated that down-regulation of extracellular superoxide dismutase (EcSOD, a.k.a. *SOD3*) is frequently detected in breast carcinomas and re-expression of *SOD3* in TNBC cell lines significantly suppressed tumor growth and metastasis *in vivo* [142]. *SOD3* is the only secreted member of the superoxide dismutase (SOD) family, which are the primary antioxidant enzymes involved in regulating reactive oxygen species (ROS) [516]. These SODs utilize metal cofactors for catalyzing one-electron oxidation followed by one-electron reduction of two O2•- anions to form hydrogen peroxide, H_2O_2, which is further reduced into water molecules by catalase and glutathione peroxidases [112, 117]. While the three mammalian SODs catalyze the same dismutation reaction at the same rate, the individual isoform is expected to provide specific and non-redundant biological function, due to their

distinctive cellular localizations and membrane impermeability of their substrate, $O_2^{\bullet-}$. In contrast to the other SODs, which are ubiquitously expressed, *SOD3* is expressed in a tissue and cell type-specific manner [62]. The presence of *SOD3* is also detectable in milk, plasma, synovium, and lymph [61, 70]. Most importantly, loss of *SOD3* expression is associated with decreased breast cancer patient survival, suggesting a potential tumor suppressive function [161, 517].

Hypermethylation of CpG islands within the promoter region of a gene is recognized as an important epigenetic mechanism of transcriptional silencing of tumor suppressor genes during cancer development [518]. The fact that *SOD3* expression is tightly controlled in a cell type and tissue-specific manner [443], and with a promoter that shows a CpG structure similar to other genes silenced by aberrant cytosine methylation [519] indicates a potential association of epigenetic regulation via DNA methylation with *SOD3* gene expression in breast cancer. The *SOD3* promoter (-550 bp upstream to 100 bp downstream) has 18 CpG sites, which have been shown to be hypermethylated in breast and lung cancer tissues when compared to the normal control tissues [142, 413]. Due to the limited number of tissues analyzed in our previous study, the association of *SOD3* promoter methylation could not be determined in a subtype-specific manner for breast cancer. This study, therefore seeks to enrich those results via pyrosequencing analysis of the *SOD3* promoter using a subset of the cohort from the Breast Cancer Collaborative Registry, which is run by the Northern Great Plains Personalized Breast Cancer Program (NGPPBCP). The NGPPBCP was designed to use whole exome DNA sequencing to find genetic drivers in breast cancer with the goal of developing new targeted therapies. Our study indicates that *SOD3* expression is significantly down-regulated in breast tumors compared to normal breast tissues. Moreover, there is an inverse correlation between the expression levels and the %

methylation in breast cancer patient samples. Pam 50-based subtype analysis further revealed that *SOD3* is most significantly down-regulated via DNA methylation in Luminal B breast cancers.

5.2 Results

5.2.1 *SOD3* Expression is Downregulated in Breast Tumors

Agendia gene array analysis performed on clinical specimens collected from the BCCR showed that there was a significant decrease in *SOD3* expression in breast tumors when compared to the normal tissues (Median = 10.991 vs. 12.215 or 2.33 fold reduction), as shown in Figure 5.1A. In the tumor subset where molecular subtypes were identified, we observed that the lowest *SOD3* expression was seen in the Luminal B subtype (Figure 5.1B). A similar trend was observed when we analyzed Oncomine® datasets, which is a publicly available microarray-based database, where significantly lower expression levels of *SOD3* were observed in the tumor tissues compared to the normal ones (Figure 5.1C). Two datasets, the Curtis Breast (Figure 5.1D) and Gluck Breast (Figure 5.1E) further showed the lowest *SOD3* expression in Luminal B breast cancers (red arrow).

5.2.2 *SOD3* Expression Levels are Inversely Correlated with Its Promoter CpG Methylation

Next, we analyzed six CpG sites within the *SOD3* promoter as depicted in Figure 5.2A. These sites were selected as they occur within known transcription factor binding sites or adjacent to them [142, 413]. In comparison to the normal breast tissues, breast

Figure 5.1. *SOD3* expression is downregulated in breast cancer

(**A-B**) Agendia gene array analysis of *SOD3* expression in the BCCR cohort. (**A**) Comparison of *SOD3* expression in normal breast tissue versus cancer breast tissue. (**B**) *SOD3* expression level in the different breast cancer subtypes. (**C**) Analysis of the *SOD3* expression in the publicly available microarray data in the Oncomine dataset comparing normal breast tissue versus breast tumor. (**D-E**) Analysis of *SOD3* expression levels in different subtypes of breast cancer compared to normal tissue in the (**D**) Curtis Breast dataset and the (**E**) Gluck Breast dataset.

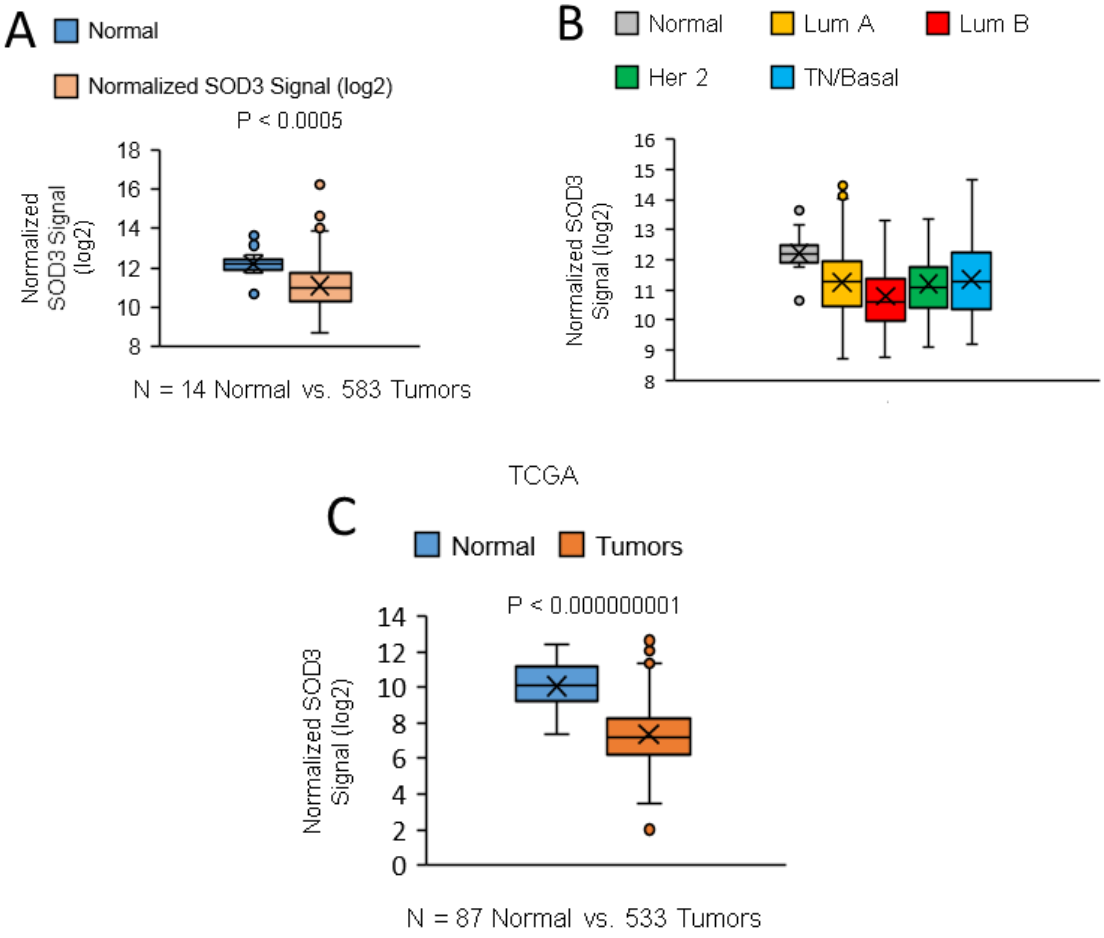
A
Normal
Normalized SOD3 Signal (log2)
P < 0.0005
Normalized SOD3 Signal (log2)
18
16
14
12
10
8
N = 14 Normal vs. 583 Tumors
B
Normal
Lum A
Lum B
Her 2
TN/Basal
Normalized SOD3 Signal (log2)
16
15
14
13
12
11
10
9
8
TCGA
C
Normal
Tumors
P < 0.000000001
Normalized SOD3 Signal (log2)
14
12
10
8
6
4
2
0
N = 87 Normal vs. 533 Tumors

D

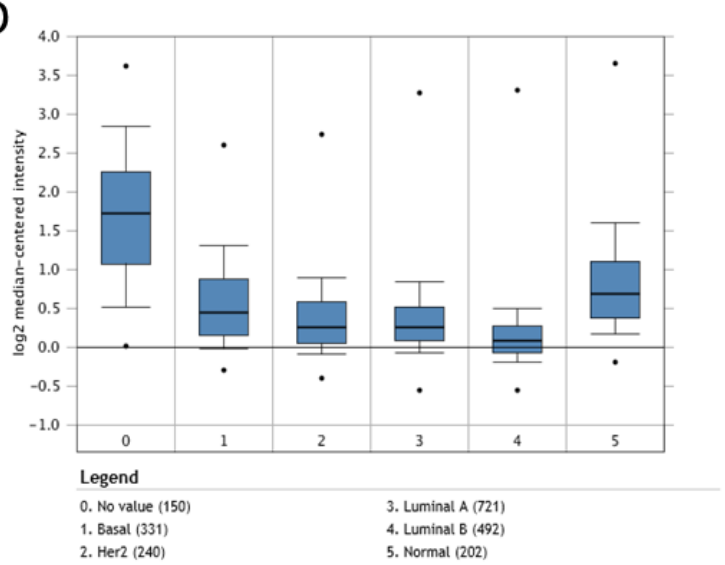
log2 median-centered intensity
4.0
3.5
3.0
2.5
2.0
1.5
1.0
0.5
0.0
-0.5
-1.0
0
1
2
3
4
5
Legend
0. No value (150)
1. Basal (331)
2. Her2 (240)
3. Luminal A (721)
4. Luminal B (492)
5. Normal (202)

E

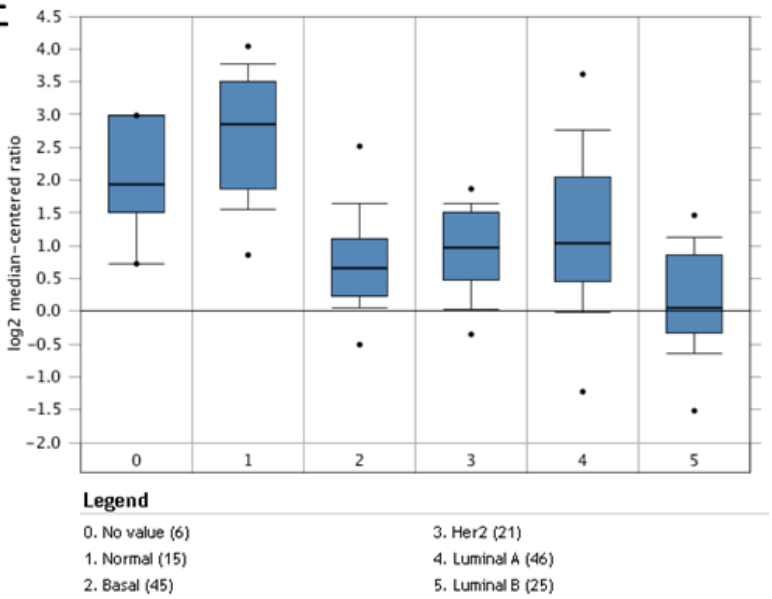
log2 median-centered ratio
4.5
4.0
3.5
3.0
2.5
2.0
1.5
1.0
0.5
0.0
-0.5
-1.0
-1.5
-2.0
0
1
2
3
4
5
Legend
0. No value (6)
1. Normal (15)
2. Basal (45)
3. Her2 (21)
4. Luminal A (46)
5. Luminal B (25)

Figure 5.2. Methylation Status of the *SOD3* Promoter

(**A**) A diagram depicting the pyrosequencing region of the *SOD3* gene. The binding sites of known transcription factors are highlighted in sequence. The CpG sites are indicated by the blank lines and the number of bases away from the transcription start site for *SOD3*. (**B**) The average methylation across all 6 CpG sites tested by pyrosequencing comparing normal to tumor tissue. (**C**) The average methylation of all CpG sites within the *SOD3* promoter comparing the different breast cancer subtypes to the normal breast tissue control. (**D**) The average methylation of each individual CpG examined in the *SOD3* promoter comparing the tumor tissue to normal breast tissue. (**E**) A heatmap indicating the methylation status of each CpG site for all the samples tested. The tissue type is indicated on the left edge of the heatmap.

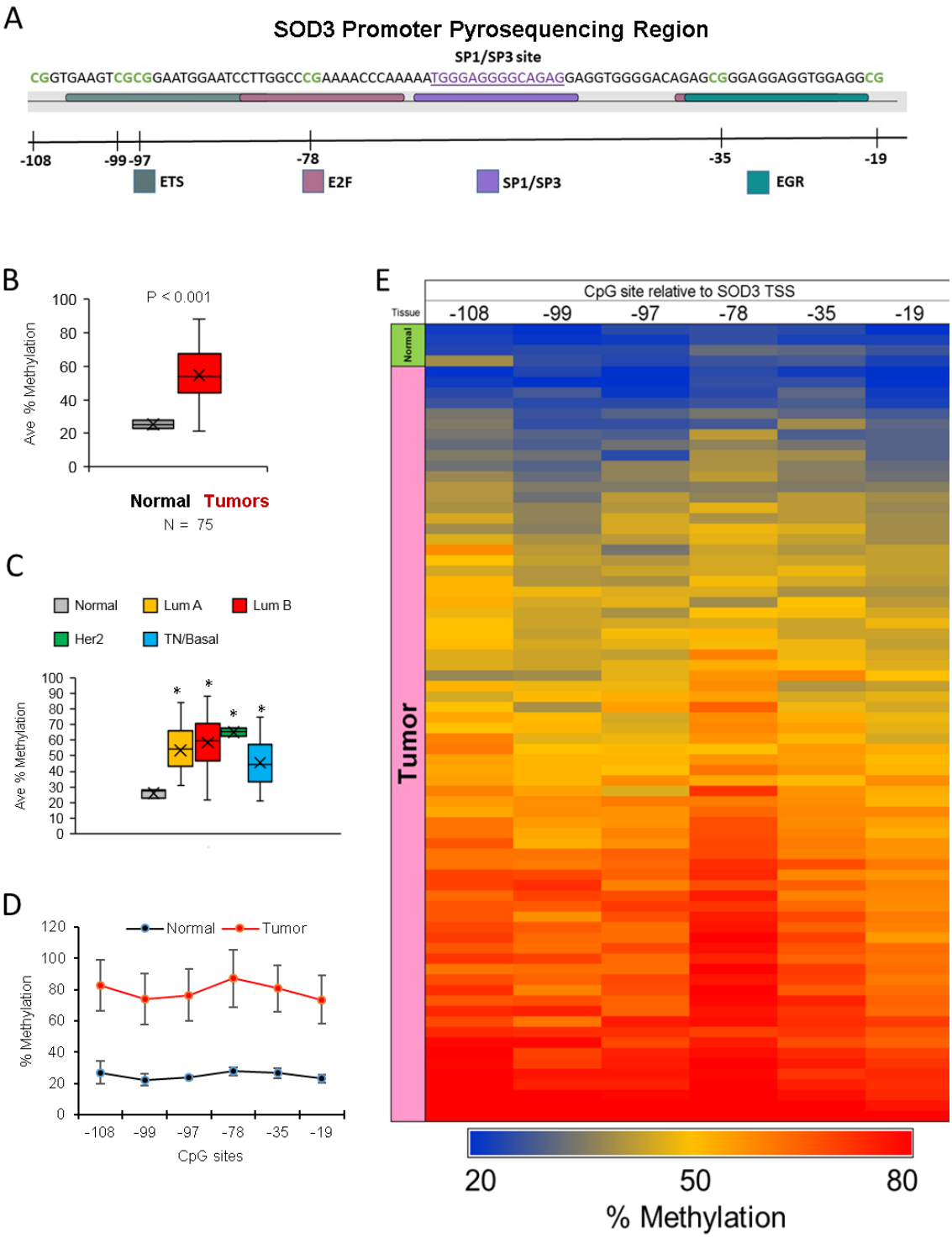
A
SOD3 Promoter Pyrosequencing Region
SP1/SP3 site
CGGTGAAGTCGCGGAATGGAATCCTTGGCCCGAAAACCCAAAAATGGGAGGGGCAGAGGAGGTGGGGACAGAGCGGGAGGAGGTGGAGGCG
-108
-99
-97
-78
-35
-19
ETS
E2F
SP1/SP3
EGR
B
P < 0.001
Ave % Methylation
Normal
Tumors
N = 75
C
Normal
Lum A
Lum B
Her2
TN/Basal
Ave % Methylation
D
Normal
Tumor
% Methylation
CpG sites
E
CpG site relative to SOD3 TSS
Tissue
Normal
Tumor
20
50
80
% Methylation

tumors showed significantly higher levels of CpG methylation in the *SOD3* promoter region (Average of the 6 CpG sites = 53.6% in tumors vs. 25.2% in normal), as presented in Figure 5.2B. A high % methylation is predicted to be associated with a suppression of *SOD3* gene expression. Our results here support *SOD3* expression being lower in breast tumors relative to normal tissue as shown in Figure 5.1A. Figure 5.2C shows the methylation pattern of *SOD3* gene across the clinical subtypes. Figure 5.2D shows the methylation pattern at each of the queried CpG sites, which indicates most tumors having significantly increased methylation across all of the 6 CpG sites while the normal tissue showed predominantly hypomethylation of CpGs in this *SOD3* promoter region ($p < 0.05$). The highest methylation levels were seen at position -78 bp in both the normal and tumor tissues. Methylation at this site is known to interfere with SP1/SP3 binding, thereby leading to a suppression of *SOD3* gene expression. The methylation pattern at the queried CpG sigtes for each sample is also shown in the heatmap in figure 5.2E.

5.2.3 Luminal B Subtype Shows the Highest Correlation of *SOD3* Methylation with Its Expression

We then determined the correlation between the % methylation and *SOD3* expression (from the Agendia array) with Spearman's correlation coefficient analysis (R values). As shown in Figure 5.3A, there was a moderate inverse correlation in all the tumor samples analyzed regardless of the molecular subtype ($R = -0.383$). A strong correlation was observed in the Luminal B subtype ($R = -0.540$), which is followed by the Luminal A subtype ($R = -0.417$) while a weak correlation was observed in the triple-negative/basal-like subtype ($R = -0.3652$), as shown in figure 5.3 A-D (left panels). Correlation analysis was not determined in the Her2+ subtype since the number of

Figure 5.3. Correlation of *SOD3* Expression with Promoter Methylation

(**A-I**) Spearman's correlation between the % methylation of the *SOD3* promoter and expression levels of *SOD3* was used to determine the strength and direction of their association. Each graph indicates in the upper left corner which data set was used either the (**A-D**) BCCR cohort or the (**E-I**) TCGA database. The subtype of breast cancer is also indicated on the top of graph.

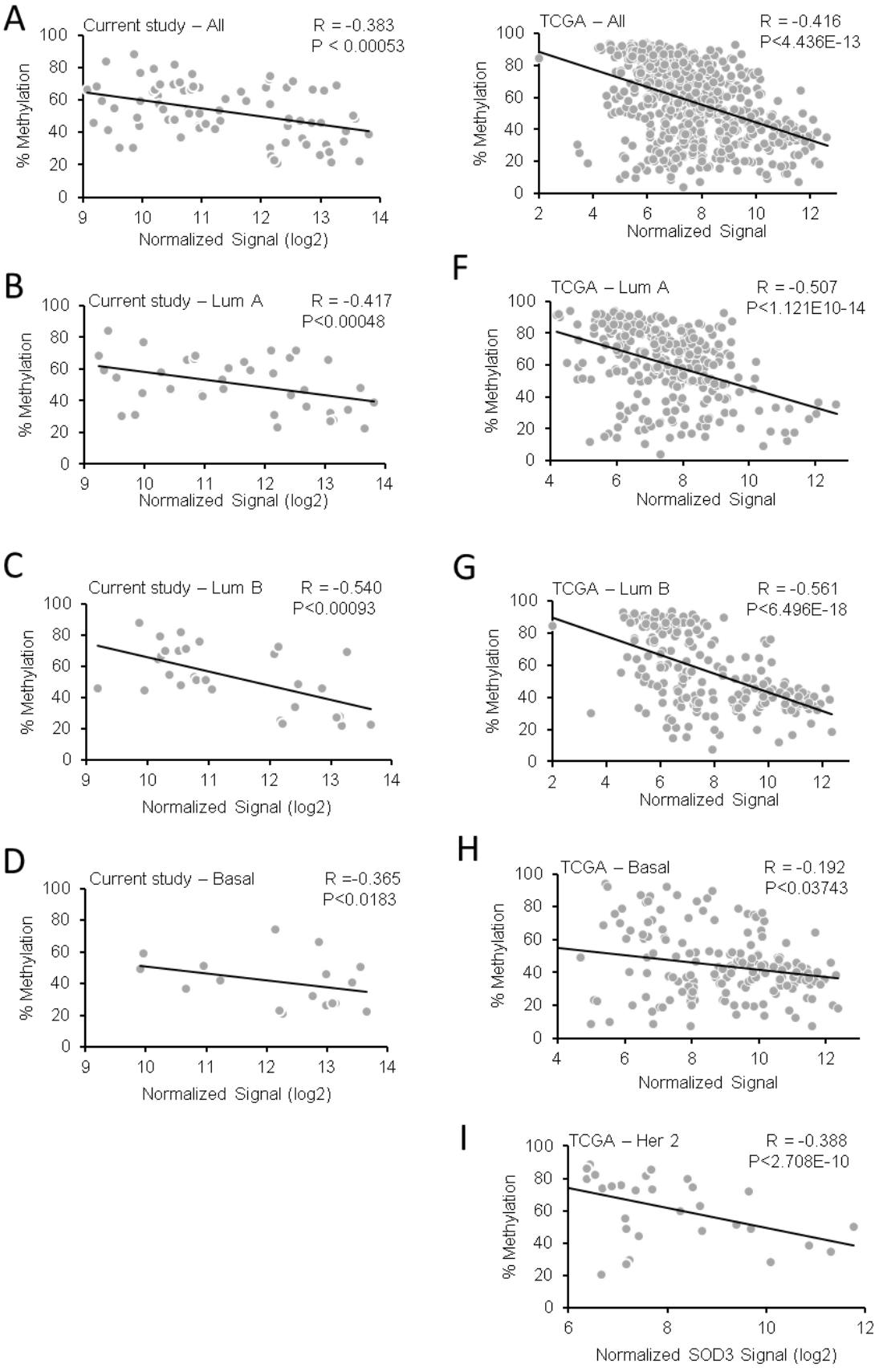
A
Current study – All
R = -0.383
P < 0.00053
% Methylation
Normalized Signal (log2)
B
Current study – Lum A
R = -0.417
P<0.00048
% Methylation
Normalized Signal (log2)
C
Current study – Lum B
R = -0.540
P<0.00093
% Methylation
Normalized Signal (log2)
D
Current study – Basal
R =-0.365
P<0.0183
% Methylation
Normalized Signal (log2)
TCGA – All
R = -0.416
P<4.436E-13
% Methylation
Normalized Signal
F
TCGA – Lum A
R = -0.507
P<1.121E10-14
% Methylation
Normalized Signal
G
TCGA – Lum B
R = -0.561
P<6.496E-18
% Methylation
Normalized Signal
H
TCGA – Basal
R = -0.192
P<0.03743
% Methylation
Normalized Signal
I
TCGA – Her 2
R = -0.388
P<2.708E-10
% Methylation
Normalized SOD3 Signal (log2)

samples available was too low to generate a statistically meaningful result. These pyrosequencing analyses suggest that promoter DNA methylation of *SOD3* is likely a major contributor to the reduced expression levels of this antioxidant in Luminal B breast cancers but less influential on the triple-negative/basal-like subtype.

5.2.4 TCGA Database Analysis Showed Similar *SOD3* Promoter Methylation Patterns

These data trends in our cohort are also seen in the breast carcinoma samples from the TGCA database. The right panels on Figure 5.3E-I show the triple-negative/basal-like subtype having the lowest correlation (R = -0.192) while the Luminal B having the highest correlations (R = -0.561) with the gene expression levels. Good to moderate correlations were also seen in the Luminal A subtype (R = -0.507) and Her2+ subtype from the TCGA database (R = -0.388), respectively. The TCGA methylome analysis (Illumina 450K array analysis) only covers two overlapping CpG sites as our pyrosequencing region (-97 and -78 from the TSS shown in Figure 5.2A). The TCGA methylome sites are marked chr4:24795366_cg03577139 and chr4:24795385_cg11372436. These data suggest that pyrosequencing analysis of the chosen *SOD3* promoter area with 323 nucleotides region used in this study is a potential predictive region and a more cost effective approach in determining the association of this epigenetic mechanism with its gene expression in breast carcinomas. The methylation study also suggests that there are likely other factors leading to down-regulation of *SOD3* expression in the triple-negative/basal-like subtype.

5.2.5 Specific CpG Methylation Status in Breast Cancer Subtypes

When correlation between methylation patterns of each CpG site and the mRNA expression of *SOD3* was further analyzed in individual breast cancer subtypes, we observed that Luminal B subtype shows the highest correlation coefficient at the -78 position while the -19 CpG location shows the highest correlations in the Luminal A and TN/basal-like subtypes (Table 5.1). These observations suggest that the association of site-specific methylation with the *SOD3* mRNA expression is subtype dependent.

5.2.6 *SOD3* gene deletion is detected in the most aggressive subtypes of breast cancers

Another known mechanism of *SOD3* silencing in cancer is genetic deletion. Therefore, we analyzed *SOD3* copy number variation (CNV) in the TCGA database. Table 5.2 shows that shallow deletion is more prevalent than a gain/amplification of the *SOD3* gene copy number in breast tumors. Amongst the subtypes, *SOD3* is deleted most often in basal (51.3%) and Her2-enriched (44.2%) cancers, suggesting gene deletion to play a more prominent role in regulating gene expression in these aggressive diseases.

Table 5.1. Correlation between Specific *SOD3* CpG Methylation Sites and mRNA Expression in Clinical Subtypes

TN/Basal	Lum B	Lum A	All subtypes		CpG sites
-0.2195	-0.5075	-0.4008	-0.3693	**Correlation**	**-108**
2.1E-06	1.7E-12	5.9E-17	5.8E-35	**p-value**	
-0.3828	-0.5222	-0.4533	-0.4062	**Correlation**	**-99**
4.5E-06	1.4E-11	7.3E-15	6.6E-32	**p-value**	
-0.3194	-0.4515	-0.4148	-0.3637	**Correlation**	**-97**
5.1E-06	2.1E-11	9.4E-16	1.1E-32	**p-value**	
-0.2948	-0.5816	-0.4302	-0.3870	**Correlation**	**-78**
5.9E-07	6.9E-12	3.6E-16	4.4E-34	**p-value**	
-0.2673	-0.5609	-0.4214	-0.3871	**Correlation**	**-35**
6.8E-07	4.7E-13	2.0E-17	1.4E-36	**p-value**	
-0.3850	-0.5732	-0.4674	-0.4184	**Correlation**	**-19**
3.0E-06	2.9E-11	1.0E-16	3.2E-33	**p-value**	

Table 5.2. Subtype-specific Copy Number Variation of *SOD3*

The *SOD3* copy number variation data in the TCGA database broken down by breast cancer subtype. The bottom row indicates the % of samples with either deep or shallow deletion.

	Lum A	Lum B	Her2	Basal-like	Normal-like
Deep Deletion	0	0	2	0	0
Shallow Deletion	25	24	21	40	1
Diploid	175	79	29	38	7
Gain	6	7	1	1	0
Amplification	0	0	0	1	0
% Deleted	**12.5%**	**23.3%**	**44.2%**	**51.3%**	**12.5%**

5.3 Discussion

The discovery that tumor suppressor genes are often epigenetically silenced during cancer development [518] has served as a foundation for the use of small molecule epigenetic modifiers in novel cancer therapy strategies. DNA promoter methylation is significantly associated with the development of various human tumors. *SOD3* lacks a standard CpG island but contains a cluster of 18 CpG sites surrounding the transcriptional start site (-550 bp upstream to 100 bp downstream) with known transcription factor binding sites, such as Sp1/Sp3. *SOD3* CpG sites have been reported to be hypermethylated in tumor tissue from gallbladder, liver, prostate, lung, and a small subset of breast cancer samples [142, 153, 192-194]. *SOD3* is also hypermethylated and downregulated in other diseases, such as coronary artery disease [195]. Highlighting the functional role of epigenetic silencing of EcSOD, treatment with 5-aza-2'-deoxycytidine (5-aza-dC), an inhibitor of DNA methylation increased EcSOD expression in both normal and cancer cells [142, 153, 159, 196-198]. This methyltransferase inhibitor increased DNA accessibility via nucleosome remodeling thereby increasing RNA polymerase II and Sp3 binding to the *SOD3* promoter [198].

In this study, we focused on the differential methylation of CpG sites, which are located in the TSS -19 to -108 region of the *SOD3* gene. We found that methylation of the six CpG sites in this region is highly associated with an inverse correlation with the mRNA expression levels of *SOD3* in breast tissues. While the normal breast tissues showed low levels of methylation in the *SOD3* promoter, higher levels of methylation were found in breast tumors of all molecular subtypes. Interestingly, the highest extent of this negative correlation was detected in the Luminal B subtype and the lowest correlation was seen in the TN/basal-like subtype. Moreover, we showed that *SOD3*

expression is most significantly down-regulated in the Luminal B subtype of breast cancer.

Luminal subtypes are the most commonly diagnosed breast cancers (60-70%). In comparison to the Luminal A subtype, the Luminal B cancers are associated with higher grade (26% grade III in luminal B compared to 8% in luminal A), micropapillary histology, and high frequency of nodal metastasis (54 vs. 43%) [520]. Patients with the Luminal B subtype also has a higher proportion of local recurrence and bone metastasis than in patients in the non-luminal groups [521]. The landscape of breast cancer methylomes have been shown to be different between biologically distinct subtypes. Stefansson et al [522] showed that DNA methylation patterns linked to the Luminal B subtype are characterized by CpG island promoter methylation events while a large fraction of basal-like tumors are mainly characterized by hypomethylation events occurring within the gene body.

In addition to DNA methylation, Alterations of *SOD3* expression, tissue distribution, and/or function can also occur via single nucleotide polymorphisms (SNPs). The *SOD3* SNPs that have been associated with cancer risk and progression include rs1799895, rs2536512, rs2284659, and rs699473, and their effects are reviewed in Griess et al [453]. However, no SNPs are identified to be associated with *SOD3* expression in our breast patient cohort, as analyzed by the whole exome DNA sequence analysis. Several reports indicate the *SOD3* gene, located on chromosome 4p15.3-4p15.1, is a hotspot for loss of heterozygocity in cancer. The deletion of chromosome 4p15.1-15.3 has been observed in many types of solid cancers, such as cervical, breast, head and neck, liver, colorectal, lung, and bladder [149, 153, 240-248]. These loses range from 30% in bladder cancer up to 60% in lung cancer [245, 248]. Our copy number variation analyses indeed revealed a higher association of *SOD3* gene deletion

in the basal-like subtype compared to the other subtypes. This data also matches previous data indicating that deletion of chromosome 4p is most common in basal-like breast cancers [523].

In conclusion, this study expands upon the data examining the role of promoter DNA methylation in regulating *SOD3* gene expression. These data provide clear evidence of the negative correlation of promoter methylation and down-regulation of *SOD3* expression in our cohort of breast cancer specimens. This study also highlights that despite reduction of *SOD3* in all breast cancer subtypes, there are key differences in the silencing mechanism for each subtype. Promoter hypermetylation of *SOD3* are more prevalent in the Luminal B cancers while *SOD3* gene silencing is affected mostly via CNV in TN/basal-like cancers. Analysis of breast cancer data by Kaplan-Meier Plotter (http://kmplot.com) showed that low *SOD3* expression is significantly associated with poor outcome (relapse free survival, RFS) in breast cancer patients [453]. This suggests that loss of this extracellular redox regulator promotes a conducive microenvironment that favors cancer progression. The vast array of genetic and/or epigenetic mechanisms reported in mediating dysregulation of *SOD3* expression, function, and cellular distribution [453] further supports that loss of this extracellular antioxidant provides a selective advantage to cancer development.

CHAPTER 6:

Summary and Future Directions

6 Summary and Future Directions

6.1 Summary of Research

Breast cancer is a highly heterogeneous disease with many different molecular subtypes. The most aggressive subtype is the basal-like subtype, which largely overlaps with the triple negative breast cancer (TNBC) subtype. TNBC is a fast growing and metastatic subtype, which unlike the other subtypes lacks any targeted therapies. Therefore, determining novel mechanisms that lead to its aggressive phenotype provide therapeutic approaches to reduce its invasive nature in breast cancer patients. One of the novel areas of research into TNBC is its ability to modify the area within the tumor, also known as the tumor microenvironment (TME). The TME is highly complex with many different activated cell types resulting in a complicated network of signaling driven by the altered signaling in the cancers cells. The major cell types within the TME are fibroblasts, macrophages, endothelial cells, and T cells. All of which can be activated by cancer cells or each other. Additionally, the ECM undergoes dramatic changes throughout cancer progression, which further contributes to complexity of the signaling network. It has become clear that the TME plays a large role in determining the aggressiveness of breast cancer. Many studies have correlated activation of fibroblasts with negative patient outcomes. Macrophages are also associated with poor survival and metastasis in breast cancer depending on the type of macrophage polarization. Thus, there is a need to determine how these cells are activated by cancer cells to help promote its own aggressive phenotype. Inhibiting these activation steps provides a novel therapeutic approach to treating aggressive breast cancers, such as TNBC, which currently lacks any suitable drug targets.

Extracellular superoxide dismutase (EcSOD) is a member of the SOD family, which are antioxidant enzymes that catalyze the dismutation reaction of superoxide into hydrogen peroxide. It is the most recently discovered and least researched member of its family. It has two unique domains that separate it from the closely related Cu/ZnSOD, which are its heparin binding domain and its signal sequence. The signal sequence results in its secretion into the extracellular space allowing it to control levels of reactive oxygen species (ROS) between cells. The heparin binding domain allows EcSOD to bind to proteoglycans on the cell surface or within the extracellular matrix (ECM). This ability to bind to the cell surface allows EcSOD to be endocytosed into the interior of cells, as well. It is expressed in a tissue- and cell-specific manner. However, in solid cancers, expression of EcSOD is lost. The loss of EcSOD correlates with poor patient outcome in many cancers, such as breast, lung, and pancreatic. Additionally, re-expression of EcSOD inhibits cancer cell growth and invasion *in vitro*, as well as inhibits tumor growth and metastasis. However, the exact mechanism behind this tumor suppressive phenotype remains unknown. Due to its unique localization, I *hypothesized* that loss of EcSOD promotes an oxidized TME (oxTME), which promotes activation of stromal cells, such as fibroblasts and macrophages, leading to an aggressive breast cancer phenotype.

Previous studies clearly showed the loss of EcSOD in breast cancer is pervasive and occurs through many different mechanisms. However, due to low sample size, the main cause of EcSOD downregulation in breast cancer remained unclear. Therefore, we sought to determine the mechanism by which EcSOD is downregulated in breast cancer. Previous studies indicated DNA methylation at its promoter can result in epigenetic silencing of EcSOD. Additionally, aberrant DNA methylation is a well-known marker of cancer. Therefore, we hypothesized that EcSOD silencing correlated with increased

DNA methylation at its promoter. We utilized patient samples from the Breast Cancer Collaborative Registry run by the Northern Great Plains Personalized Breast Cancer Program (NGPPBCP). Pyrosequencing analysis of the EcSOD promoter indicated increased DNA methylation in breast cancer patients. The DNA methylation was significantly correlated with decreased mRNA expression of EcSOD in those same patients. This correlation was strongest in the Luminal B breast cancers, which are most likely to have a local recurrence and metastasize to the bone. Despite similar levels of EcSOD expression, basal-like breast cancers had the weakest correlation. Due to the higher genetic instability within basal-like breast cancer, we analyzed the gene copy number in the TGCA database and determined the EcSOD gene is deleted frequently and most often in this subtype of breast cancer.

Previous studies in our lab have shown tumor suppressive effects of EcSOD in breast cancer cells. To determine the mechanism of these effects, a receptor tyrosine kinase (RTK) signaling array and extracellular protein array were used to determine if EcSOD overexpression inhibited specific pathways in the TNBC cell line, MDA-MB231. The c-Met receptor and its downstream kinase c-Abl were significantly inhibited by EcSOD. Additionally, thrombospondin 1 (TSP-1), a secreted factor that sequesters the c-Met ligand, hepatocyte growth factor (HGF), and prevents its signaling, was significantly increased in EcSOD expressing cells (Ec.20). In breast cancer, HGF/c-Met signaling occurs in a paracrine fashion with fibroblasts secreting HGF, which then activates c-Met on breast cancer cells. Therefore, we utilized normal mammary fibroblast (RMF) and HGF-overexpressing fibroblasts (RMF-HGF) in co-culture with breast cancer cells. EcSOD expression in MDA-MB231 significantly inhibited HGF-mediated cancer cell invasion induced by RMF-HGF to levels similar to control fibroblasts, RMF. Furthermore, 3D growth of MDA-MB231 was stimulated by RMF-HGF compared to RMF control.

However, EcSOD expression inhibited the RMF-HGF-mediated growth stimulation. Additionally, we found that long-term co-culture of MDA-MB231 and RMF-HGF increased the ability of fibroblasts to promote cancer cell invasion. Interestingly, expression of EcSOD inhibited this enhanced aggressive phenotype in the fibroblasts indicating that ROS plays a role in activation of fibroblasts. Further analysis of the RMF-HGF fibroblasts indicated that they have higher ROS production through increased expression of the ROS generating enzyme, Nox4. Nox4 knockdown or inhibition with DPI reduced fibroblast activation as evidence by their reduced ability to contract and remodel collagen. MnTE-2-PyP (MnTE), a redox active drug, also decreased collagen contraction indicating ROS is required during fibroblast activation. MnTE also replicated the results of the EcSOD inhibition of HGF/c-Met signaling in MDA-MB231 reducing their growth and invasion. We have further shown that scavenging ROS with EcSOD significantly inhibited RMF-HGF-stimulated orthotopic tumor growth of MDA-MB231. This study suggests the loss of EcSOD in breast cancer plays a pivotal role in promoting the HGF/c-Met-mediated cancer-fibroblast interactions. Additionally, this study highlights the role of ROS in activating fibroblasts during breast cancer progression.

To further study the role of the oxTME during activation of stromal cells, we tested how ROS effects macrophage polarization. Macrophages have high plasticity and are very sensitive to their surrounding environment. Macrophages polarize toward two extremes under normal conditions; the anti-tumor and pro-inflammatory M1 type and the pro-tumor and immunosuppressive M2 type. However, in cancer, macrophages are activated by cancer cells and called tumor associated macrophages (TAM), which enhance the aggressiveness of breast cancer via promoting growth, metastasis, and immunosuppression. TAM are closely related to the M2 type of macrophages. The goal of this study was to examine primary human monocyte-derived M1 and M2

macrophages for key redox differences and determine sensitivities of these macrophages to redox-active drugs. MnTE, which previously inhibited fibroblast activation, reduced levels of M2 markers. Additionally, the function of M2 macrophages was inhibited by MnTE. Treatment reduced M2 macrophage mediated-cancer cell growth. Furthermore, MnTE reduced the immunosuppressive nature of M2 macrophages, as determined by co-culture of treated macrophages and T cells during a T cell activation assay. The T cell suppressing molecule, PD-L2, was reduced by MnTE in a dose dependent manner. Additionally, this study also determined that there are key differences in ROS generation and scavenging between M1 and M2 macrophages. Our results indicate that M2 macrophages have lower levels of reactive oxygen species (ROS) and lower production of extracellular hydrogen peroxide compared to the M1 macrophages. These differences are due in part to reduced expression levels of pro-oxidants, Nox2, Nox5, and the non-enzymatic members of the Nox complex, p22phox and p47phox, as well as higher levels of antioxidant enzymes, Cu/ZnSOD, Gpx1, Gpx4, and catalase. However, analysis of ROS levels indicated that MnTE treatment reduced ROS levels in M2 but not M1 macrophages. Inhibition of Nox-derived ROS with DPI and addition of the ROS scavenger, TEMPO, also reduced M2 markers. Additionally, conditioned media from EcSOD expressing cancer cells, MDA-MB231 Ec.20, inhibited the cancer cell-mediated increase in M2 markers. Conversely, increasing ROS via direct addition of hydrogen peroxide increased M2 markers. Therefore, despite the lower ROS levels, M2 macrophage require ROS for proper polarization and pro-tumor functions. Mechanistically, MnTE decreased Stat3 activation during IL4-induced M2 polarization, as evidenced by reduced phosphorylation of Stat3 and reduced expression of downstream genes. Overall, this study reveals key redox differences between M1 and M2 primary human macrophages and that redox-active drugs can be used to inhibit the

pro-tumor and immunosuppressive phenotype of TAM-like M2 macrophages. This study also provides rationale for combining MnTE-2-PyP5+ with immunotherapies.

In conclusion, this dissertation sought to determine the role of ROS in activating stromal cells within the TME in breast cancer. We focused on fibroblasts and macrophages, since they are the most abundant stromal cells within the TME. These studies indicate that loss of EcSOD promotes an oxTME, which serves to activate fibroblasts and promote pro-tumor macrophage polarization. We also identified the use of MnTE, a drug in clinical trials, as a potential therapeutic approach to reprogram the hostile TME seen in aggressive breast cancers.

6.2 Future Directions

6.2.1 EcSOD and Its Inhibitory Role in Breast Cancer

The role of EcSOD silencing during tumorigenesis remains unclear. In normal breast epithelial cells, EcSOD is lost when polarity is lost and with long-term stimulation with estradiol. These suggest that loss of EcSOD occurs early in tumorigenesis. Therefore, we hypothesize that EcSOD expression would prevent or delay development of breast cancer. To test this hypothesis, I propose the use of the spontaneous breast cancer mouse model, MMTV-PyMT, which expresses the polyoma virus middle T antigen (PyMT) under the mouse mammary tumor virus promoter/enhancer (MMTV). This model will be crossed with *SOD3* knockout mice to examine if EcSOD plays a role in delaying tumor development [138]. Additionally, ROS alone activates CAFs and promotes immunosuppression. Therefore, this model can also be used to determine the

effect of EcSOD regulating the TME by analysis of CAF activation and immune cell infiltration.

Furthermore, the mechanism by which EcSOD inhibits HGF-c-Met signaling remains unanswered. There are two main hypotheses for how EcSOD functions in this regard: increased protein tyrosine phosphatase (PTP) activity and increased TSP1/2 secretion. The first is by reducing ROS levels to prevent ROS-mediated inhibition of PTPs. PTPs, such as PTP1B, TCPTP, SHP-1, and SHP-2, de-phosphorylate and inhibit c-Met signaling downstream [524-526]. Therefore, we hypothesize that EcSOD expression reduces PTP oxidation enhancing its activity, thereby decreasing c-Met signaling. Analysis of c-Met activation during inhibition or silencing of these PTPs will provide the initial impetus to narrow down the choices of PTPs. The second hypothesis is through increased sequestration of HGF by thrombospondin 1/2 (TSP1/2). TSP1 has a strong affinity for HGF sequestering it away and preventing binding to c-Met [431, 432]. TSP1/2 are anti-angiogenic and anti-metastatic factors that show inverse correlation with malignant progression in breast cancer [429, 430]. Therefore, we hypothesize that silencing of TSP1/2 via inducible short hairpin RNA (shRNA) in breast cancer cells overexpressing EcSOD would determine the contribution of TSP1/2 to c-Met inhibition phenotype of EcSOD overexpressing breast cancer cells. This could be tested by both direct addition of HGF, co-culture of cancer cells with RMF-HGF, or co-injection of cancer cells with RMF-HGF or RMF.

Another aspect of EcSOD function that remains unstudied is its ability to preserve nitric oxide and reduce peroxynitrite levels. By removal of superoxide, nitric oxide cannot react with it to form peroxynitrite. Both, peroxynitrite and nitric oxide are increased in breast cancer [527]. Several studies have implicated nitric oxide as a driver of cancer progression, angiogenesis, and reduced survival [528-530]. However, many

studies fail to draw the distinction between effects of nitric oxide and peroxynitrite, as it is also associated with metastasis, angiogenesis, and poor survival [373, 531, 532]. Additionally, peroxynitrite is more reactive than nitric oxide causing nitration of proteins leading to NF-κB activation, as well as reduced CXCL12 and CCL2 signaling resulting in impaired leukocyte chemotaxis and tumor infiltration [533-535]. Therefore, loss of EcSOD is believed to promote the increase of peroxynitrite levels and the potential loss of nitric oxide, due to its ability to scavenge superoxide. In particular, extracellular peroxynitrite causes nitration of ECM proteins leading to release of growth factors, such as VEGF, and enhanced fibroblast migration [536-539]. The extracellular peroxynitrite also promotes immunosuppression by nitration of T-cell receptor (TCR)-CD8 complex, inhibition of T cell activation, and reduced infiltration due to inactive nitrated chemokines [380, 540]. Due to its ability to regulate extracellular superoxide, loss of EcSOD in breast cancer may play a pivotal role in controlling peroxynitrite levels, which remains understudied. Therefore, I propose the analysis of nitrotyrosine and EcSOD in tumors to determine if EcSOD loss increases nitrotyrosine levels, a marker of peroxynitrite. Analyzing nitration levels on fibronection, CCL2, and CXCL12, may also provide a mechanism for the reduced metastasis in EcSOD expressing cells. Another potential mechanism for the EcSOD-mediated inhibition of metastasis is the preservation of nitric oxide in the pulmonary endothelial cells. Nitric oxide is a vasoprotector that prevents endothelial cell activation and limits adhesion to the vessel wall [541]. A new study implicates reduced nitric oxide in the early stages of breast cancer lung metastasis through reduced endothelial activation and permeability [542]. Additionally, vascular permeability is increased in basal-like breast cancers where it promotes metastasis and reduces efficient drug delivery [543-545].

Finally, since aggressive breast cancer cells have increased NOS2 expression, a producer of nitric oxide, and increased ROS levels, due in part to loss of EcSOD, they are likely to have higher peroxynitrite levels. Peroxynitrite, like all reactive species, can induce stress and lead to apoptosis at high levels. Therefore, loss of EcSOD may indicate cancer cells that are more sensitive to cell death induced by peroxynitrite donors through Akt inactivation and MLK activation [546]. Doxorubicin is a potent anti-tumor agent that induces cell death in a peroxynitrite-dependent manner [547]. Therefore, EcSOD expression may be a valuable marker to predict response rates in BC patients.

6.2.2 ROS and Its Role in M2 Macrophage Polarization

While my work provides strong evidence that ROS is directly affecting M2 macrophage polarization, there is also a reasonable amount of evidence that GSH also effects macrophage polarization. Previous studies have found that increasing GSH levels increased M1 polarization, while increasing oxidized GSH (GSSG) levels increased M2 polarization [367]. Interestingly, my own data suggests that addition of NAC, a GSH precursor, increases both M1 and M2 polarization. However, NAC is also used as an antioxidant that scavenges hydrogen peroxide, which contradicts the data that shows hydrogen peroxide increases M2 polarization. This may be explained by the off target effects of NAC, such as antagonism of proteasome inhibitors and reduction of disulfide bonds [548, 549]. Additionally, ROS levels were not measured after NAC addition to determine if it was functioning as an antioxidant, as some studies have found NAC to have no effect on ROS levels [550]. These results require further study into the effect of NAC and GSH in macrophage polarization.

Alterations in glutathione-S-transferases (GST), as seen in Beyer et al., between M1 and M2 macrophages may provide a potential mechanism behind the similar effects

of NAC and hydrogen peroxide on macrophage polarization, despite their likely disparate effects on ROS levels. GSTs are a family of proteins that regulate glutathionylation which can effect protein activity and act as a signaling event [551]. A recent study has found glutathionylation levels in macrophages change depending on the environmental cues [552]. Additionally, during LPS stimulation in macrophages, GSTO1 activity is required for production of ROS and pro-inflammatory cytokines, while GSTP1 activity reduced LPS-mediated iNOS and COX-2 expression [553, 554]. Since NAC also increases GST activity, the different effects of GSTs on macrophage polarization may provide an ROS-independent mechanism by which NAC effects polarization [550].

My work represents a novel function of MnTE to inhibit M2 polarization in primary human macrophages. However, this system, while very informative, is quite artificial and limited to in vitro applications. Since macrophages rely on many signals from multiple cells to control their polarization, it is important to test the ability of MnTE to inhibit M2 polarization in vivo. There are several mouse models used to study M2 polarization. The in vivo wound healing assay would provide a fast and robust method to examine the ability of MnTE to inhibit the function of M2 macrophages, as they are vital for proper and effective wound closure [503, 555]. The more relevant model to study the role of MnTE treatment on TAM in BC would be the use of MMTV-PyMT, 4T1, and E0771 mouse models. Due to the ability of cancer cells to induce specific changes and not a generalized macrophage response, it will be important to use multiple mouse models to properly assess the effect of MnTE on TAM polarization and function [556]. While MnTE can effect macrophages, it can also inhibit T_H2 response in CD4+ T cells and reduce hypoxia and angiogenesis in the 4T1 model [290, 292]. Furthermore, T_H2 cells produce IL-4 that promote M2 polarization in MMTV-PyMT mouse models. Therefore, we also

propose the use of the T cell deficient mice, such as BALB/c scid and B6 Rag1, to untangle the effect of T_H2 response and macrophage polarization [557].

While MnTE effectively inhibits macrophage polarization in vitro, it has a mild effect on tumor growth when used as a single agent [290]. Therefore, to help BC patients in the clinic, it is necessary to combine MnTE with other treatments. The research into combined treatments with MnTE has largely focused on radiation, as it acts a radioprotectant and a radiosensitizer [291, 558, 559]. Recent research has also shown efficacy in combination with chemotherapy and ascorbate [283, 560, 561]. However, to date, MnTE or any of its analogs have not been used in combination with immunotherapies. PD-L1 is a transmembrane protein that interacts with PD-1 on T cells causing their immunosuppression and is upregulated in TNBC [562]. Therefore, I hypothesize that combination of PD-L1 targeting therapies, which activate T cells, with MnTE would provide a synergistic effect in treating aggressive and metastatic BC.

Besides macrophage-mediated T cell suppression, immunotherapy also struggles to overcome “cold” tumors, which lack immune cell infiltration [563]. Chemotherapy-induced cancer cell death enhances immune cell recruitment turning the tumor “hot” [564]. This is best illustrated by a phase III clinical trial combining paclitaxel with atezolizumab, a PD-L1 targeting antibody, which has significantly increased progression-free survival in metastatic TNBC patients [8]. Interestingly, MnTE reduces chemotherapy-induced peripheral neuropathy, which is a dose-limiting side effect, without inhibiting the efficacy of paclitaxel [565, 566]. Therefore, in addition to inhibiting an immunosuppressive TME and increasing the efficacy of immunotherapies, a combination of all three modalities may provide an even more beneficial outcome while reducing the negative effects of chemotherapy. Similarly, radiation is also used to turn tumors “hot” and is being combined with immunotherapies. As highlighted earlier, the

use of MnTE in radiotherapy to reduce negative side effects and increase efficacy is well studied. Therefore, there is also strong rationale for combination of MnTE, immunotherapy, and radiotherapy in aggressive BC.

REFERENCES

1. DeSantis, C.E., et al., *Breast cancer statistics, 2019.* CA Cancer J Clin, 2019.
2. Pfeiffer, R.M., et al., *Proportion of U.S. Trends in Breast Cancer Incidence Attributable to Long-term Changes in Risk Factor Distributions.* Cancer Epidemiol Biomarkers Prev, 2018. **27**(10): p. 1214-1222.
3. Jones, M.E., et al., *Smoking and risk of breast cancer in the Generations Study cohort.* Breast Cancer Res, 2017. **19**(1): p. 118.
4. Coombs, N.J., et al., *The impact of changes in hormone therapy on breast cancer incidence in the US population.* Cancer Causes Control, 2010. **21**(1): p. 83-90.
5. Munoz, D., et al., *Effects of screening and systemic adjuvant therapy on ER-specific US breast cancer mortality.* J Natl Cancer Inst, 2014. **106**(11).
6. Waks, A.G. and E.P. Winer, *Breast Cancer Treatment: A Review.* JAMA, 2019. **321**(3): p. 288-300.
7. Slamon, D., et al., *Adjuvant trastuzumab in HER2-positive breast cancer.* N Engl J Med, 2011. **365**(14): p. 1273-83.
8. Schmid, P., et al., *Atezolizumab and Nab-Paclitaxel in Advanced Triple-Negative Breast Cancer.* N Engl J Med, 2018. **379**(22): p. 2108-2121.
9. Perou, C.M., et al., *Molecular portraits of human breast tumours.* Nature, 2000. **406**(6797): p. 747-752.
10. Toft, D.J. and V.L. Cryns, *Minireview: Basal-like breast cancer: from molecular profiles to targeted therapies.* Molecular endocrinology (Baltimore, Md.), 2011. **25**(2): p. 199-211.
11. Ahn, S.G., et al., *Molecular Classification of Triple-Negative Breast Cancer.* Journal of breast cancer, 2016. **19**(3): p. 223-230.
12. Jezequel, P., et al., *Gene-expression molecular subtyping of triple-negative breast cancer tumours: importance of immune response.* Breast Cancer Res, 2015. **17**: p. 43.
13. Burstein, M.D., et al., *Comprehensive genomic analysis identifies novel subtypes and targets of triple-negative breast cancer.* Clin Cancer Res, 2015. **21**(7): p. 1688-98.
14. Barnard, M.E., C.E. Boeke, and R.M. Tamimi, *Established breast cancer risk factors and risk of intrinsic tumor subtypes.* Biochimica et Biophysica Acta (BBA) - Reviews on Cancer, 2015. **1856**(1): p. 73-85.
15. Jones, D.P., *Redox theory of aging.* Redox Biol, 2015. **5**: p. 71-9.
16. Burgoyne, J.R., et al., *Redox signaling in cardiac physiology and pathology.* Circ Res, 2012. **111**(8): p. 1091-106.
17. Lei, Y., et al., *Redox regulation of inflammation: old elements, a new story.* Med Res Rev, 2015. **35**(2): p. 306-40.
18. Kovacic, P. and R. Somanathan, *Redox processes in neurodegenerative disease involving reactive oxygen species.* Curr Neuropharmacol, 2012. **10**(4): p. 289-302.
19. Chio, I.I.C. and D.A. Tuveson, *ROS in Cancer: The Burning Question.* Trends Mol Med, 2017. **23**(5): p. 411-429.
20. Fiaschi, T. and P. Chiarugi, *Oxidative Stress, Tumor Microenvironment, and Metabolic Reprogramming: A Diabolic Liaison.* International Journal of Cell Biology, 2012. **2012**: p. 8.
21. Parascandolo, A. and M.O. Laukkanen, *Carcinogenesis and Reactive Oxygen Species Signaling: Interaction of the NADPH Oxidase NOX1–5 and Superoxide Dismutase 1–3 Signal Transduction Pathways.* Antioxidants & Redox Signaling, 2018. **30**(3): p. 443-486.

22. Wang, Y., et al., *Superoxide dismutases: Dual roles in controlling ROS damage and regulating ROS signaling.* The Journal of Cell Biology, 2018. **217**(6): p. 1915.
23. Sharpe, M.A., S.J. Robb, and J.B. Clark, *Nitric oxide and Fenton/Haber-Weiss chemistry: nitric oxide is a potent antioxidant at physiological concentrations.* J Neurochem, 2003. **87**(2): p. 386-94.
24. Pacher, P., J.S. Beckman, and L. Liaudet, *Nitric oxide and peroxynitrite in health and disease.* Physiol Rev, 2007. **87**(1): p. 315-424.
25. Beckman, J.S. and W.H. Koppenol, *Nitric oxide, superoxide, and peroxynitrite: the good, the bad, and ugly.* Am J Physiol, 1996. **271**(5 Pt 1): p. C1424-37.
26. Flint, D.H., J.F. Tuminello, and M.H. Emptage, *The inactivation of Fe-S cluster containing hydro-lyases by superoxide.* J Biol Chem, 1993. **268**(30): p. 22369-76.
27. Winterbourn, C.C., *Revisiting the reactions of superoxide with glutathione and other thiols.* Archives of Biochemistry and Biophysics, 2016. **595**: p. 68-71.
28. Barrett, W.C., et al., *Roles of superoxide radical anion in signal transduction mediated by reversible regulation of protein-tyrosine phosphatase 1B.* J Biol Chem, 1999. **274**(49): p. 34543-6.
29. Chance, B., H. Sies, and A. Boveris, *Hydroperoxide metabolism in mammalian organs.* Physiol Rev, 1979. **59**(3): p. 527-605.
30. Go, Y.-M., J.D. Chandler, and D.P. Jones, *The cysteine proteome.* Free radical biology & medicine, 2015. **84**: p. 227-245.
31. Bienert, G.P. and F. Chaumont, *Aquaporin-facilitated transmembrane diffusion of hydrogen peroxide.* Biochim Biophys Acta, 2014. **1840**(5): p. 1596-604.
32. Dickinson, B.C. and C.J. Chang, *Chemistry and biology of reactive oxygen species in signaling or stress responses.* Nat Chem Biol, 2011. **7**(8): p. 504-11.
33. Lim, J.B., et al., *A reaction-diffusion model of cytosolic hydrogen peroxide.* Free Radic Biol Med, 2016. **90**: p. 85-90.
34. Forman, H.J., A. Bernardo, and K.J. Davies, *What is the concentration of hydrogen peroxide in blood and plasma?* Arch Biochem Biophys, 2016. **603**: p. 48-53.
35. Antunes, F. and E. Cadenas, *Estimation of H2O2 gradients across biomembranes.* FEBS Letters, 2000. **475**(2): p. 121-126.
36. Winterbourn, C.C., *Are free radicals involved in thiol-based redox signaling?* Free Radical Biology and Medicine, 2015. **80**: p. 164-170.
37. Lee, S.R., et al., *Reversible inactivation of the tumor suppressor PTEN by H2O2.* J Biol Chem, 2002. **277**(23): p. 20336-42.
38. Cho, S.-H., et al., *Redox regulation of PTEN and protein tyrosine phosphatases in H2O2-mediated cell signaling.* FEBS Letters, 2004. **560**(1): p. 7-13.
39. Denu, J.M. and K.G. Tanner, *Specific and reversible inactivation of protein tyrosine phosphatases by hydrogen peroxide: evidence for a sulfenic acid intermediate and implications for redox regulation.* Biochemistry, 1998. **37**(16): p. 5633-42.
40. Marinho, H.S., et al., *Hydrogen peroxide sensing, signaling and regulation of transcription factors.* Redox Biol, 2014. **2**: p. 535-62.
41. Adams, L., M.C. Franco, and A.G. Estevez, *Reactive nitrogen species in cellular signaling.* Exp Biol Med (Maywood), 2015. **240**(6): p. 711-7.
42. Fukumura, D., S. Kashiwagi, and R.K. Jain, *The role of nitric oxide in tumour progression.* Nat Rev Cancer, 2006. **6**(7): p. 521-34.
43. Burke, A.J., et al., *The yin and yang of nitric oxide in cancer progression.* Carcinogenesis, 2013. **34**(3): p. 503-12.
44. Vahora, H., et al., *The Potential Role of Nitric Oxide in Halting Cancer Progression Through Chemoprevention.* J Cancer Prev, 2016. **21**(1): p. 1-12.

45. Buetler, T.M., A. Krauskopf, and U.T. Ruegg, *Role of superoxide as a signaling molecule.* News Physiol Sci, 2004. **19**: p. 120-3.
46. Afanas'ev, I.B., *On mechanism of superoxide signaling under physiological and pathophysiological conditions.* Med Hypotheses, 2005. **64**(1): p. 127-9.
47. Wang, Y., et al., *Hepatocyte resistance to oxidative stress is dependent on protein kinase C-mediated down-regulation of c-Jun/AP-1.* J Biol Chem, 2004. **279**(30): p. 31089-97.
48. Dong-Yun, S., et al., *Redox stress regulates cell proliferation and apoptosis of human hepatoma through Akt protein phosphorylation.* FEBS Lett, 2003. **542**(1-3): p. 60-4.
49. Lee, S.L., et al., *Serotonin stimulates mitogen-activated protein kinase activity through the formation of superoxide anion.* Am J Physiol, 1999. **277**(2 Pt 1): p. L282-91.
50. Wang, W., et al., *Signaling by eNOS through a superoxide-dependent p42/44 mitogen-activated protein kinase pathway.* Am J Physiol Cell Physiol, 2001. **281**(2): p. C544-54.
51. Jin, Q., et al., *Differential regulation of phosphatidylinositol 3-kinase/Akt, mitogen-activated protein kinase, and AMP-activated protein kinase pathways during menadione-induced oxidative stress in the kidney of young and old rats.* Biochem Biophys Res Commun, 2004. **315**(3): p. 555-61.
52. Meng, T.C., et al., *Regulation of insulin signaling through reversible oxidation of the protein-tyrosine phosphatases TC45 and PTP1B.* J Biol Chem, 2004. **279**(36): p. 37716-25.
53. Namgaladze, D., H.W. Hofer, and V. Ullrich, *Redox control of calcineurin by targeting the binuclear Fe(2+)-Zn(2+) center at the enzyme active site.* J Biol Chem, 2002. **277**(8): p. 5962-9.
54. Afanas'ev, I.B., *Competition between superoxide and hydrogen peroxide signaling in heterolytic enzymatic processes.* Med Hypotheses, 2006. **66**(6): p. 1125-8.
55. Wang, Q., et al., *Catalytic inactivation of protein tyrosine phosphatase CD45 and protein tyrosine phosphatase 1B by polyaromatic quinones.* Biochemistry, 2004. **43**(14): p. 4294-303.
56. Pervaiz, S. and M.V. Clement, *Superoxide anion: oncogenic reactive oxygen species?* Int J Biochem Cell Biol, 2007. **39**(7-8): p. 1297-304.
57. Clement, M.V., J.L. Hirpara, and S. Pervaiz, *Decrease in intracellular superoxide sensitizes Bcl-2-overexpressing tumor cells to receptor and drug-induced apoptosis independent of the mitochondria.* Cell Death Differ, 2003. **10**(11): p. 1273-85.
58. Clement, M.V. and S. Pervaiz, *Intracellular superoxide and hydrogen peroxide concentrations: a critical balance that determines survival or death.* Redox Rep, 2001. **6**(4): p. 211-4.
59. Yamakawa, H., et al., *Activation of caspase-9 and -3 during H2O2-induced apoptosis of PC12 cells independent of ceramide formation.* Neurol Res, 2000. **22**(6): p. 556-64.
60. Hampton, M.B. and S. Orrenius, *Dual regulation of caspase activity by hydrogen peroxide: implications for apoptosis.* FEBS Lett, 1997. **414**(3): p. 552-6.
61. Marklund, S.L., E. Holme, and L. Hellner, *Superoxide dismutase in extracellular fluids.* Clin Chim Acta, 1982. **126**(1): p. 41-51.
62. Marklund, S.L., *Extracellular superoxide dismutase in human tissues and human cell lines.* J Clin Invest, 1984. **74**(4): p. 1398-403.

63. Zelko, I.N., T.J. Mariani, and R.J. Folz, *Superoxide dismutase multigene family: a comparison of the CuZn-SOD (SOD1), Mn-SOD (SOD2), and EC-SOD (SOD3) gene structures, evolution, and expression.* Free Radic Biol Med, 2002. **33**(3): p. 337-49.
64. Brigelius-Flohe, R. and L. Flohe, *Basic principles and emerging concepts in the redox control of transcription factors.* Antioxid Redox Signal, 2011. **15**(8): p. 2335-81.
65. Collins, Y., et al., *Mitochondrial redox signalling at a glance.* J Cell Sci, 2012. **125**(Pt 4): p. 801-6.
66. Mittal, M., et al., *Reactive oxygen species in inflammation and tissue injury.* Antioxid Redox Signal, 2014. **20**(7): p. 1126-67.
67. Kim, A., *Modulation of MnSOD in Cancer:Epidemiological and Experimental Evidence.* Toxicol Res, 2010. **26**(2): p. 83-93.
68. Dhar, S.K. and D.K. St Clair, *Manganese superoxide dismutase regulation and cancer.* Free Radic Biol Med, 2012. **52**(11-12): p. 2209-22.
69. Papa, L., G. Manfredi, and D. Germain, *SOD1, an unexpected novel target for cancer therapy.* Genes Cancer, 2014. **5**(1-2): p. 15-21.
70. Hicks, C.L., *Occurrence and consequence of superoxide dismutase in milk products : a review.* J Dairy Sci, 1980. **63**(7): p. 1199-204.
71. Sandstrom, J., et al., *Heparin-affinity patterns and composition of extracellular superoxide dismutase in human plasma and tissues.* Biochem J, 1993. **294 (Pt 3)**: p. 853-7.
72. Olsen, D.A., et al., *The intracellular proteolytic processing of extracellular superoxide dismutase (EC-SOD) is a two-step event.* J Biol Chem, 2004. **279**(21): p. 22152-7.
73. Chu, Y., et al., *Endocytosis of extracellular superoxide dismutase into endothelial cells: role of the heparin-binding domain.* Arterioscler Thromb Vasc Biol, 2006. **26**(9): p. 1985-90.
74. Combelles, C.M., et al., *Profiling of superoxide dismutase isoenzymes in compartments of the developing bovine antral follicles.* Reproduction, 2010. **139**(5): p. 871-81.
75. Ookawara, T., et al., *Nuclear translocation of extracellular superoxide dismutase.* Biochem Biophys Res Commun, 2002. **296**(1): p. 54-61.
76. Fattman, C.L., L.M. Schaefer, and T.D. Oury, *Extracellular superoxide dismutase in biology and medicine.* Free Radic Biol Med, 2003. **35**(3): p. 236-56.
77. Oury, T.D., et al., *Human extracellular superoxide dismutase is a tetramer composed of two disulphide-linked dimers: a simplified, high-yield purification of extracellular superoxide dismutase.* Biochem J, 1996. **317 (Pt 1)**: p. 51-7.
78. Fattman, C.L., et al., *Purification and characterization of extracellular superoxide dismutase in mouse lung.* Biochem Biophys Res Commun, 2000. **275**(2): p. 542-8.
79. Due, A.V., et al., *Extracellular superoxide dismutase exists as an octamer.* FEBS Lett, 2006. **580**(5): p. 1485-9.
80. Hjalmarsson, K., et al., *Isolation and sequence of complementary DNA encoding human extracellular superoxide dismutase.* Proc Natl Acad Sci U S A, 1987. **84**(18): p. 6340-4.
81. Stromqvist, M., J. Holgersson, and B. Samuelsson, *Glycosylation of extracellular superoxide dismutase studied by high-performance liquid chromatography and mass spectrometry.* J Chromatogr, 1991. **548**(1-2): p. 293-301.
82. Edlund, A., et al., *A non-glycosylated extracellular superoxide dismutase variant.* Biochem J, 1992. **288 (Pt 2)**: p. 451-6.

83. Ota, F., et al., *N-Glycosylation is essential for the secretion of extracellular superoxide dismutase.* FEBS Lett, 2016. **590**(19): p. 3357-3367.
84. Tibell, L., R. Aasa, and S.L. Marklund, *Spectral and physical properties of human extracellular superoxide dismutase: a comparison with CuZn superoxide dismutase.* Arch Biochem Biophys, 1993. **304**(2): p. 429-33.
85. Marklund, S.L., *Human copper-containing superoxide dismutase of high molecular weight.* Proc Natl Acad Sci U S A, 1982. **79**(24): p. 7634-8.
86. Adachi, T. and S.L. Marklund, *Interactions between human extracellular superoxide dismutase C and sulfated polysaccharides.* J Biol Chem, 1989. **264**(15): p. 8537-41.
87. Petersen, S.V., et al., *Extracellular superoxide dismutase (EC-SOD) binds to type i collagen and protects against oxidative fragmentation.* J Biol Chem, 2004. **279**(14): p. 13705-10.
88. Nguyen, A.D., et al., *Fibulin-5 is a novel binding protein for extracellular superoxide dismutase.* Circ Res, 2004. **95**(11): p. 1067-74.
89. Adachi, T., et al., *Heparin-induced release of extracellular-superoxide dismutase form (V) to plasma.* J Biochem, 1995. **117**(3): p. 586-90.
90. Bowler, R.P., et al., *Furin proteolytically processes the heparin-binding region of extracellular superoxide dismutase.* J Biol Chem, 2002. **277**(19): p. 16505-11.
91. Karlsson, K., et al., *Turnover of extracellular-superoxide dismutase in tissues.* Lab Invest, 1994. **70**(5): p. 705-10.
92. Oury, T.D., B.J. Day, and J.D. Crapo, *Extracellular superoxide dismutase: a regulator of nitric oxide bioavailability.* Lab Invest, 1996. **75**(5): p. 617-36.
93. Antonyuk, S.V., et al., *The structure of human extracellular copper-zinc superoxide dismutase at 1.7 A resolution: insights into heparin and collagen binding.* J Mol Biol, 2009. **388**(2): p. 310-26.
94. Karlsson, K., et al., *Proteolytic modification of the heparin-binding affinity of extracellular superoxide dismutase.* Biochem J, 1993. **290 (Pt 2)**: p. 623-6.
95. Sandstrom, J., et al., *10-fold increase in human plasma extracellular superoxide dismutase content caused by a mutation in heparin-binding domain.* J Biol Chem, 1994. **269**(29): p. 19163-6.
96. Gottfredsen, R.H., et al., *The cellular distribution of extracellular superoxide dismutase in macrophages is altered by cellular activation but unaffected by the naturally occurring R213G substitution.* Free Radic Biol Med, 2014. **69**: p. 348-56.
97. Adachi, T., et al., *An arginine-213 to glycine mutation in human extracellular-superoxide dismutase reduces susceptibility to trypsin-like proteinases.* J Biochem, 1996. **120**(1): p. 184-8.
98. Petersen, S.V., et al., *The concentration of extracellular superoxide dismutase in plasma is maintained by LRP-mediated endocytosis.* Free Radic Biol Med, 2010. **49**(5): p. 894-9.
99. Adachi, T., et al., *Non-enzymic glycation of human extracellular superoxide dismutase.* Biochem J, 1991. **279 (Pt 1)**: p. 263-7.
100. Adachi, T., et al., *The site of nonenzymic glycation of human extracellular-superoxide dismutase in vitro.* Free Radic Biol Med, 1992. **13**(3): p. 205-10.
101. Tamai, M., et al., *Extracellular superoxide dismutase gene polymorphism is associated with insulin resistance and the susceptibility to type 2 diabetes.* Diabetes Res Clin Pract, 2006. **71**(2): p. 140-5.
102. Yamada, H., et al., *Protective role of extracellular superoxide dismutase in hemodialysis patients.* Nephron, 2000. **84**(3): p. 218-23.

103. Yao, H., et al., *Extracellular superoxide dismutase protects against pulmonary emphysema by attenuating oxidative fragmentation of ECM.* Proc Natl Acad Sci U S A, 2010. **107**(35): p. 15571-6.
104. Sorheim, I.C., et al., *Polymorphisms in the superoxide dismutase-3 gene are associated with emphysema in COPD.* Copd, 2010. **7**(4): p. 262-8.
105. Ahmad, K.A., et al., *Antioxidant therapy for Management of Oxidative stress Induced Hypertension.* Free Radic Res, 2017: p. 1-18.
106. Schiffrin, E.L., *Antioxidants in hypertension and cardiovascular disease.* Mol Interv, 2010. **10**(6): p. 354-62.
107. Laukkanen, M.O., et al., *EC-SOD gene therapy reduces paracetamol-induced liver damage in mice.* J Gene Med, 2001. **3**(4): p. 321-5.
108. Jiang, W., et al., *Adeno-associated virus mediated SOD gene therapy protects the retinal ganglion cells from chronic intraocular pressure elevation induced injury via attenuating oxidative stress and improving mitochondrial dysfunction in a rat model.* Am J Transl Res, 2016. **8**(2): p. 799-810.
109. Gao, B., et al., *Synthesis and anti-inflammatory activity of a chimeric recombinant superoxide dismutase: SOD2/3.* Am J Physiol Lung Cell Mol Physiol, 2003. **284**(6): p. L917-25.
110. Ho, A., et al., *Synthetic protein transduction domains: enhanced transduction potential in vitro and in vivo.* Cancer Res, 2001. **61**(2): p. 474-7.
111. Zhao, J., et al., *A novel human derived cell-penetrating peptide in drug delivery.* Mol Biol Rep, 2011. **38**(4): p. 2649-56.
112. Sies, H., *Hydrogen peroxide as a central redox signaling molecule in physiological oxidative stress: Oxidative eustress.* Redox Biol, 2017. **11**: p. 613-619.
113. Furukawa, Y., A.S. Torres, and T.V. O'Halloran, *Oxygen-induced maturation of SOD1: a key role for disulfide formation by the copper chaperone CCS.* Embo j, 2004. **23**(14): p. 2872-81.
114. Getzoff, E.D., et al., *Electrostatic recognition between superoxide and copper, zinc superoxide dismutase.* Nature, 1983. **306**(5940): p. 287-90.
115. Tainer, J.A., et al., *Structure and mechanism of copper, zinc superoxide dismutase.* Nature, 1983. **306**(5940): p. 284-7.
116. Sheng, Y., et al., *Superoxide dismutases and superoxide reductases.* Chem Rev, 2014. **114**(7): p. 3854-918.
117. Perry, J.J., et al., *The structural biochemistry of the superoxide dismutases.* Biochim Biophys Acta, 2010. **1804**(2): p. 245-62.
118. Fridovich, I., *Superoxide dismutases: anti- versus pro- oxidants?* Anticancer Agents Med Chem, 2011. **11**(2): p. 175-7.
119. Liochev, S.I. and I. Fridovich, *Lucigenin luminescence as a measure of intracellular superoxide dismutase activity in Escherichia coli.* Proc Natl Acad Sci U S A, 1997. **94**(7): p. 2891-6.
120. Kawahara, T., M.T. Quinn, and J.D. Lambeth, *Molecular evolution of the reactive oxygen-generating NADPH oxidase (Nox/Duox) family of enzymes.* BMC Evol Biol, 2007. **7**: p. 109.
121. Hink, H.U., et al., *Peroxidase properties of extracellular superoxide dismutase: role of uric acid in modulating in vivo activity.* Arterioscler Thromb Vasc Biol, 2002. **22**(9): p. 1402-8.
122. Yim, M.B., P.B. Chock, and E.R. Stadtman, *Copper, zinc superoxide dismutase catalyzes hydroxyl radical production from hydrogen peroxide.* Proc Natl Acad Sci U S A, 1990. **87**(13): p. 5006-10.

123. Liochev, S.I. and I. Fridovich, *Mechanism of the peroxidase activity of Cu, Zn superoxide dismutase.* Free Radic Biol Med, 2010. **48**(12): p. 1565-9.
124. Ansenberger-Fricano, K., et al., *The peroxidase activity of mitochondrial superoxide dismutase.* Free Radic Biol Med, 2013. **54**: p. 116-24.
125. Mason, R.P., *Two hypotheses for the peroxidase activity of Mn-superoxide dismutase.* Free Radic Biol Med, 2013. **65**: p. 1533.
126. Halliwell, B. and J.M. Gutteridge, *Role of free radicals and catalytic metal ions in human disease: an overview.* Methods Enzymol, 1990. **186**: p. 1-85.
127. Folz, R.J. and J.D. Crapo, *Extracellular superoxide dismutase (SOD3): tissue-specific expression, genomic characterization, and computer-assisted sequence analysis of the human EC SOD gene.* Genomics, 1994. **22**(1): p. 162-71.
128. Zelko, I.N. and R.J. Folz, *Myeloid zinc finger (MZF)-like, Kruppel-like and Ets families of transcription factors determine the cell-specific expression of mouse extracellular superoxide dismutase.* Biochem J, 2003. **369**(Pt 2): p. 375-86.
129. Wang, Y.-D., et al., *Farnesoid X receptor antagonizes JNK signaling pathway in liver carcinogenesis by activating SOD3.* Mol Endocrinol, 2015. **29**(2): p. 322-31.
130. Stralin, P. and S.L. Marklund, *Multiple cytokines regulate the expression of extracellular superoxide dismutase in human vascular smooth muscle cells.* Atherosclerosis, 2000. **151**(2): p. 433-41.
131. Forster, D. and G. Reiser, *Nucleotides protect rat brain astrocytes against hydrogen peroxide toxicity and induce antioxidant defense via P2Y receptors.* Neurochem Int, 2016. **94**: p. 57-66.
132. Davis, S.M., et al., *Leukemia Inhibitory Factor Protects Neurons from Ischemic Damage via Upregulation of Superoxide Dismutase 3.* Mol Neurobiol, 2017. **54**(1): p. 608-622.
133. Yasuda, H., et al., *Exendin-4 induces extracellular-superoxide dismutase through histone H3 acetylation in human retinal endothelial cells.* J Clin Biochem Nutr, 2016. **59**(3): p. 174-181.
134. Davis, C.D., D.B. Milne, and F.H. Nielsen, *Changes in dietary zinc and copper affect zinc-status indicators of postmenopausal women, notably, extracellular superoxide dismutase and amyloid precursor proteins.* Am J Clin Nutr, 2000. **71**(3): p. 781-8.
135. Olin, K.L., et al., *Extracellular superoxide dismutase activity is affected by dietary zinc intake in nonhuman primate and rodent models.* Am J Clin Nutr, 1995. **61**(6): p. 1263-7.
136. Itoh, S., et al., *Novel mechanism for regulation of extracellular SOD transcription and activity by copper: role of antioxidant-1.* Free Radic Biol Med, 2009. **46**(1): p. 95-104.
137. Stralin, P. and S.L. Marklund, *Effects of oxidative stress on expression of extracellular superoxide dismutase, CuZn-superoxide dismutase and Mn-superoxide dismutase in human dermal fibroblasts.* Biochem J, 1994. **298 (Pt 2)**: p. 347-52.
138. Carlsson, L.M., et al., *Mice lacking extracellular superoxide dismutase are more sensitive to hyperoxia.* Proc Natl Acad Sci U S A, 1995. **92**(14): p. 6264-8.
139. Sentman, M.L., et al., *Phenotypes of mice lacking extracellular superoxide dismutase and copper- and zinc-containing superoxide dismutase.* J Biol Chem, 2006. **281**(11): p. 6904-9.
140. Gongora, M.C., et al., *Loss of extracellular superoxide dismutase leads to acute lung damage in the presence of ambient air: a potential mechanism underlying adult respiratory distress syndrome.* Am J Pathol, 2008. **173**(4): p. 915-26.

141. Teoh, M.L., et al., *Overexpression of extracellular superoxide dismutase attenuates heparanase expression and inhibits breast carcinoma cell growth and invasion.* Cancer Res, 2009. **69**(15): p. 6355-63.
142. Teoh-Fitzgerald, M.L., et al., *Epigenetic reprogramming governs EcSOD expression during human mammary epithelial cell differentiation, tumorigenesis and metastasis.* Oncogene, 2014. **33**(3): p. 358-68.
143. Singh, B. and H.K. Bhat, *Superoxide dismutase 3 is induced by antioxidants, inhibits oxidative DNA damage and is associated with inhibition of estrogen-induced breast cancer.* Carcinogenesis, 2012. **33**(12): p. 2601-10.
144. Hubackova, M., et al., *Association of superoxide dismutases and NAD(P)H quinone oxidoreductases with prognosis of patients with breast carcinomas.* Int J Cancer, 2012. **130**(2): p. 338-48.
145. Wang, C.-A., et al., *Vascular endothelial growth factor C promotes breast cancer progression via a novel antioxidant mechanism that involves regulation of superoxide dismutase 3.* Breast Cancer Res, 2014. **16**(5): p. 462.
146. Chatterjee, A., et al., *Natural antioxidants exhibit chemopreventive characteristics through the regulation of CNC b-Zip transcription factors in estrogen-induced breast carcinogenesis.* J Biochem Mol Toxicol, 2014. **28**(12): p. 529-38.
147. Singh, B., et al., *Resveratrol inhibits estrogen-induced breast carcinogenesis through induction of NRF2-mediated protective pathways.* Carcinogenesis, 2014. **35**(8): p. 1872-80.
148. Russo, J. and I.H. Russo, *The role of estrogen in the initiation of breast cancer.* J Steroid Biochem Mol Biol, 2006. **102**(1-5): p. 89-96.
149. Shivapurkar, N., et al., *Deletions of chromosome 4 occur early during the pathogenesis of colorectal carcinoma.* Hum Pathol, 2001. **32**(2): p. 169-77.
150. Vicini, F.A., et al., *Does local recurrence affect the rate of distant metastases and survival in patients with early-stage breast carcinoma treated with breast-conserving therapy?* Cancer, 2003. **97**(4): p. 910-9.
151. Smith, M.J., et al., *Mechanisms driving local breast cancer recurrence in a model of breast-conserving surgery.* Ann Surg Oncol, 2008. **15**(10): p. 2954-64.
152. Gyorffy, B., et al., *An online survival analysis tool to rapidly assess the effect of 22,277 genes on breast cancer prognosis using microarray data of 1,809 patients.* Breast Cancer Res Treat, 2010. **123**(3): p. 725-31.
153. Teoh-Fitzgerald, M.L.T., et al., *Genetic and epigenetic inactivation of extracellular superoxide dismutase promotes an invasive phenotype in human lung cancer by disrupting ECM homeostasis.* Mol Cancer Res, 2012. **10**(1): p. 40-51.
154. Yoo, D.G., et al., *Alteration of APE1/ref-1 expression in non-small cell lung cancer: the implications of impaired extracellular superoxide dismutase and catalase antioxidant systems.* Lung Cancer, 2008. **60**(2): p. 277-84.
155. Svensk, A.M., et al., *Differential expression of superoxide dismutases in lung cancer.* Am J Clin Pathol, 2004. **122**(3): p. 395-404.
156. Hoesel, B. and J.A. Schmid, *The complexity of NF-kappaB signaling in inflammation and cancer.* Mol Cancer, 2013. **12**: p. 86.
157. Zhang, H.-H., et al., *Array analysis for potential biomarker of gemcitabine identification in non-small cell lung cancer cell lines.* Int J Clin Exp Pathol, 2013. **6**(9): p. 1734-46.
158. Kim, J., et al., *SOD3 acts as a tumor suppressor in PC-3 prostate cancer cells via hydrogen peroxide accumulation.* Anticancer Res, 2014. **34**(6): p. 2821-31.
159. Chaiswing, L., W. Zhong, and T.D. Oberley, *Increasing discordant antioxidant protein levels and enzymatic activities contribute to increasing redox imbalance*

observed during human prostate cancer progression. Free Radic Biol Med, 2014. **67**: p. 342-52.
160. Chaiswing, L., et al., *Extracellular redox state regulates features associated with prostate cancer cell invasion.* Cancer Res, 2008. **68**(14): p. 5820-6.
161. O'Leary, B.R., et al., *Loss of SOD3 (EcSOD) Expression Promotes an Aggressive Phenotype in Human Pancreatic Ductal Adenocarcinoma.* Clin Cancer Res, 2015. **21**(7): p. 1741-51.
162. Teoh, M.L., et al., *Modulation of reactive oxygen species in pancreatic cancer.* Clin Cancer Res, 2007. **13**(24): p. 7441-50.
163. Sibenaller, Z.A., et al., *Extracellular superoxide dismutase suppresses hypoxia-inducible factor-1alpha in pancreatic cancer.* Free Radic Biol Med, 2014. **69**: p. 357-66.
164. Deng, X., D.Z. Ewton, and E. Friedman, *Mirk/Dyrk1B maintains the viability of quiescent pancreatic cancer cells by reducing levels of reactive oxygen species.* Cancer Res, 2009. **69**(8): p. 3317-24.
165. Laatikainen, L.E., et al., *Extracellular superoxide dismutase is a thyroid differentiation marker down-regulated in cancer.* Endocr Relat Cancer, 2010. **17**(3): p. 785-96.
166. Cammarota, F., et al., *Ras oncogene-mediated progressive silencing of extracellular superoxide dismutase in tumorigenesis.* Biomed Res Int, 2015. **2015**: p. 780409.
167. Cammarota, F., et al., *Clinical relevance of thyroid cell models in redox research.* Cancer Cell Int, 2015. **15**: p. 113.
168. Laatikainen, L.E., et al., *Extracellular superoxide dismutase is a thyroid differentiation marker down-regulated in cancer.* Endocr Relat Cancer, 2010. **17**(3): p. 785-96.
169. Laukkanen, M.O., et al., *Extracellular superoxide dismutase regulates the expression of small gtpase regulatory proteins GEFs, GAPs, and GDI.* PLoS One, 2015. **10**(3): p. e0121441.
170. Castellone, M.D., et al., *Extracellular superoxide dismutase induces mouse embryonic fibroblast proliferative burst, growth arrest, immortalization, and consequent in vivo tumorigenesis.* Antioxid Redox Signal, 2014. **21**(10): p. 1460-74.
171. Jeon, Y.J., et al., *IFNgamma-mediated inhibition of cell proliferation through increased PKCdelta-induced overexpression of EC-SOD.* BMB Rep, 2012. **45**(11): p. 659-64.
172. Wheeler, M.D., O.M. Smutney, and R.J. Samulski, *Secretion of extracellular superoxide dismutase from muscle transduced with recombinant adenovirus inhibits the growth of B16 melanomas in mice.* Mol Cancer Res, 2003. **1**(12): p. 871-81.
173. Kim, S.H., et al., *Overexpression of extracellular superoxide dismutase (EC-SOD) in mouse skin plays a protective role in DMBA/TPA-induced tumor formation.* Oncol Res, 2005. **15**(7-8): p. 333-41.
174. Morvan, D. and A. Demidem, *Metabolomics and transcriptomics demonstrate severe oxidative stress in both localized chemotherapy-treated and bystander tumors.* Biochim Biophys Acta, 2014. **1840**(3): p. 1092-104.
175. Liu, X., et al., *Proteomic analysis of minute amount of colonic biopsies by enteroscopy sampling.* Biochem Biophys Res Commun, 2016. **476**(4): p. 286-92.
176. Soini, Y., et al., *Antioxidant enzymes in renal cell carcinoma.* Histol Histopathol, 2006. **21**(2): p. 157-65.

177. Yang, J., et al., *Extracellular superoxide dismutase, a potential extracellular biomarker candidate for prolactinoma.* West Indian Med J, 2012. **61**(7): p. 665-9.
178. Subbannayya, Y., et al., *Identification of differentially expressed serum proteins in gastric adenocarcinoma.* J Proteomics, 2015. **127**(Pt A): p. 80-8.
179. Wei, L., et al., *Extracellular superoxide dismutase increased the therapeutic potential of human mesenchymal stromal cells in radiation pulmonary fibrosis.* Cytotherapy, 2017. **19**(5): p. 586-602.
180. Cui, R., et al., *Overexpression of superoxide dismutase 3 gene blocks high-fat diet-induced obesity, fatty liver and insulin resistance.* Gene Ther, 2014. **21**(9): p. 840-8.
181. Chan, D.S., et al., *Body mass index and survival in women with breast cancer-systematic literature review and meta-analysis of 82 follow-up studies.* Ann Oncol, 2014. **25**(10): p. 1901-14.
182. Iyengar, N.M., et al., *Systemic Correlates of White Adipose Tissue Inflammation in Early-Stage Breast Cancer.* Clin Cancer Res, 2016. **22**(9): p. 2283-9.
183. Negahdar, M., et al., *Blood superoxide dismutase and catalase activities in women affected with breast cancer.* Iran J Public Health, 2005. **34**(3): p. 39-43.
184. Sinha, R.J., et al., *Implications of free radicals and antioxidant levels in carcinoma of the breast: a never-ending battle for survival.* Indian J Cancer, 2009. **46**(2): p. 146-50.
185. Eliyasinia, F., et al., *Superoxide dismutase activities in plasma of patients with breast cancer.* Archives Breast Cancer, 2014. **1**(2): p. 29-32.
186. Khanzode, S.S., et al., *Antioxidant enzymes and lipid peroxidation in different stages of breast cancer.* Free Radic Res, 2004. **38**(1): p. 81-5.
187. Ray, G., et al., *Lipid peroxidation, free radical production and antioxidant status in breast cancer.* Breast Cancer Res Treat, 2000. **59**(2): p. 163-70.
188. Yeh, C.-C., et al., *Superoxide anion radical, lipid peroxides and antioxidant status in the blood of patients with breast cancer.* Clinica Chimica Acta, 2005. **361**(1–2): p. 104-111.
189. Battisti, V., et al., *Oxidative stress and antioxidant status in prostate cancer patients: relation to Gleason score, treatment and bone metastasis.* Biomed Pharmacother, 2011. **65**(7): p. 516-24.
190. Sandhya, B., et al., *Lipid peroxidation and antioxidant status in prostate cancer patients.* Indian J Science Technology, 2010. **3**(1): p. 83-86.
191. Shidfar, A., et al., *Protein Biomarkers for Breast Cancer Risk Are Specifically Correlated with Local Steroid Hormones in Nipple Aspirate Fluid.* Horm Cancer, 2016. **7**(4): p. 252-9.
192. Sharma, P., et al., *Global methylation profiling to identify epigenetic signature of gallbladder cancer and gallstone disease.* Tumour Biol, 2016. **37**(11): p. 14687-14699.
193. Divyya, S., et al., *GCPII modulates oxidative stress and prostate cancer susceptibility through changes in methylation of RASSF1, BNIP3, GSTP1 and Ec-SOD.* Mol Biol Rep, 2013. **40**(10): p. 5541-50.
194. Chiba, T., et al., *Cell growth inhibition and gene expression induced by the histone deacetylase inhibitor, trichostatin A, on human hepatoma cells.* Oncology, 2004. **66**(6): p. 481-91.
195. Lakshmi, S.V., et al., *Oxidative stress in coronary artery disease: epigenetic perspective.* Mol Cell Biochem, 2013. **374**(1-2): p. 203-11.
196. Kamiya, T., et al., *Epigenetic regulation of extracellular-superoxide dismutase in human monocytes.* Free Radic Biol Med, 2013. **61**: p. 197-205.

197. Zelko, I.N., et al., *Histone acetylation regulates the cell-specific and interferon-gamma-inducible expression of extracellular superoxide dismutase in human pulmonary arteries.* Am J Respir Cell Mol Biol, 2011. **45**(5): p. 953-61.
198. Zelko, I.N., M.R. Mueller, and R.J. Folz, *CpG methylation attenuates Sp1 and Sp3 binding to the human extracellular superoxide dismutase promoter and regulates its cell-specific expression.* Free Radic Biol Med, 2010. **48**(7): p. 895-904.
199. Barcellos-Hoff, M.H., et al., *Functional differentiation and alveolar morphogenesis of primary mammary cultures on reconstituted basement membrane.* Development, 1989. **105**(2): p. 223-35.
200. Le Beyec, J., et al., *Cell shape regulates global histone acetylation in human mammary epithelial cells.* Exp Cell Res, 2007. **313**(14): p. 3066-75.
201. Kamiya, T., et al., *Ten-eleven translocation 1 functions as a mediator of SOD3 expression in human lung cancer A549 cells.* Free Radic Res, 2017: p. 1-33.
202. Li, L., et al., *Epigenetic inactivation of the CpG demethylase TET1 as a DNA methylation feedback loop in human cancers.* Sci Rep, 2016. **6**: p. 26591.
203. Divyya, S., et al., *Association of glutamate carboxypeptidase II (GCPII) haplotypes with breast and prostate cancer risk.* Gene, 2013. **516**(1): p. 76-81.
204. Divyya, S., et al., *Paradoxical role of C1561T glutamate carboxypeptidase II (GCPII) genetic polymorphism in altering disease susceptibility.* Gene, 2012. **497**(2): p. 273-9.
205. Nozik-Grayck, E., et al., *Histone deacetylation contributes to low extracellular superoxide dismutase expression in human idiopathic pulmonary arterial hypertension.* Am J Physiol Lung Cell Mol Physiol, 2016. **311**(1): p. L124-34.
206. Yang, Q., et al., *Role of histone deacetylases in regulation of phenotype of ovine newborn pulmonary arterial smooth muscle cells.* Cell Prolif, 2013. **46**(6): p. 654-64.
207. Muller, B.M., et al., *Differential expression of histone deacetylases HDAC1, 2 and 3 in human breast cancer--overexpression of HDAC2 and HDAC3 is associated with clinicopathological indicators of disease progression.* BMC Cancer, 2013. **13**: p. 215.
208. Wilson, A.J., et al., *Histone deacetylase 3 (HDAC3) and other class I HDACs regulate colon cell maturation and p21 expression and are deregulated in human colon cancer.* J Biol Chem, 2006. **281**(19): p. 13548-58.
209. Liu, C., et al., *Histone deacetylase 3 participates in self-renewal of liver cancer stem cells through histone modification.* Cancer Lett, 2013. **339**(1): p. 60-9.
210. Jiao, F., et al., *Histone deacetylase 3 promotes pancreatic cancer cell proliferation, invasion and increases drug-resistance through histone modification of P27, P53 and Bax.* Int J Oncol, 2014. **45**(4): p. 1523-30.
211. Weichert, W., et al., *Histone deacetylases 1, 2 and 3 are highly expressed in prostate cancer and HDAC2 expression is associated with shorter PSA relapse time after radical prostatectomy.* Br J Cancer, 2008. **98**(3): p. 604-10.
212. Monteiro, F.L., et al., *Expression and functionality of histone H2A variants in cancer.* Oncotarget, 2014. **5**(11): p. 3428-43.
213. Hernandez-Munoz, I., et al., *Stable X chromosome inactivation involves the PRC1 Polycomb complex and requires histone MACROH2A1 and the CULLIN3/SPOP ubiquitin E3 ligase.* Proc Natl Acad Sci U S A, 2005. **102**(21): p. 7635-40.
214. Buschbeck, M., et al., *The histone variant macroH2A is an epigenetic regulator of key developmental genes.* Nat Struct Mol Biol, 2009. **16**(10): p. 1074-9.

215. Dardenne, E., et al., *Splicing switch of an epigenetic regulator by RNA helicases promotes tumor-cell invasiveness.* Nat Struct Mol Biol, 2012. **19**(11): p. 1139-46.
216. Wang, Z., et al., *DDX5 promotes proliferation and tumorigenesis of non-small-cell lung cancer cells by activating beta-catenin signaling pathway.* Cancer Sci, 2015. **106**(10): p. 1303-12.
217. Mazurek, A., et al., *DDX5 regulates DNA replication and is required for cell proliferation in a subset of breast cancer cells.* Cancer Discov, 2012. **2**(9): p. 812-25.
218. Alqahtani, H., et al., *DDX17 (P72), a Sox2 binding partner, promotes stem-like features conferred by Sox2 in a small cell population in estrogen receptor-positive breast cancer.* Cell Signal, 2016. **28**(2): p. 42-50.
219. Wortham, N.C., et al., *The DEAD-box protein p72 regulates ERalpha-/oestrogen-dependent transcription and cell growth, and is associated with improved survival in ERalpha-positive breast cancer.* Oncogene, 2009. **28**(46): p. 4053-64.
220. Shin, S., et al., *Involvement of RNA helicases p68 and p72 in colon cancer.* Cancer Res, 2007. **67**(16): p. 7572-8.
221. Janknecht, R., *Multi-talented DEAD-box proteins and potential tumor promoters: p68 RNA helicase (DDX5) and its paralog, p72 RNA helicase (DDX17).* Am J Transl Res, 2010. **2**(3): p. 223-34.
222. Clark, E.L., et al., *The RNA helicase p68 is a novel androgen receptor coactivator involved in splicing and is overexpressed in prostate cancer.* Cancer Res, 2008. **68**(19): p. 7938-46.
223. Juul, K., et al., *Genetically increased antioxidative protection and decreased chronic obstructive pulmonary disease.* Am J Respir Crit Care Med, 2006. **173**(8): p. 858-64.
224. Brenner, D.R., J.R. McLaughlin, and R.J. Hung, *Previous lung diseases and lung cancer risk: a systematic review and meta-analysis.* PLoS One, 2011. **6**(3): p. e17479.
225. Young, R.P., et al., *Lung cancer susceptibility model based on age, family history and genetic variants.* PLoS One, 2009. **4**(4): p. e5302.
226. Geng, R., et al., *Oxidative stress-related genetic polymorphisms are associated with the prognosis of metastatic gastric cancer patients treated with epirubicin, oxaliplatin and 5-fluorouracil combination chemotherapy.* PLoS One, 2014. **9**(12): p. e116027.
227. Kobylecki, C.J., S. Afzal, and B.G. Nordestgaard, *Does SOD3 R213G Homozygosity Influence Morbidity, Mortality, and Lung Function in the General Population?* Antioxid Redox Signal, 2016. **24**(15): p. 884-91.
228. Su, S., et al., *Genetic polymorphisms in antioxidant enzyme genes and susceptibility to hepatocellular carcinoma in Chinese population: a case-control study.* Tumour Biol, 2015. **36**(6): p. 4627-32.
229. Zhao, P., et al., *Genetic oxidative stress variants and glioma risk in a Chinese population: a hospital-based case-control study.* BMC Cancer, 2012. **12**: p. 617.
230. Rodrigues, P., et al., *Oxidative stress in susceptibility to breast cancer: study in Spanish population.* BMC Cancer, 2014. **14**: p. 861.
231. Bauer, S.R., et al., *Antioxidant and vitamin E transport genes and risk of high-grade prostate cancer and prostate cancer recurrence.* Prostate, 2013. **73**(16): p. 1786-95.
232. Dong, X., et al., *SOD3 and eNOS genotypes are associated with SOD activity and NOx.* Exp Ther Med, 2014. **8**(1): p. 328-334.

233. Iida, R., et al., *Multiplex single base extension method for simultaneous genotyping of non-synonymous SNP in the three human SOD genes.* Electrophoresis, 2008. **29**(23): p. 4788-94.
234. Ganguly, K., et al., *Superoxide dismutase 3, extracellular (SOD3) variants and lung function.* Physiol Genomics, 2009. **37**(3): p. 260-7.
235. Naganuma, T., et al., *Association of extracellular superoxide dismutase gene with cerebral infarction in women: a haplotype-based case-control study.* Hereditas, 2008. **145**(6): p. 283-92.
236. Yang, Y.M., X.R. Xie, and A.L. Jin, *Genetic polymorphisms in extracellular superoxide dismutase Leu53Leu, Arg213Gly, and Ala40Thr and susceptibility to type 2 diabetes mellitus.* Genet Mol Res, 2016. **15**(4).
237. Mohammedi, K., et al., *Plasma extracellular superoxide dismutase concentration, allelic variations in the SOD3 gene and risk of myocardial infarction and all-cause mortality in people with type 1 and type 2 diabetes.* Cardiovasc Diabetol, 2015. **14**: p. 845.
238. Chan, J.M., et al., *Selenium- or Vitamin E-Related Gene Variants, Interaction with Supplementation, and Risk of High-Grade Prostate Cancer in SELECT.* Cancer Epidemiol Biomarkers Prev, 2016. **25**(7): p. 1050-8.
239. Rajaraman, P., et al., *Oxidative response gene polymorphisms and risk of adult brain tumors.* Neuro Oncol, 2008. **10**(5): p. 709-15.
240. Singh, R.K., et al., *Deletions in chromosome 4 differentially associated with the development of cervical cancer: evidence of slit2 as a candidate tumor suppressor gene.* Hum Genet, 2007. **122**(1): p. 71-81.
241. Beder, L.B., et al., *Genome-wide analyses on loss of heterozygosity in head and neck squamous cell carcinomas.* Lab Invest, 2003. **83**(1): p. 99-105.
242. Dallol, A., et al., *SLIT2, a human homologue of the Drosophila Slit2 gene, has tumor suppressor activity and is frequently inactivated in lung and breast cancers.* Cancer Res, 2002. **62**(20): p. 5874-80.
243. Kim, G.J., et al., *Genomic imbalances in Korean hepatocellular carcinoma.* Cancer Genet Cytogenet, 2003. **142**(2): p. 129-33.
244. Pershouse, M.A., et al., *Deletion mapping of chromosome 4 in head and neck squamous cell carcinoma.* Oncogene, 1997. **14**(3): p. 369-73.
245. Polascik, T.J., et al., *Distinct regions of allelic loss on chromosome 4 in human primary bladder carcinoma.* Cancer Res, 1995. **55**(22): p. 5396-9.
246. Sherwood, J.B., et al., *Chromosome 4 deletions are frequent in invasive cervical cancer and differ between histologic variants.* Gynecol Oncol, 2000. **79**(1): p. 90-6.
247. Shivapurkar, N., et al., *Multiple regions of chromosome 4 demonstrating allelic losses in breast carcinomas.* Cancer Res, 1999. **59**(15): p. 3576-80.
248. Shivapurkar, N., et al., *Deletions of chromosome 4 at multiple sites are frequent in malignant mesothelioma and small cell lung carcinoma.* Clin Cancer Res, 1999. **5**(1): p. 17-23.
249. Russo, J., et al., *17-Beta-estradiol induces transformation and tumorigenesis in human breast epithelial cells.* Faseb j, 2006. **20**(10): p. 1622-34.
250. Jonas, S. and E. Izaurralde, *Towards a molecular understanding of microRNA-mediated gene silencing.* Nat Rev Genet, 2015. **16**(7): p. 421-33.
251. Zhang, X., et al., *MicroRNA-21 modulates the levels of reactive oxygen species by targeting SOD3 and TNFα.* Cancer Res, 2012. **72**(18): p. 4707-13.
252. Volinia, S., et al., *A microRNA expression signature of human solid tumors defines cancer gene targets.* Proc Natl Acad Sci U S A, 2006. **103**(7): p. 2257-61.

253. Nam, E.J., et al., *MicroRNA expression profiles in serous ovarian carcinoma.* Clin Cancer Res, 2008. **14**(9): p. 2690-5.
254. Lui, W.O., et al., *Patterns of known and novel small RNAs in human cervical cancer.* Cancer Res, 2007. **67**(13): p. 6031-43.
255. Tetzlaff, M.T., et al., *Differential expression of miRNAs in papillary thyroid carcinoma compared to multinodular goiter using formalin fixed paraffin embedded tissues.* Endocr Pathol, 2007. **18**(3): p. 163-73.
256. Krichevsky, A.M. and G. Gabriely, *miR-21: a small multi-faceted RNA.* J Cell Mol Med, 2009. **13**(1): p. 39-53.
257. Michels, K.B., et al., *Diet and breast cancer: a review of the prospective observational studies.* Cancer, 2007. **109**(12 Suppl): p. 2712-49.
258. Fortmann, S.P., et al., *Vitamin and Mineral Supplements in the Primary Prevention of Cardiovascular Disease and Cancer: An Updated Systematic Evidence Review for the U.S. Preventive Services Task Force.* Annals of Internal Medicine, 2013. **159**(12): p. 824-834.
259. Hercberg, S., et al., *The SU.VI.MAX Study: a randomized, placebo-controlled trial of the health effects of antioxidant vitamins and minerals.* Arch Intern Med, 2004. **164**(21): p. 2335-42.
260. Gaziano, J.M., et al., *Multivitamins in the prevention of cancer in men: the Physicians' Health Study II randomized controlled trial.* Jama, 2012. **308**(18): p. 1871-80.
261. Azzam, E.I., J.-P. Jay-Gerin, and D. Pain, *Ionizing radiation-induced metabolic oxidative stress and prolonged cell injury.* Cancer letters, 2012. **327**(1-2): p. 48-60.
262. Wang, J. and J. Yi, *Cancer cell killing via ROS: to increase or decrease, that is the question.* Cancer Biol Ther, 2008. **7**(12): p. 1875-84.
263. Chekhun, V.F., et al., *Expression of drug resistance proteins in triple-receptor-negative tumors as the basis of individualized therapy of the breast cancer patients.* Exp Oncol, 2009. **31**(2): p. 123-4.
264. Shen, B.Y., et al., *Is the combinational administration of doxorubicin and glutathione a reasonable proposal?* Acta Pharmacol Sin, 2019. **40**(5): p. 699-709.
265. Block, K.I., et al., *Impact of antioxidant supplementation on chemotherapeutic toxicity: a systematic review of the evidence from randomized controlled trials.* Int J Cancer, 2008. **123**(6): p. 1227-39.
266. Lincoln, D.T., et al., *The thioredoxin-thioredoxin reductase system: over-expression in human cancer.* Anticancer research, 2003. **23**(3B): p. 2425-2433.
267. Kim, S.J., et al., *High thioredoxin expression is associated with resistance to docetaxel in primary breast cancer.* Clinical cancer research : an official journal of the American Association for Cancer Research, 2005. **11**(23): p. 8425-8430.
268. Kirkpatrick, D.L. and G. Powis, *Clinically Evaluated Cancer Drugs Inhibiting Redox Signaling.* Antioxidants & redox signaling, 2017. **26**(6): p. 262-273.
269. Thompson, H.J., et al., *Sulfone metabolite of sulindac inhibits mammary carcinogenesis.* Cancer Res, 1997. **57**(2): p. 267-71.
270. Seo, S.K., et al., *Sulindac-derived reactive oxygen species induce apoptosis of human multiple myeloma cells via p38 mitogen activated protein kinase-induced mitochondrial dysfunction.* Apoptosis, 2007. **12**(1): p. 195-209.
271. Suzuki, S., et al., *Implication of mitochondria-derived reactive oxygen species, cytochrome C and caspase-3 in N-(4-hydroxyphenyl)retinamide-induced apoptosis in cervical carcinoma cells.* Oncogene, 1999. **18**(46): p. 6380-6387.

272. Veronesi, U., et al., *Fifteen-year results of a randomized phase III trial of fenretinide to prevent second breast cancer.* Annals of oncology : official journal of the European Society for Medical Oncology, 2006. **17**(7): p. 1065-1071.
273. Schoenfeld, J.D., et al., *Redox active metals and H2O2 mediate the increased efficacy of pharmacological ascorbate in combination with gemcitabine or radiation in pre-clinical sarcoma models.* Redox Biol, 2018. **14**: p. 417-422.
274. Schoenfeld, J.D., et al., *O2(-) and H2O2-Mediated Disruption of Fe Metabolism Causes the Differential Susceptibility of NSCLC and GBM Cancer Cells to Pharmacological Ascorbate.* Cancer Cell, 2017. **31**(4): p. 487-500.e8.
275. Ferreira, P.R., et al., *Protective effect of alpha-tocopherol in head and neck cancer radiation-induced mucositis: a double-blind randomized trial.* Head Neck, 2004. **26**(4): p. 313-21.
276. Anderson, C.M., et al., *Phase IIb, Randomized, Double-Blind Trial of GC4419 Versus Placebo to Reduce Severe Oral Mucositis Due to Concurrent Radiotherapy and Cisplatin For Head and Neck Cancer.* J Clin Oncol, 2019: p. Jco1901507.
277. Batinic-Haberle, I., A. Tovmasyan, and I. Spasojevic, *Mn Porphyrin-Based Redox-Active Drugs: Differential Effects as Cancer Therapeutics and Protectors of Normal Tissue Against Oxidative Injury.* Antioxid Redox Signal, 2018. **29**(16): p. 1691-1724.
278. Gad, S.C., et al., *A Nonclinical Safety Assessment of MnTE-2-PyP, a Manganese Porphyrin.* International Journal of Toxicology, 2013. **32**(4): p. 274-287.
279. Tovmasyan, A., et al., *Radiation-Mediated Tumor Growth Inhibition Is Significantly Enhanced with Redox-Active Compounds That Cycle with Ascorbate.* Antioxid Redox Signal, 2018. **29**(13): p. 1196-1214.
280. Tovmasyan, A., et al., *A comprehensive evaluation of catalase-like activity of different classes of redox-active therapeutics.* Free Radic Biol Med, 2015. **86**: p. 308-21.
281. Tong, Q., et al., *MnTE-2-PyP reduces prostate cancer growth and metastasis by suppressing p300 activity and p300/HIF-1/CREB binding to the promoter region of the PAI-1 gene.* Free Radical Biology and Medicine, 2016. **94**: p. 185-194.
282. Tong, Q., et al., *MnTE-2-PyP modulates thiol oxidation in a hydrogen peroxide-mediated manner in a human prostate cancer cell.* Free Radical Biology and Medicine, 2016. **101**: p. 32-43.
283. Jaramillo, M.C., et al., *Manganese Porphyrin, MnTE-2-PyP5+, Acts as a Pro-Oxidant to Potentiate Glucocorticoid-Induced Apoptosis in Lymphoma Cells.* Free Radical Biology and Medicine, 2012. **52**(8): p. 1272-1284.
284. Jaramillo, M.C., et al., *Manganese (III) meso-tetrakis N-ethylpyridinium-2-yl porphyrin acts as a pro-oxidant to inhibit electron transport chain proteins, modulate bioenergetics, and enhance the response to chemotherapy in lymphoma cells.* Free radical biology & medicine, 2015. **83**: p. 89-100.
285. Zhao, Y., et al., *A Mechanism-Based Antioxidant Approach for the Reduction of Skin Carcinogenesis.* Cancer Research, 2005. **65**(4): p. 1401-1405.
286. Kaewpila, S., et al., *Manganese Superoxide Dismutase Modulates Hypoxia-Inducible Factor-1α Induction via Superoxide.* Cancer Research, 2008. **68**(8): p. 2781-2788.
287. Kulich, S.M. and C.T. Chu, *Role of reactive oxygen species in extracellular signal-regulated protein kinase phosphorylation and 6-hydroxydopamine cytotoxicity.* Journal of biosciences, 2003. **28**(1): p. 83-89.

288. Shrishrimal, S., E. Kosmacek, and R. Oberley-Deegan, *341 - MnTE-2-PyP protects the prostate from radiation-induced fibrosis (RIF) by activating Nrf2/Nqo1/SIRT signaling axis.* Free Radical Biology and Medicine, 2018. **128**: p. S140-S141.
289. Jackson, I.L., et al., *Superoxide dismutase mimetic reduces hypoxia-induced , TGF-β, and VEGF production by macrophages.* Free Radical Research, 2007. **41**(1): p. 8-14.
290. Rabbani, Z.N., et al., *Antiangiogenic action of redox-modulating Mn(III) meso-tetrakis(N-ethylpyridinium-2-yl)porphyrin, MnTE-2-PyP(5+), via suppression of oxidative stress in a mouse model of breast tumor.* Free Radic Biol Med, 2009. **47**(7): p. 992-1004.
291. Ashcraft, K.A., et al., *Novel Manganese-Porphyrin Superoxide Dismutase-Mimetic Widens the Therapeutic Margin in a Preclinical Head and Neck Cancer Model.* Int J Radiat Oncol Biol Phys, 2015. **93**(4): p. 892-900.
292. Jungsuwadee, P., et al., *The Metalloporphyrin Antioxidant, MnTE-2-PyP, Inhibits Th2 Cell Immune Responses in an Asthma Model.* International Journal of Molecular Sciences, 2012. **13**(8): p. 9785-9797.
293. Snelgrove, R.J., et al., *In the Absence of Reactive Oxygen Species, T Cells Default to a Th1 Phenotype and Mediate Protection against Pulmonary Cryptococcus neoformans Infection.* The Journal of Immunology, 2006. **177**(8): p. 5509-5516.
294. MAKINDE, A.Y., et al., *Effect of a Metalloporphyrin Antioxidant (MnTE-2-PyP) on the Response of a Mouse Prostate Cancer Model to Radiation.* Anticancer Research, 2009. **29**(1): p. 107-118.
295. Dekker, T.J., et al., *Prognostic significance of the tumor-stroma ratio: validation study in node-negative premenopausal breast cancer patients from the EORTC perioperative chemotherapy (POP) trial (10854).* Breast Cancer Res Treat, 2013. **139**(2): p. 371-9.
296. Kramer, C.J.H., et al., *The prognostic value of tumour-stroma ratio in primary breast cancer with special attention to triple-negative tumours: a review.* Breast Cancer Res Treat, 2019. **173**(1): p. 55-64.
297. Houthuijzen, J.M. and J. Jonkers, *Cancer-associated fibroblasts as key regulators of the breast cancer tumor microenvironment.* Cancer Metastasis Rev, 2018. **37**(4): p. 577-597.
298. Casey, T.M., et al., *Cancer associated fibroblasts stimulated by transforming growth factor beta1 (TGF-beta 1) increase invasion rate of tumor cells: a population study.* Breast Cancer Res Treat, 2008. **110**(1): p. 39-49.
299. Cho, J.A., et al., *Exosomes from breast cancer cells can convert adipose tissue-derived mesenchymal stem cells into myofibroblast-like cells.* Int J Oncol, 2012. **40**(1): p. 130-8.
300. Weber, C.E., et al., *Osteopontin mediates an MZF1-TGF-beta1-dependent transformation of mesenchymal stem cells into cancer-associated fibroblasts in breast cancer.* Oncogene, 2015. **34**(37): p. 4821-33.
301. Avgustinova, A., et al., *Tumour cell-derived Wnt7a recruits and activates fibroblasts to promote tumour aggressiveness.* Nat Commun, 2016. **7**: p. 10305.
302. Jotzu, C., et al., *Adipose tissue derived stem cells differentiate into carcinoma-associated fibroblast-like cells under the influence of tumor derived factors.* Cellular Oncology, 2011. **34**(1): p. 55-67.
303. Kojima, Y., et al., *Autocrine TGF-beta and stromal cell-derived factor-1 (SDF-1) signaling drives the evolution of tumor-promoting mammary stromal myofibroblasts.* Proc Natl Acad Sci U S A, 2010. **107**(46): p. 20009-14.

304. Ziani, L., S. Chouaib, and J. Thiery, *Alteration of the Antitumor Immune Response by Cancer-Associated Fibroblasts.* Front Immunol, 2018. **9**: p. 414.
305. Takahashi, H., et al., *Cancer-associated fibroblasts promote an immunosuppressive microenvironment through the induction and accumulation of protumoral macrophages.* Oncotarget, 2017. **8**(5): p. 8633-8647.
306. Fu, Z., et al., *The crosstalk: Tumor-infiltrating lymphocytes rich in regulatory T cells suppressed cancer-associated fibroblasts.* Acta Oncol, 2013. **52**(8): p. 1760-70.
307. Bergamaschi, A., et al., *Extracellular matrix signature identifies breast cancer subgroups with different clinical outcome.* J Pathol, 2008. **214**(3): p. 357-67.
308. Robertson, C., *The extracellular matrix in breast cancer predicts prognosis through composition, splicing, and crosslinking.* Exp Cell Res, 2016. **343**(1): p. 73-81.
309. Liu, T., et al., *Cancer-Associated Fibroblasts Build and Secure the Tumor Microenvironment.* Frontiers in cell and developmental biology, 2019. **7**: p. 60-60.
310. Erdogan, B., et al., *Cancer-associated fibroblasts promote directional cancer cell migration by aligning fibronectin.* J Cell Biol, 2017. **216**(11): p. 3799-3816.
311. Yoshimura, H., et al., *Cellular sources of tenascin-C in canine mammary carcinomas.* Vet Pathol, 2015. **52**(1): p. 92-6.
312. Radisky, E.S. and D.C. Radisky, *Matrix metalloproteinases as breast cancer drivers and therapeutic targets.* Frontiers in bioscience (Landmark edition), 2015. **20**: p. 1144-1163.
313. Cid, S., et al., *Prognostic Influence of Tumor Stroma on Breast Cancer Subtypes.* Clinical Breast Cancer, 2018. **18**(1): p. e123-e133.
314. Navab, R., et al., *Prognostic gene-expression signature of carcinoma-associated fibroblasts in non-small cell lung cancer.* Proceedings of the National Academy of Sciences, 2011. **108**(17): p. 7160-7165.
315. Conklin, M.W., et al., *Aligned collagen is a prognostic signature for survival in human breast carcinoma.* Am J Pathol, 2011. **178**(3): p. 1221-32.
316. Barcus, C.E., et al., *Elevated collagen-I augments tumor progressive signals, intravasation and metastasis of prolactin-induced estrogen receptor alpha positive mammary tumor cells.* Breast Cancer Res, 2017. **19**(1): p. 9.
317. Levental, K.R., et al., *Matrix crosslinking forces tumor progression by enhancing integrin signaling.* Cell, 2009. **139**(5): p. 891-906.
318. El-Mohri, H., et al., *Impact of matrix stiffness on fibroblast function.* Materials Science and Engineering: C, 2017. **74**: p. 146-151.
319. Asano, S., et al., *Matrix stiffness regulates migration of human lung fibroblasts.* Physiological Reports, 2017. **5**(9): p. e13281.
320. Ahn, S., et al., *The prognostic significance of tumor-associated stroma in invasive breast carcinoma.* Tumour Biol, 2012. **33**(5): p. 1573-80.
321. Yang, Z., et al., *Tenascin C is a prognostic determinant and potential cancer-associated fibroblasts marker for breast ductal carcinoma.* Experimental and Molecular Pathology, 2017. **102**(2): p. 262-267.
322. Yamashita, M., et al., *Role of stromal myofibroblasts in invasive breast cancer: stromal expression of alpha-smooth muscle actin correlates with worse clinical outcome.* Breast Cancer, 2012. **19**(2): p. 170-6.
323. Liu, L., et al., *Stromal Myofibroblasts Are Associated with Poor Prognosis in Solid Cancers: A Meta-Analysis of Published Studies.* PLOS ONE, 2016. **11**(7): p. e0159947.
324. Park, S.Y., H.M. Kim, and J.S. Koo, *Differential expression of cancer-associated fibroblast-related proteins according to molecular subtype and stromal histology*

in breast cancer. Breast Cancer Research and Treatment, 2015. **149**(3): p. 727-741.
325. Tchou, J., et al., *Human breast cancer associated fibroblasts exhibit subtype specific gene expression profiles.* BMC Medical Genomics, 2012. **5**(1): p. 39.
326. Busch, S., et al., *Cellular organization and molecular differentiation model of breast cancer-associated fibroblasts.* Molecular Cancer, 2017. **16**(1): p. 73.
327. Bartoschek, M., et al., *Spatially and functionally distinct subclasses of breast cancer-associated fibroblasts revealed by single cell RNA sequencing.* Nature Communications, 2018. **9**(1): p. 5150.
328. Chen, D. and G. Che, *Value of caveolin-1 in cancer progression and prognosis: Emphasis on cancer-associated fibroblasts, human cancer cells and mechanism of caveolin-1 expression (Review).* Oncology letters, 2014. **8**(4): p. 1409-1421.
329. Sloan, E.K., et al., *Stromal cell expression of caveolin-1 predicts outcome in breast cancer.* Am J Pathol, 2009. **174**(6): p. 2035-43.
330. Witkiewicz, A.K., et al., *Loss of stromal caveolin-1 expression predicts poor clinical outcome in triple negative and basal-like breast cancers.* Cancer Biol Ther, 2010. **10**(2): p. 135-43.
331. Chiavarina, B., et al., *HIF1-alpha functions as a tumor promoter in cancer associated fibroblasts, and as a tumor suppressor in breast cancer cells: Autophagy drives compartment-specific oncogenesis.* Cell cycle (Georgetown, Tex.), 2010. **9**(17): p. 3534-3551.
332. Lisanti, M.P., U.E. Martinez-Outschoorn, and F. Sotgia, *Oncogenes induce the cancer-associated fibroblast phenotype: metabolic symbiosis and "fibroblast addiction" are new therapeutic targets for drug discovery.* Cell cycle (Georgetown, Tex.), 2013. **12**(17): p. 2723-2732.
333. Martinez-Outschoorn, U.E., et al., *Cancer cells metabolically "fertilize" the tumor microenvironment with hydrogen peroxide, driving the Warburg effect: implications for PET imaging of human tumors.* Cell cycle (Georgetown, Tex.), 2011. **10**(15): p. 2504-2520.
334. Rőszer, T., *Understanding the Mysterious M2 Macrophage through Activation Markers and Effector Mechanisms.* Mediators of Inflammation, 2015. **2015**: p. 16.
335. Murray, Peter J., et al., *Macrophage Activation and Polarization: Nomenclature and Experimental Guidelines.* Immunity, 2014. **41**(1): p. 14-20.
336. Martinez, F.O. and S. Gordon, *The M1 and M2 paradigm of macrophage activation: time for reassessment.* F1000prime reports, 2014. **6**: p. 13-13.
337. Kadl, A., et al., *Identification of a novel macrophage phenotype that develops in response to atherogenic phospholipids via Nrf2.* Circ Res, 2010. **107**(6): p. 737-46.
338. Gleissner, C.A., *Macrophage Phenotype Modulation by CXCL4 in Atherosclerosis.* Frontiers in physiology, 2012. **3**: p. 1-1.
339. Mantovani, A., et al., *Macrophage polarization: tumor-associated macrophages as a paradigm for polarized M2 mononuclear phagocytes.* Trends in Immunology, 2002. **23**(11): p. 549-555.
340. Noy, R. and J.W. Pollard, *Tumor-associated macrophages: from mechanisms to therapy.* Immunity, 2014. **41**(1): p. 49-61.
341. Valeta-Magara, A., et al., *Inflammatory Breast Cancer Promotes Development of M2 Tumor-associated Macrophages and Cancer Mesenchymal Cells Through a Complex Cytokine Network.* Cancer Research, 2019: p. canres.2158.2017.
342. Su, S., et al., *A Positive Feedback Loop between Mesenchymal-like Cancer Cells and Macrophages Is Essential to Breast Cancer Metastasis.* Cancer Cell, 2014. **25**(5): p. 605-620.

343. Ding, J., et al., *CSF1 is involved in breast cancer progression through inducing monocyte differentiation and homing.* Int J Oncol, 2016. **49**(5): p. 2064-2074.
344. Zhou, J., et al., *Cancer-Associated Fibroblasts Correlate with Tumor-Associated Macrophages Infiltration and Lymphatic Metastasis in Triple Negative Breast Cancer Patients.* J Cancer, 2018. **9**(24): p. 4635-4641.
345. Orimo, A., et al., *Stromal fibroblasts present in invasive human breast carcinomas promote tumor growth and angiogenesis through elevated SDF-1/CXCL12 secretion.* Cell, 2005. **121**(3): p. 335-48.
346. Comito, G., et al., *Cancer-associated fibroblasts and M2-polarized macrophages synergize during prostate carcinoma progression.* Oncogene, 2014. **33**(19): p. 2423-31.
347. Garvin, S., et al., *Tumor cell expression of CD163 is associated to postoperative radiotherapy and poor prognosis in patients with breast cancer treated with breast-conserving surgery.* Journal of cancer research and clinical oncology, 2018. **144**(7): p. 1253-1263.
348. Chao Ni, L.Y., Qiuran Xu, Hongjun Yuan, Wei Wang, Wenjie Xia, Dihe Gong, Wei Zhang, Kun Yu, *CD68- and CD163-positive tumor infiltrating macrophages in non-metastatic breast cancer: a retrospective study and meta-analysis.* Journal of Cancer, 2019. **10**(19): p. 4463-4472.
349. Medrek, C., et al., *The presence of tumor associated macrophages in tumor stroma as a prognostic marker for breast cancer patients.* BMC Cancer, 2012. **12**(1): p. 306.
350. Volodko, N., et al., *Low infiltration of tumor-associated macrophages in high c-Myb-expressing breast tumors.* Scientific Reports, 2019. **9**(1): p. 11634.
351. Ivan, S., et al., *Breast cancer expression of CD163, a macrophage scavenger receptor, is related to early distant recurrence and reduced patient survival.* International Journal of Cancer, 2008. **123**(4): p. 780-786.
352. Qian, B., et al., *A Distinct Macrophage Population Mediates Metastatic Breast Cancer Cell Extravasation, Establishment and Growth.* PLOS ONE, 2009. **4**(8): p. e6562.
353. Guiducci, C., et al., *Redirecting In vivo Elicited Tumor Infiltrating Macrophages and Dendritic Cells towards Tumor Rejection.* Cancer Research, 2005. **65**(8): p. 3437.
354. Yoshimura, T., et al., *Monocyte chemoattractant protein-1/CCL2 produced by stromal cells promotes lung metastasis of 4T1 murine breast cancer cells.* PLoS One, 2013. **8**(3): p. e58791.
355. Fujimoto, H., et al., *Stromal MCP-1 in mammary tumors induces tumor-associated macrophage infiltration and contributes to tumor progression.* International Journal of Cancer, 2009. **125**(6): p. 1276-1284.
356. Arendt, L.M., et al., *Obesity Promotes Breast Cancer by CCL2-Mediated Macrophage Recruitment and Angiogenesis.* Cancer Research, 2013. **73**(19): p. 6080.
357. Fang, W.B., et al., *Targeted gene silencing of CCL2 inhibits triple negative breast cancer progression by blocking cancer stem cell renewal and M2 macrophage recruitment.* Oncotarget, 2016. **7**(31): p. 49349-49367.
358. Ries, C.H., et al., *Targeting tumor-associated macrophages with anti-CSF-1R antibody reveals a strategy for cancer therapy.* Cancer Cell, 2014. **25**(6): p. 846-59.
359. Strachan, D.C., et al., *CSF1R inhibition delays cervical and mammary tumor growth in murine models by attenuating the turnover of tumor-associated*

macrophages and enhancing infiltration by CD8(+) T cells. Oncoimmunology, 2013. **2**(12): p. e26968-e26968.
360. Cassetta, L. and J.W. Pollard, *Targeting macrophages: therapeutic approaches in cancer.* Nature Reviews Drug Discovery, 2018. **17**: p. 887.
361. Guerriero, J.L., et al., *Class IIa HDAC inhibition reduces breast tumours and metastases through anti-tumour macrophages.* Nature, 2017. **543**(7645): p. 428-432.
362. Hoves, S., et al., *Rapid activation of tumor-associated macrophages boosts preexisting tumor immunity.* J Exp Med, 2018. **215**(3): p. 859-876.
363. Georgoudaki, A.-M., et al., *Reprogramming Tumor-Associated Macrophages by Antibody Targeting Inhibits Cancer Progression and Metastasis.* Cell Reports, 2016. **15**(9): p. 2000-2011.
364. Kaneda, M.M., et al., *PI3Kgamma is a molecular switch that controls immune suppression.* Nature, 2016. **539**(7629): p. 437-442.
365. Xiao, Z., et al., *Antibody mediated therapy targeting CD47 inhibits tumor progression of hepatocellular carcinoma.* Cancer Lett, 2015. **360**(2): p. 302-9.
366. Le Mercier, I., et al., *Tumor promotion by intratumoral plasmacytoid dendritic cells is reversed by TLR7 ligand treatment.* Cancer Res, 2013. **73**(15): p. 4629-40.
367. Murata, Y., T. Shimamura, and J. Hamuro, *The polarization of T(h)1/T(h)2 balance is dependent on the intracellular thiol redox status of macrophages due to the distinctive cytokine production.* Int Immunol, 2002. **14**(2): p. 201-12.
368. Zhang, Y., et al., *ROS play a critical role in the differentiation of alternatively activated macrophages and the occurrence of tumor-associated macrophages.* Cell Res, 2013. **23**(7): p. 898-914.
369. Festjens, N., et al., *Butylated hydroxyanisole is more than a reactive oxygen species scavenger.* Cell Death Differ, 2006. **13**(1): p. 166-9.
370. Padgett, L.E., et al., *Loss of NADPH Oxidase–Derived Superoxide Skews Macrophage Phenotypes to Delay Type 1 Diabetes.* Diabetes, 2015. **64**(3): p. 937.
371. He, C., et al., *Accelerated development of pulmonary fibrosis via Cu,Zn-superoxide dismutase-induced alternative activation of macrophages.* J Biol Chem, 2013. **288**(28): p. 20745-57.
372. Panis, C., et al., *Can Breast Tumors Affect the Oxidative Status of the Surrounding Environment? A Comparative Analysis among Cancerous Breast, Mammary Adjacent Tissue, and Plasma.* Oxidative medicine and cellular longevity, 2015. **2015**: p. 6429812-6429812.
373. Nakamura, Y., et al., *Nitric oxide in breast cancer: induction of vascular endothelial growth factor-C and correlation with metastasis and poor prognosis.* Clin Cancer Res, 2006. **12**(4): p. 1201-7.
374. Aryal, B. and V.A. Rao, *Specific protein carbonylation in human breast cancer tissue compared to adjacent healthy epithelial tissue.* PloS one, 2018. **13**(3): p. e0194164-e0194164.
375. Mannello, F., G.A. Tonti, and V. Medda, *Protein oxidation in breast microenvironment: Nipple aspirate fluid collected from breast cancer women contains increased protein carbonyl concentration.* Cell Oncol, 2009. **31**(5): p. 383-92.
376. Panis, C., et al., *Differential oxidative status and immune characterization of the early and advanced stages of human breast cancer.* Breast Cancer Res Treat, 2012. **133**(3): p. 881-8.

377. Gonenc, A., et al., *Lipid peroxidation and antioxidant status in blood and tissue of malignant breast tumor and benign breast disease.* Cell Biol Int, 2006. **30**(4): p. 376-80.
378. Sarmiento-Salinas, F.L., et al., *Breast Cancer Subtypes Present a Differential Production of Reactive Oxygen Species (ROS) and Susceptibility to Antioxidant Treatment.* Frontiers in oncology, 2019. **9**: p. 480-480.
379. Chan, J.S.K., et al., *Cancer-associated fibroblasts enact field cancerization by promoting extratumoral oxidative stress.* Cell death & disease, 2017. **8**(1): p. e2562-e2562.
380. Nagaraj, S., et al., *Altered recognition of antigen is a mechanism of CD8+ T cell tolerance in cancer.* Nature Medicine, 2007. **13**: p. 828.
381. Kraaij, M.D., et al., *Induction of regulatory T cells by macrophages is dependent on production of reactive oxygen species.* Proc Natl Acad Sci U S A, 2010. **107**(41): p. 17686-91.
382. Adair-Kirk, T.L. and R.M. Senior, *Fragments of extracellular matrix as mediators of inflammation.* The international journal of biochemistry & cell biology, 2008. **40**(6-7): p. 1101-1110.
383. McKee, C.M., et al., *Hyaluronan fragments induce nitric-oxide synthase in murine macrophages through a nuclear factor kappaB-dependent mechanism.* J Biol Chem, 1997. **272**(12): p. 8013-8.
384. McKee, C.M., et al., *Hyaluronan (HA) fragments induce chemokine gene expression in alveolar macrophages. The role of HA size and CD44.* The Journal of Clinical Investigation, 1996. **98**(10): p. 2403-2413.
385. Noble, P.W., et al., *Hyaluronate activation of CD44 induces insulin-like growth factor-1 expression by a tumor necrosis factor-alpha-dependent mechanism in murine macrophages.* The Journal of Clinical Investigation, 1993. **91**(6): p. 2368-2377.
386. Schwertfeger, K.L., et al., *Hyaluronan, Inflammation, and Breast Cancer Progression.* Frontiers in immunology, 2015. **6**: p. 236-236.
387. Wu, M., et al., *A novel role of low molecular weight hyaluronan in breast cancer metastasis.* Faseb j, 2015. **29**(4): p. 1290-8.
388. Kliment, C.R., et al., *Extracellular superoxide dismutase protects against matrix degradation of heparan sulfate in the lung.* Antioxid Redox Signal, 2008. **10**(2): p. 261-8.
389. Kato, Y., K. Uchida, and S. Kawakishi, *Oxidative fragmentation of collagen and prolyl peptide by Cu(II)/H2O2. Conversion of proline residue to 2-pyrrolidone.* J Biol Chem, 1992. **267**(33): p. 23646-51.
390. Giri, R.K., et al., *Metal-catalyzed oxidation of extracellular matrix components perturbs hepatocyte survival with activation of intracellular signaling pathways.* Experimental Cell Research, 2003. **291**(2): p. 451-462.
391. Bacakova, L., et al., *Oxidized collagen stimulates proliferation of vascular smooth muscle cells.* Exp Mol Pathol, 1997. **64**(3): p. 185-94.
392. Kraft-Sheleg, O., et al., *Localized LoxL3-Dependent Fibronectin Oxidation Regulates Myofiber Stretch and Integrin-Mediated Adhesion.* Developmental Cell, 2016. **36**(5): p. 550-561.
393. Yakubenko, V.P., et al., *Oxidative modifications of extracellular matrix promote the second wave of inflammation via beta2 integrins.* Blood, 2018. **132**(1): p. 78-88.
394. Cui, K., et al., *Inhibition of integrin alphaDbeta2-mediated macrophage adhesion to end product of docosahexaenoic acid (DHA) oxidation prevents macrophage accumulation during inflammation.* J Biol Chem, 2019. **294**(39): p. 14370-14382.

395. Cui, K., et al., *Distinct Migratory Properties of M1, M2, and Resident Macrophages Are Regulated by alphaDbeta2 and alphaMbeta2 Integrin-Mediated Adhesion.* Front Immunol, 2018. **9**: p. 2650.
396. Fattman, C.L., et al., *Enhanced bleomycin-induced pulmonary damage in mice lacking extracellular superoxide dismutase.* Free Radic Biol Med, 2003. **35**(7): p. 763-71.
397. Gao, F., et al., *Extracellular superoxide dismutase inhibits inflammation by preventing oxidative fragmentation of hyaluronan.* J Biol Chem, 2008. **283**(10): p. 6058-66.
398. Rabbani, Z.N., et al., *Overexpression of extracellular superoxide dismutase reduces acute radiation induced lung toxicity.* BMC Cancer, 2005. **5**(1): p. 59.
399. Na, K., et al., *EC-SOD Suppresses Contact Hypersensitivity in Mouse Skin by Impairing Langerhans Cell Migration.* Journal of Investigative Dermatology, 2007. **127**(8): p. 1930-1937.
400. Kim, Y., et al., *Regulation of skin inflammation and angiogenesis by EC-SOD via HIF-1α and NF-κB pathways.* Free Radical Biology and Medicine, 2011. **51**(11): p. 1985-1995.
401. Laurila, J.P., et al., *SOD3 reduces inflammatory cell migration by regulating adhesion molecule and cytokine expression.* PLoS One, 2009. **4**(6): p. e5786.
402. Goswami, K.K., et al., *Tumor promoting role of anti-tumor macrophages in tumor microenvironment.* Cell Immunol, 2017.
403. Kwon, M.J., et al., *Superoxide dismutase 3 controls adaptive immune responses and contributes to the inhibition of ovalbumin-induced allergic airway inflammation in mice.* Antioxid Redox Signal, 2012. **17**(10): p. 1376-92.
404. Grivennikov, S.I., F.R. Greten, and M. Karin, *Immunity, inflammation, and cancer.* Cell, 2010. **140**(6): p. 883-99.
405. Tang, X., et al., *A critical role of Gbetagamma in tumorigenesis and metastasis of breast cancer.* J Biol Chem, 2011. **286**(15): p. 13244-54.
406. Kuperwasser, C., et al., *Reconstruction of functionally normal and malignant human breast tissues in mice.* Proc Natl Acad Sci U S A, 2004. **101**(14): p. 4966-71.
407. Lee, G.Y., et al., *Three-dimensional culture models of normal and malignant breast epithelial cells.* Nat Methods, 2007. **4**(4): p. 359-65.
408. Mia, S., et al., *An optimized protocol for human M2 macrophages using M-CSF and IL-4/IL-10/TGF-β yields a dominant immunosuppressive phenotype.* Scandinavian journal of immunology, 2014. **79**(5): p. 305-314.
409. Teoh, M.L.T., et al., *Overexpression of Extracellular Superoxide Dismutase Attenuates Heparanase Expression and Inhibits Breast Carcinoma Cell Growth and Invasion.* Cancer Research, 2009. **69**(15): p. 6355-6363.
410. Weydert, C.J. and J.J. Cullen, *MEASUREMENT OF SUPEROXIDE DISMUTASE, CATALASE, AND GLUTATHIONE PEROXIDASE IN CULTURED CELLS AND TISSUE.* Nature protocols, 2010. **5**(1): p. 51-66.
411. Teoh, M.L.T., et al., *Modulation of Reactive Oxygen Species in Pancreatic Cancer.* Clinical Cancer Research, 2007. **13**(24): p. 7441-7450.
412. Timpson, P., et al., *Organotypic collagen I assay: a malleable platform to assess cell behaviour in a 3-dimensional context.* J Vis Exp, 2011(56): p. e3089.
413. Teoh-Fitzgerald, M.L., et al., *Genetic and epigenetic inactivation of extracellular superoxide dismutase promotes an invasive phenotype in human lung cancer by disrupting ECM homeostasis.* Mol Cancer Res, 2012. **10**(1): p. 40-51.
414. Frank, G.D. and S. Eguchi, *Activation of tyrosine kinases by reactive oxygen species in vascular smooth muscle cells: significance and involvement of EGF*

receptor transactivation by angiotensin II. Antioxid Redox Signal, 2003. **5**(6): p. 771-80.
415. Jagadeeswaran, R., et al., *Activation of HGF/c-Met pathway contributes to the reactive oxygen species generation and motility of small cell lung cancer cells.* Am J Physiol Lung Cell Mol Physiol, 2007. **292**(6): p. L1488-94.
416. Trusolino, L., A. Bertotti, and P.M. Comoglio, *MET signalling: principles and functions in development, organ regeneration and cancer.* Nat Rev Mol Cell Biol, 2010. **11**(12): p. 834-48.
417. Ghoussoub, R.A., et al., *Expression of c-met is a strong independent prognostic factor in breast carcinoma.* Cancer, 1998. **82**(8): p. 1513-20.
418. Gusenbauer, S., P. Vlaicu, and A. Ullrich, *HGF induces novel EGFR functions involved in resistance formation to tyrosine kinase inhibitors.* Oncogene, 2012.
419. Cecchi, F., D.C. Rabe, and D.P. Bottaro, *Targeting the HGF/Met signalling pathway in cancer.* Eur J Cancer, 2010. **46**(7): p. 1260-70.
420. Tsao, M.S., et al., *Hepatocyte growth factor is predominantly expressed by the carcinoma cells in non-small-cell lung cancer.* Hum Pathol, 2001. **32**(1): p. 57-65.
421. Jiang, W., et al., *Hepatocyte growth factor/scatter factor, its molecular, cellular and clinical implications in cancer.* Crit Rev Oncol Hematol, 1999. **29**(3): p. 209-48.
422. Buchsbaum, R.J. and S.Y. Oh, *Breast Cancer-Associated Fibroblasts: Where We Are and Where We Need to Go.* Cancers (Basel), 2016. **8**(2).
423. Torres, S., et al., *Proteome profiling of cancer-associated fibroblasts identifies novel proinflammatory signatures and prognostic markers for colorectal cancer.* Clin Cancer Res, 2013. **19**(21): p. 6006-19.
424. Giannoni, E., et al., *Cancer associated fibroblasts exploit reactive oxygen species through a proinflammatory signature leading to epithelial mesenchymal transition and stemness.* Antioxid Redox Signal, 2011. **14**(12): p. 2361-71.
425. Li, R., et al., *Abl Kinases Regulate HGF/Met Signaling Required for Epithelial Cell Scattering, Tubulogenesis and Motility.* PLoS One, 2015. **10**(5): p. e0124960.
426. Furlan, A., et al., *Abl interconnects oncogenic Met and p53 core pathways in cancer cells.* Cell Death Differ, 2011. **18**(10): p. 1608-16.
427. Furlan, A., et al., *Met acts through Abl to regulate p53 transcriptional outcomes and cell survival in the developing liver.* J Hepatol, 2012. **57**(6): p. 1292-8.
428. Case, A.J., et al., *Rational design of a secreted enzymatically inactive mutant of extracellular superoxide dismutase.* Redox Rep, 2012. **17**(6): p. 239-45.
429. Weinstat-Saslow, D.L., et al., *Transfection of thrombospondin 1 complementary DNA into a human breast carcinoma cell line reduces primary tumor growth, metastatic potential, and angiogenesis.* Cancer Res, 1994. **54**(24): p. 6504-11.
430. Koch, M., et al., *CD36-mediated activation of endothelial cell apoptosis by an N-terminal recombinant fragment of thrombospondin-2 inhibits breast cancer growth and metastasis in vivo.* Breast Cancer Res Treat, 2011. **128**(2): p. 337-46.
431. Lamszus, K., et al., *Scatter factor binds to thrombospondin and other extracellular matrix components.* Am J Pathol, 1996. **149**(3): p. 805-19.
432. Margosio, B., et al., *Thrombospondin 1 as a scavenger for matrix-associated fibroblast growth factor 2.* Blood, 2003. **102**(13): p. 4399-406.
433. Nazarewicz, R.R., A. Bikineyeva, and S.I. Dikalov, *Rapid and specific measurements of superoxide using fluorescence spectroscopy.* Journal of biomolecular screening, 2013. **18**(4): p. 498-503.

434. Batinic-Haberle, I., J.S. Reboucas, and I. Spasojevic, *Superoxide dismutase mimics: chemistry, pharmacology, and therapeutic potential.* Antioxid Redox Signal, 2010. **13**(6): p. 877-918.
435. Menashe, I., et al., *Pathway analysis of breast cancer genome-wide association study highlights three pathways and one canonical signaling cascade.* Cancer Res, 2010. **70**(11): p. 4453-9.
436. Miura, Y., Y. Kozuki, and K. Yagasaki, *Potentiation of invasive activity of hepatoma cells by reactive oxygen species is mediated by autocrine/paracrine loop of hepatocyte growth factor.* Biochem Biophys Res Commun, 2003. **305**(1): p. 160-5.
437. Ivanovska, I., et al., *Gene Signatures Derived from a c-MET-Driven Liver Cancer Mouse Model Predict Survival of Patients with Hepatocellular Carcinoma.* PLoS ONE, 2011. **6**(9): p. e24582.
438. Srinivasan, D., J.T. Sims, and R. Plattner, *Aggressive breast cancer cells are dependent on activated Abl kinases for proliferation, anchorage-independent growth and survival.* Oncogene, 2008. **27**(8): p. 1095-105.
439. Ghajar, C.M., et al., *The perivascular niche regulates breast tumour dormancy.* Nat Cell Biol, 2013. **15**(7): p. 807-17.
440. Resovi, A., et al., *Current understanding of the thrombospondin-1 interactome.* Matrix Biol, 2014. **37**: p. 83-91.
441. Zhang, Y.W., et al., *Hepatocyte growth factor/scatter factor mediates angiogenesis through positive VEGF and negative thrombospondin 1 regulation.* Proc Natl Acad Sci U S A, 2003. **100**(22): p. 12718-23.
442. Casbas-Hernandez, P., et al., *Role of HGF in epithelial–stromal cell interactions during progression from benign breast disease to ductal carcinoma in situ.* Breast Cancer Research, 2013. **15**(5): p. R82.
443. Ho-Yen, C.M., J.L. Jones, and S. Kermorgant, *The clinical and functional significance of c-Met in breast cancer: a review.* Breast Cancer Res, 2015. **17**: p. 52.
444. Zhao, Q.D., et al., *NADPH Oxidase 4 Induces Cardiac Fibrosis and Hypertrophy Through Activating Akt/mTOR and NFkappaB Signaling Pathways.* Circulation, 2015.
445. Cucoranu, I., et al., *NAD(P)H oxidase 4 mediates transforming growth factor-beta1-induced differentiation of cardiac fibroblasts into myofibroblasts.* Circ Res, 2005. **97**(9): p. 900-7.
446. Lookene, A., P. Stenlund, and L.A. Tibell, *Characterization of heparin binding of human extracellular superoxide dismutase.* Biochemistry, 2000. **39**(1): p. 230-6.
447. Ookawara, T., et al., *Nuclear translocation of extracellular superoxide dismutase.* Biochemical and Biophysical Research Communications, 2002. **296**(1): p. 54-61.
448. Nisimoto, Y., et al., *Nox4: a hydrogen peroxide-generating oxygen sensor.* Biochemistry, 2014. **53**(31): p. 5111-20.
449. Altenhofer, S., et al., *The NOX toolbox: validating the role of NADPH oxidases in physiology and disease.* Cell Mol Life Sci, 2012. **69**(14): p. 2327-43.
450. Altenhöfer, S., et al., *The NOX toolbox: validating the role of NADPH oxidases in physiology and disease.* Cellular and Molecular Life Sciences, 2012. **69**(14): p. 2327-2343.
451. Liochev, S.I. and I. Fridovich, *The effects of superoxide dismutase on H2O2 formation.* Free Radic Biol Med, 2007. **42**(10): p. 1465-9.
452. Irwin, F., *Superoxide Dismutases: Anti- Versus Pro- Oxidants?* Anti-Cancer Agents in Medicinal Chemistry, 2011. **11**(2): p. 175-177.

453. Griess, B., et al., *Extracellular superoxide dismutase and its role in cancer.* Free Radic Biol Med, 2017. **112**: p. 464-479.
454. Leek, R.D., et al., *Association of Macrophage Infiltration with Angiogenesis and Prognosis in Invasive Breast Carcinoma.* Cancer Research, 1996. **56**(20): p. 4625-4629.
455. Mantovani, A., et al., *Tumour-associated macrophages as treatment targets in oncology.* Nature Reviews Clinical Oncology, 2017. **14**: p. 399.
456. Bingle, L., N.J. Brown, and C.E. Lewis, *The role of tumour-associated macrophages in tumour progression: implications for new anticancer therapies.* J Pathol, 2002. **196**(3): p. 254-65.
457. Baghdadi, M., et al., *High co-expression of IL-34 and M-CSF correlates with tumor progression and poor survival in lung cancers.* Sci Rep, 2018. **8**(1): p. 418.
458. Chen, X., et al., *Prognostic value of diametrically polarized tumor-associated macrophages in multiple myeloma.* Oncotarget, 2017. **8**(68): p. 112685-112696.
459. Jensen, T.O., et al., *Macrophage markers in serum and tumor have prognostic impact in American Joint Committee on Cancer stage I/II melanoma.* J Clin Oncol, 2009. **27**(20): p. 3330-7.
460. Klein, J.L., et al., *CD163 immunohistochemistry is superior to CD68 in predicting outcome in classical Hodgkin lymphoma.* Am J Clin Pathol, 2014. **141**(3): p. 381-7.
461. Komohara, Y., et al., *Macrophage infiltration and its prognostic relevance in clear cell renal cell carcinoma.* Cancer Sci, 2011. **102**(7): p. 1424-31.
462. Kridel, R., et al., *The Prognostic Impact of CD163-Positive Macrophages in Follicular Lymphoma: A Study from the BC Cancer Agency and the Lymphoma Study Association.* Clin Cancer Res, 2015. **21**(15): p. 3428-35.
463. Lee, C.H., et al., *Prognostic significance of macrophage infiltration in leiomyosarcomas.* Clin Cancer Res, 2008. **14**(5): p. 1423-30.
464. Maniecki, M.B., et al., *Tumor-promoting macrophages induce the expression of the macrophage-specific receptor CD163 in malignant cells.* Int J Cancer, 2012. **131**(10): p. 2320-31.
465. Yu, M., et al., *Prognostic value of tumor-associated macrophages in pancreatic cancer: a meta-analysis.* Cancer Manag Res, 2019. **11**: p. 4041-4058.
466. Biswas, S.K. and A. Mantovani, *Macrophage plasticity and interaction with lymphocyte subsets: cancer as a paradigm.* Nature Immunology, 2010. **11**: p. 889.
467. Klingen, T.A., et al., *Tumor-associated macrophages are strongly related to vascular invasion, non-luminal subtypes, and interval breast cancer.* Human Pathology, 2017. **69**: p. 72-80.
468. Satu, T., et al., *High numbers of macrophages, especially M2-like (CD163-positive), correlate with hyaluronan accumulation and poor outcome in breast cancer.* Histopathology, 2015. **66**(6): p. 873-883.
469. Fritz, J.M., et al., *Depletion of Tumor-Associated Macrophages Slows the Growth of Chemically Induced Mouse Lung Adenocarcinomas.* Frontiers in Immunology, 2014. **5**(587).
470. Galmbacher, K., et al. *Shigella mediated depletion of macrophages in a murine breast cancer model is associated with tumor regression*. PloS one, 2010. **5**, e9572 DOI: 10.1371/journal.pone.0009572.
471. Rogers, T.L. and I. Holen, *Tumour macrophages as potential targets of bisphosphonates.* Journal of Translational Medicine, 2011. **9**(1): p. 177.

472. Tan, H.Y., et al., *The Reactive Oxygen Species in Macrophage Polarization: Reflecting Its Dual Role in Progression and Treatment of Human Diseases.* Oxid Med Cell Longev, 2016. **2016**: p. 2795090.
473. Policastro, L.L., et al., *The Tumor Microenvironment: Characterization, Redox Considerations, and Novel Approaches for Reactive Oxygen Species-Targeted Gene Therapy.* Antioxid Redox Signal, 2012.
474. Cross, A.R. and O.T.G. Jones, *The effect of the inhibitor diphenylene iodonium on the superoxide-generating system of neutrophils. Specific labelling of a component polypeptide of the oxidase.* Biochemical Journal, 1986. **237**(1): p. 111-116.
475. Yeung, O.W.H., et al., *Alternatively activated (M2) macrophages promote tumour growth and invasiveness in hepatocellular carcinoma.* Journal of Hepatology, 2015. **62**(3): p. 607-616.
476. Yuan, A., et al., *Opposite Effects of M1 and M2 Macrophage Subtypes on Lung Cancer Progression.* Scientific Reports, 2015. **5**: p. 14273.
477. Parsa, R., et al., *Adoptive Transfer of Immunomodulatory M2 Macrophages Prevents Type 1 Diabetes in NOD Mice.* Diabetes, 2012. **61**(11): p. 2881-2892.
478. Sharma, A., et al., *77 - Immunotherapy of Cancer*, in *Clinical Immunology (Fifth Edition)*, R.R. Rich, et al., Editors. 2019, Content Repository Only!: London. p. 1033-1048.e1.
479. Huber, S., et al., *Alternatively activated macrophages inhibit T-cell proliferation by Stat6-dependent expression of PD-L2.* Blood, 2010. **116**(17): p. 3311-3320.
480. Lawrence, T. and G. Natoli, *Transcriptional regulation of macrophage polarization: enabling diversity with identity.* Nat Rev Immunol, 2011. **11**(11): p. 750-61.
481. Dwivedi, G., et al., *Dynamic Redox Regulation of IL-4 Signaling.* PLOS Computational Biology, 2015. **11**(11): p. e1004582.
482. Kim, H.J., et al., *Exogenous Hydrogen Peroxide Induces Lipid Raft-Mediated STAT-6 Activation in T Cells.* Cellular Physiology and Biochemistry, 2017. **42**(6): p. 2467-2480.
483. Hirakawa, S., et al., *Dual Oxidase 1 Induced by Th2 Cytokines Promotes STAT6 Phosphorylation via Oxidative Inactivation of Protein Tyrosine Phosphatase 1B in Human Epidermal Keratinocytes.* The Journal of Immunology, 2011. **186**(8): p. 4762-4770.
484. Wills-Karp, M. and F.D. Finkelman, *Untangling the Complex Web of IL-4– and IL-13–Mediated Signaling Pathways.* Science Signaling, 2008. **1**(51): p. pe55-pe55.
485. Rahaman, S.O., M.A. Vogelbaum, and S.J. Haque, *Aberrant Stat3 Signaling by Interleukin-4 in Malignant Glioma Cells: Involvement of IL-13Rα2.* Cancer Research, 2005. **65**(7): p. 2956-2963.
486. Liu, J., et al., *The ROS-mediated activation of IL-6/STAT3 signaling pathway is involved in the 27-hydroxycholesterol-induced cellular senescence in nerve cells.* Toxicology in Vitro, 2017. **45**: p. 10-18.
487. Choi, S.Y., et al., *Reactive oxygen species mediate Jak2/Stat3 activation and IL-8 expression in pulmonary epithelial cells stimulated with lipid-associated membrane proteins from Mycoplasma pneumoniae.* Inflammation Research, 2012. **61**(5): p. 493-501.
488. Cheng, Z., et al., *CD163 as a novel target gene of STAT3 is a potential therapeutic target for gastric cancer.* Oncotarget, 2017. **8**(50): p. 87244-87262.
489. Hedrich, C.M., et al., *Stat3 promotes IL-10 expression in lupus T cells through trans-activation and chromatin remodeling.* Proceedings of the National Academy of Sciences, 2014. **111**(37): p. 13457-13462.

490. Garcia-Diaz, A., et al., *Interferon Receptor Signaling Pathways Regulating PD-L1 and PD-L2 Expression.* Cell Reports, 2017. **19**(6): p. 1189-1201.
491. Chen, X., et al., *Reactive Oxygen Species Regulate T Cell Immune Response in the Tumor Microenvironment.* Oxidative Medicine and Cellular Longevity, 2016. **2016**: p. 1580967.
492. Sklavos, M.M., H.M. Tse, and J.D. Piganelli, *Redox modulation inhibits CD8 T cell effector function.* Free Radical Biology and Medicine, 2008. **45**(10): p. 1477-1486.
493. Kraaij, M.D., et al., *Dexamethasone increases ROS production and T cell suppressive capacity by anti-inflammatory macrophages.* Molecular Immunology, 2011. **49**(3): p. 549-557.
494. Beyer, M., et al., *High-resolution transcriptome of human macrophages.* PLoS One, 2012. **7**(9): p. e45466.
495. Simon, A.R., et al., *Activation of the JAK-STAT pathway by reactive oxygen species.* American Journal of Physiology-Cell Physiology, 1998. **275**(6): p. C1640-C1652.
496. Yu, M.O., et al., *Reactive oxygen species production has a critical role in hypoxia-induced Stat3 activation and angiogenesis in human glioblastoma.* Journal of Neuro-Oncology, 2015. **125**(1): p. 55-63.
497. Millonig, G., et al., *Sustained Submicromolar H2O2 Levels Induce Hepcidin via Signal Transducer and Activator of Transcription 3 (STAT3).* Journal of Biological Chemistry, 2012. **287**(44): p. 37472-37482.
498. Carballo, M., et al., *Oxidative Stress Triggers STAT3 Tyrosine Phosphorylation and Nuclear Translocation in Human Lymphocytes.* Journal of Biological Chemistry, 1999. **274**(25): p. 17580-17586.
499. Ju, K.D., et al., *Potential role of NADPH oxidase-mediated activation of Jak2/Stat3 and mitogen-activated protein kinases and expression of TGF-β1 in the pathophysiology of acute pancreatitis.* Inflammation Research, 2011. **60**(8): p. 791-800.
500. Tawfik, A., et al., *Hyperglycemia and reactive oxygen species mediate apoptosis in aortic endothelial cells through Janus kinase 2.* Vascular Pharmacology, 2005. **43**(5): p. 320-326.
501. Riganti, C., et al., *Diphenyleneiodonium inhibits the cell redox metabolism and induces oxidative stress.* J Biol Chem, 2004. **279**(46): p. 47726-31.
502. Galván-Peña, S. and L.A.J. O'Neill, *Metabolic reprograming in macrophage polarization.* Frontiers in immunology, 2014. **5**: p. 420-420.
503. Xu, Q., et al., *NADPH Oxidases Are Essential for Macrophage Differentiation.* J Biol Chem, 2016. **291**(38): p. 20030-41.
504. Xu, D. and C.-K. Qu, *Protein tyrosine phosphatases in the JAK/STAT pathway.* Frontiers in bioscience : a journal and virtual library, 2008. **13**: p. 4925-4932.
505. Persson, C., et al., *Preferential oxidation of the second phosphatase domain of receptor-like PTP-alpha revealed by an antibody against oxidized protein tyrosine phosphatases.* Proceedings of the National Academy of Sciences of the United States of America, 2004. **101**(7): p. 1886-1891.
506. Gross, S., et al., *Inactivation of protein-tyrosine phosphatases as mechanism of UV-induced signal transduction.* J Biol Chem, 1999. **274**(37): p. 26378-86.
507. Meng, T.-C., et al., *Regulation of Insulin Signaling through Reversible Oxidation of the Protein-tyrosine Phosphatases TC45 and PTP1B.* Journal of Biological Chemistry, 2004. **279**(36): p. 37716-37725.
508. Wei Luo, B.Y., Qin-Yi Qin, Jiong-Min Lu, Shan-Yu Qin, Hai-Xing Jiang, *Interleukin-22 promotes macrophage M2 polarization via STAT3 pathway.*

International Journal of Clinical and Experimental Medicine, 2016. **9**(10): p. 19574-19580.
509. Fu, X.-L., et al., *Interleukin 6 induces M2 macrophage differentiation by STAT3 activation that correlates with gastric cancer progression.* Cancer Immunology, Immunotherapy, 2017. **66**(12): p. 1597-1608.
510. Niemand, C., et al., *Activation of STAT3 by IL-6 and IL-10 in primary human macrophages is differentially modulated by suppressor of cytokine signaling 3.* J Immunol, 2003. **170**(6): p. 3263-72.
511. Vasquez-Dunddel, D., et al., *STAT3 regulates arginase-I in myeloid-derived suppressor cells from cancer patients.* J Clin Invest, 2013. **123**(4): p. 1580-9.
512. Stritesky, G.L., et al., *The Transcription Factor STAT3 Is Required for T Helper 2 Cell Development.* Immunity, 2011. **34**(1): p. 39-49.
513. Sawa-Wejksza, K. and M. Kandefer-Szerszeń, *Tumor-Associated Macrophages as Target for Antitumor Therapy.* Archivum Immunologiae et Therapiae Experimentalis, 2018. **66**(2): p. 97-111.
514. Coscia, M., et al., *Zoledronic acid repolarizes tumour-associated macrophages and inhibits mammary carcinogenesis by targeting the mevalonate pathway.* J Cell Mol Med, 2010. **14**(12): p. 2803-15.
515. Cassetta, L. and T. Kitamura, *Targeting Tumor-Associated Macrophages as a Potential Strategy to Enhance the Response to Immune Checkpoint Inhibitors.* Frontiers in Cell and Developmental Biology, 2018. **6**: p. 38.
516. Griess, B., et al., *Extracellular superoxide dismutase and its role in cancer.* Free radical biology & medicine, 2017. **112**: p. 464-479.
517. Golden, B.O., et al., *Extracellular superoxide dismutase inhibits hepatocyte growth factor-mediated breast cancer-fibroblast interactions.* Oncotarget, 2017. **8**(64): p. 107390-107408.
518. Jones, P.A., *DNA methylation and cancer.* Oncogene, 2002. **21**(35): p. 5358-60.
519. Laukkanen, M.O., et al., *Local hypomethylation in atherosclerosis found in rabbit ec-sod gene.* Arterioscler Thromb Vasc Biol, 1999. **19**(9): p. 2171-8.
520. Hashmi, A.A., et al., *Prognostic parameters of luminal A and luminal B intrinsic breast cancer subtypes of Pakistani patients.* World Journal of Surgical Oncology, 2018. **16**(1): p. 1.
521. Li, Z.-H., et al., *Luminal B breast cancer: patterns of recurrence and clinical outcome.* Oncotarget, 2016. **7**(40): p. 65024-65033.
522. Stefansson, O.A., et al., *A DNA methylation-based definition of biologically distinct breast cancer subtypes.* Molecular Oncology, 2015. **9**(3): p. 555-568.
523. Kwei, K.A., et al., *Genomic instability in breast cancer: pathogenesis and clinical implications.* Molecular oncology, 2010. **4**(3): p. 255-266.
524. Kakazu, A., G. Sharma, and H.E.P. Bazan, *Association of protein tyrosine phosphatases (PTPs)-1B with c-Met receptor and modulation of corneal epithelial wound healing.* Investigative ophthalmology & visual science, 2008. **49**(7): p. 2927-2935.
525. Sangwan, V., et al., *Regulation of the Met receptor-tyrosine kinase by the protein-tyrosine phosphatase 1B and T-cell phosphatase.* The Journal of biological chemistry, 2008. **283**(49): p. 34374-34383.
526. Maroun, C.R., et al., *The Tyrosine Phosphatase SHP-2 Is Required for Sustained Activation of Extracellular Signal-Regulated Kinase and Epithelial Morphogenesis Downstream from the Met Receptor Tyrosine Kinase.* Molecular and Cellular Biology, 2000. **20**(22): p. 8513.
527. Meena S.K., K.R., Sairoz, *Serum nitric oxide and peroxynitrite in breast cancer patients.* International Journal of Current Research, 2017. **9**(8): p. 55725-55727.

528. Basudhar, D., et al., *Nitric Oxide Synthase-2-Derived Nitric Oxide Drives Multiple Pathways of Breast Cancer Progression.* Antioxid Redox Signal, 2017. **26**(18): p. 1044-1058.
529. Glynn, S.A., et al., *Increased NOS2 predicts poor survival in estrogen receptor-negative breast cancer patients.* J Clin Invest, 2010. **120**(11): p. 3843-54.
530. Loibl, S., et al., *The role of early expression of inducible nitric oxide synthase in human breast cancer.* Eur J Cancer, 2005. **41**(2): p. 265-71.
531. Samoszuk, M., et al., *Association Between Nitrotyrosine Levels and Microvascular Density in Human Breast Cancer.* Breast Cancer Research and Treatment, 2002. **74**(3): p. 271-278.
532. Ashki, N., et al., *Peroxynitrite Upregulates Angiogenic Factors VEGF-A, BFGF, and HIF-1α in Human Corneal Limbal Epithelial Cells.* Investigative Ophthalmology & Visual Science, 2014. **55**(3): p. 1637-1646.
533. Gochman, E., J. Mahajna, and A.Z. Reznick, *NF-kappaB activation by peroxynitrite through IkappaBalpha-dependent phosphorylation versus nitration in colon cancer cells.* Anticancer Res, 2011. **31**(5): p. 1607-17.
534. Janssens, R., et al., *Peroxynitrite Exposure of CXCL12 Impairs Monocyte, Lymphocyte and Endothelial Cell Chemotaxis, Lymphocyte Extravasation in vivo and Anti-HIV-1 Activity.* Frontiers in Immunology, 2018. **9**(1933).
535. Molon, B., et al., *Chemokine nitration prevents intratumoral infiltration of antigen-specific T cells.* J Exp Med, 2011. **208**(10): p. 1949-62.
536. Fields, M.A., et al., *Nitrite Modification of Extracellular Matrix Alters CD46 Expression and VEGF Release in Human Retinal Pigment Epithelium.* Investigative Ophthalmology & Visual Science, 2015. **56**(8): p. 4231-4238.
537. Thao, M.T., et al., *Nitrite ion modifies tyrosine and lysine residues of extracellular matrix proteins.* Nitric Oxide, 2018. **79**: p. 51-56.
538. Fields, M.A., et al., *Extracellular matrix nitration alters growth factor release and activates bioactive complement in human retinal pigment epithelial cells.* PLoS One, 2017. **12**(5): p. e0177763.
539. Sato, E., et al., *Reactive oxygen and nitrogen metabolites modulate fibronectin-induced fibroblast migration in vitro.* Free Radic Biol Med, 2001. **30**(1): p. 22-9.
540. Lukacs-Kornek, V., et al., *Regulated release of nitric oxide by nonhematopoietic stroma controls expansion of the activated T cell pool in lymph nodes.* Nat Immunol, 2011. **12**(11): p. 1096-104.
541. Liao, J.K., *Linking endothelial dysfunction with endothelial cell activation.* J Clin Invest, 2013. **123**(2): p. 540-1.
542. Smeda, M., et al., *Nitric oxide deficiency and endothelial-mesenchymal transition of pulmonary endothelium in the progression of 4T1 metastatic breast cancer in mice.* Breast cancer research : BCR, 2018. **20**(1): p. 86-86.
543. Harrell, J.C., et al., *Endothelial-like properties of claudin-low breast cancer cells promote tumor vascular permeability and metastasis.* Clinical & experimental metastasis, 2014. **31**(1): p. 33-45.
544. Azzi, S., J.K. Hebda, and J. Gavard, *Vascular permeability and drug delivery in cancers.* Frontiers in oncology, 2013. **3**: p. 211-211.
545. Baldus, S., et al., *Endothelial transcytosis of myeloperoxidase confers specificity to vascular ECM proteins as targets of tyrosine nitration.* The Journal of Clinical Investigation, 2001. **108**(12): p. 1759-1770.
546. Shacka, J.J., et al., *Two distinct signaling pathways regulate peroxynitrite-induced apoptosis in PC12 cells.* Cell Death & Differentiation, 2006. **13**(9): p. 1506-1514.

547. Mukhopadhyay, P., et al., *Role of superoxide, nitric oxide, and peroxynitrite in doxorubicin-induced cell death in vivo and in vitro.* Am J Physiol Heart Circ Physiol, 2009. **296**(5): p. H1466-83.
548. Song, D., et al., *Downregulation of c-FLIP, XIAP and Mcl-1 protein as well as depletion of reduced glutathione contribute to the apoptosis induction of glycyrrhetinic acid derivatives in leukemia cells.* Cancer Biol Ther, 2010. **9**(2): p. 96-108.
549. Samuni, Y., et al., *The chemistry and biological activities of N-acetylcysteine.* Biochimica et Biophysica Acta (BBA) - General Subjects, 2013. **1830**(8): p. 4117-4129.
550. Horst, A., et al., *Effect of N-acetylcysteine on the spinal-cord glutathione system and nitric-oxide metabolites in rats with neuropathic pain.* Neurosci Lett, 2014. **569**: p. 163-8.
551. Short, J.D., et al., *Protein Thiol Redox Signaling in Monocytes and Macrophages.* Antioxidants & Redox Signaling, 2016. **25**(15): p. 816-835.
552. Ullevig, S.L., et al., *Protein S-Glutathionylation Mediates Macrophage Responses to Metabolic Cues from the Extracellular Environment.* Antioxidants & Redox Signaling, 2016. **25**(15): p. 836-851.
553. Menon, D., et al., *GSTO1-1 modulates metabolism in macrophages activated through the LPS and TLR4 pathway.* J Cell Sci, 2015. **128**(10): p. 1982-90.
554. Cao, X., et al., *Glutathione S-transferase P1 suppresses iNOS protein stability in RAW264.7 macrophage-like cells after LPS stimulation.* Free Radic Res, 2015. **49**(12): p. 1438-48.
555. Troidl, C., et al., *Classically and alternatively activated macrophages contribute to tissue remodelling after myocardial infarction.* Journal of Cellular and Molecular Medicine, 2009. **13**(9b): p. 3485-3496.
556. Yu, Y.-R.A., et al., *A Protocol for the Comprehensive Flow Cytometric Analysis of Immune Cells in Normal and Inflamed Murine Non-Lymphoid Tissues.* PLOS ONE, 2016. **11**(3): p. e0150606.
557. DeNardo, D.G., et al., *CD4(+) T cells regulate pulmonary metastasis of mammary carcinomas by enhancing protumor properties of macrophages.* Cancer cell, 2009. **16**(2): p. 91-102.
558. Oberley-Deegan, R.E., et al., *The antioxidant, MnTE-2-PyP, prevents side-effects incurred by prostate cancer irradiation.* PloS one, 2012. **7**(9): p. e44178-e44178.
559. Moeller, B.J., et al., *A manganese porphyrin superoxide dismutase mimetic enhances tumor radioresponsiveness.* International Journal of Radiation Oncology*Biology*Physics, 2005. **63**(2): p. 545-552.
560. Keir, S.T., et al., *Cellular redox modulator, ortho Mn(III) meso-tetrakis(N-n-hexylpyridinium-2-yl)porphyrin, MnTnHex-2-PyP(5+) in the treatment of brain tumors.* Anti-cancer agents in medicinal chemistry, 2011. **11**(2): p. 202-212.
561. Tovmasyan, A., et al., *Anticancer therapeutic potential of Mn porphyrin/ascorbate system.* Free Radical Biology and Medicine, 2015. **89**: p. 1231-1247.
562. Gatalica, Z., et al., *Programmed cell death 1 (PD-1) and its ligand (PD-L1) in common cancers and their correlation with molecular cancer type.* Cancer Epidemiol Biomarkers Prev, 2014. **23**(12): p. 2965-70.
563. Bonaventura, P., et al., *Cold Tumors: A Therapeutic Challenge for Immunotherapy.* Frontiers in Immunology, 2019. **10**(168).
564. Demaria, S., et al., *Development of tumor-infiltrating lymphocytes in breast cancer after neoadjuvant paclitaxel chemotherapy.* Clin Cancer Res, 2001. **7**(10): p. 3025-30.

565. Doyle, T., et al., *Targeting the overproduction of peroxynitrite for the prevention and reversal of paclitaxel-induced neuropathic pain.* The Journal of neuroscience : the official journal of the Society for Neuroscience, 2012. **32**(18): p. 6149-6160.
566. Janes, K., et al., *Bioenergetic deficits in peripheral nerve sensory axons during chemotherapy-induced neuropathic pain resulting from peroxynitrite-mediated post-translational nitration of mitochondrial superoxide dismutase.* Pain, 2013. **154**(11): p. 2432-2440.